SWECLIM
SWEDISH REGIONAL CLIMATE MODELLING PROGRAMME

SMHI

No. 30, 2002

Reports Oceanography

Simulating Baltic Sea climate for the period 1902-1998 with the Rossby Centre coupled ice-ocean model

H.E. Markus Meier
Swedish Meteorological and Hydrological Institute
Rossby Centre, Sweden

Frank Kauker
Alfred Wegener Institute for Polar and Marine Research
Germany

Cover illustration: Photography by Berndt-Joel Gunnarsson.

RO
No. 30, 2002

Simulating Baltic Sea climate for the period 1902-1998 with the Rossby Centre coupled ice-ocean model

H.E. Markus Meier
Swedish Meteorological and Hydrological Institute
Rossby Centre, Sweden

Frank Kauker
Alfred Wegener Institute for Polar and Marine Research
Germany

Report Summary / Rapportsammanfattning

Issuing Agency/Utgivare	Report number/Publikation
Swedish Meteorological and Hydrological Institute S-601 76 NORRKÖPING Sweden	RO No. 30
	Report date/Utgivningsdatum December 2002

Author (s)/Författare

H.E. Markus Meier, Swedish Meteorological and Hydrological Institute, Rossby Centre, Sweden
Frank Kauker, Alfred Wegener Institute for Polar and Marine Research, Germany

Title (and Subtitle/Titel

Simulating Baltic Sea climate for the period 1902-1998 with the Rossby Centre coupled ice-ocean model

Abstract/Sammandrag

Hindcast simulations for the period 1902-1998 have been performed using a 3D coupled ice-ocean model for the Baltic Sea. Daily sea level observations in Kattegat, monthly basin-wide discharge data, and reconstructed atmospheric surface data have been used to force the Baltic Sea model. The reconstruction utilizes a statistical model to calculate daily sea level pressure and monthly surface air temperature, dew-point temperature, precipitation, and cloud cover fields on a 1° x 1° regular horizontal grid for the Baltic Sea region. An improved turbulence scheme has been implemented into the Baltic Sea model to simulate saltwater inflows realisticly. The results are validated against available observational datasets for sea level, salinity, saltwater inflow, volume transport, and sea ice. In addition, a comparison is performed with simulations for the period 1980-1993 using 3-hourly gridded atmospheric observations from synoptic stations. It is shown that the results of the Baltic Sea model forced with the reconstructed data are satisfactory. Sensitivity experiments have been performed to explore the impact of internal mixing, fresh- and saltwater inflows, sea ice, and the sea level in Kattegat on the salinity of the Baltic Sea. It is found that the decadal variability of mean salinity is explained partly by decadal volume variations of the accumulated freshwater inflow from river runoff and net precipitation and partly by decadal variations of the large-scale sea level pressure over Scandinavia. During the last century two exceptionally long stagnation periods are found, the 1920s to the 1930s and the 1980s to the mid 1990s. During these periods precipitation, runoff and westerly winds were stronger than normal. Stronger westerly winds caused increased eastward surface-layer transports. Consequently, the mean eastward lower-layer transports through the Stolpe Channel is reduced. The response time scale of the Baltic Sea is of the order of 30-40 years. The large inter-annual variability of the freshwater supply has no significant impact on the decadal variability of the mean salinity. Also the impact of river regulation which changes the discharge seasonality is only minor. Finally, the response of the Baltic Sea salinity to extreme changes of the freshwater inflow is investigated. We found that even with a 100 % increased freshwater supply compared to the period 1902-1998 the Baltic Sea cannot be classified as a lake. The relationship between freshwater supply and mean salinity of the final steady-state is non-linear.

Key words/sök-, nyckelord

Baltic Sea, ice-ocean modeling, decadal variability, stagnation period, major Baltic inflows, large-scale atmospheric circulation, extreme freshwater inflow

Supplementary notes/Tillägg	Number of pages/Antal sidor	Language/Språk
This work is part of the SWECLIM program.	111	English

ISSN and title/ISSN och titel

0283-1112 SMHI Reports Oceanography

Report available from/Rapporten kan köpas från:

SMHI
S-601 76 NORRKÖPING
Sweden

Contents

1 Introduction

The hydrography of the Baltic Sea estuary depends on the water exchange with the world ocean which is restricted by the narrows and sills of the Danish Straits (Fig.1) and on river runoff into the Baltic. The highly variable bottom topography separates the water masses

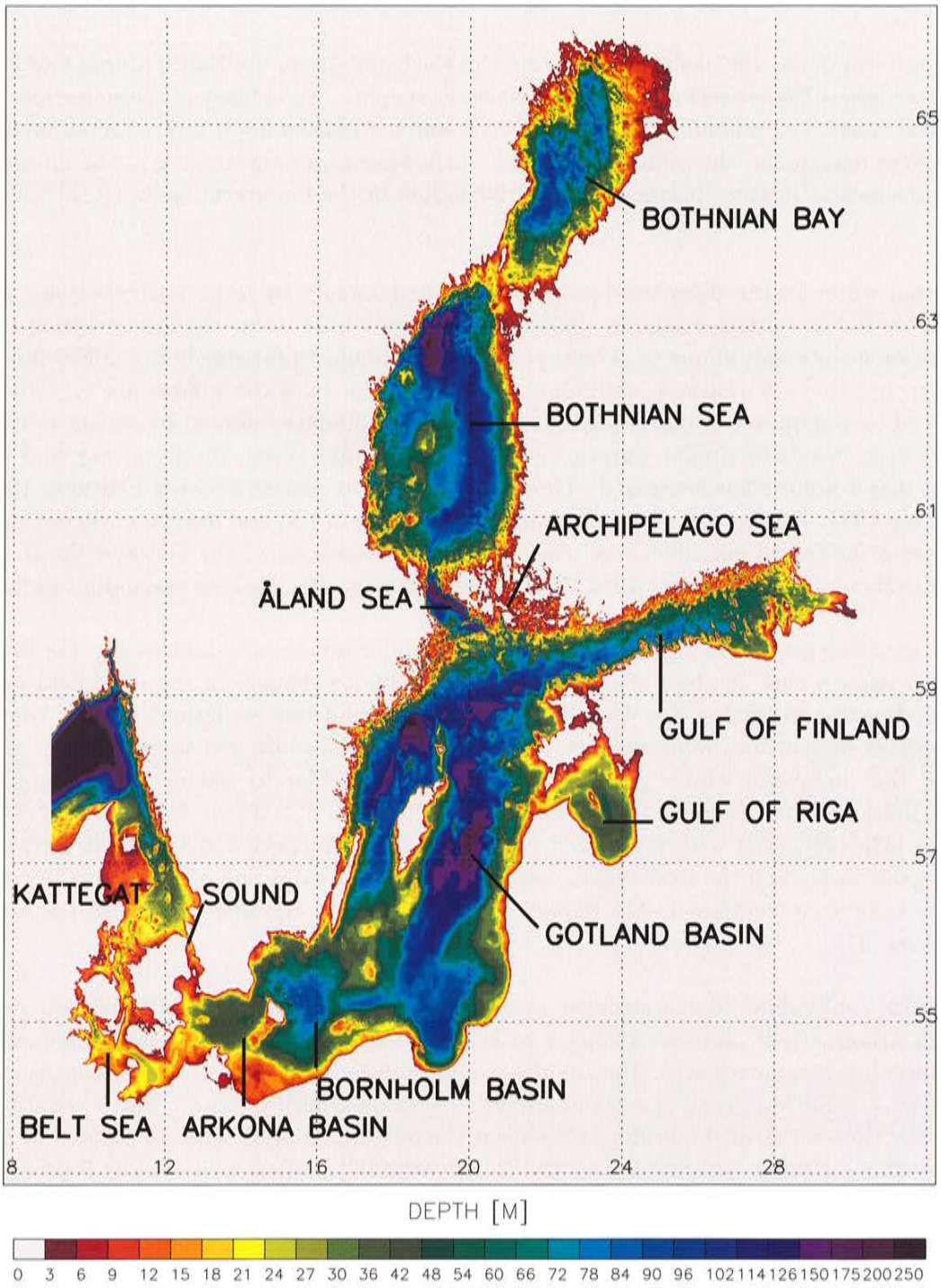

Figure 1: *Bottom topography of the Baltic Sea including Kattegat and Skagerrak (data from [100]).*

into separate basins, delimited by high sills, or bays. These are, listed from North to South, Bothnian Bay, Bothnian Sea, Åland Sea, Archipelago Sea, Gulf of Finland, Gulf of Riga, Northwestern and Eastern Gotland Basin, Bornholm Basin and Arkona Basin (Fig.1). Important channels or sills of the inner Baltic are the Quark separating Bothnian Bay and Bothnian Sea (sill depth of 25 m), the Southern Quark separating Bothnian Sea and Åland Sea (100 m), Stolpe or Slupsk Channel separating Gotland and Bornholm Basin (sill depth of 60 m) and Bornholm Channel separating Bornholm and Arkona Basin (40 m).

In the long-term mean, high saline water from the Kattegat enters the Baltic proper and low saline water leaves the estuary due to the freshwater surplus. An estuary is characterized by two vertical layers, i.e., a homogeneous upper layer and a stratified lower layer. Mixing in the entrance area determines the salinity of in- and outflowing water and mixing in the interior, so-called deepwater mixing, balances vertical advection in the long-term mean ([115], [106], [107]).

The bottom water in the deep sub-basins is ventilated mainly by large perturbations, so-called major Baltic saltwater inflows ([63], [29]). These events occur randomly during the winter season at intervals of one to several years. They are most probable between November to January, but they occur also in autumn and spring. Major saltwater inflows are very likely to be forced by a sequence of easterly winds lasting for 20-30 days followed by strong to very strong westerly winds of similar duration [56]. Since the mid-1970s, the frequency and intensity of major inflows has decreased. They were completely absent between February 1983 and January 1993. During this phase a significant depletion of salt and oxygen occurred, and an increase of hydrogen sulphide were observed in the deep layer of the Gotland Basin. A major saltwater inflow in January 1993 terminated this exceptionally long stagnation period.

Different mechanisms for the decreased frequency of major inflows are discussed in the literature. It is argued that the lack of major inflows was due to changes in the wind field over the North Sea and the Baltic Sea [56]. Recently, it was found that variations in river runoff have a greater impact on the occurrence of major inflows than hitherto supposed [97]. [66] suggested that increased winter runoff (from September to March) reduce the probability of major Baltic inflows. Increased zonal circulation (high North Atlantic Oscillation (NAO) index, see [42], [48], [87]) with intensified precipitation and increased river runoff, and the anthropogenic impact on the freshwater cycle by seasonal redistribution of runoff due to river regulation have been mentioned. The impact of river regulation on saltwater inflows has been discussed by [91].

Indeed, [119] could show that a stronger meridional sea level pressure (SLP) gradient over the North Atlantic, and therefore stronger westerly winds, causes positive rainfall anomalies in the Baltic Sea catchment area. Hence, increased runoff reduces salinities at all depths and at all stations included in their statistical analysis based on monthly values. The correlations between the time series of the leading Canonical Correlation Analysis (CCA) pattern of the SLP (describing a zonal circulation over the North Atlantic) and salinities in the Baltic Sea are $r = 0.7$ for the mean salinity in the upper 50 m and $r = 0.85$ for the mean salinity below 100 m.

In accordance with these results, [39] proposed a general chain-of-events relationship between the NAO and the Baltic Sea salinity: Westerly winds measured over the British Isles followed changes in the NAO with a lag of less than one month. Total freshwater runoff to the Baltic

Sea followed changes in the NAO with a lag of less than two months. Furthermore, salinity at Gotland Deep in 200 m of depth between 1953-1990 responded to freshwater runoff with a time lag of less than one year.

Several other publications show also the strong link between the large-scale atmospheric circulation, e.g. described by the NAO index, and Baltic Sea variables, e.g. sea ice ([54], [60], [109], [83]), sea level ([47], [3]), and circulation [58].

Inter-annual salinity variations in the Baltic Sea during the period 1954-1990 have been discussed by [95]. Even 100 years of hydrographic data have been analyzed with focus on the freshwater budget by [117]. They found that variations of the mean salinity reflect the accumulated changes of river runoff. The system is 'truly time-dependent' with a time scale much longer than the forcing time scale, identified as the runoff essentially [117]. [117] concluded that there must be a strong positive feedback between the freshwater content of the Baltic Sea and the return of freshwater equivalents with the inflows. The responsible mechanism behind the feedback is a very effective mixing in the Danish Straits [92]. Using a time dependent 'Knudsen like' conservation equation for the Baltic Sea inside the Danish Straits, [92] achieved a relation between the freshwater supply and the steady-state salinity of the Baltic Sea surface water. They found that the inflow of Kattegat deepwater vanishes at a freshwater supply of about $21,500\, m^3\, s^{-1}$.

The sensitivity of Baltic Sea climate has been investigated earlier using process oriented models. For example, the sensitivity of Baltic Sea surface salinity on the barotropic transport between the Baltic and the Kattegat, on the freshwater supply, on the wind speed, and on the salinity of the Skagerrak water have been investigated by [106]. [85] showed the sensitivity of sea ice to air temperature increase. The sensitivity of median salinities for Kattegat and for the eastern Gotland Basin on net precipitation was explored by [82]. [35] stated using a process oriented model of the Baltic entrance area that increased wind mixing does not significantly change the major inflows from the Arkona pool. Both increased amplitudes of sea level variations in Kattegat and decreased freshwater supply substantially increase the magnitude of the inflows. He found that the deepwater renewal is obstructed during years with high freshwater supply even if the sea level forcing is favorable to a major inflow.

[77] performed a series of process studies of the inflow period 1992/93 using a high-resolution primitive equation model for the Baltic Sea. Their results for the impact of river runoff, wind speed, and sea level in Kattegat were in agreement with those by [35]. Natural inter-annual runoff variations modify saltwater inflows into the Bornholm Basin significantly.

In this study, we present sensitivity studies period 1902-1998 using a 3D coupled ice-ocean model for the Baltic Sea. The model used is the Rossby Centre Ocean model, RCO ([76], [68], [69], [70], [71], [78], [72], [73], [77]). The atmospheric forcing for this period has been reconstructed [51]. The study aims to answer the following questions:

- Is the performance of 3D general circulation models good enough to perform 100-year simulations of the Baltic Sea?
- Is the quality of the reconstructed atmospheric data set sufficient to model climate and decadal variability of the Baltic Sea? Especially, are major Baltic inflows correctly simulated?

- What is the reason for the decreased frequency and intensity of major saltwater inflows since the mid-1970s? In general, what is the influence of salt- and freshwater inflows on decadal variability of salinity in the Baltic Sea?
- What are the extremes to which the Baltic Sea system might drift on the time scale of 100 years if extremely increased or decreased fresh- and saltwater inflows are applied? For example, is it possible that the Baltic Sea will become a lake at a 34% increased freshwater supply compared to todays climate as found by [92]?

Regarding the last question, we emphasize that it is not our aim to perform a climate change scenario of Baltic Sea salinity for the next 100 years. Exploring the impacts of global climate change for the Baltic Sea is beyond the scope of this study. The report describes sensitivity experiments to determine the space of steady-state salinity as a function of the forcing. Within the Swedish Regional Climate Modeling program (SWECLIM) scenarios for the Nordic countries have been produced which indicate that the river runoff to the Baltic Sea might increase in case of global warming [72]. However, it was earlier impossible to address the question how salinity will evolve during the next 100 years as the time slice approach has been applied [72]. Now we have the possibility to perform such scenarios with the reconstructed atmospheric forcing together with the relative monthly changes of atmospheric surface variables between scenario and control time slice experiments assuming that the variability of the past 100 years will not change in future ('Δ-change' technique). Results will be reported in forthcoming publications.

The report is organized as follows: In the second section, RCO is presented briefly. In the third section, a revised mixing parameterization is derived. In Sections 4 to 7, the model setup is described. In the eighth section, model results of sea level, salinity, salt and volume transports, and sea ice are validated compared to observations. In Section 9, sensitivity studies are presented. In Section 10, the relation between the large-scale atmospheric circulation and regional variables is discussed. Extreme states of the Baltic Sea stratification are presented in Section 11. The experiments performed for this study are listed in Appendix A (Tables 15, 16 and 17). The report ends with a discussion, conclusions and a future outlook.

2 The Rossby Centre coupled ice-ocean model

Decade-long integrations of the Baltic Sea require ice-ocean models with high technical performance. In addition, the evolution of stratification in time has to be stable and the flow of dense water over the sills into the Baltic has to be simulated realisticly. When SWECLIM started, none of the available Baltic Sea models including sea ice was suitable for parallel computing. Hence, the Rossby Centre Ocean Model (RCO) has been developed using the version of the Ocean Circulation Climate Advanced Modelling (OCCAM) project of the Bryan–Cox–Semtner primitive equation ocean model with a free surface [114]. As the OCCAM project focuses on global scales it was necessary to add parameterizations important for the Baltic Sea. A two-equation turbulence closure scheme, open boundary conditions, and a sea ice model were main features that had to be added for our purposes ([76], [69], [71], [77]).

The model depths are based on realistic bottom topography data [100], as shown in Fig.1. RCO uses 41 levels with layer thicknesses from 3 m close to the surface to 12 m near the bottom. The maximum depth in RCO is 250 m. For the long-term simulations described here, a horizontal resolution of 6 *nautical miles* is used. Standard bulk formulae are utilized

[72].

For a more detailed model description of RCO the reader is referred to [76], [71] and [77]. The computational performance of RCO has been investigated by [78]. The RCO code is optimized for massively parallel computer architectures with horizontal partitioning. An improved domain partitioning technique minimizes load imbalance. For 100-year simulations it was necessary to improve the mixing parameterization. The revised turbulence model is described in the next section.

3 Mixing parameterization

Firstly, the framework of the $k-\varepsilon$ model (Section 3.1) and of the k model (Section 3.2) as described by [69] and [71] are repeated briefly. Both turbulence models are utilized with flux boundary conditions for the turbulence equation(s) (Section 3.3). A parameterization for the turbulence generation of breaking internal waves is included (Section 3.4). As shown by [71], the results for the seasonal thermocline of a k model with appropriately chosen length scales are more or less equivalent to the results of the so-called standard $k-\varepsilon$ model. However, in Section 9.1, it will be shown that this equivalence is not valid for the evolution of the stratification on a 100-year time scale. The deepwater renewal is quite sensitive to the mixing parameterization used. As the standard $k-\epsilon$ model underestimates saltwater inflows (e.g. [71], [77]), an improved turbulence model has been developed with better performance concerning saltwater inflows. In Section 3.5, it is shown that for the non-diffusive steady-state both model types (k and $k-\varepsilon$) are physically equivalent if appropriately chosen modifications to the earlier versions are applied. However, it should be noted that in general the k and the $k-\varepsilon$ model are not physically identical because the k model does not include a time scale and vertical diffusion for the turbulent master length scale. In addition, differences between the two numerical equation solvers may cause significant performance differences. Readers familiar with the earlier publications by [69] and [71] can continue with Section 3.5.

3.1 The standard $k-\varepsilon$ turbulence model

In this section the so-called standard $k-\varepsilon$ turbulence model is presented. As shown by [7], the two commonly used two-equation turbulence closure schemes, the $k-\varepsilon$ [108], [93] and the Mellor-Yamada level 2.5 model [79], [80], can be written in a joint form with different parameters. [15] have shown that the two model types perform similarly.

The $k-\varepsilon$ model consists of two prognostic equations for turbulent kinetic energy (k) and for dissipation (ε) of k. These two equations have to be solved at every grid point of the 3D ocean model:

$$\frac{\partial k}{\partial t} - \frac{\partial}{\partial z}\left(\frac{\nu_t}{\sigma_k}\,\frac{\partial k}{\partial z}\right) = P + G - \varepsilon\,, \tag{1}$$

$$\frac{\partial \varepsilon}{\partial t} - \frac{\partial}{\partial z}\left(\frac{\nu_t}{\sigma_\varepsilon}\,\frac{\partial \varepsilon}{\partial z}\right) = c_{\varepsilon 1}\,\frac{\varepsilon}{k}\,(P + c_{\varepsilon 3}\,G) - c_{\varepsilon 2}\,\frac{\varepsilon^2}{k}\,, \tag{2}$$

$$\text{with}\quad P = \nu_t\left[\left(\frac{\partial u}{\partial z}\right)^2 + \left(\frac{\partial v}{\partial z}\right)^2\right],\quad G = -\frac{\nu_t}{\sigma_t}\,N^2\,, \tag{3}$$

$$\nu_t = c_\mu\,\frac{k^2}{\varepsilon}\,. \tag{4}$$

Here, t denotes time. N is the Brunt-Väisälä frequency and σ_t is the turbulent Prandtl number. The constants c_μ, $c_{\varepsilon 1}$, $c_{\varepsilon 2}$, $c_{\varepsilon 3}$, σ_k and σ_ε are given in Table 1 according to [93].

c_μ	$c_{\varepsilon 1}$	$c_{\varepsilon 2}$	$c_{\varepsilon 3}$	σ_k	σ_ε
0.09	1.44	1.92	0/1	1	1.3

Table 1: *Constants of the standard $k-\varepsilon$ model [93].*

In case of unstable stratification the constant $c_{\varepsilon 3}$ is set equal to 1 to ensure complete mixing between adjacent grid boxes. Otherwise, $c_{\varepsilon 3}$ is zero. However, the interaction of turbulence with stratification is not very well understood as indicated by the wide spread of values used in the literature for $c_{\varepsilon 3}$ (Tab.2).

$c_{\varepsilon 3}$	author(s)
-1.9	[13], advanced
-1.4	[13], standard
-0.48	[71], $Ri^{st} = 0.25$
$0 \ldots 0.2$	[93]
0.56	Omstedt (1996, pers.comm.)
0.67	[8]
0.8	[86]

Table 2: *Different values of $c_{\varepsilon 3}$ used by a couple of authors in case of stable stratification.*

The turbulence model gives no information about σ_t. An empirical formula is used to complete the mixing scheme. In several experiments the best results are obtained using a Richardson number dependent Prandtl number [10]:

$$\sigma_t = \begin{cases} 1 & : \quad Ri \leq 0.2 \\ 5\,Ri & : \quad 0.2 < Ri \leq 2 \\ 10 & : \quad 2 < Ri \end{cases} . \tag{5}$$

With (5), diffusivity of tracers is calculated according to $\nu_t' = \nu_t/\sigma_t$.

Penetrative radiation additionally heats the water column. Conservation of potential temperature (T) is given in the circulation model by

$$\frac{\partial T}{\partial t} + \Gamma(T) = \frac{\partial}{\partial z}\left(\frac{\nu_t}{\sigma_t}(z)\,\frac{\partial T}{\partial z}\right) + A_T\,\nabla^2 T + \frac{1}{\rho_0\,c_{pw}}\,\frac{\partial I}{\partial z} \tag{6}$$

with the advection operator

$$\Gamma(T) = \frac{1}{R\cos\phi}\left[\frac{\partial}{\partial\lambda}(u\,T) + \frac{\partial}{\partial\phi}\,(v\,T\,\cos\phi)\right] + \frac{\partial}{\partial z}(w\,T)\,, \tag{7}$$

the Earth radius R, specific heat capacity of water c_{pw}, horizontal austausch coefficient A_T and solar intensity I. I is parameterized according to [89] with two extinction lengths

$$I = Q_{SW}\left[R_{SW}\,e^{\frac{z}{\zeta_1}} + (1 - R_{SW})\,e^{\frac{z}{\zeta_2}}\right] \tag{8}$$

with $R_{SW} = 0.64$, $\zeta_1 = 1.78\,m$, and $\zeta_2 = 3.26\,m$. Q_{SW} is the shortwave energy flux. Usually, optical water types are classified according to [46], but not very detailed information is available for the Baltic Sea. Jerlov classified the Skagerrak water as coastal water type 1 and the Baltic proper as coastal water type 3 without giving the corresponding extinction lengths. Hence, climatology data from [24] (see his Tab. 5.3.1) have been used to optimize the unknown constant R_{SW} and the extinction lengths ζ_1 and ζ_2 utilizing a least-squares fit according to [89]. The available data are average monthly means of solar energy over the entire spectrum reaching particular depths in the southern Baltic. For comparison, the most turbid optical water type III for oceans according to [46] uses the values $R_{SW} = 0.78$, $\zeta_1 = 1.4\,m$, and $\zeta_2 = 7.9\,m$.

The impact of solar insolation is illustrated in Figure 2. Shown is the 13-year mean temper-

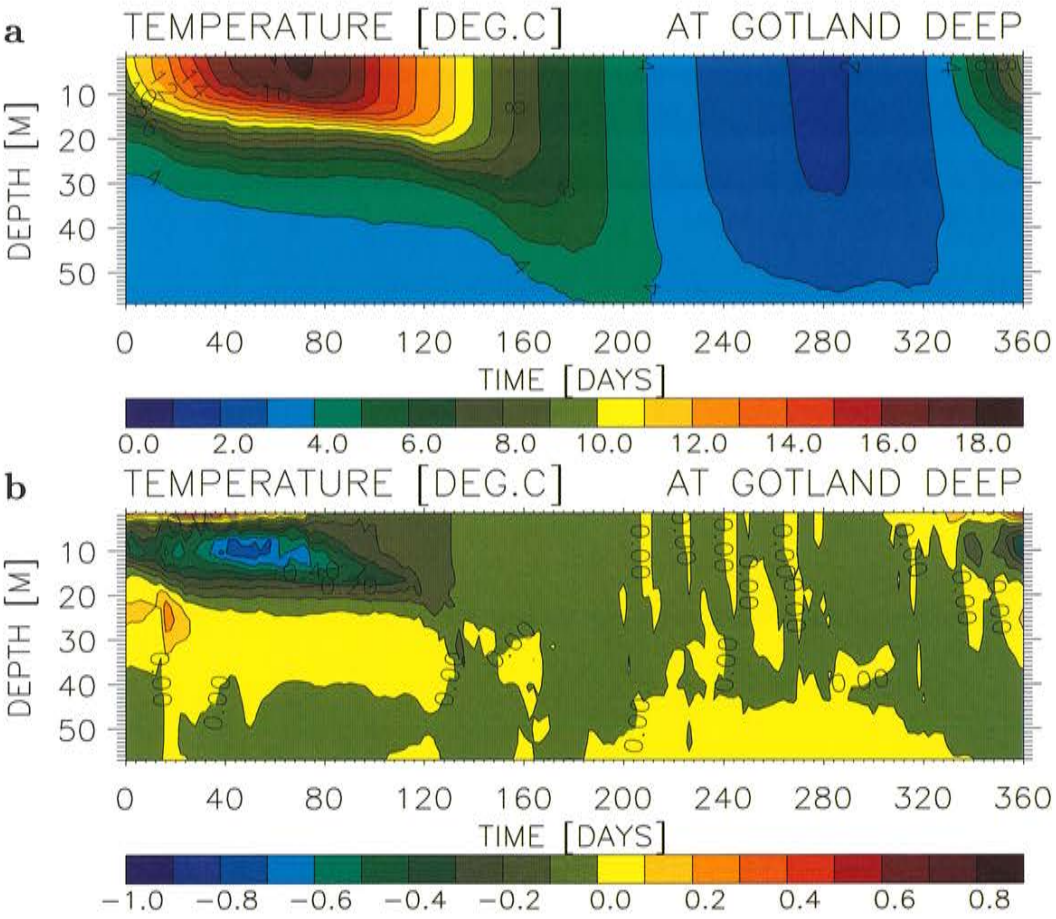

Figure 2: *The 13-year mean seasonal cycle of isotherm depths (in °C) at Gotland Deep (BY15): (a) reference run using the $k-\varepsilon$ model (run 240), (b) difference between simulations without and with penetrating short wave radiation (run 339 minus run 240). The time axis starts with May 27.*

ature difference between two simulations without and with penetrating short wave radiation. In the experiment without penetration the short wave radiation is heating only the first model layer. Maximum differences are found in July when the water in $10\,m$ depth is $0.8°C$ colder without penetrative radiation and in June when the surface water is $0.5°C$ warmer.

3.2 The k turbulence model

Instead of an equation for dissipation of turbulent kinetic energy an algebraic relationship for the turbulent length scale (l) is used in so-called k models. Using Kolmogorov's hypothesis [53] for the dissipation of k

$$\varepsilon = c_d \frac{k^{\frac{3}{2}}}{l} \tag{9}$$

with the empirical constant c_d, the equation for k results in

$$\frac{\partial k}{\partial t} - \frac{\partial}{\partial z}\left(\frac{\nu_t}{\sigma_k}\frac{\partial k}{\partial z}\right) = P + G - c_d \frac{k^{\frac{3}{2}}}{l} \tag{10}$$

with

$$\nu_t = \frac{c_\mu}{c_d}\, l\, \sqrt{k}\,. \tag{11}$$

The value of the empirical constant c_d is related to the applied stability function c_μ. Following [16] or [14] c_d can be calculated from the quasi-equilibrium momentum stability function for neutral flow, for example, from [31] resulting in $c_d = 0.17$ or from [17] resulting in $c_d = 0.15$. Here, the value $c_d = 0.1618$ is used. In addition, $\sigma_k = 1$ and the turbulent Prandtl number in (5) are adopted from the $k - \varepsilon$ model.

According to [116] the equation for k (10) can be scaled using the following length scales

$$l_b = \frac{\sqrt{2\,k}}{N}\,, \tag{12}$$

$$l_u = \frac{\sqrt{k}}{\sqrt{\left(\frac{\partial u}{\partial z}\right)^2 + \left(\frac{\partial v}{\partial z}\right)^2}} \tag{13}$$

and l_d, the distance to the sea surface or bottom. Neglecting time tendency and assuming stable stratification (10) can be written for scale analysis as

$$\frac{l^2}{l_d^2} + \frac{l^2}{l_u^2} - \frac{l^2}{l_b^2} - 1 = 0\,. \tag{14}$$

The only relevant length scales contained in (10) which determine the turbulent length scale l are l_d, l_u and l_b. Further, it follows from (14) that physically sound solutions of the k equation (10) have to consider always dissipation.

As $\sqrt{2\,k}$ is the velocity of the turbulent eddies, l_u can be interpreted as characteristic length scale for the background shear of mean velocity. If the turbulent length scale l is larger than l_u the classical hypothesis from Prandtl is violated. Thus, the austausch ansatz applied to the k equation is valid if always $l \leq l_u$ is fulfilled.

Further, l_b is the characteristic length scale of a turbulent eddy in stratified fluid which is elevated from equilibrium position z_0 so that its change of potential energy equals its turbulent kinetic energy:

$$k(z_0) = \frac{g}{\rho_0}\int_{z_0}^{z_0+l_b} (\rho(z_0) - \rho(z))\, dz\,. \tag{15}$$

Expanding density into a Taylor series

$$\rho(z) = \rho(z_0) + \left.\frac{\partial \rho}{\partial z}\right|_{z_0} (z - z_0) + \dots \tag{16}$$

the integral can be solved analytically

$$k = \frac{1}{2} N^2 l_b^2 , \tag{17}$$

which is equivalent to (12). It is assumed that the potential energy of turbulent eddies is smaller than their kinetic energy (k). Thus, the turbulent length scale is limited by $l \leq l_b$.

A third limitation, $l \leq l_d$, follows from simple geometrical arguments. As the turbulent length scale is limited by three characteristic length scales simultaneously, the most simple model for l would be to choose just the minimum:

$$l = \min[l_d, l_u, l_b] . \tag{18}$$

However, there is still a degree of freedom for the choice of the proportionality constants of the three characteristic length scales (with magnitude of the order of 1). To consider roughness lengths z_0 and z_{0H} at the sea surface and bottom, respectively, and to use only one length scale l_d for the whole water column, the following expression for l_d is used here:

$$l_d = \kappa (z_0 - z) \left(1 + \frac{(z_{0H} + z)}{H}\right) \tag{19}$$

with von Kármán's constant $\kappa = 0.4$ and water depth H (recall that z is positive upward and zero at the sea surface).

To ensure that in the shear layer the balance $P = \varepsilon$ replaces the full equation (10), the following k model has been tested by [69] and [71]:

$$l = \min \left[\kappa (z_0 - z) \left(1 + \frac{(z_{0H} + z)}{H}\right) , \quad \frac{c_d}{\sqrt{c_\mu}} \frac{\sqrt{k}}{\sqrt{\left(\frac{\partial u}{\partial z}\right)^2 + \left(\frac{\partial v}{\partial z}\right)^2}} , \quad \frac{\sqrt{2\,k}}{N} \right] . \tag{20}$$

3.3 Surface flux boundary conditions

Commonly, Dirichlet boundary conditions are used for turbulence models. At the surface a logarithmic boundary layer is assumed with balance between shear production (P), interaction with stratification (G) and dissipation (ε) [108]:

$$P + G = \varepsilon, \quad l = \kappa (z_0 - z) . \tag{21}$$

In case of high vertical resolution, these boundary conditions are only slightly dependent on the surface roughness length. Within the boundary layer dissipation decays inversely proportional with the distance from the surface. Contrary, measurements show that dissipation decays much faster with the second or third power [21], [20]. Because of breaking surface gravity waves, a turbulence enhanced layer is developed, which controls the vertical flux of

k from the wave field to the mixed layer interior. Therefore, flux boundary conditions (Neumann boundary conditions) are included which are calculated from an analytical solution of the k equation based on the assumption of a balance of k diffusion and dissipation [21]:

$$\frac{\partial}{\partial z}\left(\frac{\nu_t}{\sigma_k}\frac{\partial k}{\partial z}\right) = \varepsilon, \quad l = \kappa\,(z_0 - z) \quad . \tag{22}$$

Neglecting the term, which represents reflected energy from the bottom, the solution of (22) within the turbulence enhanced layer is

$$\sqrt{k} = C\,(z_0 - z)^{-\frac{n}{3}} \tag{23}$$

with

$$n = \sqrt{\frac{3}{2}\frac{\sigma_k}{c_\mu}}\frac{c_d}{\kappa} = 1.65\,. \tag{24}$$

The constant C is determined by the boundary condition at the surface

$$\left.\frac{\nu_t}{\sigma_k}\frac{\partial k}{\partial z}\right|_{z=0} = m\,u_\star^3 + \kappa\,z_0\,B_0 \tag{25}$$

with friction velocity in the ocean $u_\star$, surface buoyancy flux B_0 and a constant $m = 100$ given by [21] or estimated by [61]. From (23) and (25) follows

$$C = \left(\frac{3\,\sigma_k}{2\,c_\mu}\right)^{\frac{1}{6}} z_0^{\frac{n}{3}}\,\left(m\,u_\star^3 + \kappa\,z_0\,B_0\right)^{\frac{1}{3}}\,. \tag{26}$$

Using (23), (24) and (26) one can calculate dissipation within the boundary layer

$$\varepsilon = C^3\,\frac{c_d}{\kappa}\,(z_0 - z)^{-n-1} \tag{27}$$

or fluxes of k and ε

$$\frac{\nu_t}{\sigma_k}\frac{\partial k}{\partial z} = C^3\sqrt{\frac{2\,c_\mu}{3\,\sigma_k}}\,(z_0 - z)^{-n}\,, \tag{28}$$

$$\frac{\nu_t}{\sigma_\varepsilon}\frac{\partial \varepsilon}{\partial z} = C^4\,\frac{c_\mu}{\sigma_\varepsilon}\,(n+1)\,(z_0 - z)^{-\frac{4n}{3}-1}\,, \tag{29}$$

.

For the discretization of the $k-\varepsilon$ model a staggered grid is used in vertical direction with ν_t, k and ε at edges of the grid boxes of thickness Δz. Contrary, the prognostic variables of the circulation model u, v, T, S are located in box centers. Hence, fluxes of k and ε have to be prescribed at $z = -\Delta z/2$. Assuming that this depth is within the turbulence enhanced boundary layer, the following flux boundary conditions are derived from (28) and (29):

$$\left.\frac{\nu_t}{\sigma_k}\frac{\partial k}{\partial z}\right|_{z=-\frac{\Delta z}{2}} = \frac{m\,u_\star^3 + \kappa\,z_0\,B_0}{\left(1 + \frac{\Delta z}{2\,z_0}\right)^n}\quad , \tag{30}$$

$$\left.\frac{\nu_t}{\sigma_\varepsilon}\frac{\partial \varepsilon}{\partial z}\right|_{z=-\frac{\Delta z}{2}} = a_\varepsilon\,\frac{\left(m\,u_\star^3 + \kappa\,z_0\,B_0\right)^{\frac{4}{3}}}{z_0\,\left(1 + \frac{\Delta z}{2\,z_0}\right)^{\frac{4n}{3}+1}}\quad . \tag{31}$$

The value of the constant a_ε is given by

$$a_\varepsilon = \frac{c_\mu^{\frac{1}{3}}}{\sigma_\varepsilon} \left(\frac{3\,\sigma_k}{2}\right)^{\frac{2}{3}} \left(\sqrt{\frac{3\,\sigma_k}{2\,c_\mu}}\,\frac{c_d}{\kappa} + 1\right) \quad . \tag{32}$$

The surface roughness length is calculated adopting Charnok's formula [18]:

$$z_0 = \alpha_C\,\frac{u_\star^2}{g} \tag{33}$$

with $\alpha_C = 1400$ [62], justified by analogy with the atmosphere. Using $z_0 = 10\,cm$ and $\Delta z = 3\,m$ the denominator in (30) reduces the k flux in $\Delta z/2 = 1.5\,m$ depth to 1 % of the corresponding surface flux. Most of the k generated by breaking surface gravity waves is dissipated within the uppermost grid box of the circulation model.

The depth (z_{crit}) of the transition from the turbulence enhanced surface layer to the shear layer ($P = \varepsilon$) can be estimated as follows. Assuming that z_{crit} is smaller than the Ekman depth, rotation can be neglected in the steady Ekman equations for momentum:

$$\rho_0\,\nu_t\,\frac{\partial \vec{u}}{\partial z} = \vec{\tau} = \text{const} \tag{34}$$

with $|\vec{\tau}| = \rho_0\,u_\star^2$. Thus, $P = \varepsilon$ is transformed to

$$\frac{u_\star^4}{\nu_t} = \varepsilon \tag{35}$$

and with (4)

$$k = \frac{u_\star^2}{\sqrt{c_\mu}} = \text{const}\,. \tag{36}$$

If the surface buoyancy flux B_0 is considered too according to [108], (36) has to be modified to

$$k = \frac{1}{\sqrt{c_\mu}}\,(u_\star^3 + \kappa\,z_0\,B_0)^{\frac{2}{3}}\,. \tag{37}$$

Except the case of convective boundary layers, the buoyancy flux is smaller than the momentum flux. By equating (23) and (36), the critical depth results in

$$z_{crit} = z_0\left(1 - \left[m\,c_\mu^{\frac{1}{4}}\sqrt{\frac{3}{2}\sigma_k}\right]^{\frac{1}{n}}\right) = -11.8\,z_0\,. \tag{38}$$

The depth of the turbulence enhanced surface layer depends only on the roughness length.

3.4 Deepwater mixing

For multi-year integrations deepwater mixing needs to be taken into account. The $k-\varepsilon$ model is extended to include a parameterization for breaking internal waves [107]:

$$\nu = \nu_t + \sigma_t \min\left(\frac{\alpha}{N}, \nu_{0,max}\right) \tag{39}$$

with $\alpha = 0.5 \cdot 10^{-3}\, cm^2\, s^{-2}$, $\nu_{0,max} = 0.5\, cm^2\, s^{-1}$. The inverse proportionality between the deep mixing and the Brunt-Väisälä frequency is in accordance with ocean observations [32].

Alternatively, it is possible to include the effect of breaking internal waves into the $k - \varepsilon$ model directly. As in stable stratified layers the turbulent macro length scale l is limited by

$$l \leq \frac{\sqrt{2\,k}}{N}\,, \tag{40}$$

as shown in Section 3.2, a corresponding lower limit for the dissipation rate ε using Kolmogorov's equation can be derived:

$$\varepsilon \geq \frac{c_d}{\sqrt{2}}\, k\, N\,. \tag{41}$$

Hence, a necessary condition to fulfill (40) is given by

$$\varepsilon \geq \varepsilon_{min} \cong 0.1144\, k_{min}\, N\,. \tag{42}$$

Using the relationship of Kolmogorov and Prandtl (4) the viscosity is limited by

$$\nu_t \geq \nu_{t,min} = c_\mu\, \frac{k_{min}^2}{\varepsilon_{min}}\,. \tag{43}$$

Comparison with (39) gives a lower limit for k:

$$k \geq k_{min} = \frac{\alpha\, c_d\, \sigma_{t,max}}{c_\mu\, \sqrt{2}} \cong 6.356 \cdot 10^{-3}\, cm^2 s^{-2}\,. \tag{44}$$

The results of both approaches are rather similar [69]. In the following, the second alternative with lower limits for k and ε are used.

3.5 The improved k model

Assuming a non-diffusive steady-state for dissipation, it follows from (2)

$$0 = c_{\varepsilon 1}\; (P + c_{\varepsilon 3}\, G) - c_{\varepsilon 2}\, \varepsilon\,. \tag{45}$$

With the modified definitions for the length scales

$$l_b = \frac{\sqrt{2\,k}}{N}\,, \tag{46}$$

$$l_u = \frac{c_d}{\sqrt{c_\mu}}\, \frac{\sqrt{k}}{\sqrt{\left(\frac{\partial u}{\partial z}\right)^2 + \left(\frac{\partial v}{\partial z}\right)^2}} \tag{47}$$

it follows from (3) utilizing (4)

$$P = \nu_t \left[\left(\frac{\partial u}{\partial z}\right)^2 + \left(\frac{\partial v}{\partial z}\right)^2\right] = \frac{k^3}{\varepsilon}\, \frac{c_d^2}{l_u^2}\,, \tag{48}$$

$$G = -\frac{\nu_t}{\sigma_t}\, N^2 = -c_\mu\, \frac{k^2\, N^2}{\varepsilon\, \sigma_t}\,. \tag{49}$$

Replacing in (45) P, G, and ε with (48), (49), and (9), the result is after reordering

$$\frac{1}{l^2} = \frac{c_{\varepsilon 1}}{c_{\varepsilon 2}} \frac{1}{l_u^2} - \frac{c_{\varepsilon 1}\, c_{\varepsilon 3}\, c_\mu}{c_{\varepsilon 2}\, c_d^2\, \sigma_t} \frac{1}{l_b^2} \,. \tag{50}$$

Equation (50) is similar to the result of the scale analysis (14) presented by [116], but the length scale l_d is missing per definition. The proportionality constants, derived from the ϵ-equation (2), are now considered. A straight forward extension of (50) to the diffusive case (important for boundary layers) would be

$$\frac{1}{l^2} = \frac{1}{l_d^2} + \frac{c_{\varepsilon 1}}{c_{\varepsilon 2}} \frac{1}{l_u^2} - \frac{c_{\varepsilon 1}\, c_{\varepsilon 3}\, c_\mu}{c_{\varepsilon 2}\, c_d^2\, \sigma_t} \frac{1}{l_b^2} \,. \tag{51}$$

(51) and (20) differ mathematically as two different algebraic functions are used. However, more important is the physical difference. The two length scales l_u and l_b are considered with weights (with magnitude of the order of 1) relative to the length scale l_d. In sensitivity experiments performed for the period 1902-1998 (Section 9), it is found that the modified k model utilizing

$$l = \min\left[\kappa\,(z_0 - z)\left(1 + \frac{(z_{0H} + z)}{H}\right)\,,\quad c_u\,\frac{c_d}{\sqrt{c_\mu}}\,\frac{\sqrt{k}}{\sqrt{\left(\frac{\partial u}{\partial z}\right)^2 + \left(\frac{\partial v}{\partial z}\right)^2}}\,,\quad c_b\,\frac{\sqrt{2\,k}}{N}\right]\,, \tag{52}$$

with $c_u = \sqrt{c_{\varepsilon 2}/c_{\varepsilon 1}} = 1.1547$ and $c_b = 1$, yields good results compared to observations (Section 8).

Although in this study the value for the constant c_b has not been optimized, the results suggest that the corresponding $k-\varepsilon$ model performs better if $c_{\varepsilon 3}$ is a function of the turbulent Prandtl number (σ_t) or of the stability function ($c'_\mu = c_\mu/\sigma_t$) rather than a constant:

$$c_{\varepsilon 3} = -\frac{c_{\varepsilon 2}\, c_d^2}{c_{\varepsilon 1}\, c'_\mu} \,. \tag{53}$$

$c_{\varepsilon 3}$ should be negative because otherwise no stationary solution exists for the $k-\varepsilon$ model ([13], [7]). Applying the Richardson number dependent Prandtl number of [10] (Eq.5), the following function for $c_{\varepsilon 3}$ is derived:

$$c_{\varepsilon 3} = \begin{cases} -0.39 & : \quad Ri \le 0.2 \\ -1.94\,Ri & : \quad 0.2 < Ri \le 2 \\ -3.88 & : \quad 2 < Ri \end{cases} \,. \tag{54}$$

For the non-diffusive steady-state, the gradient Richardson number follows from (1) and (2):

$$Ri^{st} = \frac{c_\mu}{c'_\mu}\,\frac{c_{\varepsilon 2} - c_{\varepsilon 1}}{c_{\varepsilon 2} - c_{\varepsilon 3}} \,. \tag{55}$$

Taking $\sigma_t = 1$, from (55) follows $Ri^{st} = 0.2080$. Assuming the Richardson number dependent Prandtl number of [10], from (55) follows $Ri^{st} = 0.2475$. Both results are in accordance with earlier estimates used in the literature [99].

In Figures 3 and 4, temperature and salinity results of the improved k model and of the $k-\varepsilon$ model with Equation (54) and with $\sigma_\varepsilon = 10$ are compared for the period 1980-1993.

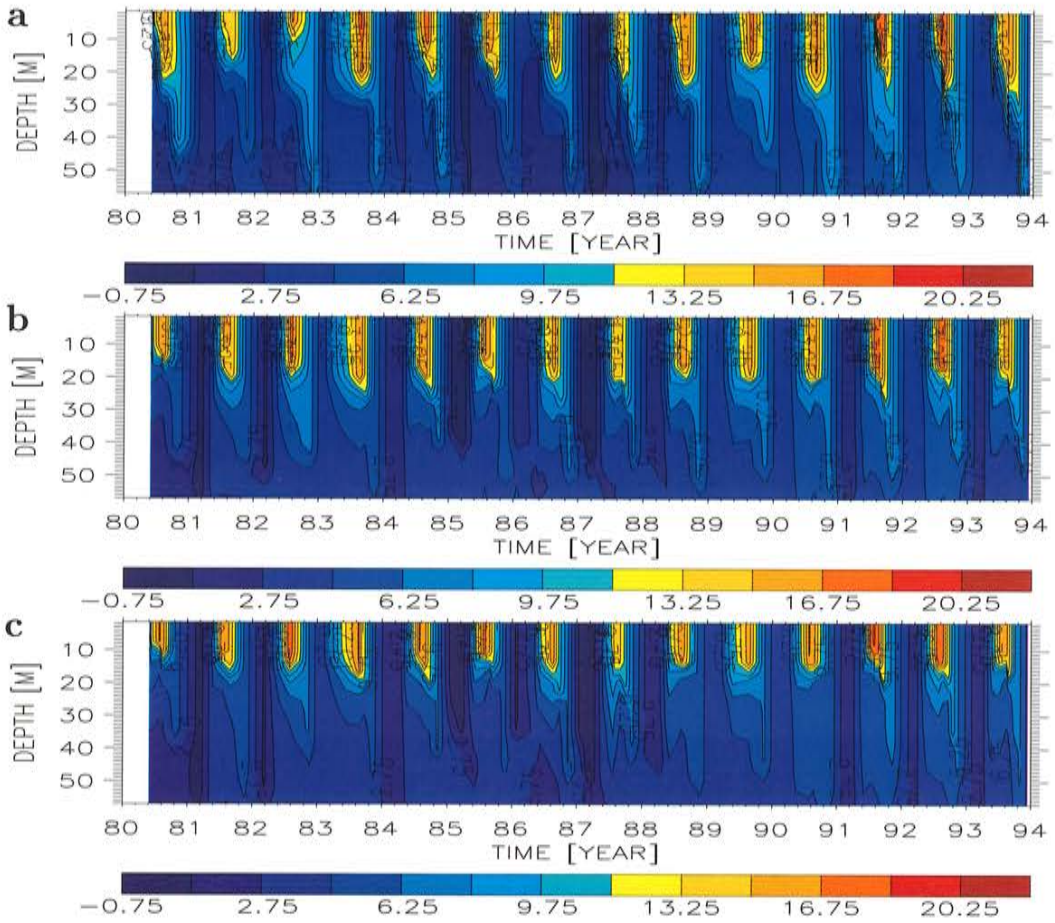

Figure 3: *Isotherm depths (in °C) in the eastern Gotland Basin (BY15): (a) observations, (b) improved k model (run 414), (c) $k-\varepsilon$ model with Eq.54 and with $\sigma_\varepsilon = 10$ (run 426b). Only the upper 60 m are shown.*

The results of the two turbulence models are almost identical. The depth of the seasonal thermocline is somewhat shallower and deepwater salinities are slightly higher utilizing the $k-\varepsilon$ model compared to the k model. The reason for this discrepancy is that in the $k-\varepsilon$ model the vertical diffusion of dissipation cannot be neglected completely due to numerical reasons. In addition, mathematical differences of the formulations may cause performance differences.

It is believed that the diffusion of turbulent kinetic energy is an important process within the surface mixed layer (e.g. [4], [69]). However, it is still unclear if a transport equation or a length scale formulation should be applied to calculate dissipation (cf. discussion by [71]).

4 Initial conditions

Initial fields for temperature and salinity are generated for 14 basins. The borders have been chosen according to topographic features. The hydrography of each sub-basin is assumed to be homogeneous. Profiles from the Marine Data Centre of the International Council for the

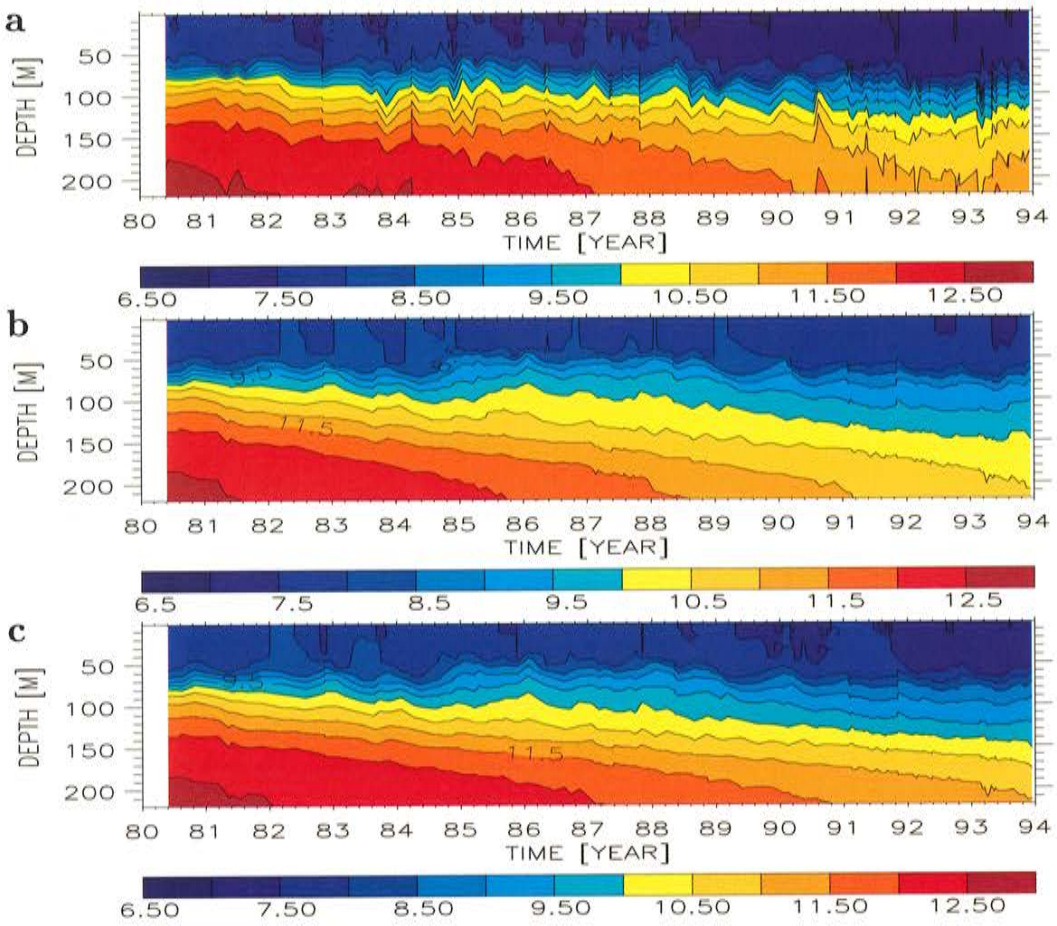

Figure 4: *Isohaline depths (in psu) in the eastern Gotland Basin (BY15): (a) observations, (b) improved k model (run 414), (c) $k-\varepsilon$ model with Eq.54 and with $\sigma_\varepsilon = 10$ (run 426b).*

Exploration of the Sea (ICES) have been selected to compile initial conditions for November 1, 1902. Initial sea level and current velocities have been set to zero.

5 Atmospheric forcing

5.1 Reconstructed surface variables

Whereas 100-year long records of river runoff and sea level data in the Kattegat are available, an observational data set of atmospheric surface fields applicable to force a coupled ice-ocean model of the Baltic Sea is missing. High resolutions in space and time are required. Therefore, we developed a statistical model using a *Redundancy Analysis* to reconstruct daily sea level pressure and monthly surface air and dew-point temperature, precipitation, and cloud cover fields on a $1^\circ \times 1^\circ$ regular horizontal grid for the Baltic Sea region [51]. A gridded atmospheric data set based on synoptic stations, which is available for the period 1970-1998, is used as input to the statistical model. The predictor fields are depending on the predictand variables: 100-years of sea level pressure at 18 locations, 100-years of sea-surface air temperature on a $5^\circ \times 5^\circ$ regular horizontal grid, and 100-years of precipitation on a $2.5^\circ \times 3.75^\circ$ regular grid.

Spatial patterns are selected by maximizing predictand variance during the 'learning' period 1980-1998. The remainder period 1970-1979 is used for validation. The statistical model works reasonable well for all variables. We found the highest skill for sea level pressure and the lowest skill for cloud cover. For details, the reader is referred to [51].

5.2 Wind speed

In a first approach (run 373b), the same bulk formulae as used earlier by [72] have been applied. Wind speeds in $10\,m$ height ($\vec{U}_{10}$) are calculated according to [12]:

$$\left|\vec{U}_{10}\right| = a_{red} \left|\vec{G}\right| \tag{56}$$

and

$$\cos\,\alpha = \frac{\vec{U}_{10} \cdot \vec{G}}{\left|\vec{U}_{10}\right| \left|\vec{G}\right|} \tag{57}$$

with the geostrophic wind speed $\vec{G}$, the reduction coefficient $a_{red} = 0.5 \ldots 0.6$, which is a function of the distance to the coast, and the ageostrophic angle $\alpha = 17°$ [11]. As the reconstruction of the sea level pressure is based on daily mean values instead of 3-hourly values available from the SMHI database, the wind speeds in $10\,m$ height are too smooth in time. Therefore, simulated mixed layer depths are too shallow compared with observations (see Section 8). However, it is impossible to increase just the vertical sea surface flux of turbulent kinetic energy (e.g., the coefficient m in Equation (25)) to enhance the mixing because in the turbulence enhanced surface layer the divergence of the turbulent kinetic energy flux balances dissipation (22). Turbulence generated below this layer is mainly produced via the vertical velocity shear of inertial waves and near-inertial currents. Therefore, the wind speed parameterization has been improved to simulate realistic mixed layer depths.

In Figure 5, the relative frequency of simulated and observed wind speed at Landsort is shown. At the station Landsort, a long record of observations is available which is assumed to represent sea wind with almost no disturbance (Hans Alexandersson SMHI, 2002, pers. comm.). Daily mean wind speeds smaller than $4\,m/s$ and larger than $11\,m/s$ are less frequent than observations sampled every three hours. Even a 3-hourly resolution may cause an underestimation of the energy flux to inertial motions by 20 % as shown by [23]. The frequency distribution of reconstructed wind speeds using a reduction coefficient of $a_{red} = 0.6$ (over sea) is significantly shifted to lower wind speeds with a maximum at $4\,m/s$ instead of a maximum at $6\,m/s$ in case of daily mean observations. Using $a_{red} = 0.78$ (run 403), the simulated frequency distribution is more realistic, especially for wind speeds larger than $17\,m/s$. As the flux of energy from the wind into inertial motions is proportional to U_{10}^4 [23], only the tail of the distribution for high wind speeds is important for mixing. A few storm events in autumn or winter may deliver all the energy necessary to generate the observed depth of the well mixed surface layer.

In a third approach (run 394), a random wind component with an amplitude of $6\,m/s$ has been added. This spatially homogeneous wind component rotates anti-clockwise with a period of 12 hours. In addition, wind direction changes instantaneously every 12 hours randomly. The frequency distribution is shown on the right panel of Figure 5. At least, the agreement with the daily mean observations for wind speeds larger than $11\,m/s$ is perfect.

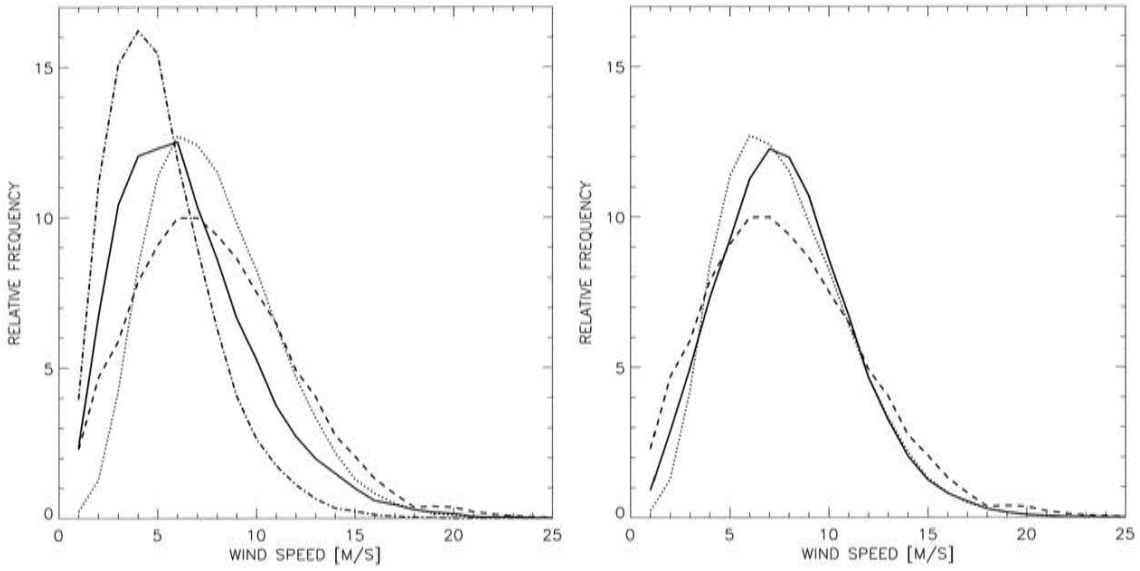

Figure 5: *Left: Relative frequency of wind speed at Landsort 1961-2001 based on 3-hourly observations (dashed) and based on 1-day running mean values (dotted), daily reconstructed wind with* $a_{red} = 0.6$ *(dashed-dotted) and with* $a_{red} = 0.78$ *(solid). Right: The same dashed and dotted curves as on the left. In addition, the relative frequency of the reconstructed wind speed at Landsort with an additional random wind component with an amplitude of* $6\,m/s$ *is shown (solid).*

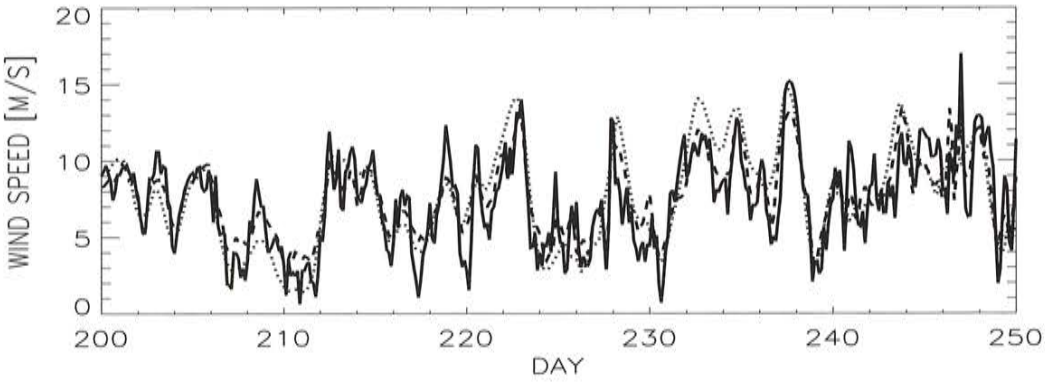

Figure 6: *Assembled time record of wind speed at Östergarnsholm in days with observations after June 1, 1995 (solid), wind parameterization according to Omstedt and Axell (submitted manuscript, 2002) (dashed), 1-day running mean geostrophic wind speed (SMHI database) with* $a_{red} = 0.78$ *(dotted).*

Wind data from Östergarnsholm [105] have been used for validation (Fig.6). Östergarnsholm is a small and very flat island $4\,km$ east of Gotland. Observations of $10\,m$ wind speed casted between June 1995 and December 1998 are available. However, the time record has many missing values. In Figures 6 and 7 (right panel), the wind parameterization using $a_{red} = 0.78$ and the wind parameterization presented by Omstedt and Axell (Modeling the variations of salinity and temperature in the large gulfs of the Baltic Sea, submitted to Continental Shelf Research, 2002, hereinafter referred to as Omstedt and Axell, submitted manuscript, 2002)

have been compared with observations. Omstedt and Axell (submitted manuscript, 2002)

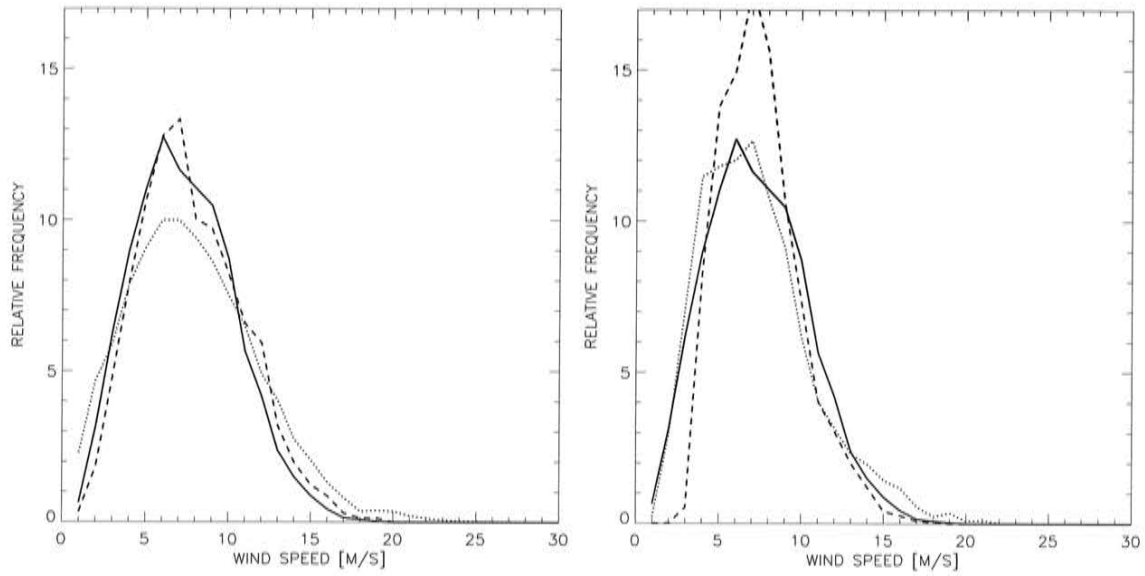

Figure 7: *Left: Relative frequency of 3-hourly observed wind speed calculated at Östergarnsholm 1995-1998 (solid), at Landsort 1961-2001 (dotted), and at Landsort 1996-1998 (dashed). Right: Relative frequency of wind speed at Östergarnsholm: 3-hourly observations 1995-1998 (solid), wind parameterization according to Omstedt and Axell (submitted manuscript, 2002) (dashed), 1-day running mean geostrophic wind speed (SMHI database) with* $a_{red} = 0.78$ *(dotted).*

optimized the following relationship:

$$U_{10} = c_5 + c_6\, G + c_7\, \Delta T + c_8\, G\, \Delta T\,. \tag{58}$$

G is the geostrophic wind speed of the SMHI database, and ΔT is the temperature difference between corrected air temperature (T_a) and sea surface temperature (T_s):

$$\Delta T = T_a - T_s\,. \tag{59}$$

The turning angle in the reduction to $10\,m$ wind is neglected by Omstedt and Axell (submitted manuscript, 2002). To correct for the land influence, the air temperatures given in the SMHI database were corrected according to

$$T_a = c_1 + c_2\, T_{db} + c_3\, T_s + c_4\, T_{db}\, T_s \tag{60}$$

where T_{db} is the temperature given in the SMHI database. The optimization resulted in $c_1 = -0.398$, $c_2 = 0.676$, $c_3 = 0.396$, $c_4 = -0.00380$, $c_5 = 2.56$, $c_6 = 0.489$, $c_7 = -0.0870$, $c_8 = -0.0138$ (in SI units) [1]. The rms error of the wind parameterization by Omstedt and Axell (submitted manuscript, 2002) is $1.74\,m/s$ compared with $2.32\,m/s$ using the constant reduction $a_{red} = 0.78$. In general, the problem of this approach is illustrated in Figure 7. During the period 1995-1998, wind speeds higher than $11\,m/s$ are less frequent at station Östergarnsholm compared to Landsort which might indicate that Östergarnsholm is more

[1] The calculated surface wind speeds used in Baltic Sea simulations by Omstedt and Axell (submitted manuscript, 2002) are multiplied additionally with a factor of 0.75 (Lars Axell SMHI, 2002, pers. comm.).

land influenced than Landsort. Östergarnsholm is located at a distance of 4 km from Gotland, i.e. the wind might be influenced by the land effect [12]. Thus, the optimization using only one land station may cause a bias. In addition, calculated wind speeds higher than 9 m/s (using Eqs.(58) and (60)) are less frequent than observed (Fig.7, right panel) causing underestimated mixing in the ocean model. Although the parameterized wind speed by Omstedt and Axell (submitted manuscript, 2002) is perfect with respect to the rms error, the frequency distribution shows a bias towards wind speeds in the range between 4 m/s and 9 m/s. Therefore, we suggest for climate applications, when mixing gets important, a statistical approach using an additional random wind component. Unfortunately, only few wind observations over sea are available to optimize such a random wind component. In Section 8, model results of the three approaches for the surface wind parameterization (run 373b, 394, and 403) will be compared and validated against observations.

6 Freshwater forcing

6.1 River runoff

The mean annual river discharge to the Baltic Sea amounts to 15,310 m^3/s for the period 1950-1990 [9]. The river flow is highly variable through the year and there are large inter-annual variations. The lowest (11,132 m^3/s in 1976) and highest (18,660 m^3/s in 1981) annual values differ from the mean value by -27% and $+22\%$, respectively. In addition, surface freshwater fluxes (i.e., precipitation minus evaporation) have to be considered. For the period 1981-1994, [84] calculated the total mean atmospheric freshwater inflow to be 1,986 m^3/s. The inter-annual variability is large as well, with values ranging from 502 m^3/s (in 1983) to 4,069 m^3/s (in 1987).

In RCO, the 29 most important rivers are considered. For them, monthly mean discharges for the period 1902-1998 have been calculated from three data sources:

- River runoff data for the period 1950-1998 from the Baltic Sea Experiment Hydrological Data Centre (BHDC) at SMHI. The monthly data do not only represent the inflow by major rivers, but the runoff through coastal segments including estimated smaller runoff ways [9].
- Basin river discharge for the period 1921-1975 by [81]. 17 rivers representative for the selected drainage areas are considered.
- Total discharge into the Baltic Sea for the period 1901-1990 calculated by [22]. [22] supplemented and corrected historical hydrometric results from 17 rivers for the period 1901-1920.

Firstly, climatological mean ratios between runoff of the selected 29 rivers and the corresponding sub-basin discharges are calculated for the period 1950-1998 using the data by [9]. In addition, the ratios between individual river runoff and the whole Baltic Sea discharge are calculated. Secondly, monthly sub-basin discharges are calculated for the period 1921-1998 and missing values have been replaced by results of the HBV model, a large-scale hydrological model by [33]. This homogeneous data set is published by [40]. Finally, monthly river discharges for the period 1902-1998 are reconstructed utilizing either monthly basin discharges for the period 1902-1920 or monthly sub-basin discharges for the period 1921-1998. The available higher spatial resolution for most of the period 1950-1998 has not been utilized for homogeneity reasons. The results are shown in Figure 8. The total mean river runoff for the

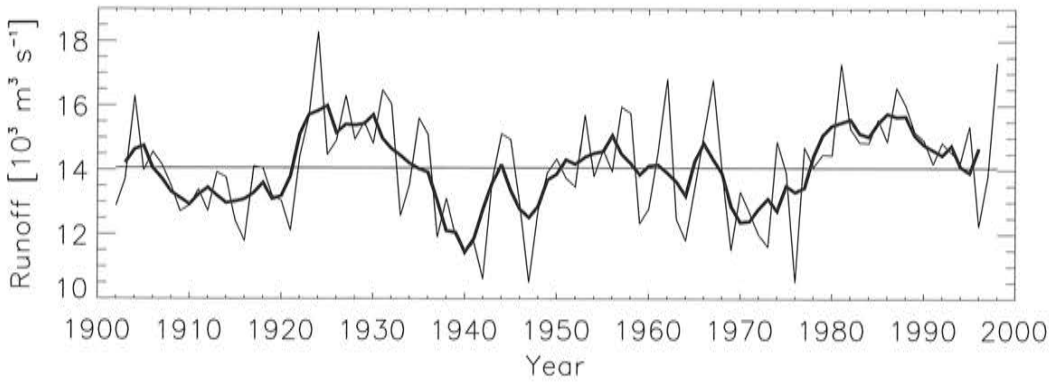

Figure 8: *Annual mean river runoff (in $m^3\,s^{-1}$) to the Baltic Sea without Kattegat (thin line). In addition, the 4-year running mean (thick line) and the total mean for the period 1902-1998 (horizontal line) are shown.*

period 1902-1998 amounts to $14,085\,m^3\,s^{-1}$. As mentioned by [22], there is no significant trend in the annual mean runoff.

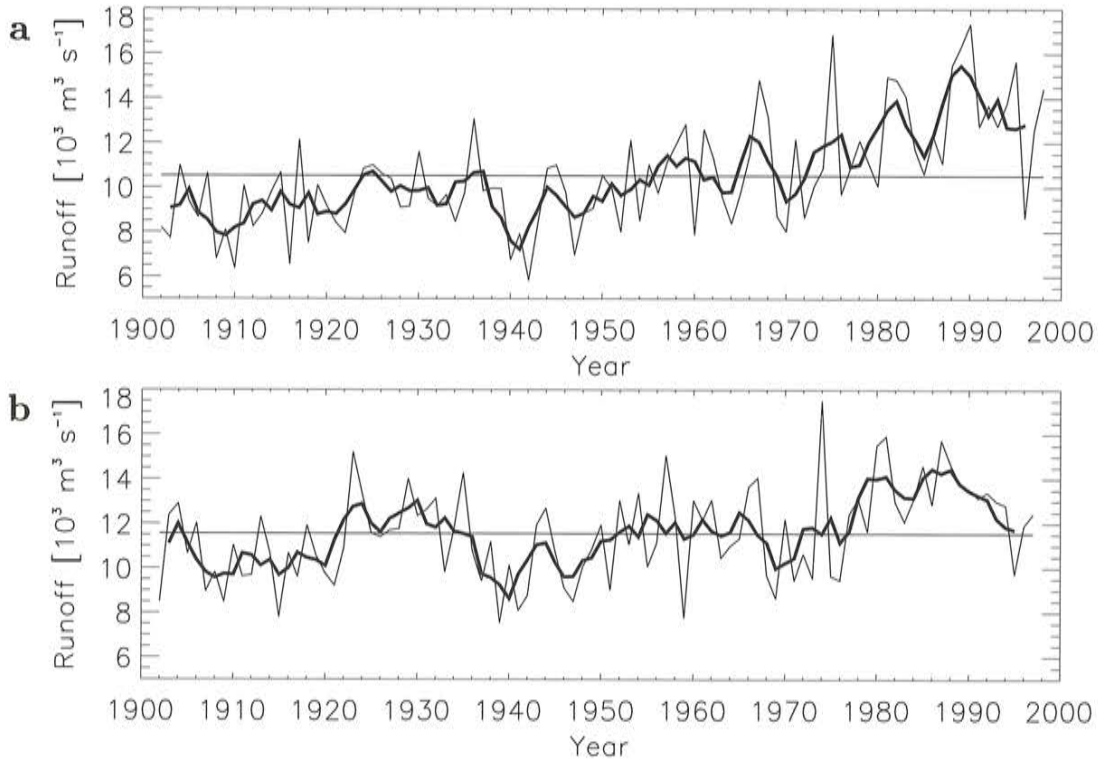

Figure 9: *Annual winter mean river runoff (in $m^3\,s^{-1}$) to the Baltic Sea without Kattegat (thin line): (a) January-February-March, (b) September to March (cf. [66]). In addition, the 4-year running mean (thick line) and the total mean for the period 1902-1998 (horizontal line) are shown.*

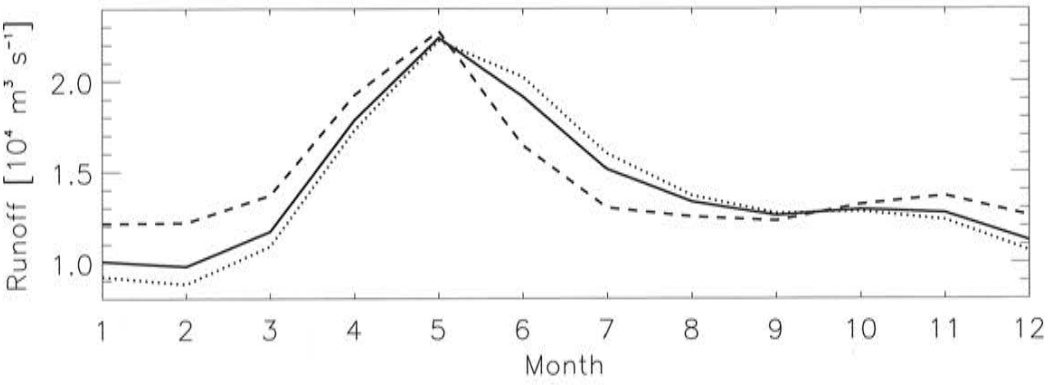

Figure 10: *Climatological monthly mean river runoff (in $m^3\,s^{-1}$) to the Baltic Sea without Kattegat for the period: 1902-1998 (solid line), 1902-1970 (dotted line), 1971-1998 (dashed line).*

Period	Jan	Feb	Mar	Apr	May	Jun	Jul	Aug	Sep	Oct	Nov	Dec
1902-98	1.01	0.98	1.17	1.79	2.24	1.91	1.51	1.33	1.26	1.29	1.27	1.12
1902-70	0.92	0.88	1.09	1.73	2.22	2.02	1.60	1.37	1.27	1.28	1.23	1.06
1971-98	1.22	1.22	1.37	1.93	2.28	1.65	1.30	1.25	1.23	1.32	1.37	1.26
change	32	39	26	11	2	-19	-19	-8	-3	3	11	18

Table 3: *Monthly mean river runoff (in $10^4\,m^3\,s^{-1}$) to the Baltic Sea without Kattegat for the periods 1902-1998, 1902-1970, and 1971-1998. In the last row the relative changes (in %) between 1902-1970 and 1971-1998 are given.*

However, the seasonal cycle has changed during the past century (Figs.9 and 10, Tab.3). Especially, the winter mean runoff for January-February-March has increased significantly since the 1970s. Correspondingly, summer mean runoff for June-July-August has decreased. It is believed that this change in the seasonality of river runoff is caused mainly by river regulation (see discussion below). The construction of dams in Sweden and Finland became conspicuous since the 1970s. In comparison with the period 1902-1970, the spring (March-May) outflow of the period 1971-1998 has increased by 13 %, the summer (June-August) outflow has decreased by 15 %, and the winter (December-February) outflow has risen by 30 %. In autumn (September-November) the change is only small (+4 %). These results are in accordance with [22]. [22] calculated the quarterly trends during 1901-1990 and found significant figures for spring (+13 %), summer (−28 %) and winter (+30 %), while the figures for autumn and the entire year remained practically unaltered.

The observed changes of the seasonal cycle of the total runoff (Fig.10) cannot completely be explained by river regulation. This is the conclusion from the analysis of trends calculated for the period 1921-2000 from discharge data of 20 smaller catchment areas without regulation [59]. In northern Sweden, an increased spring flood (May-June) is found for 1971-2000 compared to 1941-1970. In southern Sweden, increased winter runoff (December-March) and decreased summer runoff (August-September) are observed. The latter trend may contribute to the overall trend found for all regulated and unregulated rivers of the Baltic catchment area. However, further investigations are still necessary.

6.2 Precipitation

The precipitation over the Baltic Sea (without Kattegat) is correlated with river runoff (Fig.11). The linear correlation between the annual mean precipitation over the Baltic Sea

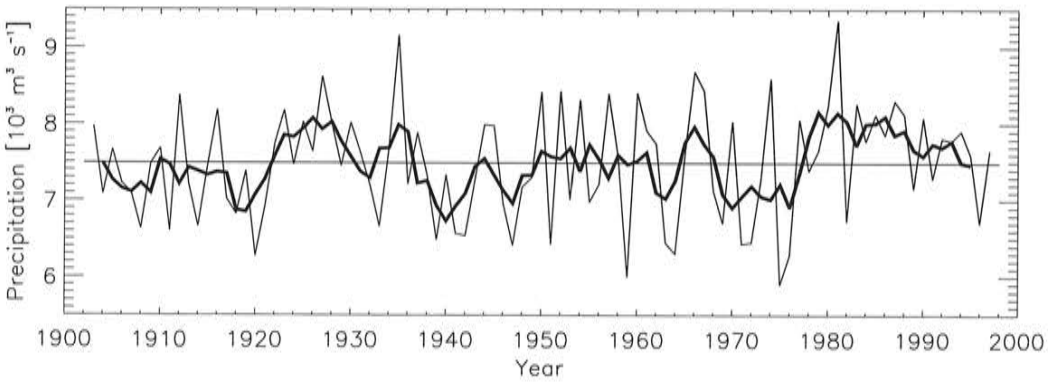

Figure 11: *Annual mean precipitation (in* $10^3\, m^3\, s^{-1}$*) to the Baltic Sea without Kattegat (thin line). In addition, the 4-year running mean (thick line) and the total mean for the period 1902-1998 (horizontal line) are shown.*

and the annual mean runoff amounts to $r = 0.54$. The corresponding correlation based on 4-year annual mean values is 0.82. The total mean precipitation for the period 1902-1998 amounts to $7,490\, m^3\, s^{-1}$. Minimum and maximum annual mean precipitation are $5,901\, m^3\, s^{-1}$ (1975) and $9,358\, m^3\, s^{-1}$ (1981), respectively.

7 Open boundary conditions in the Kattegat

7.1 Sea level

At the open boundary in the Kattegat daily sea level data are prescribed. For the period 1902-01-01 to 1910-06-19 Swedish observations are available at Strömstad. For the period 1910-06-20 to 1999-12-31 we used observations at Smögen. Missing values have been replaced by linear interpolation. The linear trend due to land uplift are subtracted from the data according to [26], i.e. $1.99\, mm\, yr^{-1}$ for Smögen and $3.53\, mm\, yr^{-1}$ for Strömstad. In addition, the mean values of the time records have been subtracted and replaced by the values of the Nordic height system 1960 (NH60), a geodetic solution published by [27]. As the open boundary follows a line between Frederikshavn in Denmark and Ringhals in Sweden approximately, the mean sea levels in the model have been chosen to be $\bar{\zeta_F} = -11.1\, cm$ at Frederikshavn and $\bar{\zeta_R} = -1.4\, cm$ at Ringhals. Between these two locations the sea level at the open boundary is linear interpolated.

The sensitivity of the long-term simulations to the sea level forcing in Kattegat is investigated in Section 9. For comparison, the sea level observations have been replaced by an empirical relationship between the meridional atmospheric SLP difference across the North Sea and the sea level in Kattegat by [36]. [36] found for daily sea levels ζ at Hornbæk (Denmark):

$$\zeta = a\, w(t - \tau) + b \tag{61}$$

with the constants $a = 2.0\,cm\,hPa^{-1}$, $b = -4\,cm$, $\tau = 0.7\,days$, and with the south-north SLP difference $w(t-\tau)$ between deBilt (Netherlands) and Oksøy (Norway). [36] found that more than 70% of the sea level variance is explained by oscillations in the pressure difference for periods between 15 and 200 days. In the sensitivity experiment, we have replaced the calculated mean sea level at Hornbæk for the period 1902-1998 of $\bar{\zeta_H} = 1.5\,cm$ with the mean sea levels of the Nordic height system 1960 at Frederikshavn ($\bar{\zeta_F} = -11.1\,cm$) and Ringhals ($\bar{\zeta_R} = -1.4\,cm$), respectively. In NH60, the mean sea level at Hornbæk would be $\bar{\zeta_H} = -4.5\,cm$ [27]. A phase lag τ is not considered because the daily sampling does not include any information for periods less than one day.

7.2 Temperature and salinity profiles

In the area of the model boundary the Skagerrak-Kattegat front is located with rapid changes of its position on daily timescales [44]. Due to the lack of data resolving the northern Kattegat hydrography climatological mean temperature and salinity profiles from observations at the open sea monitoring station P2 in the northern Kattegat ($57°N\,52'$, $11°E\,18'$) are used as open boundary conditions. The sensitivity of the model interior to the salinity profiles used for the open boundary conditions has been investigated by [76].

8 Model validation

The results of three long simulations (run 373b, 403, and 394), hereinafter referred to as standard experiments, are compared and validated against observations for the period 1902-1998. In these experiments the improved k turbulence model (Section 3.5) and three different approaches for the surface wind parameterization (Section 5.2) have been utilized:

In run 373b, the same surface wind parameterization as used earlier for the geostrophic winds of the SMHI database for the period 1980-1993 is applied [12]. The reduction coefficient depends on the distance to the coast and varies between $a_{red} = 0.5$ (land) and $a_{red} = 0.6$ (open sea). The ageostrophic angles are constant (17°). The coefficient c_u of the improved k turbulence model has been adjusted to simulate deepwater salinity in the Gotland Basin realisticly ($c_u = 1.2$).

In run 403, the surface wind parameterization is revised to deepen the simulated halocline depth. The reduction coefficient in this experiment varies in the range of $a_{red} = 0.65$ (land) and $a_{red} = 0.78$ (open sea). The theoretically calculated value for $c_u = \sqrt{c_{\varepsilon 2}/c_{\varepsilon 1}} = 1.1547$ of the improved k model is used.

In run 394, a random wind component with an amplitude of $6\,m/s$ is added to the surface winds calculated from the reconstructed sea level pressure fields according to [12]. This spatially homogeneous wind component rotates anti-clockwise with a period of 12 hours (see Section 5.2). In this experiment, $c_u = 1.1547$ is used. Compared to earlier experiments performed with the standard $k-\varepsilon$ model by [71], deepwater mixing in run 373b and 394 is increased by 50 %, i.e. $\alpha' = 1.5\,\alpha = 0.75\,cm^2\,s^{-2}$ (Section 3.4).

An overview of the standard experiments is given in Appendix A (Tab.15).

8.1 Sea level

8.1.1 Landsort

The tide gauge at Landsort is located close to the nodal line of the first seiche of the system between the western Baltic and the Gulf of Finland. Thus, the sea level at Landsort measures mainly variations of the Baltic Sea volume with a period longer than 20 - 30 days rather than high-frequent sea surface gravity waves within the Baltic. Major saltwater inflows have a period of 20 days typically giving rise to significant volume variations. Thus, the agreement between observed and simulated sea levels with periods longer than 20 days indicates that those transports through the Danish Straits are simulated correctly which are relevant for major Baltic inflows (Fig.12). For the standard experiments, we found mean errors between -0.4 and $3.0\,cm$ and rms errors between 9.3 and $11.3\,cm$ (Tab.4).

RUN	ME (cm)	RMSE (cm)
373b	-0.4	9.3
403	3.0	11.3
394	1.3	10.2
411	3.2	12.0

Table 4: *Model errors of 2-daily sea levels at Landsort during the period 1902-1998 for different RCO experiments (see Appendix A, Tabs.15 and 16). (ME = mean error, $RMSE$ = root mean square error.)*

These errors are of the same magnitude as found by [77] for the period 1980 to 1993 using observed atmospheric forcing. Here, the best results are obtained using run 373b. Only slightly higher errors are obtained if the sea level observations of Strömstad and Smögen prescribed at the open boundary in Kattegat are replaced by the results of the empirical formula by [36] (see Equation (61), run 411). The role of the sea level boundary conditions is further discussed in Section 9.4.

The unfiltered sea level at Landsort is shown in Figure 13. Three 4-year periods are selected including the saltwater inflows in November/December 1951, December 1975/January 1976, and January 1993. In all three cases the simulated sea level is in good agreement with observations. For the events 1951 and 1993, the modeled sea level rise during the inflow phase is somewhat faster than observed.

10-year running mean sea levels of the three standard experiments are shown in Figure 14. There are two distinct maxima during the 1920s and during the second half of the 1980s to the 1990s and one distinct minimum during the second half of the 1930s to the first half of the 1940s. There seems to be a positive trend during the 1980s and 1990s. In all three experiments, we found the same decadal variability as in observations but the sea level in run 403 is constantly higher than observed. The mean error in run 403 is $3\,cm$ compared to only $-0.4\,cm$ in run 373b (Tab.4). The higher mean wind speed from south westerly direction causes an additional rise of the mean sea level in the entire Baltic Sea. In run 394 the first maximum during the 1920s is somewhat overestimated.

[47] have shown that the annual mean sea level of all Finnish tide gauges is correlated significantly with the NAO index. In addition, they found that the annual standard deviation of the sea level also correlates with the NAO, but the correlation is not statistically significant

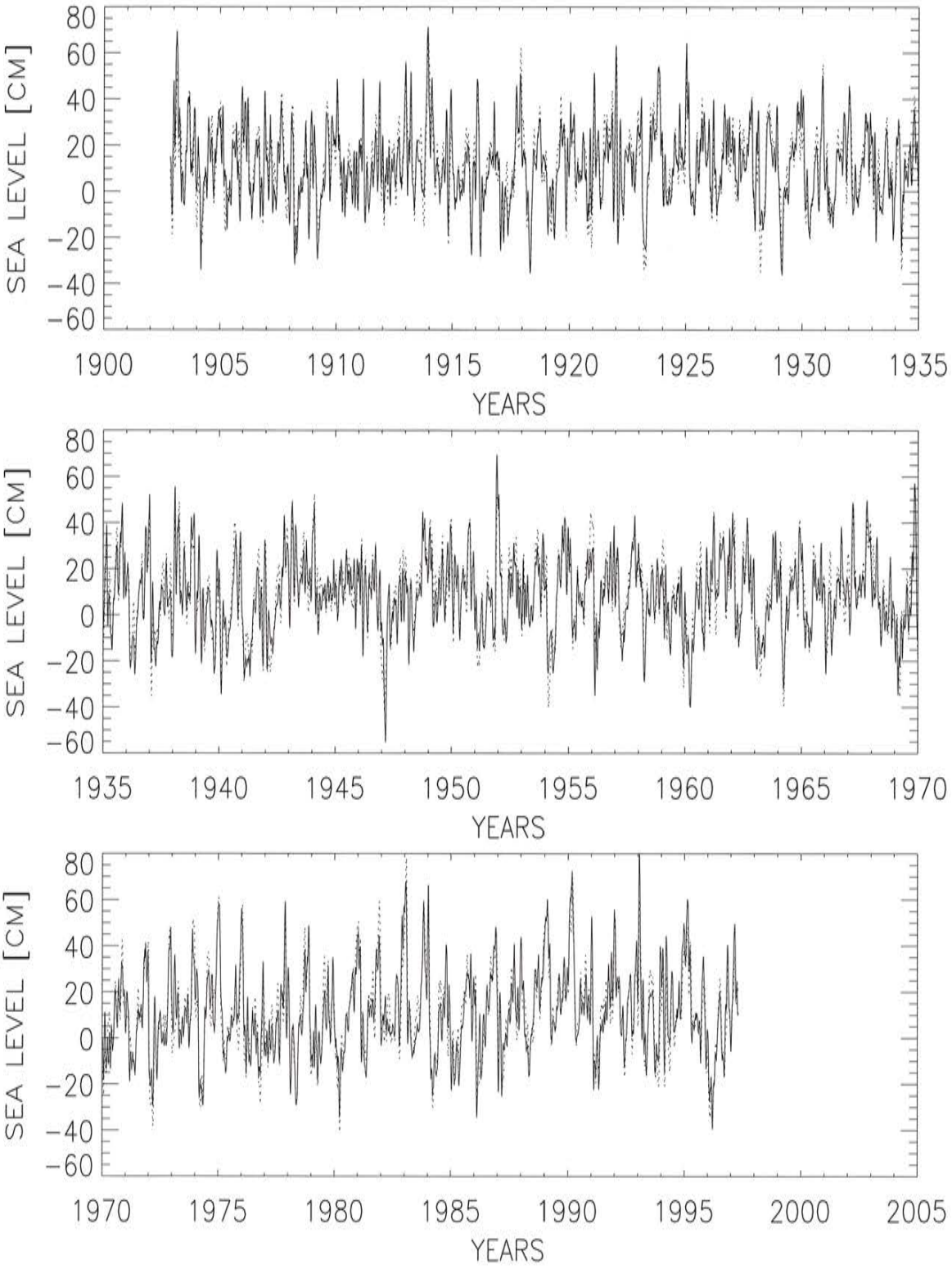

Figure 12: *20-day running mean sea level (in cm) at Landsort. Solid line: model results (run 373b). Dotted line: observations.*

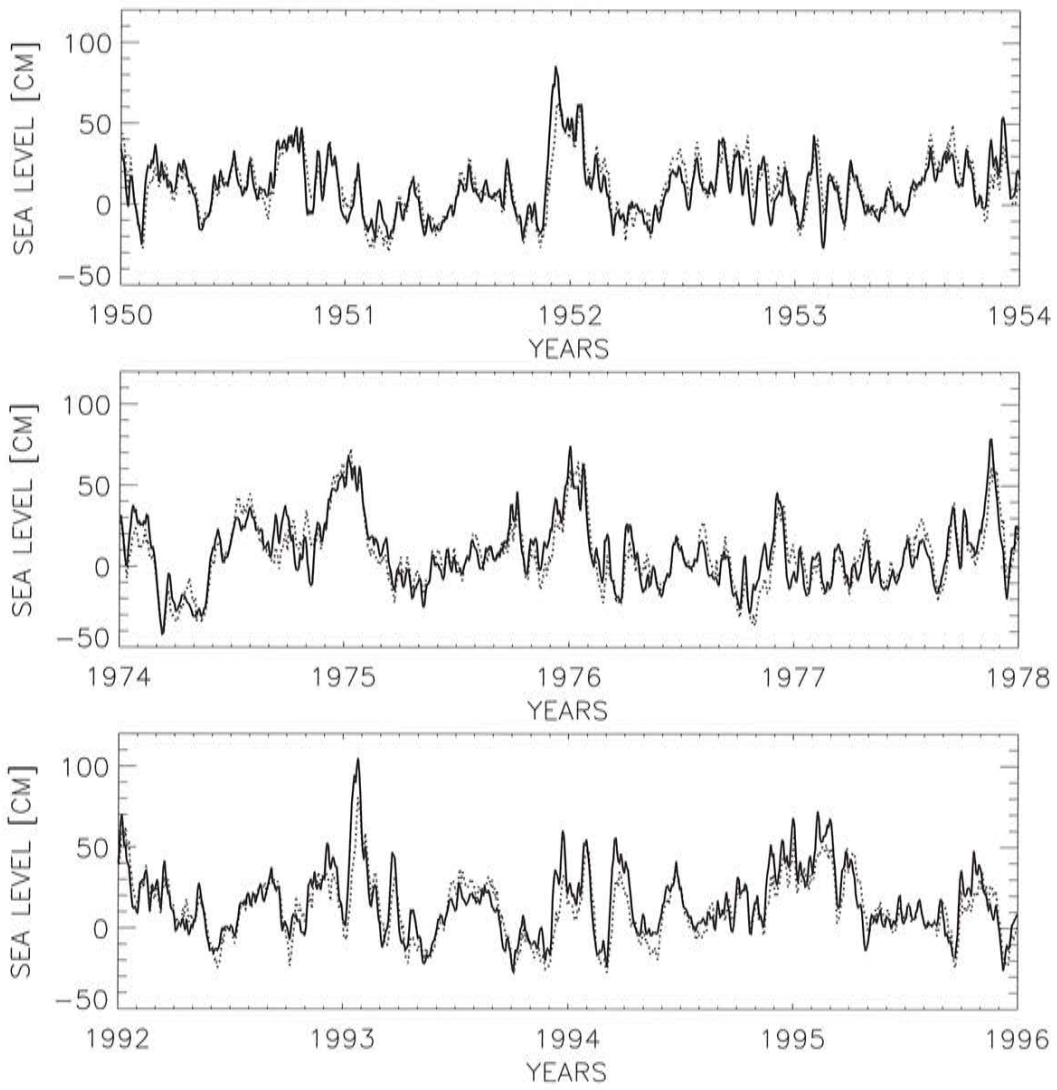

Figure 13: *2-daily sea level (in cm) at Landsort: run 373b (solid), data (dotted).*

in every basin. We found that the impact of the freshwater inflow on the sea surface height is very small (Section 9.2.6). Thus, we conclude that the decadal variability of the Landsort sea level is mainly determined by wind variations. The recent increase of storm frequency reported by [1] and [2] might contribute to the positive trend during the 1980s and 1990s.

8.1.2 Varberg/Ringhals

Observations of the tide gauges Strömstad and Smögen are prescribed at the open boundary in Kattegat (Section 7.1). The border is located close to the station Varberg/Ringhals. Thus, the mean sea level at this tide gauge is used for the forcing data. Hereinafter, the observations are referred to as data from Varberg/Ringhals.

The input sea level at Varberg/Ringhals in Kattegat is compared to the simulated output sea level at Landsort in the Baltic proper (Figs.15 and 16). The short-period variability

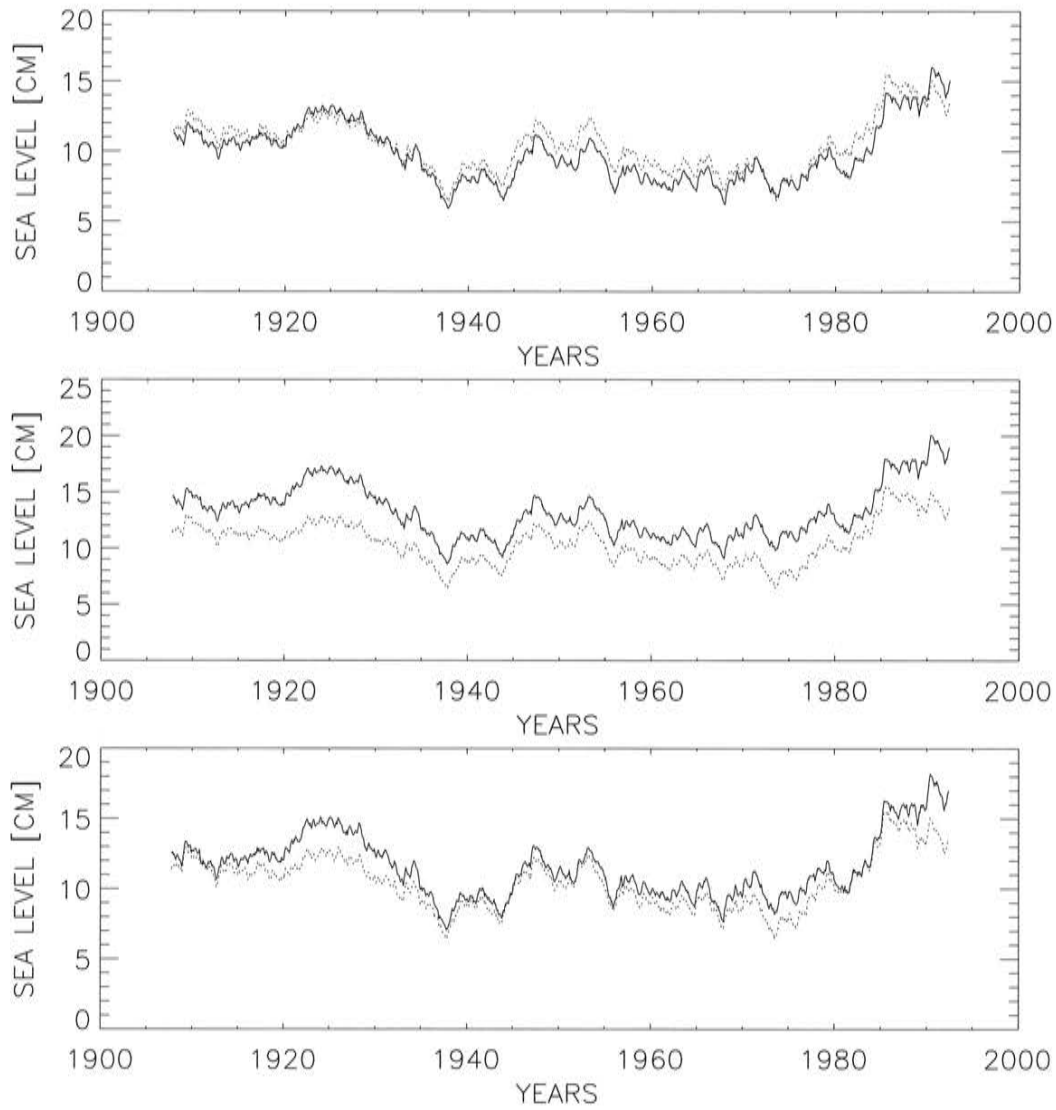

Figure 14: *10-year running mean sea level (in cm) at Landsort. Solid line: model results (upper: run 373b, middle: run 403, lower: run 394). Dotted line: observations.*

of the order of a few days is much higher in the Kattegat than at Landsort but the decadal variability is similar. The mean sea levels at Landsort and Varberg/Ringhals are $\bar{\zeta} = 10.2\,cm$ and $\bar{\zeta} = -1.4\,cm$, respectively. Thus, the difference between both stations of $11.6\,cm$ is close to the geodetic result of $12\,cm$ by [27]. In the Nordic height system 1960 (NH60), the mean sea levels at Landsort and Ringhals are $\bar{\zeta} = 10.6\,cm$ and $\bar{\zeta} = -1.4\,cm$, respectively. As shown by [96], the limited transport capacity of the Danish Straits causes a low-pass filtering of the external forcing provided by the Kattegat sea level with a cut-off period of about one month. The Baltic Sea acts either as an open bay/fjord or as a closed basin depending on the time scale considered. Within the Baltic Sea the variance of the sea level is increasing from south to north for periods longer than two weeks. For shorter periods the highest variance occurs at the extreme ends, in the Arkona Basin/western Baltic, in the Gulf of Finland, and in the Bay of Bothnia.

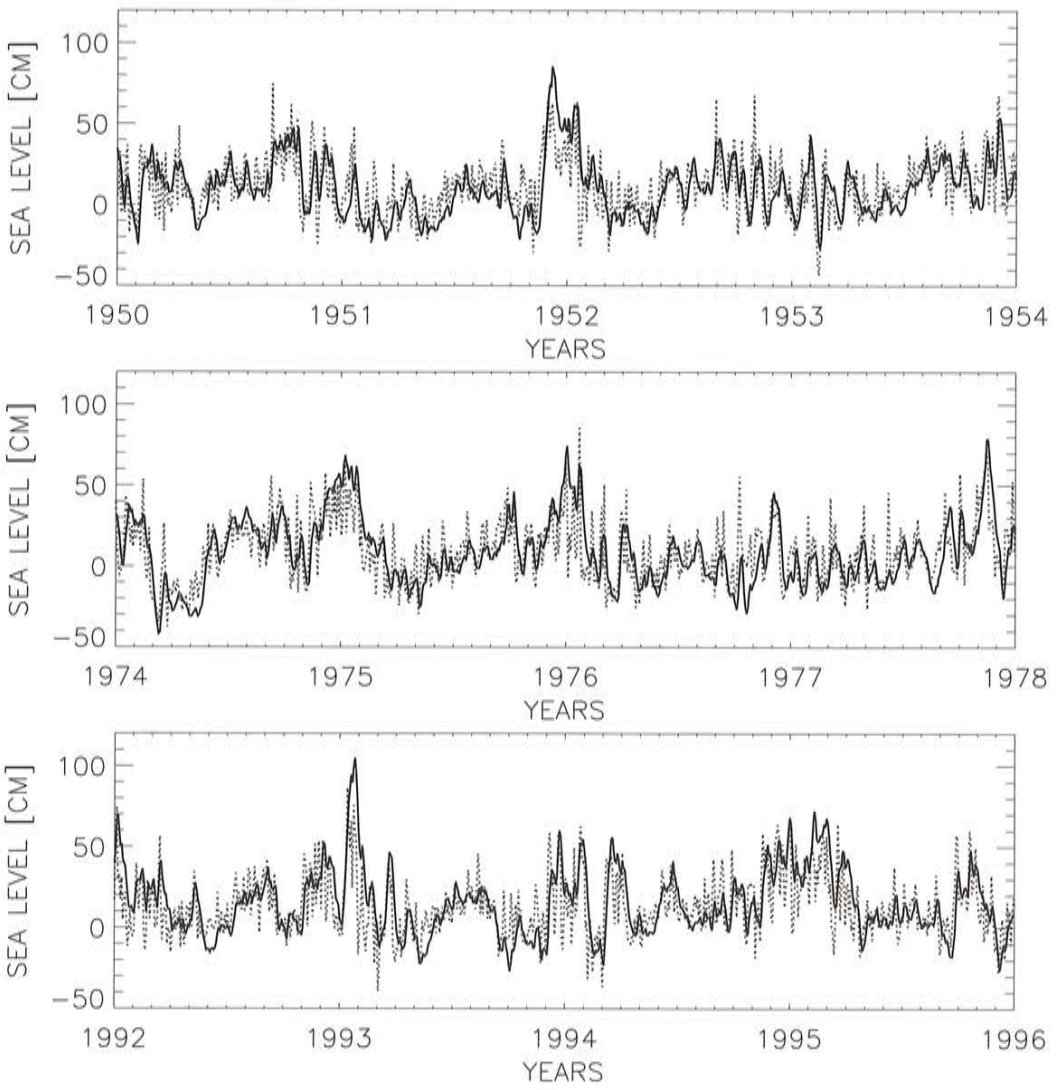

Figure 15: *2-daily sea level (in cm): run 373b at Landsort (solid), data at Varberg/Ringhals (dotted).*

8.2 Salinity profile in the eastern Gotland Basin

Figure 17 shows the time evolution of a vertical salinity profile in the eastern Gotland Basin (BY15, Gotland Deep) for the period 1902-1998. The three standard experiments and a sensitivity run with modified mixing parameterization are shown. In all experiments, the minima of lower layer salinity during the 1930s and during the 1990s and the pronounced maximum during the 1950s are simulated correctly. Even individual major saltwater inflows are reproduced well, e.g. the events during November/December 1951 and during January 1993. Especially, the agreement between model results from run 403 and observations is satisfactory (Fig.17d). The mean salinities in the depicted experiments differ significantly with lowest value in run 394 (Fig.17e) and highest value in run 375 (Fig.17c). The latter experiment is identical with the standard run 373b but $c_u = \sqrt{c_{\varepsilon 2}/c_{\varepsilon 1}}$ has been chosen. This experiment enables a comparison between different surface wind parameterizations using the same mixing parameterizations. Deepwater salinity differences between run 394 and run

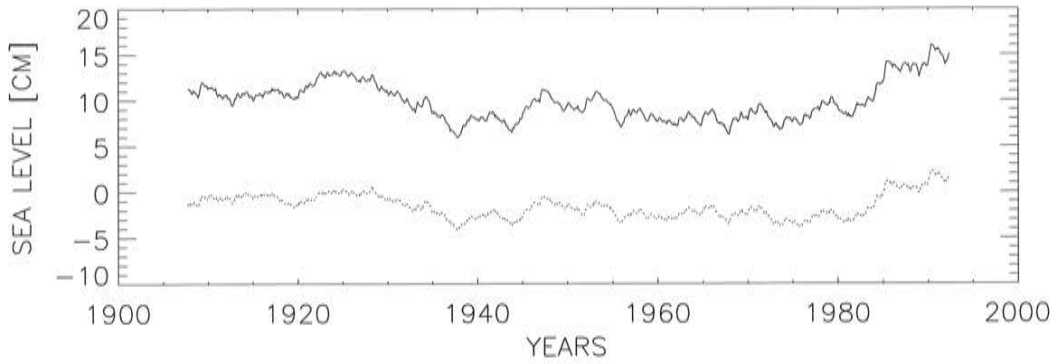

Figure 16: *10-year running mean sea levels (in cm): run 373b at Landsort (solid), data at Varberg/Ringhals (dotted).*

373b amount up to $1\,psu$ (Fig.18b). In both experiments with surface wind parameterization according to [12] (run 373b and run 375), the halocline depths are underestimated. We found improved results when using either constantly increased wind speeds (run 403) or an additional random wind component (run 394). Additional wind induced mixing improves the results quite much. The halocline is about $30\,m$ deeper in run 403 than in run 373b (Fig.18a). However, the halocline depth is still somewhat underestimated compared to observations. In all experiments decadal variations are smaller than observed. For example, in run 375 the salinity maximum of more than $13.5\,psu$ after the major inflow in November/December 1951 is simulated correctly but the salinity minima during the 1930s and during the 1990s are underestimated. In contrast, the simulated stagnation periods in run 403 are close to the observations but the maximum during the 1950s is underestimated by $1\,psu$ approximately. The large sensitivity of deepwater salinity in the Baltic Sea on the chosen mixing parameterization is discussed further in Section 9.1.

8.3 Saltwater inflows

8.3.1 Events during 1902-1998

The saltwater inflow into the Baltic Sea is mainly intermittent. The only effective mechanism renewing the central Baltic deepwater is the advective transport of large amounts of highly saline and oxygenated water from the Kattegat into the Baltic known as major Baltic inflows ([63], [29]). [30] employed the following empirical criteria to salinity observations at Darss Sill from the light vessel *L/V Gedser Rev* to identify the events

$$S_0/S_b \geq 0.8 \quad \text{and} \quad S_b \geq 17\,psu \tag{62}$$

with the surface salinity S_0 and the bottom salinity S_b. 96 major events have been detected during the period from 1897 to 1995 excluding the two world wars ([30], [63]). The intensity of major inflows were estimated using a relative intensity index

$$Q = 50\left(\frac{k_{GR}-5}{25} + \frac{S_{GR}-17}{7}\right) \tag{63}$$

with the duration k_{GR} in days and with the mean salinity $S_{GR} \geq 17\,psu$ at the Darss Sill. To assess the role of the Öresund for major inflows, [29] investigated additionally observations at the Drogden Sill from the light vessel *L/V Drogden*. They calculated the re-assessed

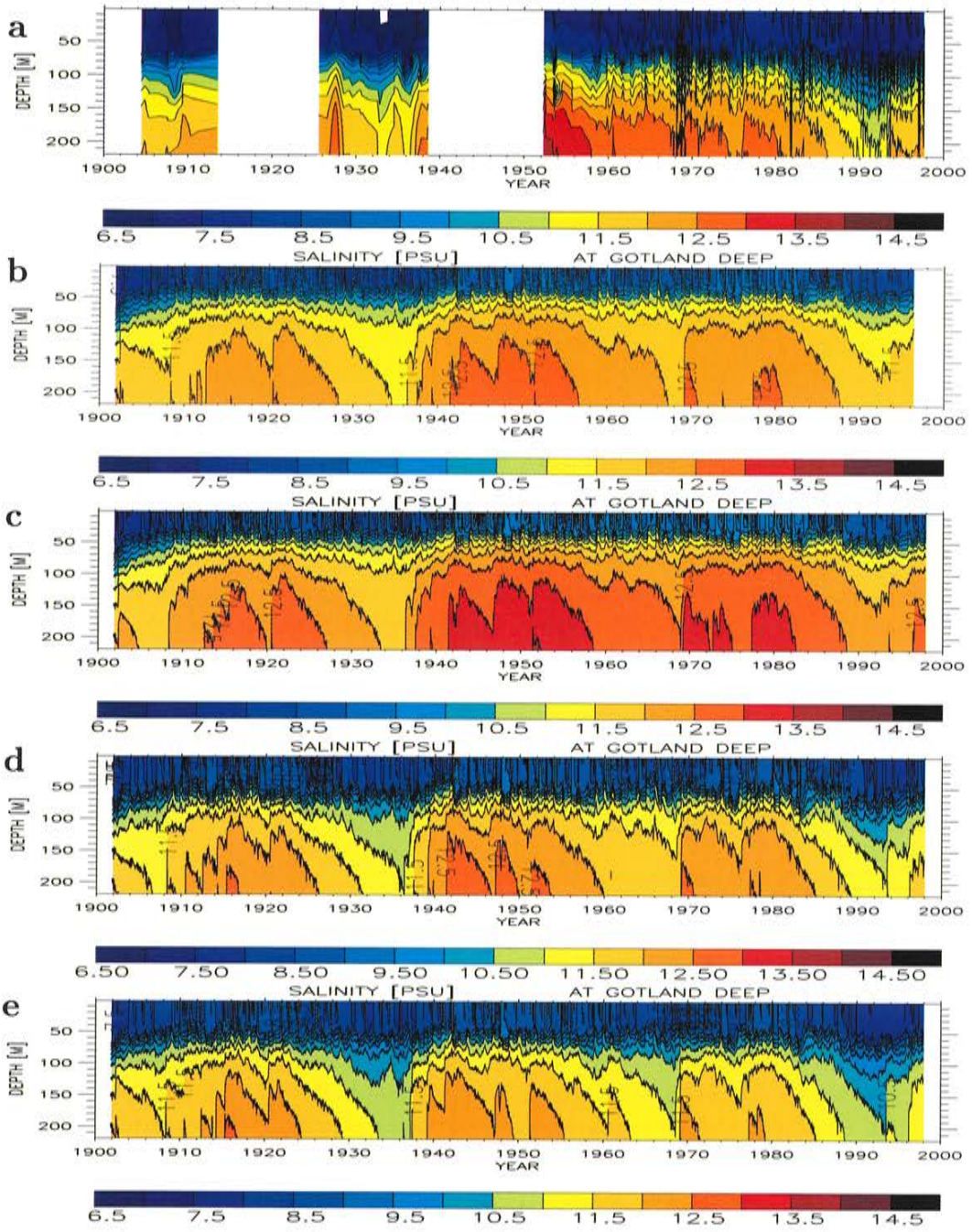

Figure 17: *Isohaline depths (in psu) in the eastern Gotland Basin (BY15): (a) observations, (b) standard experiment with* $c_u = 1.2$, $\alpha = 0.75 \cdot 10^{-3}\, cm^2\, s^{-2}$ *(run 373b), (c) modified k model with* $c_u = \sqrt{c_{\varepsilon 2}/c_{\varepsilon 1}}$, $\alpha = 0.75 \cdot 10^{-3}\, cm^2\, s^{-2}$ *(run 375), (d) as (c) but modified wind reduction with* $a_{red} = 0.78$ *and modified deepwater mixing with* $\alpha = 0.5 \cdot 10^{-3}\, cm^2\, s^{-2}$ *(run 403), (e) as (c) but additional random wind component (run 394). Observations are not available for periods covering the world wars.*

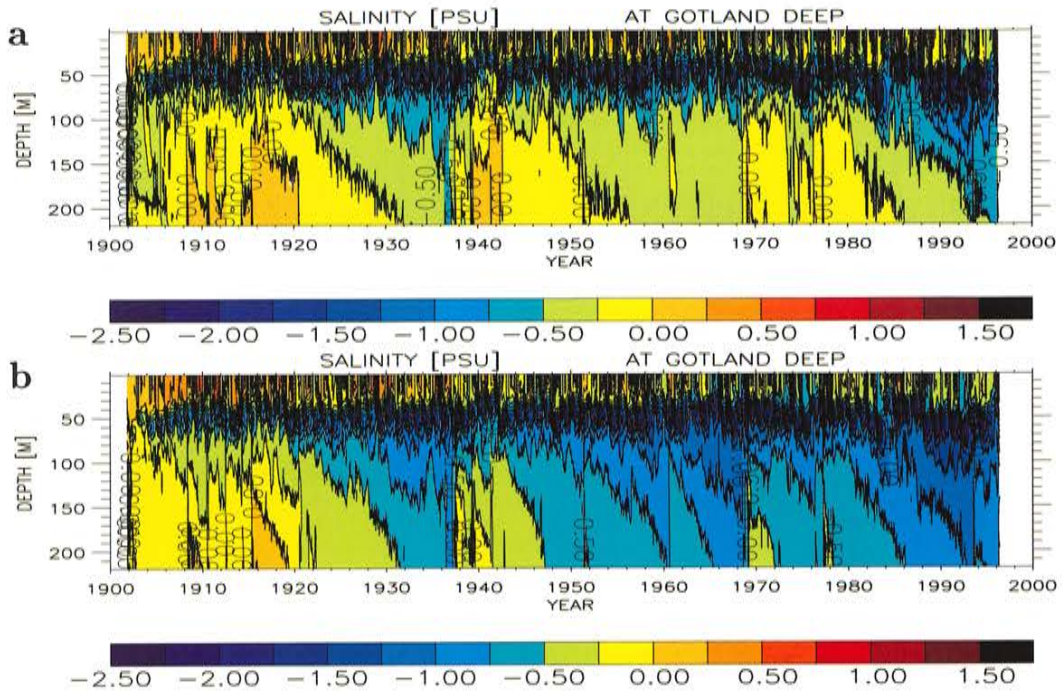

Figure 18: *Isohaline depths (in psu) in the eastern Gotland Basin (BY15): (a) difference between Fig.17d and Fig.17b (run 403 minus run 373b), (b) difference between Fig.17e and Fig.17b (run 394 minus run 373b)*

total intensity of a major inflow (Q_T) from the amount of salt transported across both sills in water bodies with $S \geq 17psu$ (M_{17}) divided by $10^{11}\,kg$. The criteria of Equation (62) and a corresponding criterium for Drogden Sill are still applied to identify saltwater inflows. [29] documented the different contributions of the two passages, Belt Sea and Öresund, on the basis of 90 events that took place between 1897 and 1976. This dataset is used here to validate simulated saltwater inflows.

Due to the coarse horizontal resolution of the model, the topography of the Danish Straits, especially of the Öresund, is not well represented. Thus, a correct ratio of simulated salt transports is not expected although the results of the high-resolution version of RCO using a grid distance of *2 nautical miles* have been proven to be quite accurate [77]. A definition of major inflows in RCO using a criterium at one or both sills like in [29] would not be very useful. Therefore, we have defined an event to be a major inflow if the simulated volume of high saline water with $S \geq 17\,psu$ (V_{17}) in the Arkona Basin is higher than $50\,km^3$ during at least 6 consecutive days. This definition should approximately correspond to the criteria in (62). 6 instead of 5 days are used because model snapshots are sampled only every second day. The limit of $50\,km^3$ of water with $S \geq 17psu$ has also been used by [36].

The volumes of high saline water as a function of time for the different sub-basins are shown in Figures 19 and 20. As the salinity of the inflowing water decreases on its path from the sills into the Baltic proper due to entrainment, the salinity in the eastern Gotland Basin is never higher than $14\,psu$. Therefore, the high saline water body is defined by $S \geq 12\,psu$. The depicted results indicate the high non-linearity of the system. A large inflow of high saline water into the Arkona Basin does not necessarily mean a corresponding large saltwater

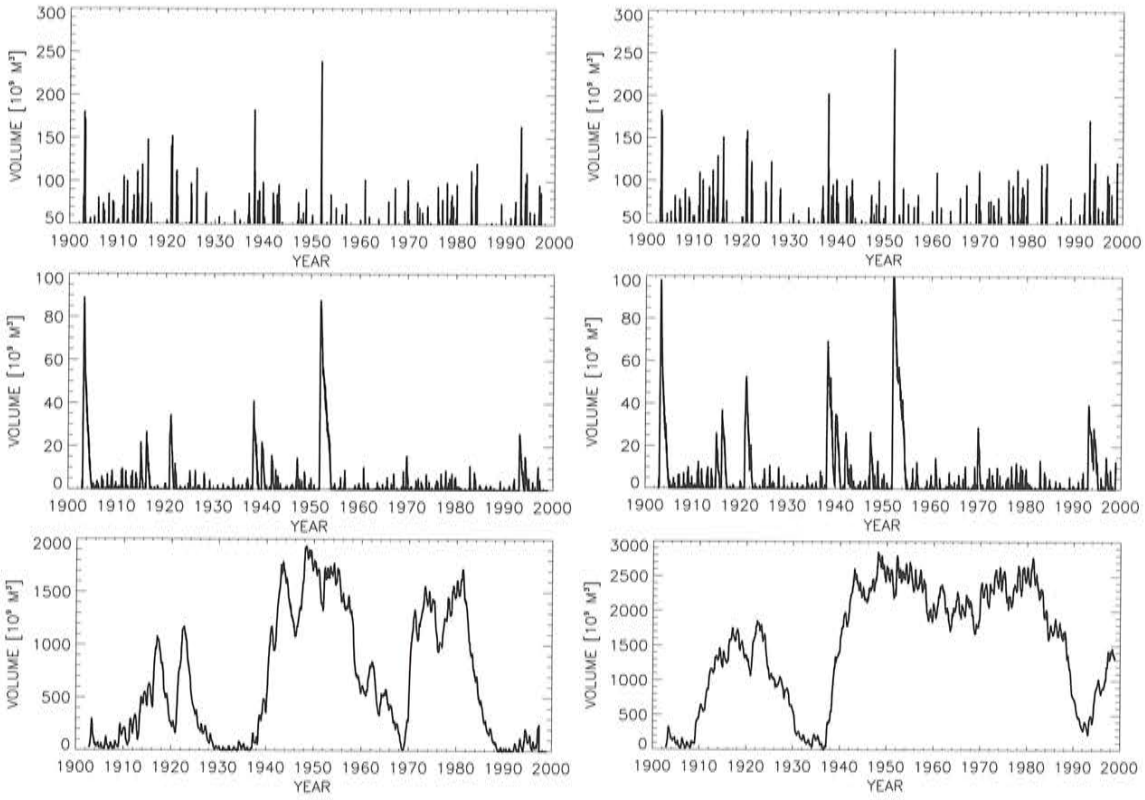

Figure 19: *Volume (in km^3) of high saline water in (upper panels) Arkona Basin ($S \geq 17\,psu$), (middle panels) Bornholm Basin ($S \geq 17\,psu$), and (lower panels) Gotland Basin ($S \geq 12\,psu$). The model results are from run 373b (left) and from run 375 (right).*

inflow into the Gotland Basin. Entrainment, diapycnical mixing and water storage in deep upstream basins are important processes changing the water mass on its pathways. We found the largest saltwater inflows into Arkona Basin in run 403 but the highest saltwater amount in Gotland Basin in run 373b. Increased mixing due to an additional random wind component in run 394 results in somewhat increased saltwater inflows into Arkona Basin and in a decreased amount of saltwater in the Gotland Basin compared to run 375. (Figs.19 and 20).

Observed and simulated saltflows into the Arkona Basin are shown in Figure 21. As observations are not available for periods covering the world wars, the number of observed inflows is certainly underestimated by at least 20 % (Tab.5).

Thus, the basic characteristics of simulated major Baltic inflows in run 373b are quite close to the observations. Even the time records show similarities (Fig.21). Only the mean salt amount is somewhat overestimated by 19 % (Tab.5). We found too many major Baltic inflows in run 403 with a too high mean salt amount. The results of run 394 are in between. However, it is difficult to draw any final conclusions for the correct saltwater flow into the Baltic. The number of observed inflows is very likely underestimated as observations are not available for periods covering the world wars and after 1976 (except the inflow event 1993). Even the amount of inflowing salt during an event might be underestimated by the observations. For example, [67] found with his regional high-resolution model of the western Baltic Sea that during the inflow phase in January 1993 $2.8 \times 10^{12}\,kg$ salt (all salinities) enters the

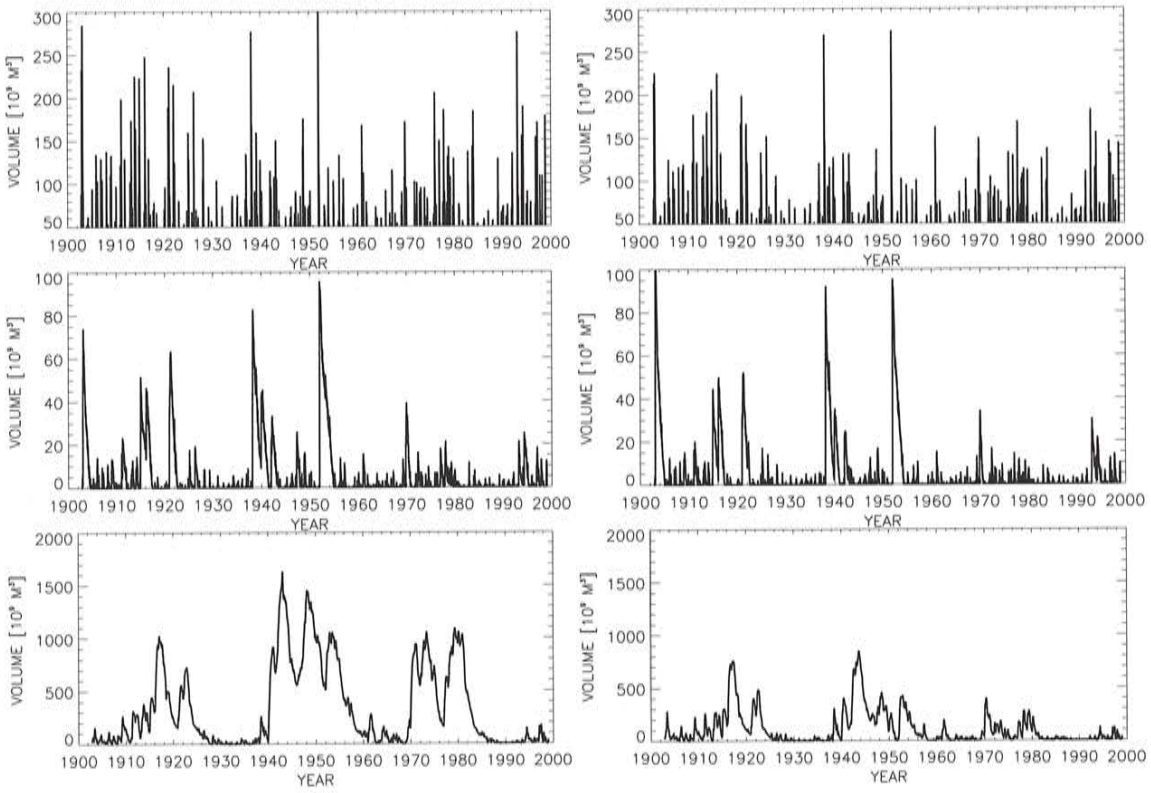

Figure 20: *As Fig.19 but for run 403 (left) and for run 394 (right).*

	Data	Model		
	[29]	Run 373b	Run 403	Run 394
Number of inflows	82[1]	99[3]	180	157
Mean volume ($\bar{V}_{17}$ in km^3)	81.1[2]	85.2[3]	105.0	97.7
Mean salt amount ($\bar{M}_{17}$ in $10^{12}\,kg$)	1.55[1]	1.85[3]	2.30	2.11

Table 5: *Basic characteristics of observed and simulated major Baltic inflows ($V_{17} \geq 50\,km^3$, $\geq 6\,days$). The comparison of model results and observations is slightly biased due to different periods considered. ([1]For the period November 1902 to January 1976 but without the two world wars. The inflow event 1993 has been added. [2]For the period 1897-1976 excluding the two world wars. [3]In contrast to the simulation period of the other model runs (1902-1998), run 373b ends already in April 1997.)*

Baltic via Darss Sill. The corresponding figure for Drogden Sill is $2.1 \times 10^{12}\,kg$, i.e., 43 % of the total salt inflow. [38] found the same result for Drogden Sill analyzing observations at Oskarsgrundet. However, [64] calculated from observations a saltflow across Darss Sill of only $0.9 \times 10^{12}\,kg$. After re-assessment of the data [29] found $1.74 \times 10^{12}\,kg$ and $1.66 \times 10^{12}\,kg$ for Darss and Drogden Sill, respectively ($S \geq 17\,psu$). The latter figure is adopted from [43]. The complicated current conditions at the Darss Sill area might be the reason for the large uncertainty of the analyzed results based on observations only. In addition, the inaccuracy of the intensity estimations increases with decreasing number of consecutive days [29], i.e., the amount of salt transported during weak inflows might be biased.

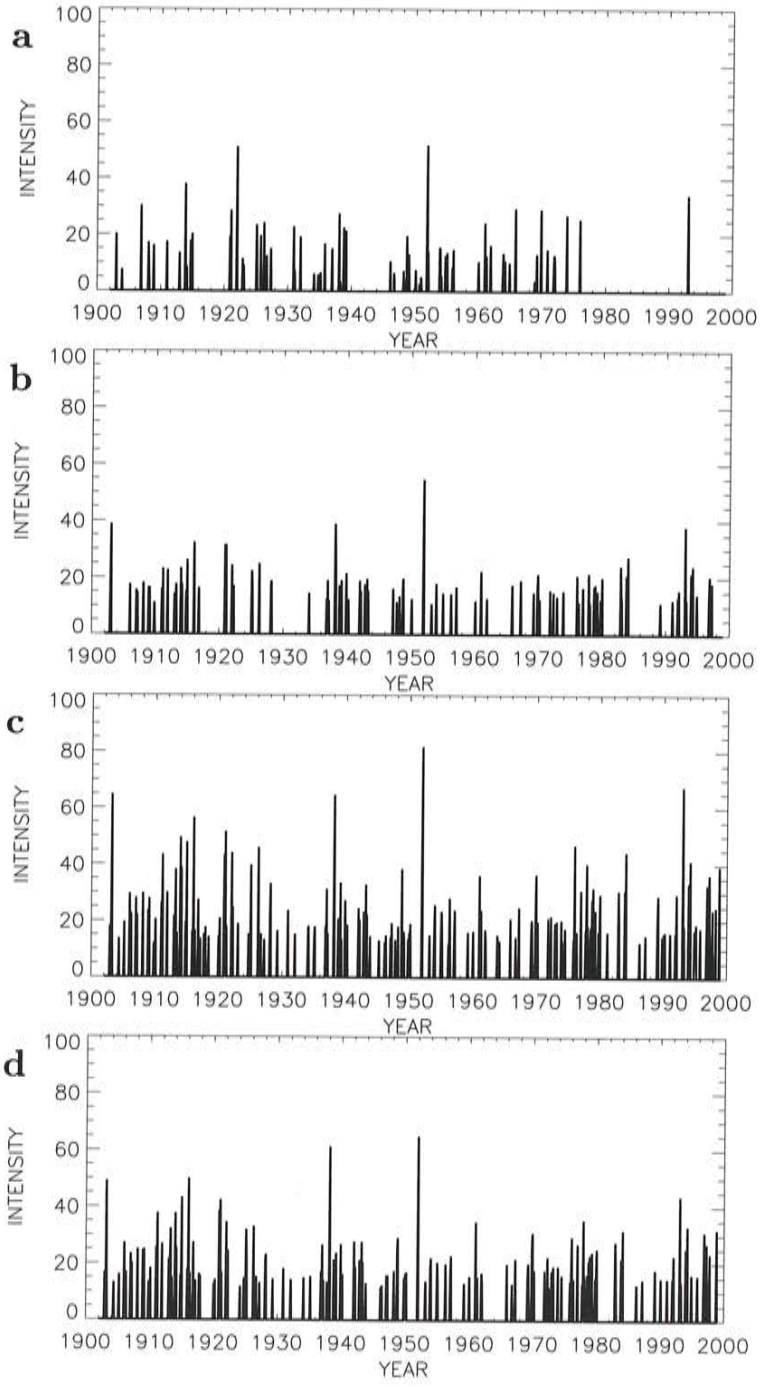

Figure 21: *Major Baltic inflows during the period 1902-1998 as characterized by an intensity index based on the amount of salt (in kg) transported across the sills in water bodies with salinities $S \geq 17psu$ divided by 10^{11} kg according to [29]: (a) observations according to [29], (b) run 373b, (c) run 403, and (d) run 394. Observations are not available for periods covering the world wars and after 1976 but the inflow event 1993 has been added.*

Therefore, we have further concentrated on the analysis of the 16 most intensive inflows with a ranking in terms of observed M_{17} between 1897 and 1993 (Tab.6) and on the analysis of the 22 most intensive inflows with a ranking in terms of simulated M_{17} in run 394 between

November 1902 and December 1998 (Tab.7, Fig.22).

		Data		Run 373b		Run 403		Run 394		Model GA		Model G	
No.	Period	M_{17}	V_{17}	M_{17}	V_{17}	M_{17}	V_{17}	M_{17}	V_{17}	M_{17}	V_{17}	M_{17}	V_{17}
1	Nov. 25 to Dec. 19, 1951	5.17	225	5.47	239	8.17	334	6.50	274	2.89	136	3.16	-
2	Dec. 16, 1921, to Jan. 6, 1922	5.12	258	2.45	112	4.41	215	3.47	166	3.32	153	-	-
3	Nov. 18 to Dec. 16, 1913	3.80	174	2.33	111	4.95	225	3.77	180	2.51	127	-	-
4	Jan. 18-28, 1993	3.40	159	3.82	164	6.76	275	4.38	182	3.48	154	2.05	78
5	Nov. 20 to Dec. 4, 1897	3.35	177	-	-	-	-	-	-	-	-	-	-
6	Nov. 26 to Dec. 13, 1906	3.03	151	1.57	74	2.82	130	2.35	111	1.72	87	-	-
7	Oct. 30 to Nov. 8, 1965	2.95	155	1.76	77	2.09	92	2.00	87	0.67	35	-	-
8	Oct. 29 to Nov. 25, 1969	2.92	153	2.15	102	3.66	172	3.10	149	1.69	88	2.39	-
9	Jan. 17-31, 1921	2.87	130	3.17	153	5.16	236	4.24	199	2.57	127	-	-
10	Dec. 7-22, 1898	2.79	142	-	-	-	-	-	-	-	-	-	-
11	Jan. 7-22, 1902	2.77	143	-	-	-	-	-	-	2.12	105	-	-
12	Jan. 24 to Feb. 6, 1938	2.75	144	3.90	183	6.46	277	6.13	270	2.63	122	-	-
13	Nov. 13-29, 1973	2.70	138	1.54	71	2.03	95	1.91	88	2.67	133	1.20	-
14	Dec. 22, 1975 to Jan. 14, 1976	2.56	125	2.09	94	4.69	200	2.95	133	2.67	134	1.75	-
15	Dec. 18-28, 1900	2.55	128	-	-	-	-	-	-	-	-	-	-
16	Jan. 20 to Feb. 7, 1898	2.50	133	-	-	-	-	-	-	-	-	-	-

Table 6: *Characteristic properties of the 16 most intensive Baltic inflows between 1897 and 1993 according to [29]. Tabulated are the volume (V_{17} in km^3) and amount of salt (M_{17} in $10^{12}\,kg$) transported into the Arkona Basin in water bodies with salinities $S > 17\,psu$. In addition, model results for the three standard experiments using RCO and results of [36] (GA) and [35] (G) are shown. A ranking in terms of observed M_{17} between 1897 and 1993 is performed.*

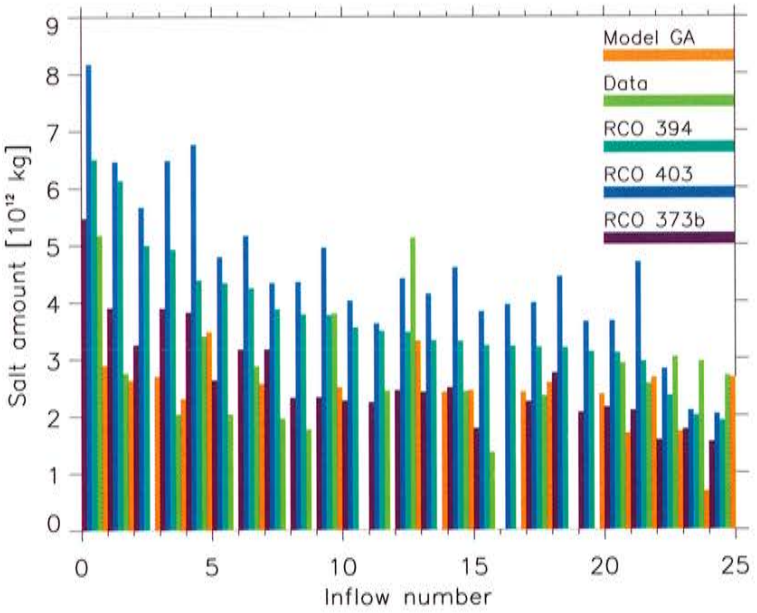

Figure 22: *The 22 (+3) largest simulated inflows 1902-1998 according to Tab.7 compared with observations [29] and the semi-empirical model by [36] (GA).*

So far information is available, the results of RCO have been compared with the results of the semi-empirical model presented by [36] (1902-98) and with the results of the process-oriented model for stratification and circulation within the entrance area presented by [35] (1950-53, 1961-93). Biases of simulated M_{17} are summarized in Table 8.

No.	Start date	Run 373b	Run 403	Run 394	Data	GA
1	Nov. 1951	5.47	8.17	6.50	5.17	2.89
2	Jan. 1938	3.90	6.46	6.13	2.75	2.63
3	Jan. 1916	3.25	5.66	4.99	-	2.70
4	Dec. 1902	3.89	6.48	4.92	2.03	2.31
5	Jan. 1993	3.82	6.76	4.38	3.40	3.48
6	Dec. 1914	2.63	4.79	4.33	2.03	-
7	Jan. 1921	3.17	5.16	4.24	2.87	2.57
8	Oct. 1920	3.17	4.33	3.87	1.95	-
9	Dec. 1910	2.32	4.35	3.78	1.76	-
10	Nov. 1913	2.33	4.95	3.77	3.80	2.51
11	Nov. 1977	2.27	4.02	3.55	-	-
12	Dec. 1960	2.24	3.62	3.49	2.44	-
13	Dec. 1921	2.45	4.41	3.47	5.12	3.32
14	Jan. 1994	2.42	4.14	3.32	-	2.42
15	Mar. 1926	2.50	4.60	3.31	2.43	2.45
16	Dec. 1912	1.78	3.83	3.23	1.36	-
17	Oct. 1998	-	3.95	3.22	-	2.42
18	Jan. 1925	2.25	3.98	3.20	2.35	2.58
19	Jan. 1984	2.75	4.44	3.19	-	-
20	Nov. 1996	2.06	3.65	3.12	-	2.38
21	Oct. 1969	2.15	3.66	3.10	2.92	1.69
22	Dec. 1975	2.09	4.69	2.95	2.56	2.67
...						
48	Nov. 1906	1.57	2.82	2.35	3.03	1.72
...						
66	Oct. 1965	1.76	2.09	2.00	2.95	0.67
...						
69	Nov. 1973	1.54	2.03	1.91	2.70	2.67

Table 7: *The 22 largest saltwater inflows in RCO (run 394) in terms of the salt amount in water bodies with salinities $S > 17\,psu$ compared with results of the other standard experiments (run 403, 394), with observations [29], and with results of the semi-empirical model by [36] (GA). Those inflows from Tab.6 which are not among the 22 largest are added.*

Among the 11 most intensive observed inflows between 1902 and 1993 (Tab.6) we found significant negative biases for RCO run 373b of $-0.64 \times 10^{12}\,kg$ and for the model by [36] of even $-0.95 \times 10^{12}\,kg$ (Tab.8). A significant positive bias is detected for RCO run 403. The best results are found for RCO run 394 concerning the mean error and for RCO run 373b concerning the rms error. Among the 19 most intensive simulated and observed inflows between 1902 and 1993 (Tab.7, Fig.22) the smallest bias and the smallest rms error are found for RCO run 373b. Among that part of these inflows with available values by [36] the smallest bias is found for RCO run 373b and the smallest rms error for the model by [36] and RCO run 373b.

The seasonal distribution of saltwater inflows is shown in Figure 23. All observed inflows occurred between the end of August and the end of April. They are most frequent between October and February, when about 90% of all events take place, and are less common in August/September and in March/April. Major events have never been observed between May and middle of August. [63] and [29] have classified major inflows by their intensity index into weak ($Q_T \leq 15$), moderate ($15 < Q_T \leq 30$), strong ($30 < Q_T \leq 45$), and very strong ($Q_T > 45$). Weak inflows, which account for about half of all observed inflow events, never last more than eight days and have a maximum mean salinity of $18.6\,psu$. Very strong inflows are observed only in November, December, and January. In general, the seasonal distributions of the standard experiments agree well with the observed distribution (Fig.23).

Statistics based on the 11 largest observed inflows 1902-1993 (Tab.6)		
Model	Mean error (in $10^{12}\,kg$)	RMS error (in $10^{12}\,kg$)
RCO run 373b	-0.64	1.23
RCO run 403	1.27	2.08
RCO run 394	0.32	1.38
Model GA	-0.95	1.30
Statistics based on the 19 largest simulated and observed inflows 1902-1993 (Tab.7)		
Model	Mean error (in $10^{12}\,kg$)	RMS error (in $10^{12}\,kg$)
RCO run 373b	-0.14	1.09
RCO run 403	1.77	2.32
RCO run 394	0.91	1.60
Statistics based on the 14 largest simulated and observed inflows 1902-1993 with available values by [36] (Tab.7)		
Model	Mean error (in $10^{12}\,kg$)	RMS error (in $10^{12}\,kg$)
RCO run 373b	-0.37	1.20
RCO run 403	1.58	2.31
RCO run 394	0.58	1.48
Model GA	-0.71	1.16

Table 8: *Model errors of the largest major Baltic inflows in terms of M_{17} for RCO and for the semi-empirical model by [36] (GA).*

Simulated inflows are most frequent between October and March. In run 373b, the maximum occurs in December as in the observations, but in run 403 and in run 394 February is the month with the most inflows. In all three standard experiments we found no weak inflows. The definition used for simulated events requires that $Q_T \geq 8.5$. However, it is not clear why we have not found inflows in the range $8.5 \leq Q_T \leq 15$. In the runs 403 and 394 the relative number of strong and very strong inflows compared to moderate inflows is higher than in run 373b. Very strong inflows occur even in October, February and March, and moderate inflows even in June.

Summarizing, saltwater inflows are most realisticly represented in run 373b (with the lowest surface wind speeds) compared to available observations. However, due to large uncertainties of the analyzed saltwater inflows a proper model validation is almost impossible.

8.3.2 The event in January 1993

The recent major Baltic inflow in January 1993 has been studied earlier (e.g. [67], [77]). Measurements of this event were described and analyzed in several publications (e.g., [38], [65], [43], [64]). At the end of December 1992 and during the first days in January 1993, a distinct outflow situation is established with low salinities in the Danish Straits. After the onset of strong westerly winds the salinity fronts are moved towards Arkona Basin and the Belt Sea is filled up with salty water. Between January 6 and 27, a mean salinity of 26.75 psu was observed at Drogden Sill [38]. At Darss Sill, vertical mean maximum salinities of about 22 psu were observed between January 26 and 28 [65].

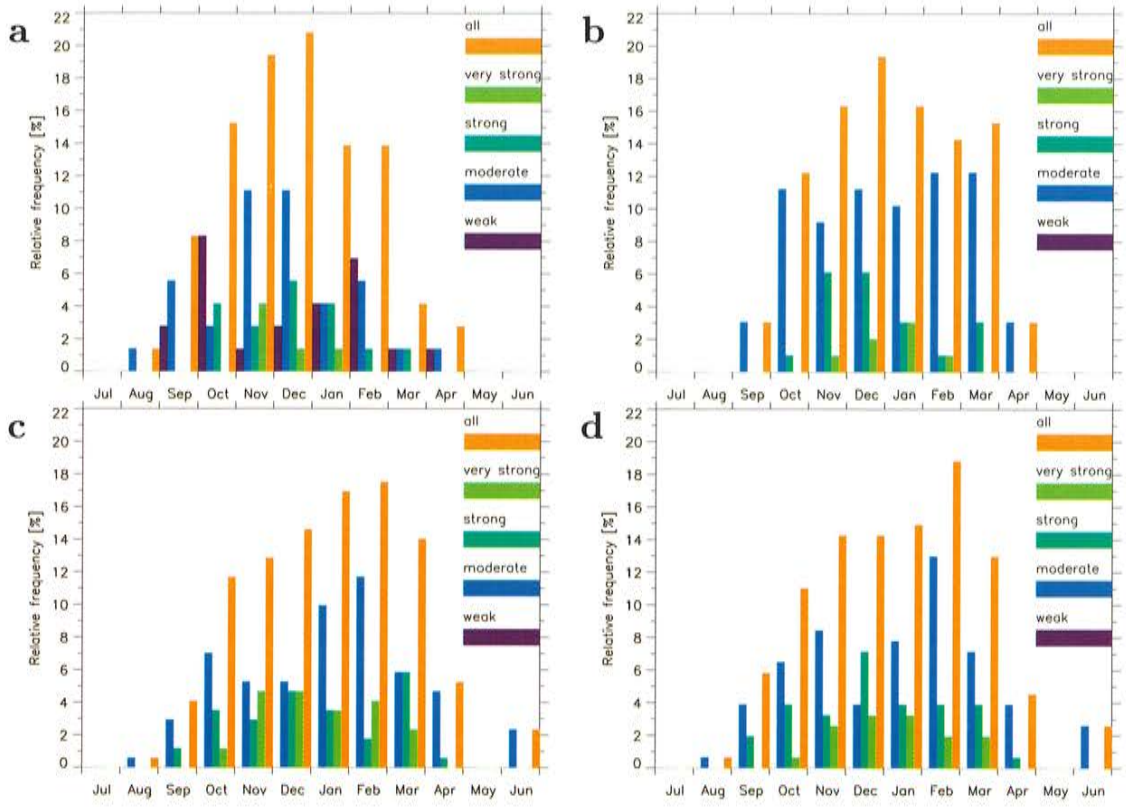

Figure 23: *Seasonal distribution of classified events. (a) observations according to [29], (b) run 373b, (c) run 403, and (d) run 394.*

The event has been simulated also with the high-resolution version of RCO using a horizontal grid distance of *2 nautical miles* [77]. As these model results agree very well with available observations, the time evolutions of simulated V_{17} in the Arkona Basin and in the Bornholm Basin have been compared using horizontal resolutions of *2 nautical miles* (run 349: atmospheric forcing from the SMHI database, initial conditions May 1992) and of *6 nautical miles* (runs 373b, 403, and 394: reconstructed atmospheric forcing, initial conditions November 1902), (Fig.24). In the Arkona Basin and in the Bornholm Basin the best agreements are found for run 373b and run 394, respectively. In run 403 the inflowing high-saline water into the Arkona Basin is overestimated compared to run 349. In contrast, the deepwater renewal in the Bornholm Basin is underestimated. Due to higher surface wind speeds the barotropic transports across the shallow sills are increased. In addition, increased wind induced diapycnical mixing in the Arkona Basin during and after the inflow event is also enhanced. The net effect is a reduced baroclinic transport into the Bornholm Basin. In run 403, the wind speed is increased by 30 % compared to run 373b. A similar effect has been reported already by [77] utilizing a sensitivity experiment with 20 % increased wind speed compared to run 349.

8.4 The stagnation period 1980-92

In earlier studies RCO has been validated for the test period 1980-1993 ([68], [69], [70], [71], [72], [73], [77]). During this period several homogeneous observational data sets for atmo-

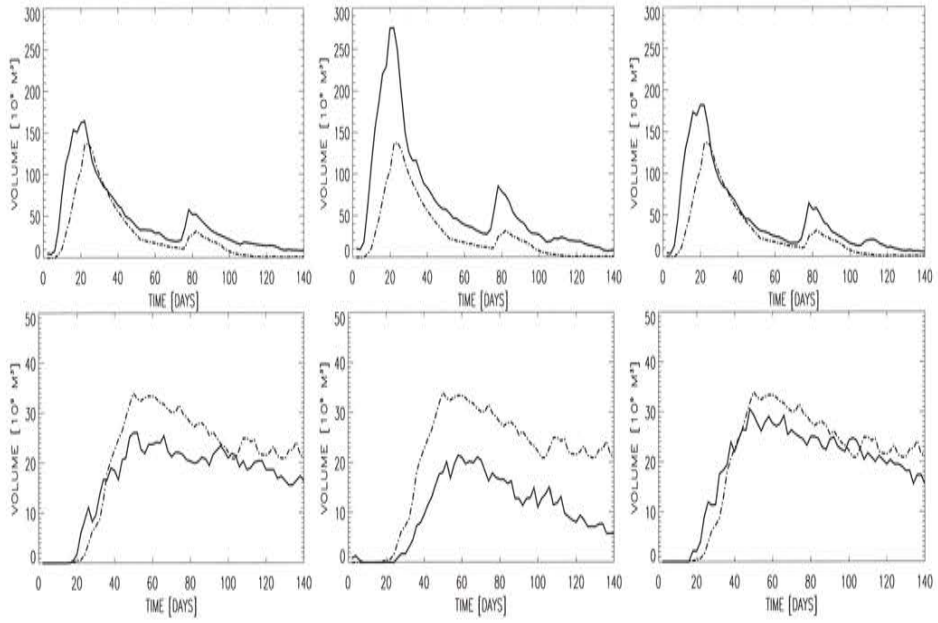

Figure 24: *Volume (in km^3) of high saline water ($S > 17\,psu$) in the Arkona Basin (upper panels) and in the Bornholm Basin (lower panels). From left to right, the solid curves show model results of run 373b, run 403, and run 394. In all panels, the dashed curve denotes the 2 nautical miles run 349 presented by [77]. The time axis starts January 2, 1993.*

spheric variables (SMHI database, ECMWF reanalysis data, etc.), river runoff and ocean data of sufficient quality are available. The latter are used for initialization and verification. The main conclusion of the above mentioned publications is that the stagnation period is simulated realisticly. Deepwater salinity in the Baltic proper decreases as observed. During the 13-year long integration unphysical erosion of the density structure is not observed, which has been a major obstacle in older models. Therefore, in this sub-section the results of the 100-year simulations are compared with the earlier findings. The impact of the initial conditions are illustrated for the results of the stagnation period 1980-1993. However, this period does not allow a model performance test for overflows between the Bornholm Basin and the eastern Gotland Basin. Indeed, the period is a very special one as shown below.

8.4.1 A part of the long simulations

The results of the standard experiments for the isohaline depths at Gotland Deep for the period 1980-1993 are depicted in Figure 25. In addition, the observations and results of the sensitivity run 375 are shown. Thus, Figure 25 shows just a part of the whole period 1902-1998 as depicted in Figure 17. As mentioned earlier, the halocline is too shallow in the experiments 373b and 375. The upper layer tends to be too saline. In 375, also the deep layer is too saline. In both experiments 373b and 375 the small signal of the inflow event in January 1993 is clearly visible. Despite of that, we found better results for the halocline depth and the upper layer salinity in the runs 403 and 394. However, the deeper layer salinity at the beginning of the stagnation period is somewhat too low, especially in run 394. For this period, we found the most realistic results compared to the observations in run 403.

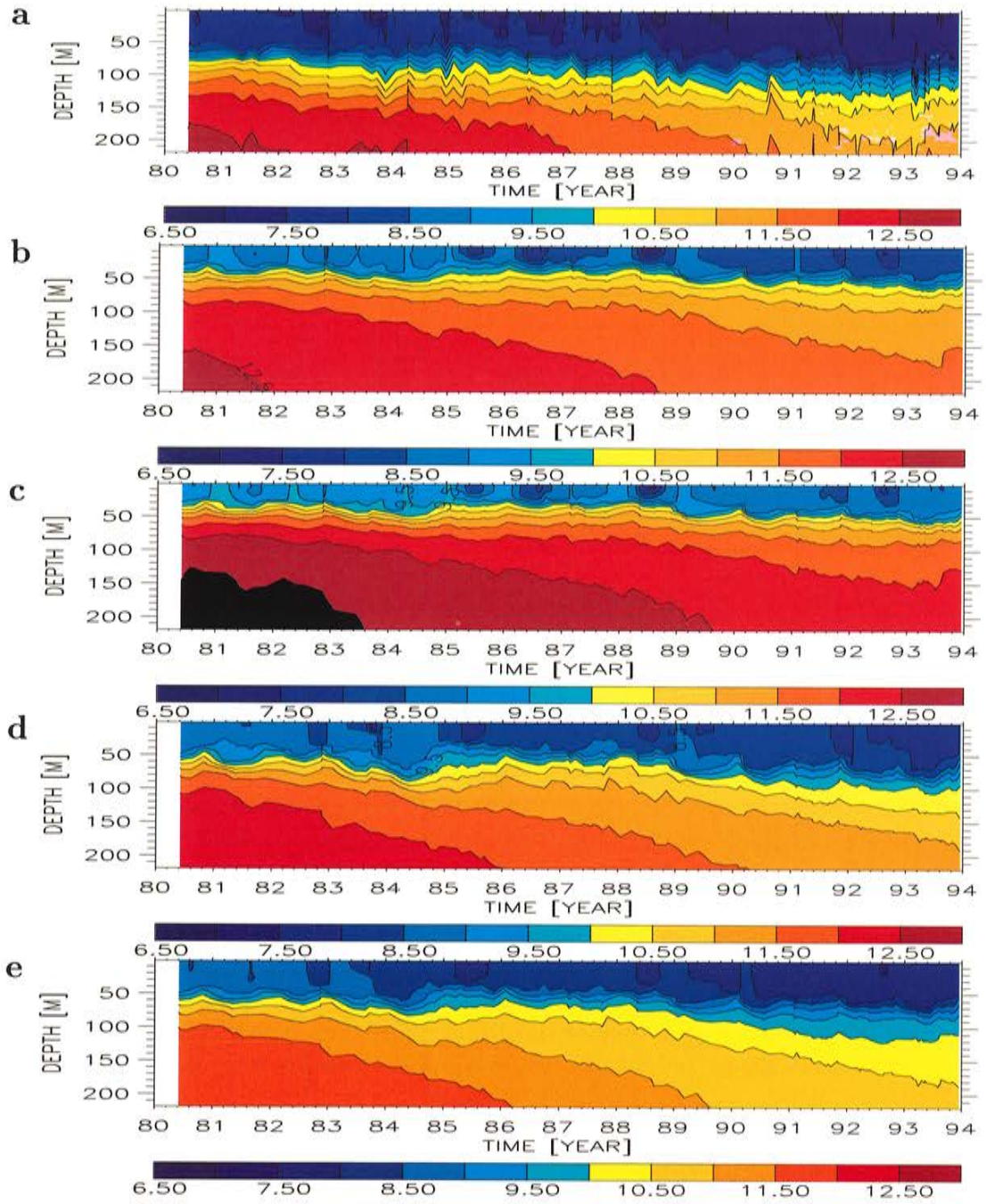

Figure 25: *(a) Observed and (b-e) simulated isohaline depths (in psu) at Gotland Deep (BY15) for the period 1980-1993 (a part of the long simulations, cf. Fig.17): (b) run 373b, (c) run 375, (d) run 403, and (e) run 394.*

8.4.2 Initialization in May 1980

The same experiments as in sub-section 8.4.1 have been repeated but with initial conditions from May 1980. The experiment 413 corresponds to run 373b, run 376 to run 375, run 402c to run 403, and run 414 to run 394 (see Tab.15 in Appendix A). As all experiments start with the same initial conditions, the results are relatively similar (Fig.26). Due to the long

response time scale of salinity in the deep layer of the Baltic Sea, differences caused by the mixing parameterization or by the wind speed parameterization are only small for the short period 1980-1993. However, some features can be identified also in the short runs. As in the long simulations, the halocline is too shallow in the runs 413 and 376 (Fig.26b and c). Only in these two experiments the signal of the major inflow in January 1993 is visible as in the observations. In run 414 the bottom salinity decreases too fast during the stagnation period

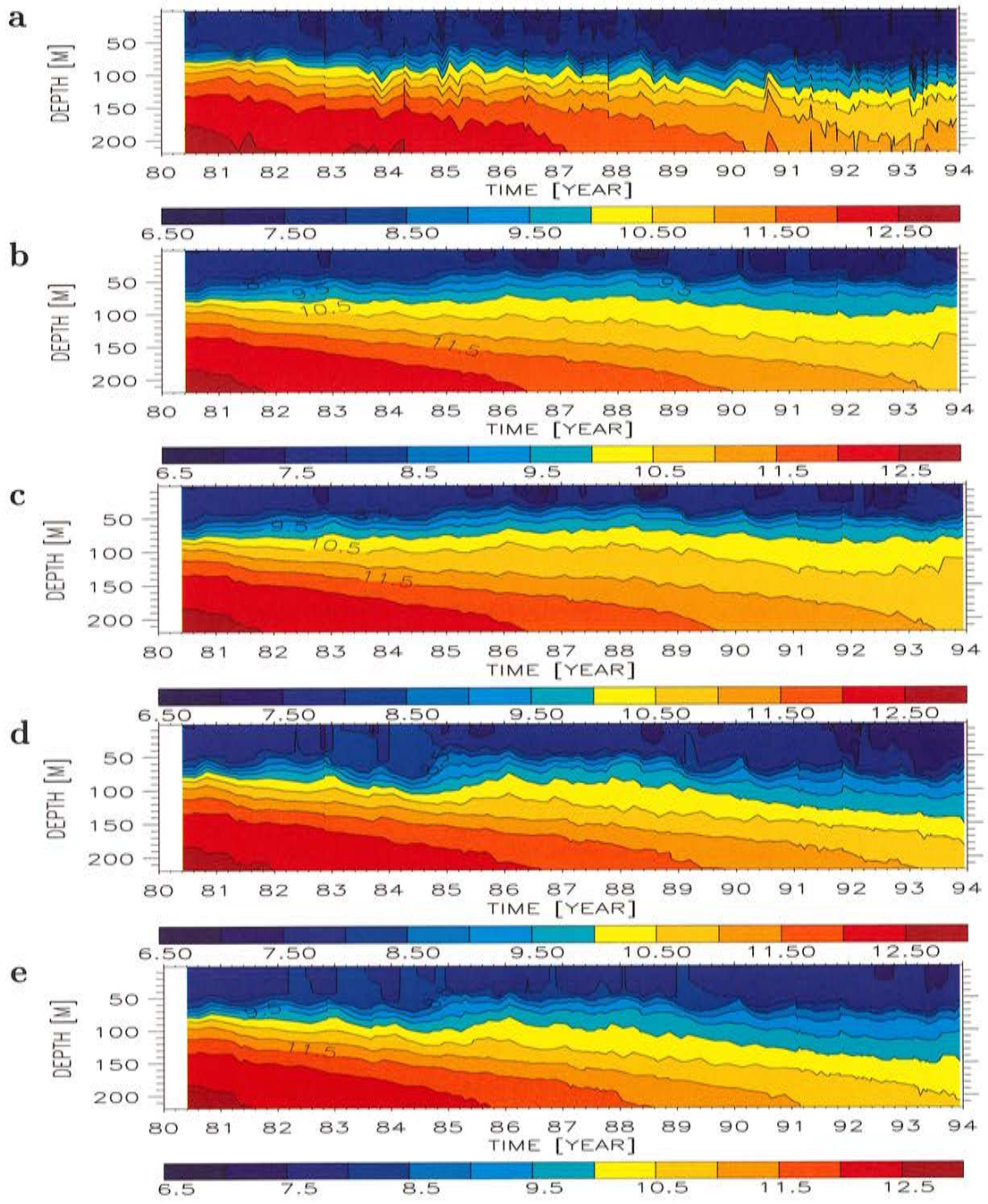

Figure 26: *As Fig.25 but initial conditions from May 1980: (a) observations, (b) run 413, (c) run 376, (d) run 402c, and (e) run 414.*

(Fig.26e). In this experiment, a decreased constant for the parameterization of deepwater

mixing would improve the results ($\alpha = 0.75 \cdot 10^{-3}\, cm^2\, s^{-2}$ is actually used). Despite of the missing inflow signal in 1993, the best agreement between model results and observations are found for run 402c (Fig.26d).

8.5 Deepwater transport in the eastern Gotland Basin

In Figure 27, the mean simulated horizontal advection of denser water ventilating the halocline and the upper deepwater in the East Gotland Basin is shown and compared with results calculated from observations for the period 1979-94 by [28] using a diagnostic model (Fig.28). We have chosen a section between the island of Gotland and Estonia to calculate the horizon-

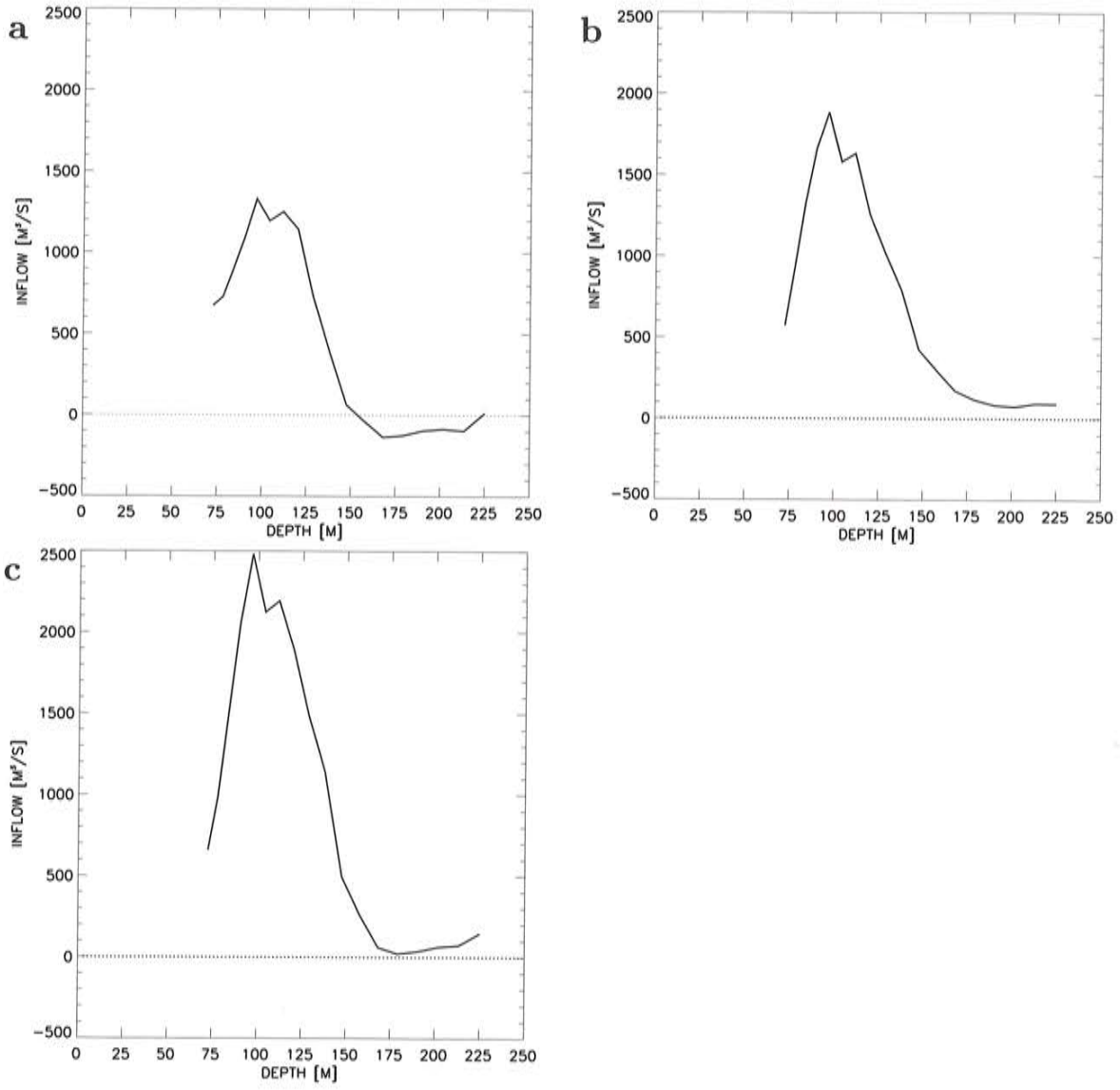

Figure 27: *Simulated mean horizontally averaged volume transport entering the eastern Gotland Basin from the Bornholm Basin: (a) short run 240 from May 1980 to December 1993, (b) standard experiment run 373b from January 1979 to December 1994, and (c) standard experiment run 403 from January 1979 to December 1994.*

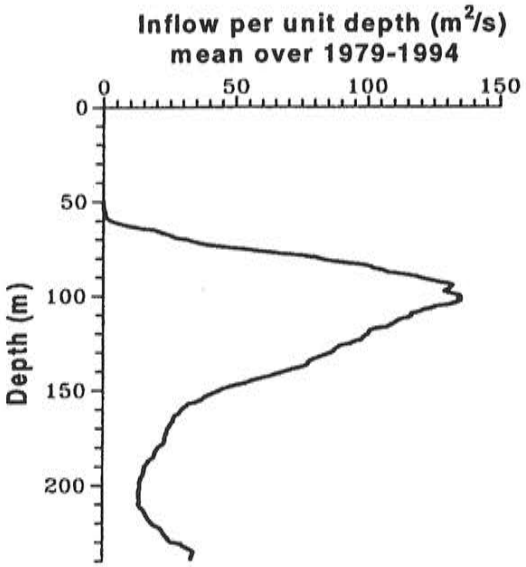

Figure 28: *Mean horizontally averaged volume transport entering the eastern Gotland Basin from the Bornholm Basin. The results are adopted from [28] who used a diagnostic model together with observations for the period 1979-1994.*

tally averaged volume transports. The vertically integrated results are summarized in Table 9. According to the diagnostic model from [28], the mean inflow rate of dense water from

Run	Deepwater inflow (m^3/s)	Total transport (m^3/s)
1980-1993		
run 240	8,928	96,018
1979-1994		
[28]	10,900	-
run 373b	13,993	95,905
run 403	17,706	114,053
1970-1990		
[50]	33,200	-
run 373b	16,216	97,124
run 403	19,648	114,408
1902-1998		
run 373b	16,390	95,722
run 403	19,707	118,165

Table 9: *Mean volume transports entering the eastern Gotland Basin. The deepwater inflow is calculated between 78 m of depth and the bottom. The total transport is calculated between the surface and the bottom.*

Bornholm Basin amounts to $10,900\,m^3/s$ for the period 1979-1994. A much larger value of $33,200\,m^3/s$ has been calculated by [50] for the period 1970-1990. In both diagnostic models the mean wind driven circulation is not considered.

8.6 Mean salinity

In Figure 29, the mean salinities of the Baltic Sea as a function of time during the period 1902-1998 for the three standard experiments are shown. The total mean salinities amount

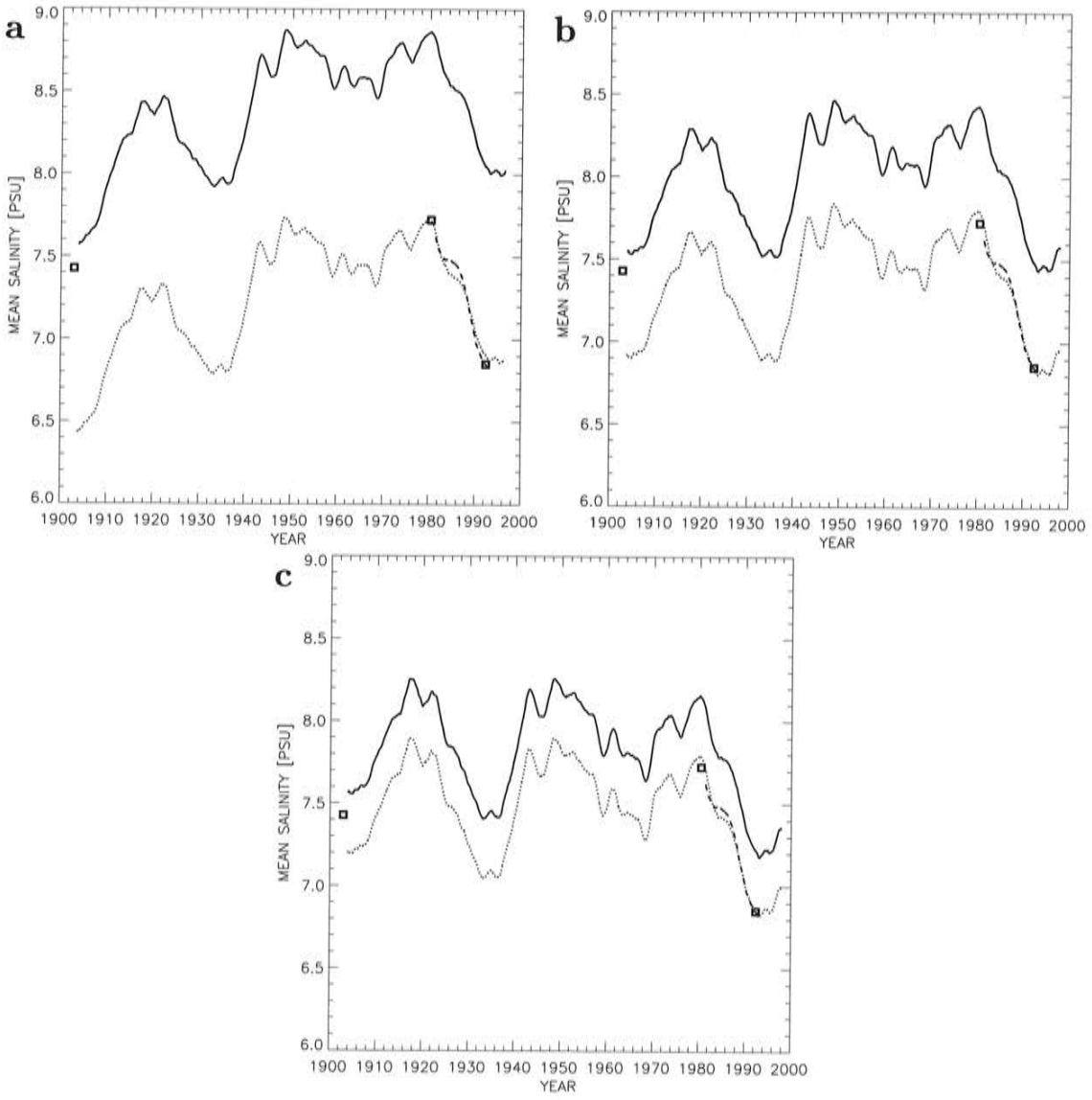

Figure 29: *2-year running mean salinity in the Baltic Sea without Kattegat (in psu): (a) run 373b, (b) run 403, and (c) run 394. The solid and dotted curves denote the uncorrected and corrected model results, respectively. The dashed line denotes the short run 240. The squares denote mean salinities calculated from observations for November 1902, May 1980, and May 1992.*

to $8.38\,psu$ in run 373b, to $7.99\,psu$ in run 403, and to $7.82\,psu$ in run 394 (Tab.10). Daily salinity variations of the unfiltered record are of the magnitude of $0.1 - 0.2\,psu$. The inflow event in January 1993 causes the mean salinity of the Baltic to increase by $0.13\,psu$ (run 349).

As a consequence of the discretization algorithm used for the topography, the model volume on tracer grid points is about 9 % larger than the volume calculated from independent data

Run	$\bar{S}$	difference to run 240	corrected $\bar{S}$	minimum	maximum
373b	8.38	1.13	7.24	6.28	7.90
403	7.99	0.63	7.36	6.65	8.06
394	7.82	0.36	7.46	6.69	8.08

Table 10: *Total mean salinities calculated with the three standard experiments. In addition, the differences between these long simulations and run 240 for the period 1980-93, correspondingly corrected total mean salinities, and the extrema of the corrected unfiltered time record are listed.*

(Tab.18 in Appendix B). The corresponding error of the mean salinity is estimated to be smaller than $0.3\,psu$. The uncertainty due to the precise definition of the Baltic Sea domain is even smaller. Here, we have chosen a border located in the Great Belt and in the Öresund.

A comparison between the long standard experiments and a simulation with observed initial conditions from May 1980 (run 240) shows that the mean salinities during the period 1980-1993 are overestimated in all long simulations (Fig.29). We found the largest positive bias of $1.13\,psu$ for run 373b and the smallest bias of $0.36\,psu$ in run 394 (Tab.10). However, when the bias is subtracted from the records, the results of the long standard experiments and run 240 fit perfectly (Fig.29). The corrected mean salinity for the whole period 1902-1998 amounts to $7.24 - 7.46\,psu$. After the correction the total mean salinities in all three standard experiments are very close (Tab.10). The variability of the mean salinity amounts to $1.4 - 1.6\,psu$. Thus, the corrected mean salinity varies between 6.3 and $8.1\,psu$ (Tab.10).

As the biases of the mean salinity differ quite much between different experiments, we conclude that the overestimation cannot be caused only by biased initial conditions in November 1902. Instead, it is quite likely that the model drifts to higher salinities during the first two decades. This is further confirmed by a sensitivity experiment without decadal variations in freshwater supply and atmospheric forcing as discussed in Section 9 (Fig.56). As the halocline is too shallow (most obvious in run 373b), increased saltwater inflow occurs until the system is in a new quasi steady-state. The drift is largest in run 373b and smallest in run 394. The biased mixing is partly improved by the additional random wind component in run 394.

The decadal variations in our experiments agree very well with the results presented by [117] (see their Fig.15). [117] calculated freshwater content and mean salinity of the Baltic Sea from data at one station in the eastern Gotland Basin (BY15) for the period 1902-1996. They found that BY15 is representative for the whole Baltic Sea. To show this, [117] computed the freshwater volume in all major sub-basins (Arkona Basin, Bornholm Basin, Baltic Proper, Bothnian Sea, and Bothnian Bay) separately, with their own hypsographic curves, and compared these with the total freshwater volume obtained by using BY15 only. The comparison was done for the 1977 to 1987 period, with good data coverage in all sub-basins. [117] found that the average difference amounts to $219\,km^3$ or some 2 % of the total freshwater content. The mean salinities calculated by [117] are significant smaller. They found mean salinities between 5.5 and $6.5\,psu$ during the 20th century and a total mean of about $6\,psu$ which is more than $1\,psu$ smaller than our result[2].

[2]The calculations of the Baltic Sea freshwater content and mean salinity presented by [117] and [92] were erroneous due to a fault in the hypsographic data used as meanwhile confirmed by the authors (Johan Rodhe,

In addition to the model results, mean salinities calculated from observations only are shown in Figure 29 for November 1902 ($\bar{S} = 7.43\,psu$), May 1980 ($\bar{S} = 7.73\,psu$), and May 1992 ($\bar{S} = 6.85\,psu$). The latter two figures agree very well with the corrected mean salinities of the long simulations.

Our model results are further confirmed by other studies. [57] calculated the mean salinity of the Baltic Sea between December 1, 1992 and March 31, 1993. He found variations between 6.81 and $6.92\,psu$. During the inflow event in January 1993 he found an increase of about $0.1\,psu$. The models used at the Baltic Sea Research Institute Warnemünde (IOW) are initialized by assimilating profile data of regular monitoring cruises into climatological mean temperature and salinity fields (Torsten Seifert IOW, 2002, pers. comm.). During autumn 1992 the mean salinity in the area $13 - 30°E$, $54 - 66°N$ amounts to $6.94\,psu$ for a *3 nautical mile* model and $6.96\,psu$ for a *9 nautical mile* model. During autumn 1997 Seifert (2002, pers. comm.) found a mean salinity of $6.94\,psu$. Further, mean salinities calculated from the climatological dataset for the North Sea and the Baltic Sea [45] amount to $7.2 - 7.4\,psu$ for the different months within the same area. In this dataset observations from the period 1902-1996 are included. As more than 50 % of the data are recorded after 1977 (for greater depths the data density maximum is shifted even more towards the stagnation period of the 1980s and 1990s), the total mean salinity of the whole period 1902-1996 is very likely underestimated by the dataset (Frank Janssen IOW, 2002, pers. comm.).

8.7 Freshwater budget

Annual mean net precipitation, i.e. precipitation minus evaporation, is shown in Figure 30. The total mean net precipitation amounts to $2,224\,m^3\,s^{-1}$ in run 373b (for the period November 1902 to April 1997), to $2,030\,m^3\,s^{-1}$ in run 403, and to $1,280\,m^3\,s^{-1}$ in run 394. The latter two figures are calculated for the period November 1902 to November 1998. The inter-annual variability is large (Tab.11).

Run	Minimum	Mean	Maximum
373b	-19	2,224	4,078
403	-384	2,030	3,917
394	-1,148	1,280	3,142

Table 11: *Minimum, mean, and maximum of annual mean net precipitation (in $m^3\,s^{-1}$) for the three standard experiments.*

From RCO results using the SMHI database as atmospheric forcing [75] calculated a total mean net precipitation of $1,843\,m^3\,s^{-1}$ for the relatively wet period 1980-1993.

The mean freshwater volume stored in the Baltic Sea is shown in Figure 31. The total mean freshwater content amounts to $17,461\,km^3$ in run 373b, to $17,734\,km^3$ in run 403, and to $17,853\,km^3$ in run 394. These numbers are uncorrected, i.e. the model drift towards higher salinities during the first two decades is not corrected. Using an average freshwater volume of $1.8 \times 10^4\,km^3$ and an average freshwater inflow of $16,000\,m^3\,s^{-1}$ (see sub-section 6.1), we

Göteborg University, 2002, pers. comm.)

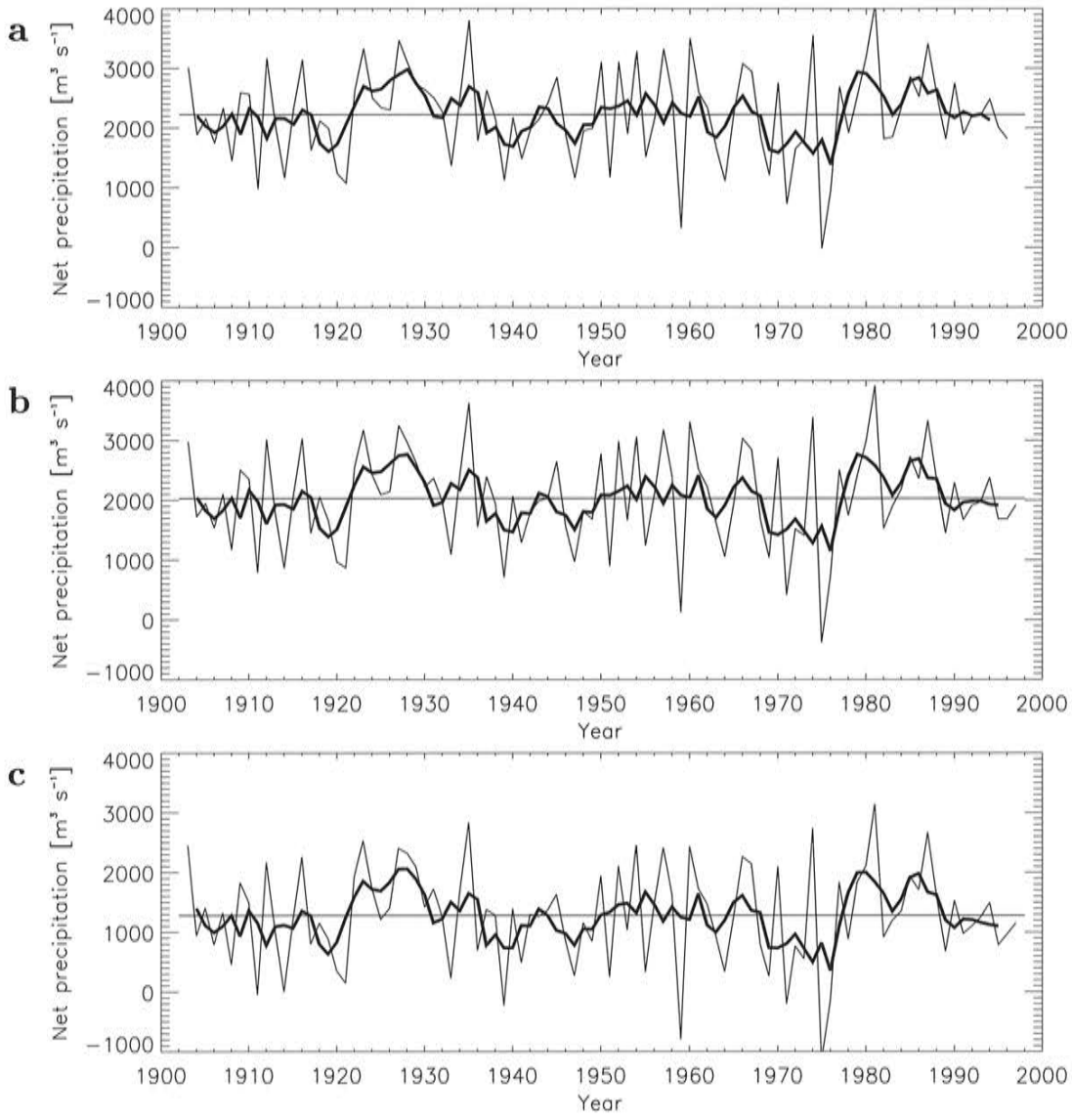

Figure 30: *Annual mean net precipitation (in $m^3\ s^{-1}$), i.e. precipitation minus evaporation, to the Baltic Sea (without Kattegat) for the period 1902-1998: (a) run 373b, (b) run 403, and (c) run 394. In addition to the annual means, the 4-year running means (thick line) and the total means for the period 1902-1998 (horizontal line) are shown.*

found a freshwater residence time of about 36 years which is only slightly longer than calculated by [117] (34 years).

In Figure 32, the simulated freshwater storage anomaly is shown. Our results are very similar to the freshwater storage calculated by [117] from observations (cf. their Fig.17). We also found that the freshwater storage anomaly and the accumulated freshwater inflow are well correlated.

To check if this relationship also holds for parts of the estuary, i.e. the large Gulfs, we have calculated also the accumulated river runoff and net precipitation anomalies and freshwater

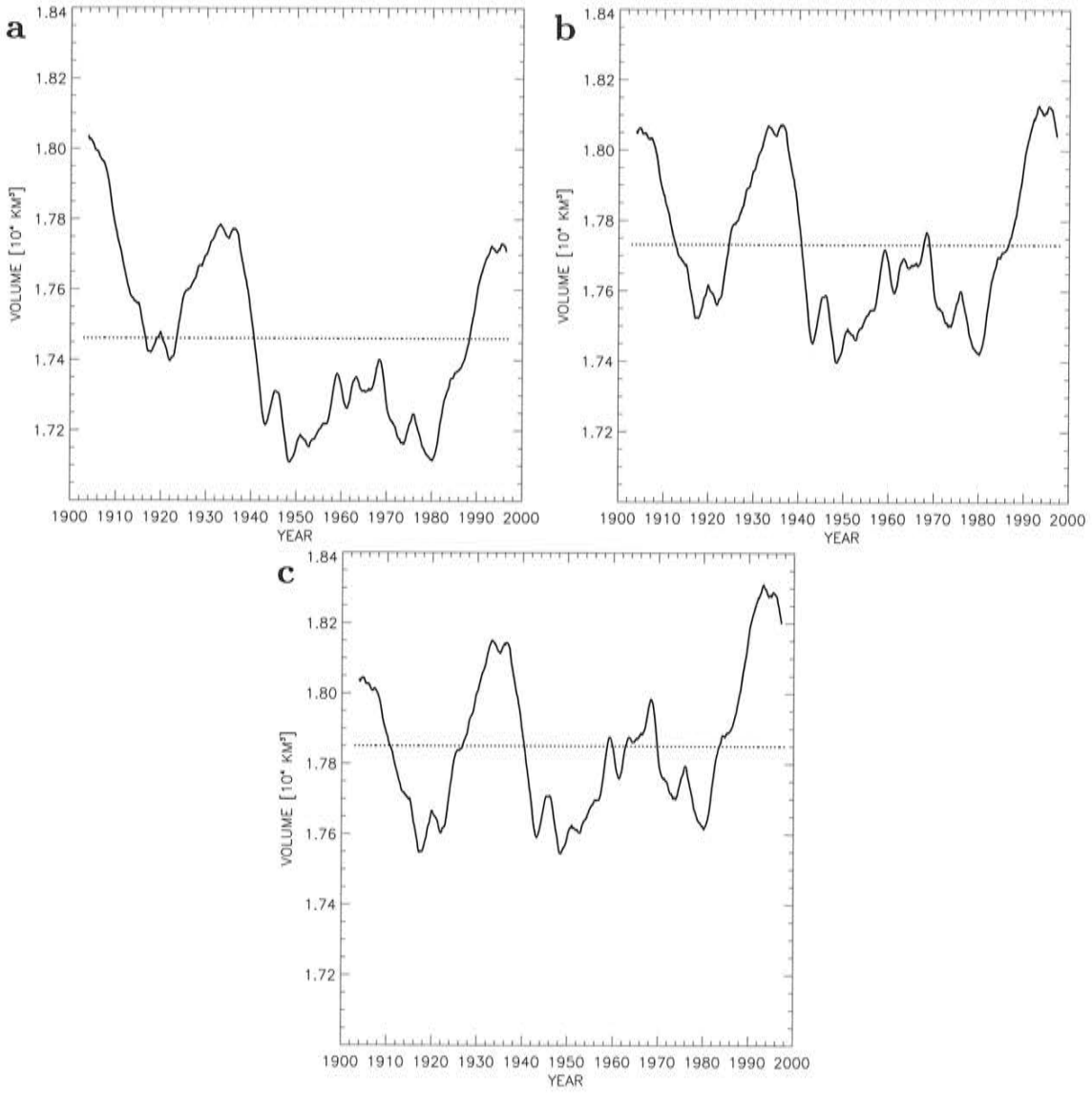

Figure 31: *2-year running mean (solid) and total mean (dotted) of freshwater storage (in* $10^4\,km^3$*): (a) run 373b, (b) run 403, and (c) run 394.*

storage anomalies in the Gulf of Bothnia and in the Gulf of Finland separately (Fig.33). We found no significant correlations in the Gulfs.

8.8 Sea ice

8.8.1 Maximum ice extent

Data of the annual maximum ice extent of the Baltic Sea (MIB) are collected by the Finnish Institute of Marine Research (FIMR). Original data by [49] were destroyed in World War II. However, the time series was reconstructed by [88] and subsequently extended by [102]. The method is described by [101]. Statistical parameters of the MIB data are presented by [109]. Data from winter 1719/1720 to winter 1999/2000 were available.

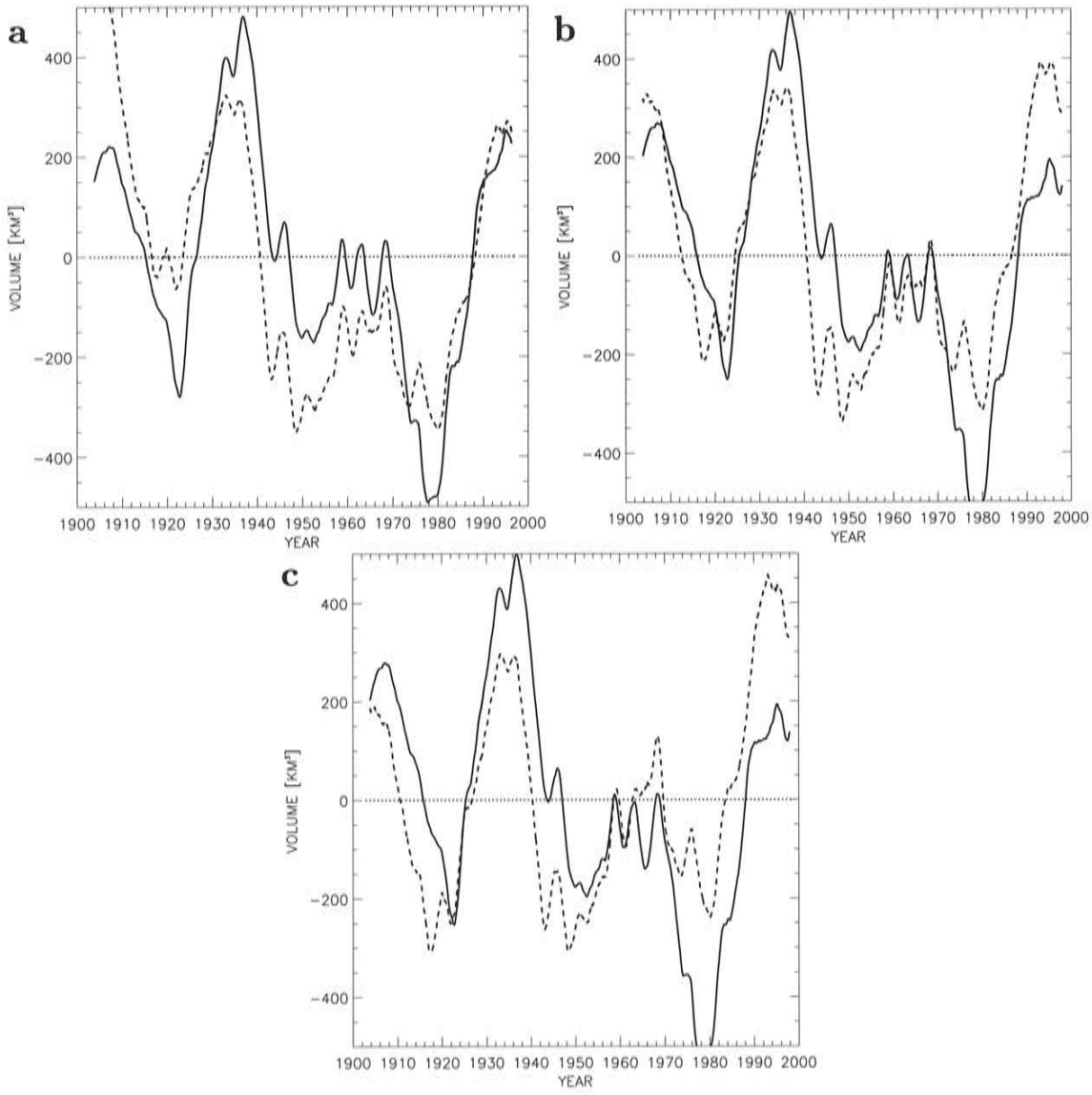

Figure 32: *2-year running mean of accumulated river runoff and net precipitation anomaly (solid) and 2-year running mean of freshwater storage anomaly (dashed), in km^3: (a) run 373b, (b) run 403, and (c) run 394.*

The variability of maximum ice extent is simulated in good agreement with the observations but the ice cover is somewhat overestimated (Fig.34a-c, Tab.12). In Table 12 the model errors are listed for the whole period 1903-1998, the fitting period 1980-1998, the remainder period 1903-1979, etc. We found the best results for run 394 (random wind component) and the worst results for run 373b (original wind parameterization) with the largest mean error. The results of run 403 (increased wind speed) are close to run 394. During 1903-1998 79 % of the observed variance is explained in run 394 by the simulated MIB. The heat content of the water column in autumn has a significant impact for the beginning of the following ice season and also on the maximum ice extent [69]. As the seasonal mixed layer depth is underestimated in run 373b, the ice cover is overestimated with a mean error for the period

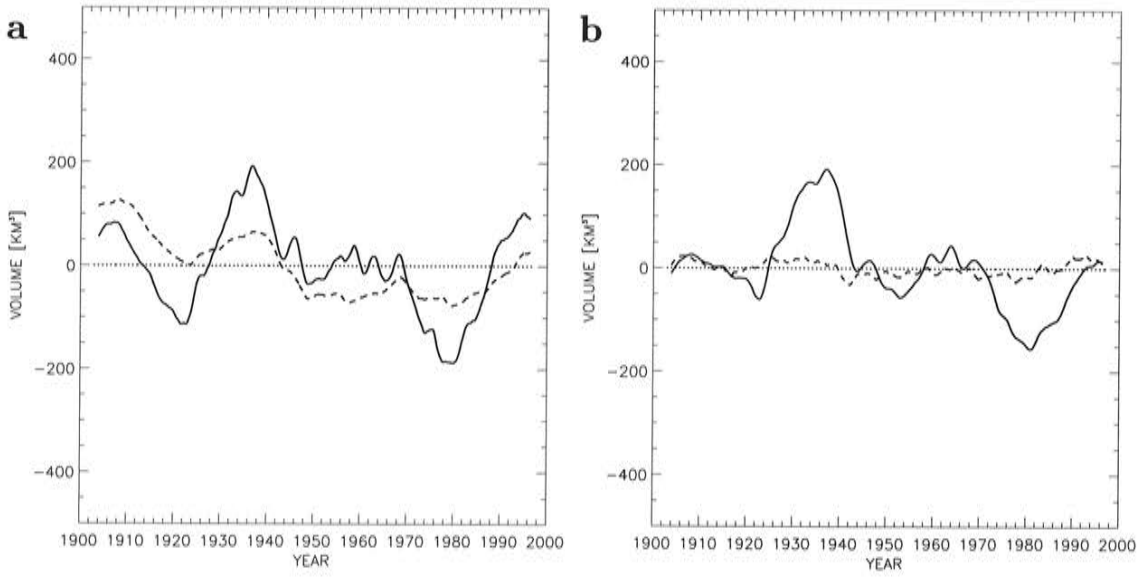

Figure 33: *2-year running mean of accumulated river runoff and net precipitation anomaly (solid) and 2-year running mean of freshwater storage anomaly (dashed), in km^3: (a) Gulf of Bothnia, (b) Gulf of Finland. Depicted are model results of the standard experiment run 373b.*

1903-1998 which is about 80 % larger than the bias in run 394. The overall positive bias in all standard experiments even during the fitting period is very likely caused by a latent heat flux bias so that the ocean looses heat too rapidly in autumn.

To show the impact of specific humidity and cloudiness (the variables with the lowest skill in the reconstruction) on the simulated ice cover, an additional experiment has been performed. In run 420, climatological monthly mean specific humidity and cloudiness calculated from the SMHI database for the period 1980-1995 have been used. The results are shown in Figure 34d. The errors should be compared with those from run 403 (Tab.12). The mean error is much reduced especially after 1966 including the fitting period showing that the latent heat flux is improved. However, the variabilities for the whole period 1903-1998 and for the periods after 1966 are worse simulated than in run 403 (cf. rms errors, correlation coefficients, and explained variances in Tab.12). Although specific humidity and cloudiness are less important variables than air temperature explaining ice cover variability, there is a significant impact even from these variables.

The error increases back in time in two steps, i.e. around 1966 and around 1926 (Fig.34). The reason might be a decreasing quality of the ice observations. Interestingly, the two steps with decreasing MIB error coincide with increases of intensity and area coverage of the observations (Jouko Launiainen FIMR, 2002, pers.comm.):

1. In the late 1960s the activity of aircraft ice reconnaissance was increased and first satellite observations became available.

2. On February 11, 1927 the Finnish merchant vessels were ordered by the Finnish Government to keep on-track sea ice diaries and to deliver those data to the Finnish Institute of Marine Research [34]. Hourly data of ice cover, ice severity, ice velocity, wind speed,

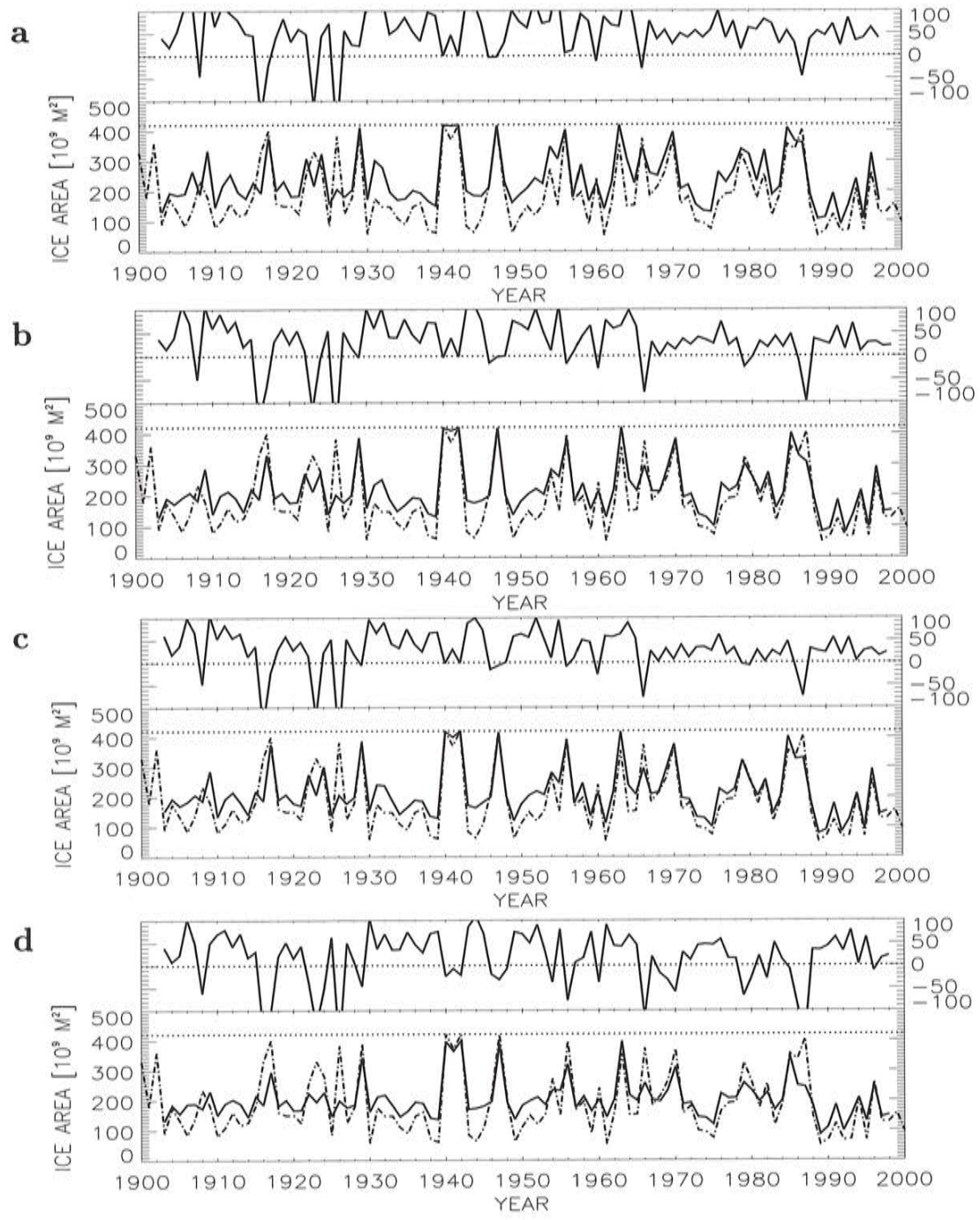

Figure 34: *Annual maximum ice extent (in $10^9\,m^2$): observations (dashed-dotted), model results (solid). The difference between model results and observations is shown above every panel. (a) run 373b, (b) run 403, (c) run 394, and (d) run 420.*

etc. were recorded. According to Launiainen (2002, pers.comm.) this order has put much attention to ice observations and it is a very likely candidate of improved data quality in those years.

Alternatively, the quality of the input data to the statistical model (e.g. air temperature and

Run	ME ($10^9\,m^2$)	RMSE ($10^9\,m^2$)	R	VAR
1903-1998				
run 373b*	51.7	74.7	0.86	0.73
run 403	30.8	59.6	0.88	0.76
run 394	28.8	55.6	0.89	0.79
run 420	16.3	61.5	0.85	0.67
1903-1979				
run 373b	53.1	78.5	0.83	0.69
run 403	33.3	63.6	0.86	0.72
run 394	31.7	59.9	0.88	0.76
run 420	18.5	63.0	0.85	0.66
1980-1998				
run 373b*	36.1	60.0	0.90	0.79
run 403	20.5	39.5	0.95	0.90
run 394	17.1	32.7	0.97	0.93
run 420	7.5	55.4	0.90	0.72
1966-1998				
run 373b*	40.1	57.6	0.91	0.83
run 403	19.7	39.1	0.95	0.89
run 394	17.1	33.8	0.96	0.91
run 420	4.1	53.0	0.92	0.72
1966-1995				
run 373b	45.1	54.1	0.96	0.92
run 403	19.3	40.4	0.95	0.88
run 394	16.5	34.7	0.96	0.91
run 420	3.7	55.3	0.91	0.71
model OC	-	-	0.78	0.60
1981-1995				
run 394	17.6	35.3	0.97	0.93
model ON	14.	-	0.91	-
model OC	-9.	-	0.8	-

Table 12: *Model errors of annual maximum ice extent. Different periods are investigated to compare the RCO results with the statistical model (OC) by [83] and with the dynamical model (ON) by [85]. (*Note that for run 373b only 94 winters are available. ME = mean error, $RMSE$ = root mean square error, R = correlation coefficient, VAR = explained variance.)*

precipitation) could have decreased back in time or the statistical relationship between predictor and predictand variables could have changed. A changing correlation between maximum ice extent and the large-scale atmospheric circulation via a meridional SLP index has been reported already by [109] (see his Fig.8a). He showed further that the correlation between MIB and the mean air temperature from November to March of the 10° grid area ($55-65°N$, $20-30°E$) of the Climatic Research Unit dataset (University of East Anglia, Cambridge) varies as well but is much more constant in time than using a zonal index (Fig.8b by [109]). Similar results were reported later also by [83] for the winter NAO index and for the mean air temperature at Stockholm during December to February (see Figs.3b and 4b by [83]). The question of changing correlation is further discussed in Section 10.

In Table 12 also results of the statistical model (OC) by [83] and of the dynamical model (ON) by [85] are shown. [83] established a statistical model between MIB and a westerly wind index, southerly wind index, and total vorticity. For details the reader is referred to [83]. The statistical model has been calibrated for the period 1874-1965. The MIB data of the period 1966-1995 were used for an independent verification of the statistical model. [83] found that 60 % of the MIB variance can be captured by the indices. This is significant lower than our results with an explained variance of 91 % in run 394 for the same period.

As already mentioned, [109] correlated MIB and the mean air temperature from November to March of the 10° grid area ($55-65°N$, $20-30°E$) for the period 1855-1990, and MIB and a zonal winter index of SLP for the period 1899-1993. Using a linear (exponential) statistical model, he found a rms error of $46 \times 10^9\, m^2$ ($45 \times 10^9\, m^2$) and an explained variance of 70 % (86 %) utilizing the mean winter air temperature. Correspondingly, he calculated a rms error of $81 \times 10^9\, m^2$ ($85 \times 10^9\, m^2$) and an explained variance of 52 % (54 %) utilizing the zonal SLP index. The rms errors utilizing the mean winter air temperature are slightly smaller than for our results of the period 1903-1998 but only the exponential statistical model can explain slightly more variance than in the best RCO run (Tab.12). This is not surprisingly as the figures by [109] are calculated for the fitting period. Therefore, we regard our results as satisfactory. In addition to biases of the reconstruction, biases of the bulk formulae for the parameterization of the surface fluxes and biases of the ice model itself have to be considered.

8.8.2 Ice cover 1960-1994

Figure 35 shows simulated total ice coverage with an ice concentration larger than 0.1 compared with calibrated gridded weekly ice cover data from the Global Digital Sea Ice Data Bank of the USA National Ice Center, see [98]. The agreement between model results and

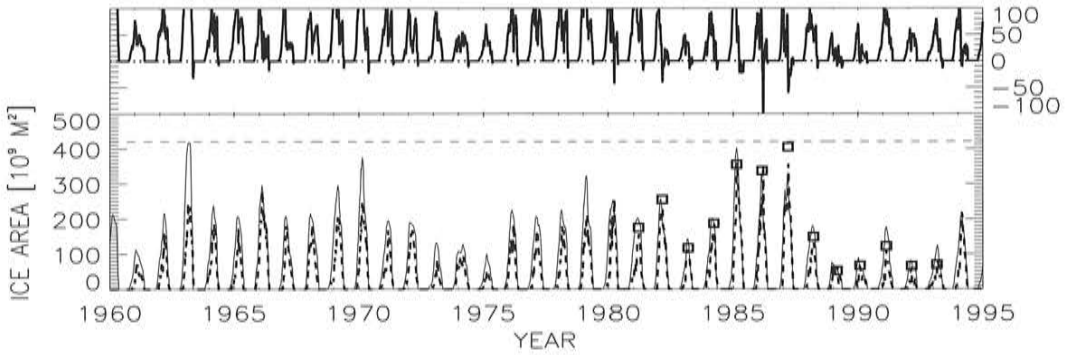

Figure 35: *Ice extent (in $10^9\, m^2$): observations (dashed), model results (solid, run 394). The squares denote observed maximum ice extent regularly published by FIMR. The difference between model results and observations is shown in the upper panel.*

observations is good but the ice cover is overestimated generally. This finding corresponds to the already mentioned positive bias of the annual maximum ice extent.

8.8.3 Ice cover 1980-1993

The period 1980-1993 has been investigated earlier with RCO using observations from the SMHI database as atmospheric forcing [73], [77]. Therefore, we have compared the errors of the long simulations with the errors calculated from the earlier performed simulations (Fig.36). Table 13 lists the errors compared to the calibrated weekly observations from the Global Digital Sea Ice Data Bank.

RUN	ME ($10^9\,m^2$)	RMSE ($10^9\,m^2$)	R	VAR
run 240	12.6	27.4	0.94	0.87
run 353	5.1	20.8	0.95	0.91
run 373b	32.6	52.0	0.93	0.63
run 403	23.1	40.2	0.92	0.76
run 394	20.5	36.6	0.94	0.79
run 420	20.3	37.7	0.90	0.77

Table 13: *Model errors of weekly mean ice cover for the period 1980-1993 for different RCO experiments (see Appendix A). (ME = mean error, $RMSE$ = root mean square error, R = correlation coefficient, VAR = explained variance.)*

We found for run 394 a mean error of ME = $21 \cdot 10^9\,m^2$ and a rms error of RMSE = $37 \cdot 10^9\,m^2$. Corresponding numbers of the best RCO hindcast run using the SMHI database as atmospheric forcing are ME = $5 \cdot 10^9\,m^2$ and RMSE = $21 \cdot 10^9\,m^2$ [77]. This run 353 has a horizontal resolution of 2 *nautical miles*. The corresponding experiment with a horizontal resolution of 6 *nautical miles* is run 240. We found a mean error of ME = $13 \cdot 10^9\,m^2$ and a rms error of RMSE = $27 \cdot 10^9\,m^2$. In all RCO runs, the ice cover during mild winters is slightly overestimated.

As the period 1980-1993 is a part of the fitting period, the discussed biases cannot be caused by the reconstruction of the variability. They might be related to the coarse sampling. The reconstruction yields only monthly surface fields for air temperature, dew point temperature, precipitation and cloudiness whereas the SMHI database contains three-hourly data. In the long simulations the ice season starts earlier (Fig.36). As this is also the case for run 420 (not shown), the latent heat bias may be caused not only by the underestimated specific humidity in the reconstruction but in addition also by too large wind speeds.

The three standard experiments are compared in Figure 37. The differences between run 394 and run 403 are actually small.

8.9 Seasonal thermocline

In Figure 38 temperature results of the standard experiments with initial conditions from May 1980 are compared for the period 1980-1993. The experiment 413 corresponds to run 373b, run 376 to run 375, run 402c to run 403, and run 414 to run 394 (see Tab.15 in Appendix A). In the runs 413, 376, and 402c the depths of the seasonal thermocline are underestimated whereas in run 414 (additional random wind component) we found quite realistic results.

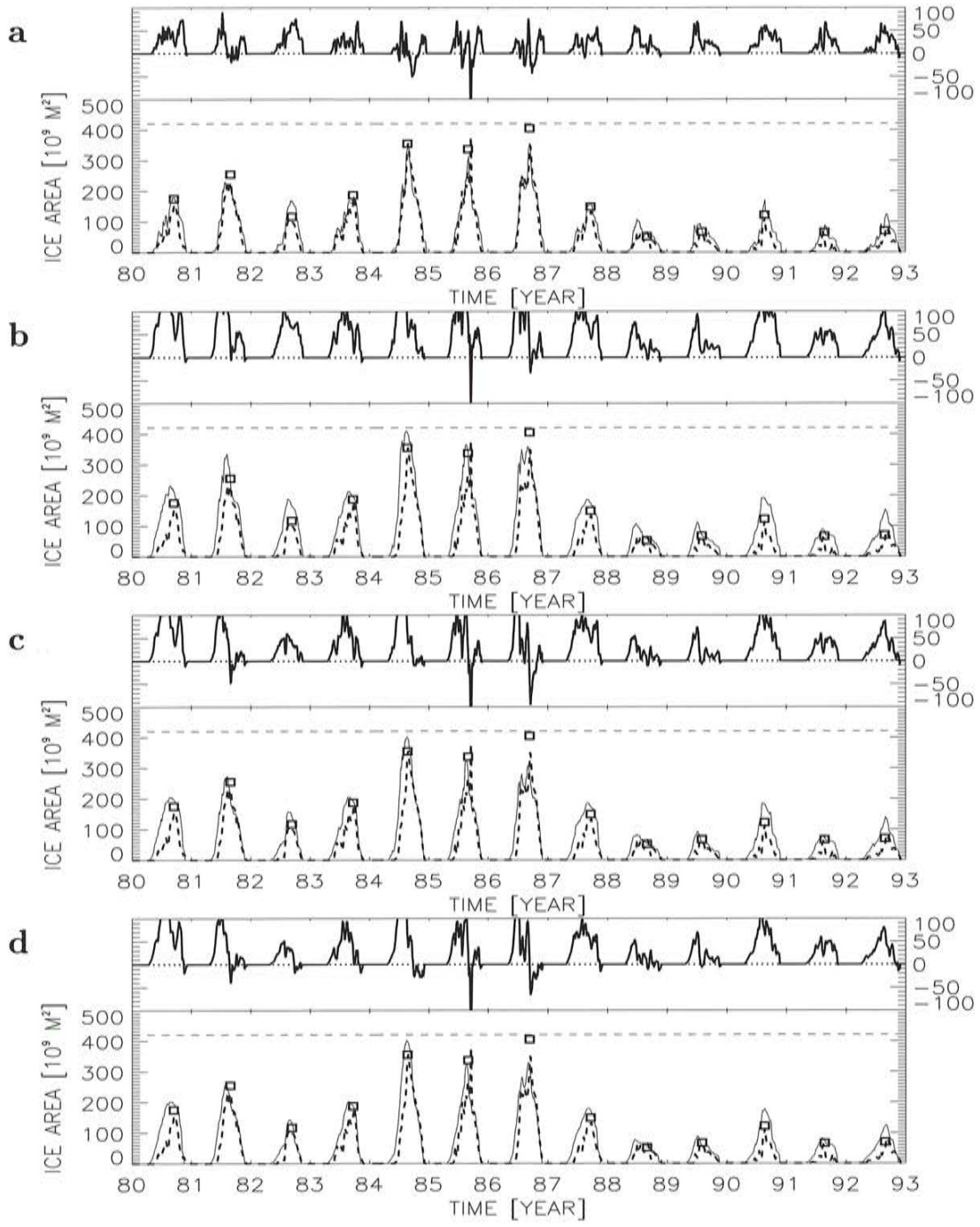

Figure 36: *Ice extent (in $10^9\,m^2$): observations (dashed), model results (solid). The squares denote observed maximum ice extent regularly published by FIMR. The difference between model results and observations is shown above every panel. (a) run 240 (three-hourly atmospheric forcing calculated from the SMHI database), (b) run 373b, (c) run 403, and (d) run 394.*

9 Sensitivity studies

The stratification of an estuary in humid climate like the Baltic Sea is mainly governed by the high saline water entering the system from the North Sea, by the freshwater surplus includ-

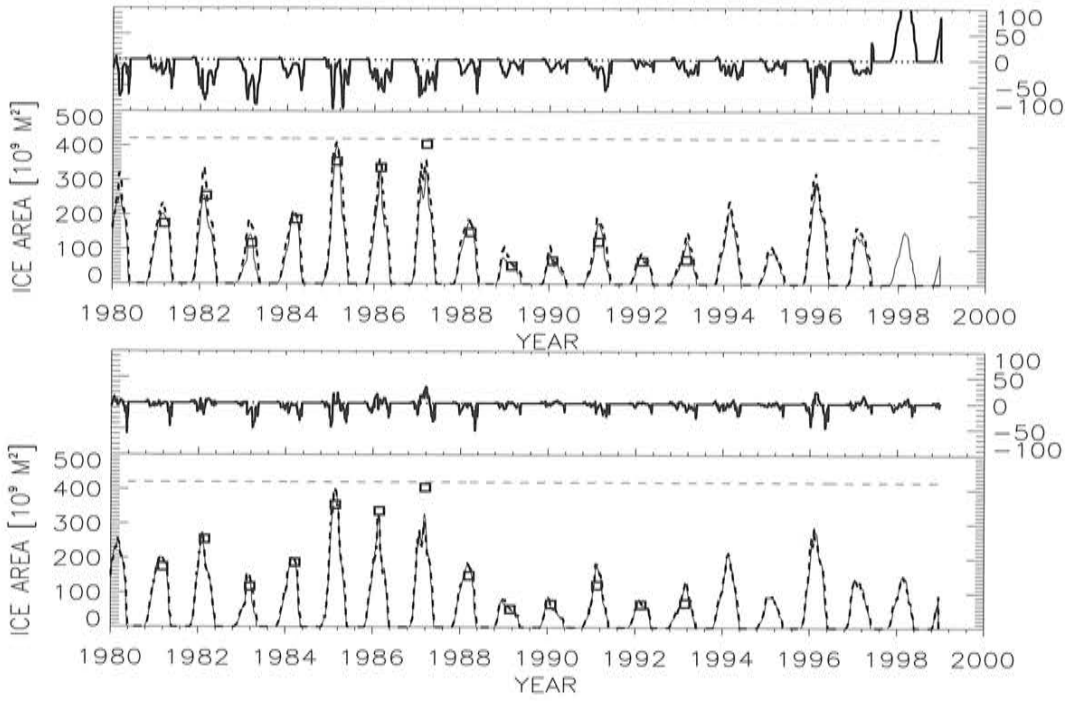

Figure 37: *Simulated ice extent (in* $10^9\ m^2$*). Upper panel: run 394 (solid), run 373b (dashed), and difference between run 394 and run 373b (upper part of the panel). Lower panel: run 394 (solid), run 403 (dashed), and difference between run 394 and run 403 (upper part of the panel). The squares denote observed maximum ice extent regularly published by FIMR. Note that run 373b ends already in April 1997.*

ing positive net precipitation, and by mixing between water masses. The relative impacts of these factors for decadal variability of salinity will be quantified in the following.

In addition, less obvious factors like sea ice are addressed. [118] have modeled the influence of ice on sea level variations in the Baltic Sea for three study cases each covering a period of 120 hours. They have shown that the water piling-up with ice is decreased to one-third and that for severe ice conditions the current field magnitude dropped to 20 % from the ice-free case. As saltwater inflows have never been observed in the second part of the inflow season, i.e. from January to April, during severe winters [29], one might speculate whether saltwater inflows are hampered by the rigid lid of sea ice especially during extremely severe winters when the entire surface area becomes ice covered. Thus, a colder climate would have an impact on Baltic Sea salinity via reduced saltwater inflows. This hypothesis is checked in this section.

The sea level in Kattegat is important for the barotropic transports through the Danish Straits. Thus, a realistic long simulation requires high quality data at the open boundary. For the past century these observations are available at Strömstad and Smögen (see Section 7.1). However, for even longer periods no data exist. In addition, the assessment of saltwater inflows in climate change scenarios requires a predictive relationship between the meridional SLP difference across the North Sea and the Kattegat sea level as presented by [36]. This relationship has been utilized in the latest, at the Rossby Centre performed scenario time slice experiments [74], [25]. Here, the impact of the calculated sea level in Kattegat for the water exchange between North Sea and Baltic Sea is investigated.

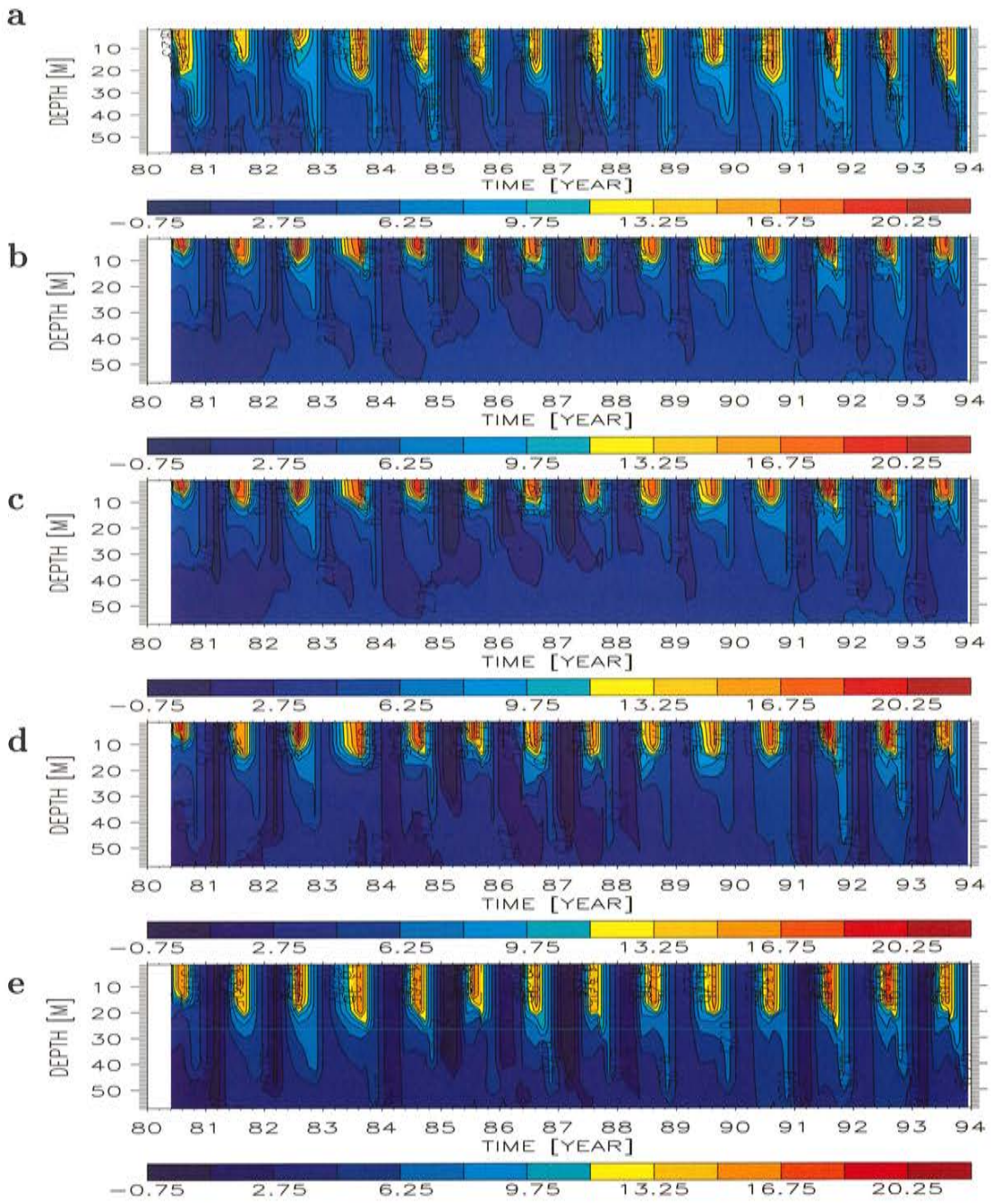

Figure 38: *Isotherm depths (in °C) in the eastern Gotland Basin (BY15): (a) observations, (b) reference experiment with $c_u = 1.2$ (run 413), (c) modified k model with $c_u = \sqrt{c_{\varepsilon 2}/c_{\varepsilon 1}}$ (run 376), (d) as (c) but modified wind reduction with $a_{red} = 0.78$ (run 402c), (e) as (c) but additional random wind component (run 414). Only the upper 60 m are shown.*

9.1 The influence of mixing

9.1.1 Experiments for the period 1980-1993

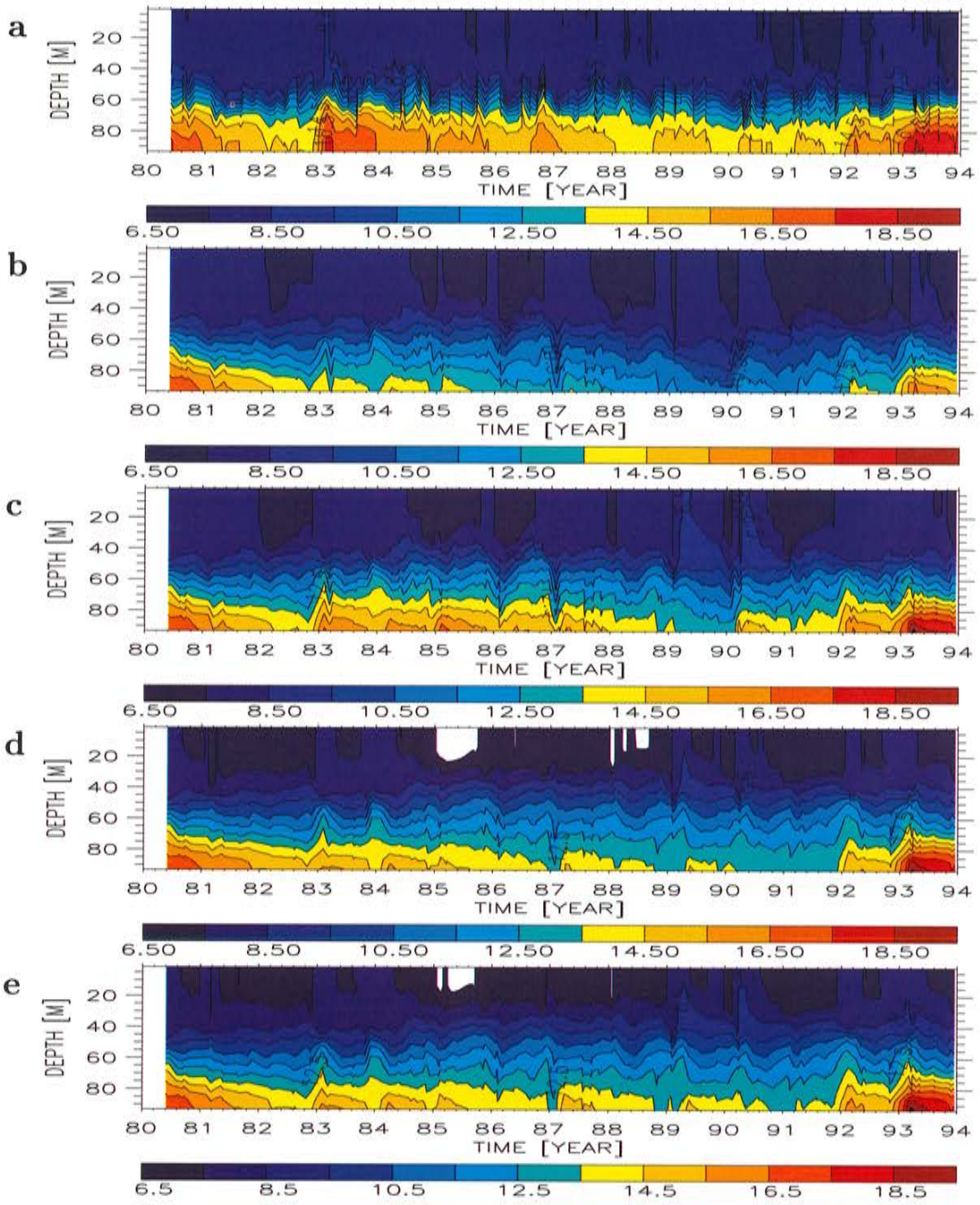

Figure 39: *(a) Observed and (b-e) simulated isohaline depths (in psu) at Bornholm Deep (BY5): (b) $k-\varepsilon$ model and SMHI database (run 240), (c) k model and SMHI database (run 264), (d) improved k model with increased flux of turbulent kinetic energy at the surface and reconstructed atmospheric forcing (run 361), (e) improved k model, increased deepwater mixing and reconstructed atmospheric forcing (run 362c).*

A series of 13-year long simulations for the period 1980-1993 has been performed. Observed temperature and salinity profiles from May 1980 in each sub-basin have been used to initialize

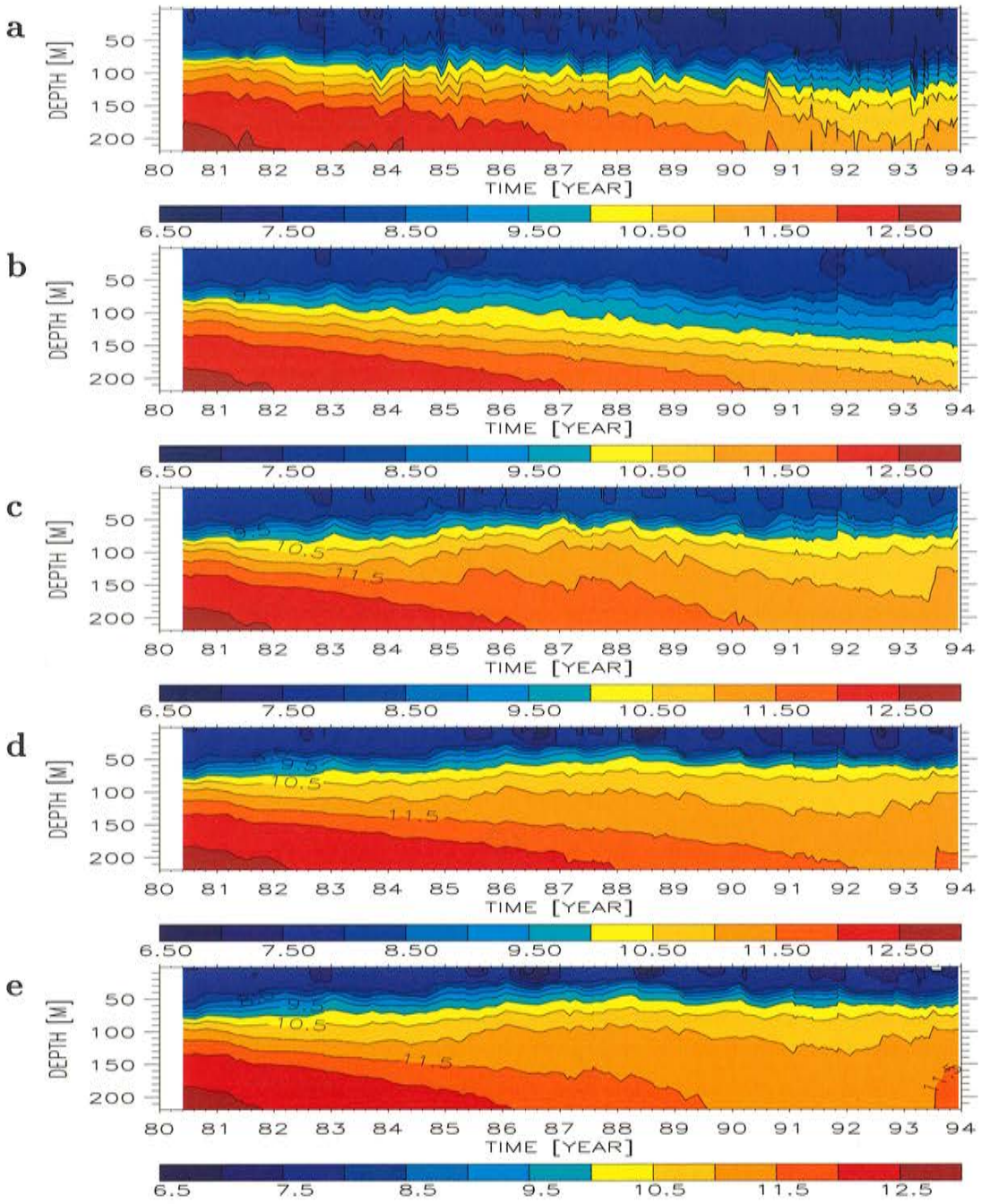

Figure 40: *(a) Observed and (b-e) simulated isohaline depths (in psu) at Gotland Deep (BY15): (b) $k-\varepsilon$ model and SMHI database (run 240), (c) k model and SMHI database (run 264), (d) improved k model with increased flux of turbulent kinetic energy at the surface and reconstructed atmospheric forcing (run 361), (e) improved k model, increased deepwater mixing and reconstructed atmospheric forcing (run 362c).*

the experiments. The atmospheric forcing is either based on three-hourly gridded observations of the SMHI database (run 240, 264) or calculated with the statistical model described in Section 5.1 (run 361, 362c). Observed and simulated salinity profiles in Bornholm and Gotland Basin are shown in Figures 39 and 40, respectively.

In run 240, the standard $k-\varepsilon$ model has been utilized (Section 3.1). During the stagnation period, the halocline depth in Gotland Basin is simulated realisticly but the salt transports into the Bornholm Basin are underestimated (Fig.39b, cf. [71]). As the deepwater salinity in Bornholm Basin has decreased too much at the end of the simulation period, a deepwater renewal in Gotland Basin after the major saltwater inflow in January 1993 does not occur (Fig.40b).

In run 264, the standard $k-\varepsilon$ model has been replaced with a k turbulence model based on Equation (20) (Section 3.2). The amount of inflowing saltwater into the Bornholm Basin is improved significantly (Fig.39c). Even the Gotland Basin deepwater is ventilated during 1993 (Fig.40c). However, the observed deepening of the halocline depth with a maximum depth during 1992 cannot be reproduced by the model. The results are even worse if the daily atmospheric forcing of the statistical model is used instead of three-hourly observations of the SMHI database (not shown). Surface layer mixing is underestimated.

To increase the vertical flux of turbulent kinetic energy, the coefficient m of Equation (25) has been increased by a factor of 5 in run 361. As in the turbulence enhanced surface layer the divergence of the turbulent kinetic energy flux balances dissipation (22), the effect for the halocline depth is negligible (Fig.40d). However, good results are obtained concerning the saltwater inflows (Figs.39d and 40d). As the reduction of deepwater salinity in the Gotland Basin during the stagnation period is somewhat too low in this experiment, the coefficient for the deepwater mixing (39) has been adjusted in run 362c to $\alpha = 0.75 \cdot 10^{-3}\, cm^2\, s^{-2}$ (Figs.39e and 40e).

9.1.2 Experiments for the period 1902-1998

During the unique stagnation period 1983-1992, the problem of the standard $k-\varepsilon$ model simulating overflows into the Gotland Basin does not seriously appear. However, the results for the Bornholm Basin are not satisfactory as shown in the previous sub-section. The problem is more severe for the Baltic proper when periods with several major saltwater inflows are simulated. The results for the long period 1902-1998 show that salinity in the lower layer of the Gotland Basin is underestimated significantly although many saltwater inflows (including the one from January 1993) appear correctly (Fig.41).

To improve simulated saltwater inflows, the k model utilizing Equation (52) has been implemented in RCO (see Section 3.5). A series of sensitivity experiments has been performed testing different values for the model coefficient c_u. The simulation results are extremely sensitive to this model parameter (Fig.42). If $c_u = 1$ is used, salinity in the lower layer of the Gotland Basin is very much overestimated (Fig.42a) whereas significant underestimation occurs with $c_u = 1.5$ (Fig.42d), comparable with the results of the standard $k-\varepsilon$ model. As the theoretically derived value should be $c_u = \sqrt{c_{\varepsilon 2}/c_{\varepsilon 1}} = 1.1547$ (Section 3.5), the somewhat overestimated deepwater salinities in Figure 42b indicate that the baroclinic transports are too large due to the too shallow halocline depth. Thus, it is very important that in connection with the improved mixing parameterization the wind driven turbulence generation is as realistic as possible. In the experiments presented in Figure 42 a surface wind parameterization has been used with a significantly shifted frequency distribution of wind speeds towards lower than observed values as shown in Figure 5 of Section 5.2. Thus,

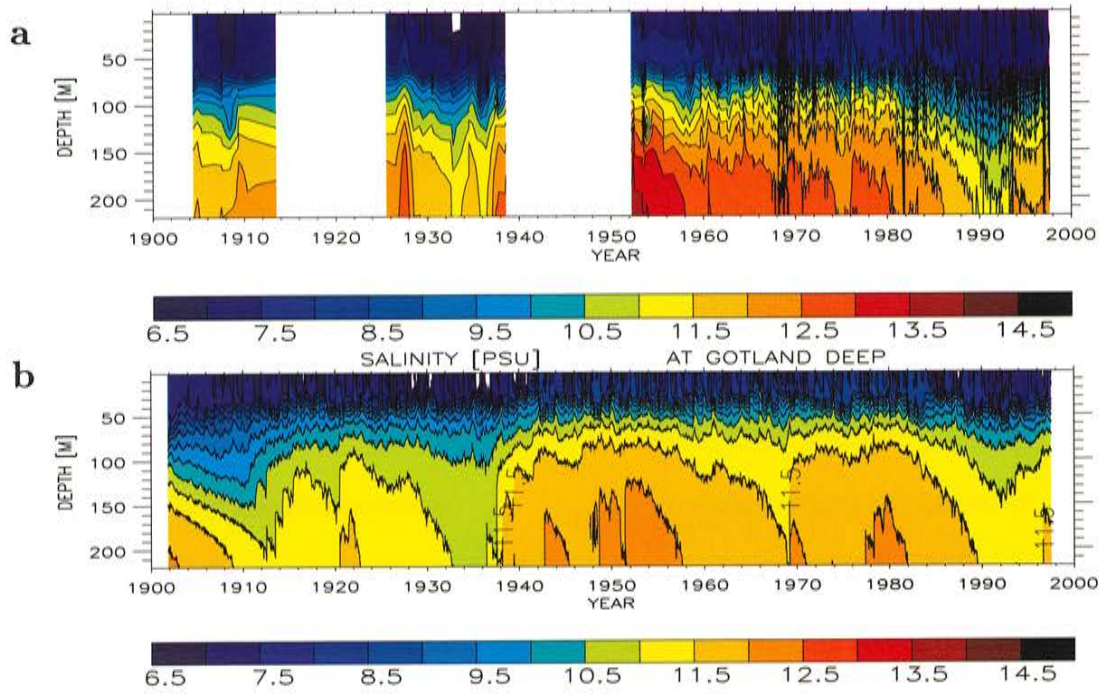

Figure 41: *Isohaline depths (in psu) in the eastern Gotland Basin (BY15): (a) observations, (b) $k-\varepsilon$ model with $\alpha = 0.5 \cdot 10^{-3}\, cm^2\, s^{-2}$ (run 368).*

mixing is underestimated causing a too shallow halocline. Better results are obtained if an increased wind reduction coefficient as in run 403 is used (Fig.17d). Indeed, in experiment 403 an appropriate choice for the model parameter c_u is found to be $c_u = \sqrt{c_{\varepsilon 2}/c_{\varepsilon 1}} = 1.1547$.

Although the approach adding a random wind component (run 394) results in a realistic frequency wind speed distribution at Landsort (Fig.5), deepwater salinity is somewhat underestimated (Fig.43b). If $c_u = 1.11$ is used instead of $c_u = 1.1547$ (run 396), the simulated lower layer salinity is very close to observations (Fig.43c). However, a drift of simulated upper layer salinity to higher than observed values is the drawback of this modification. Obviously, too much salt is mixed from the lower into the upper layer.

9.2 The influence of fresh- and saltwater forcing

In this sub-section, the sensitivity of Baltic Sea salinity on precipitation and river runoff is explored. As mentioned in the introduction, [66] suggested that increased winter runoff reduce the probability of major inflows. As indeed a stronger meridional SLP gradient across the North Atlantic is correlated with lower salinities in the Baltic Sea at all depths [119], the question is whether increased runoff really hampers saltwater inflows. Alternatively, it might be possible that during decades with increased precipitation and runoff saltwater inflows occur less often due to the atmospheric wind stress conditions. To check the hypothesis of [66], we performed a series of sensitivity experiments with modified freshwater inflow. In addition, we investigated the impact of the decadal variability of the wind forcing on saltwater inflows and finally on Baltic Sea salinity. Thereby, two standard experiments for the period 1902-1998 have been used as a reference, i.e. run 373b and run 403.

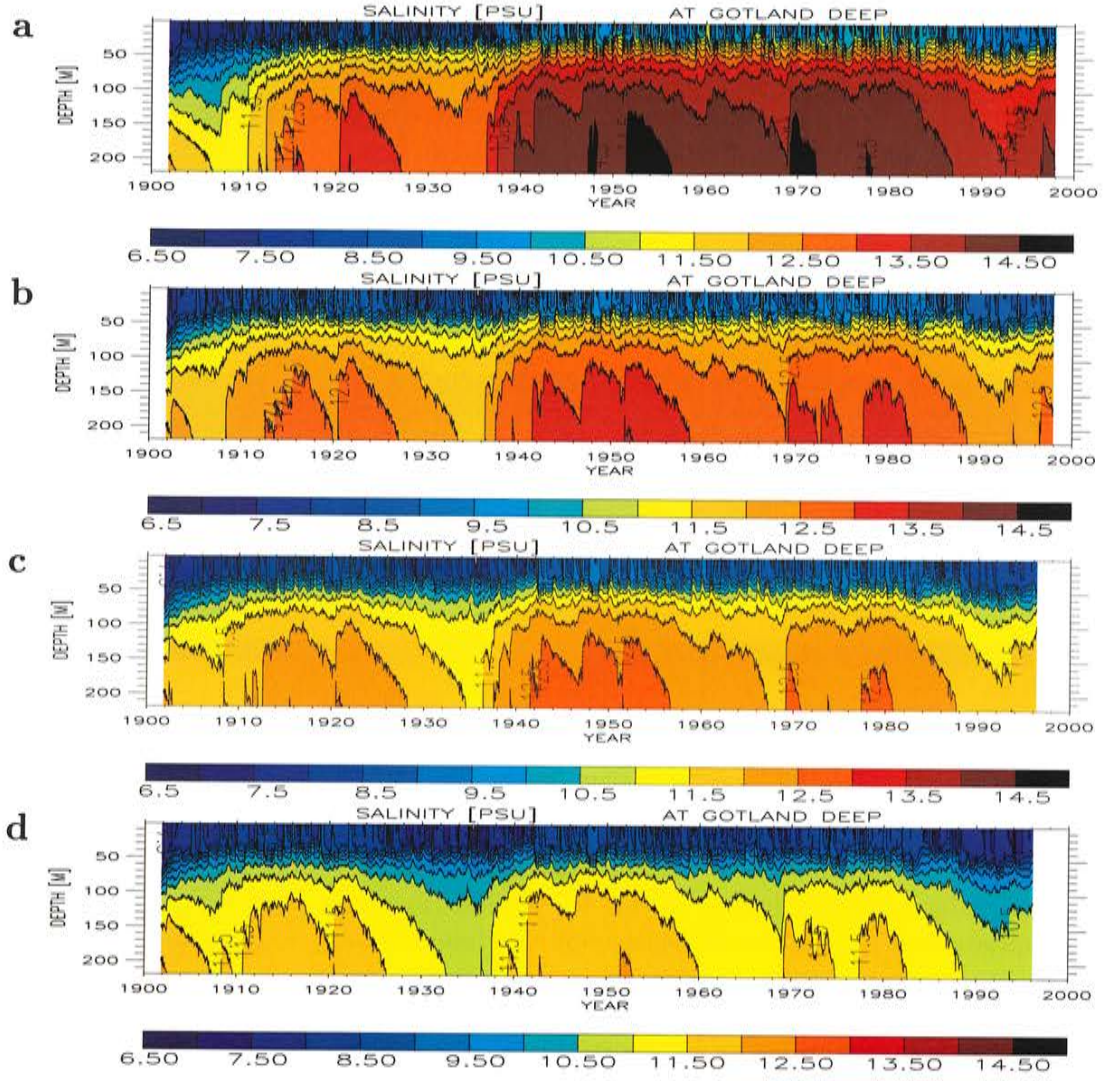

Figure 42: *Isohaline depths (in psu) in the eastern Gotland Basin (BY15): k model with (a)* $c_u = 1$ *(run 366), (b)* $c_u = \sqrt{c_{\varepsilon 2}/c_{\varepsilon 1}} = 1.1547$ *(run 375), (c)* $c_u = 1.2$ *(run 373b), and (d)* $c_u = 1.5$ *(run 371). In all experiments, the coefficient for deepwater mixing is* $\alpha = 0.75 \cdot 10^{-3}\, cm^2\, s^{-2}$. *Observations are shown in Fig.41a.*

9.2.1 Salinity in the Gotland Basin

In Figures 44 and 45 results of the sensitivity experiments based on the standard experiment 373b are shown for salinity profiles in the eastern Gotland Basin. Correspondingly, the reference experiment in Figures 46 and 47 is run 403. Experiments with climatological monthly mean runoff, i.e. without inter-annual variability, are runs 383, 404, 406, 409, and 418 (Tab.16). To exclude the period since the construction of dams in Sweden and Finland became conspicuous (since the 1970s), in 404, 406, 409, and 418 the mean seasonal cycle is calculated for the period 1902-1970 (Fig.10). In addition, in these experiments inter-annual variability of precipitation is removed as well. In the shorter run 406 even inter-annual variabilities of air temperature, specific humidity (or dew point temperature), and total cloudiness

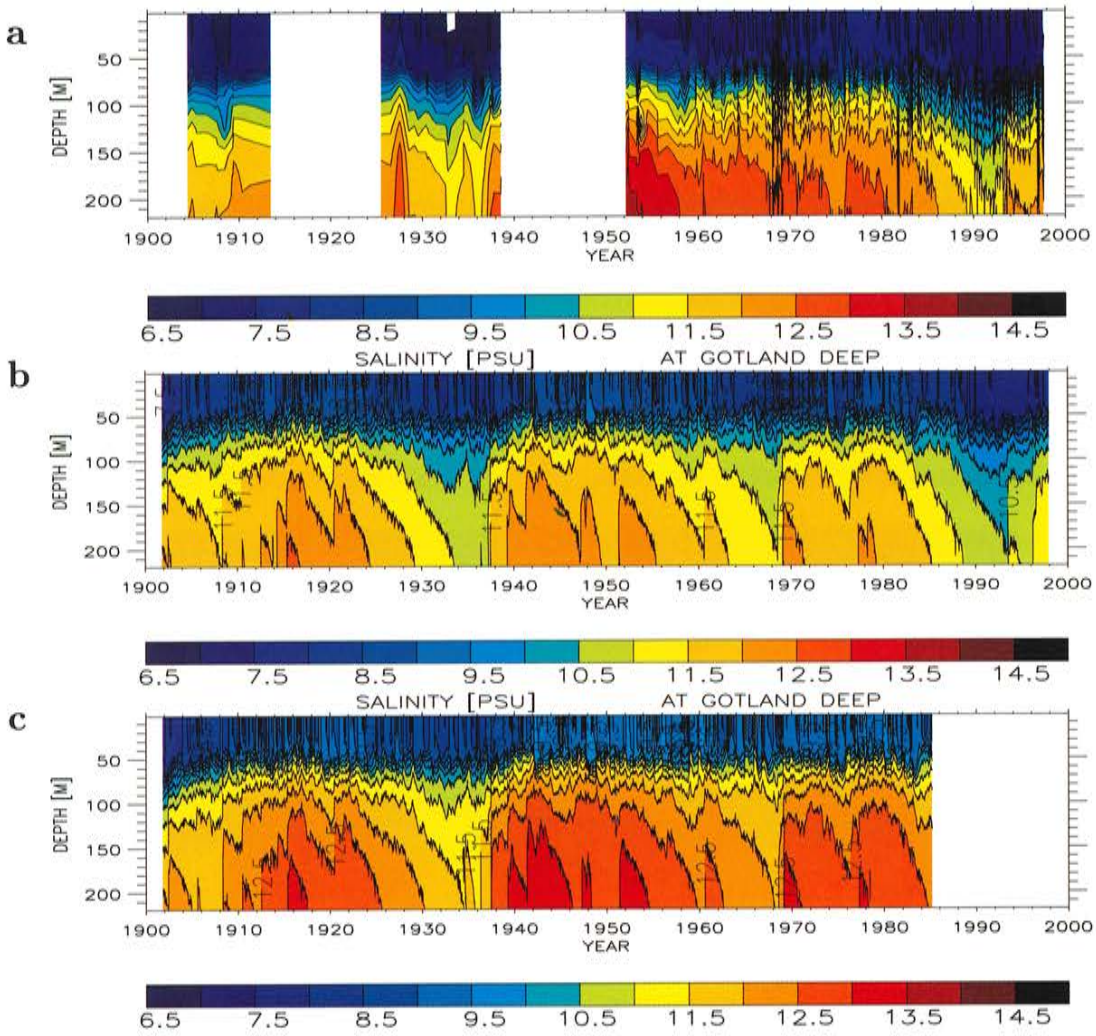

Figure 43: *Isohaline depths (in psu) in the eastern Gotland Basin (BY15): (a) observations, (b) k model with* $c_u = \sqrt{c_{\varepsilon 2}/c_{\varepsilon 1}} = 1.1547$ *and random wind component (run 394), (c) k model with* $c_u = 1.11$ *and random wind component (run 396).*

have been omitted.

The variability of salinity is clearly reduced showing the important impact of freshwater inflow variations on decadal time scale (Figs.44c, 44d, 45a, 45b, and 46c). As simulated net precipitation amounts to 13 % of the total freshwater inflow of $16,115\,m^3\,s^{-1}$ (Section 8.7, run 403), also net precipitation influences decadal salt variability but to a smaller extent (Fig.44d).

However, there is still significant decadal variability left in the system which can only be explained by saltwater inflow variations because inter-annual variabilities of air temperature, specific humidity and total cloudiness have a negligible impact (Fig.45c). The still pronounced minima in the 1930s and in the 1990s indicate that fresh- and saltwater inflows are not independent forcing mechanisms but anti-correlated during certain decades. During the 1920s and during the 1980s runoff and precipitation were larger than the climatological

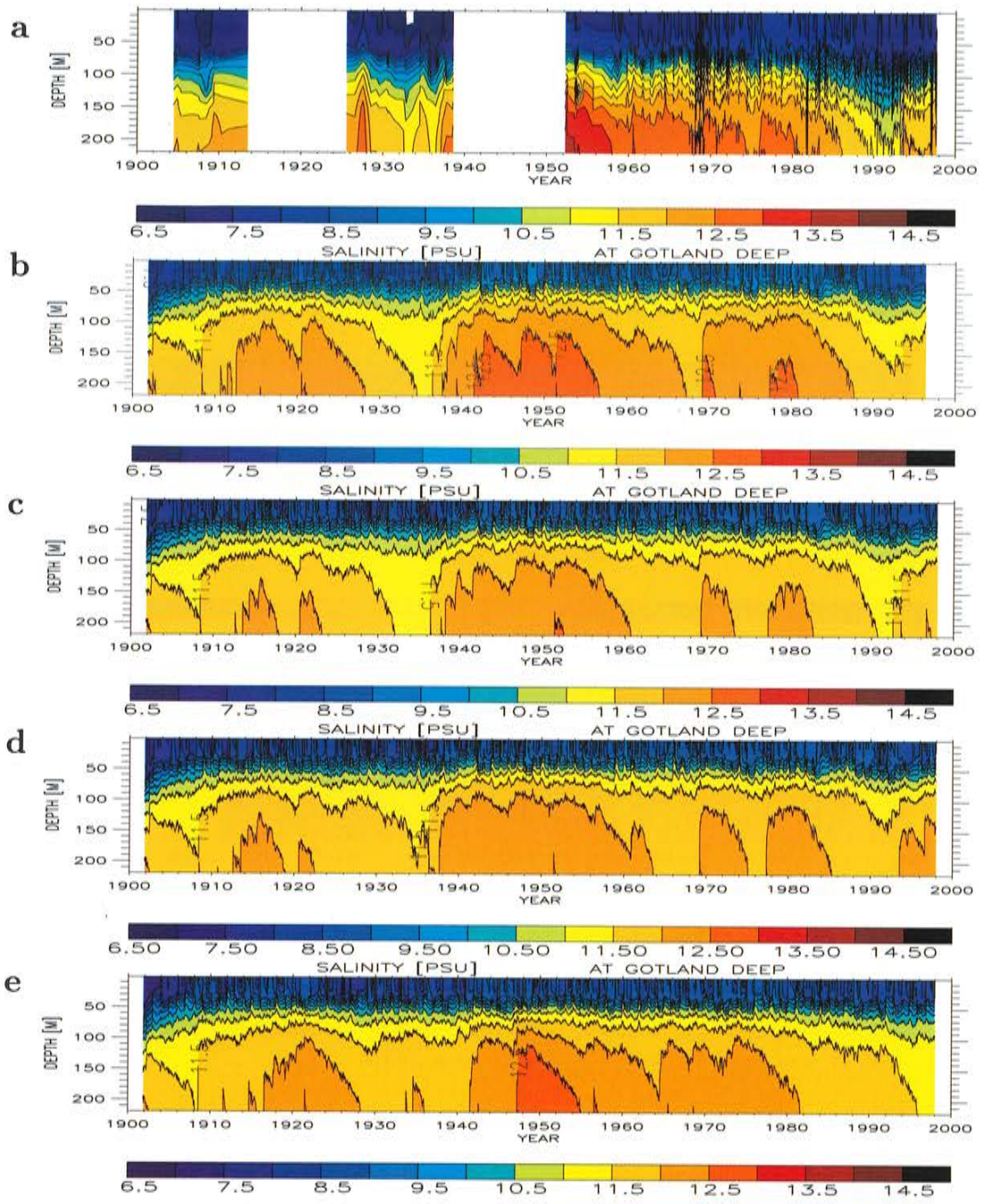

Figure 44: *Isohaline depths (in psu) in the eastern Gotland Basin (BY15): (a) observations, (b) reference experiment (run 373b, cf. Fig.17b), (c) as (b) but with climatological monthly mean river runoff of the period 1902-1998 (run 383), (d) as (b) but with climatological monthly mean river runoff and precipitation of the period 1902-1970 (run 404), (e) as (b) but forced with a series of random years for SLP, surface wind and sea level in Kattegat (run 393).*

mean (Figs.8 and 11).

A second set of sensitivity experiments was performed with a series of random years for sea level pressure, surface wind and sea level in Kattegat but with observed freshwater inflow, i.e. saltwater inflows occur randomly in time but with the statistics for the period 1902-1998.

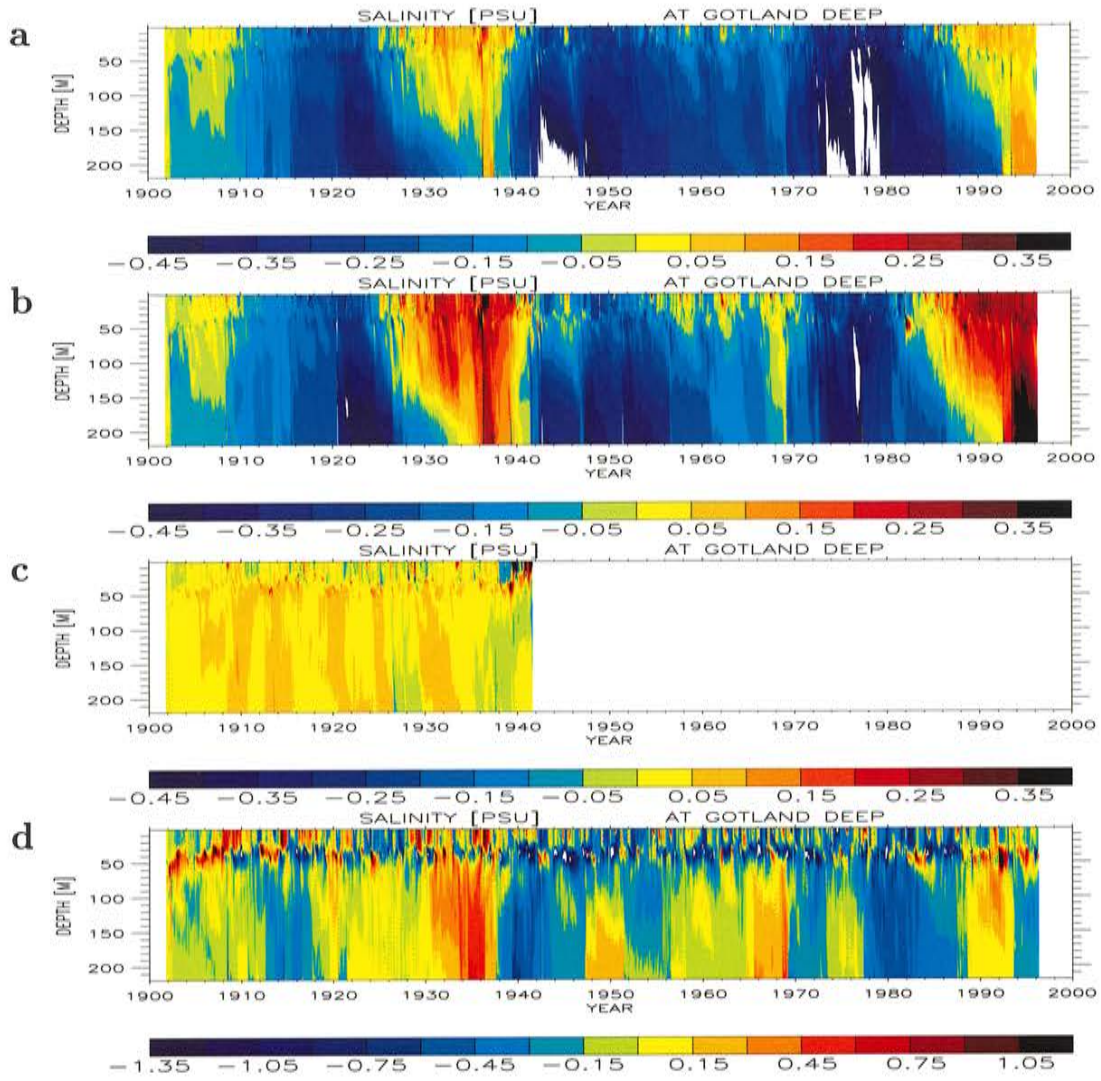

Figure 45: *Isohaline depths (in psu) in the eastern Gotland Basin (BY15): (a) difference between Fig.44c and Fig.44b (run 383 minus run 373b), (b) difference between Fig.44d and Fig.44b (run 404 minus run 373b), (c) difference between the experiment with climatological monthly mean river runoff, precipitation, air temperature, specific humidity and cloudiness of the period 1902-1970 and the run shown in Fig.44d (run 406 minus run 404), (d) difference between Fig.44e and Fig.44b (run 393 minus run 373b). Note the different color bar in (d).*

The "saltwater inflow years" are defined from July 1 to June 30 of the following calendar year. The random procedure does not include restrictions, i.e. the time series may include a "saltwater inflow year" more than once. The results show that the variability of salinity changes tremendously but there is still a minimum during the 1990s (Figs.44e, 45d, and 46e).

The influence of river regulation is addressed in another experiment (run 408) for the period 1942-1998 with climatological monthly mean river runoff and precipitation of the period 1902-1970 and observed inter-annual variability, i.e. the positive trend of winter runoff is removed (Fig.9) and a mean seasonal cycle of natural river discharge is applied (Fig.10). Thus, it is assumed that river regulation only redistributes the discharge from summer to winter without

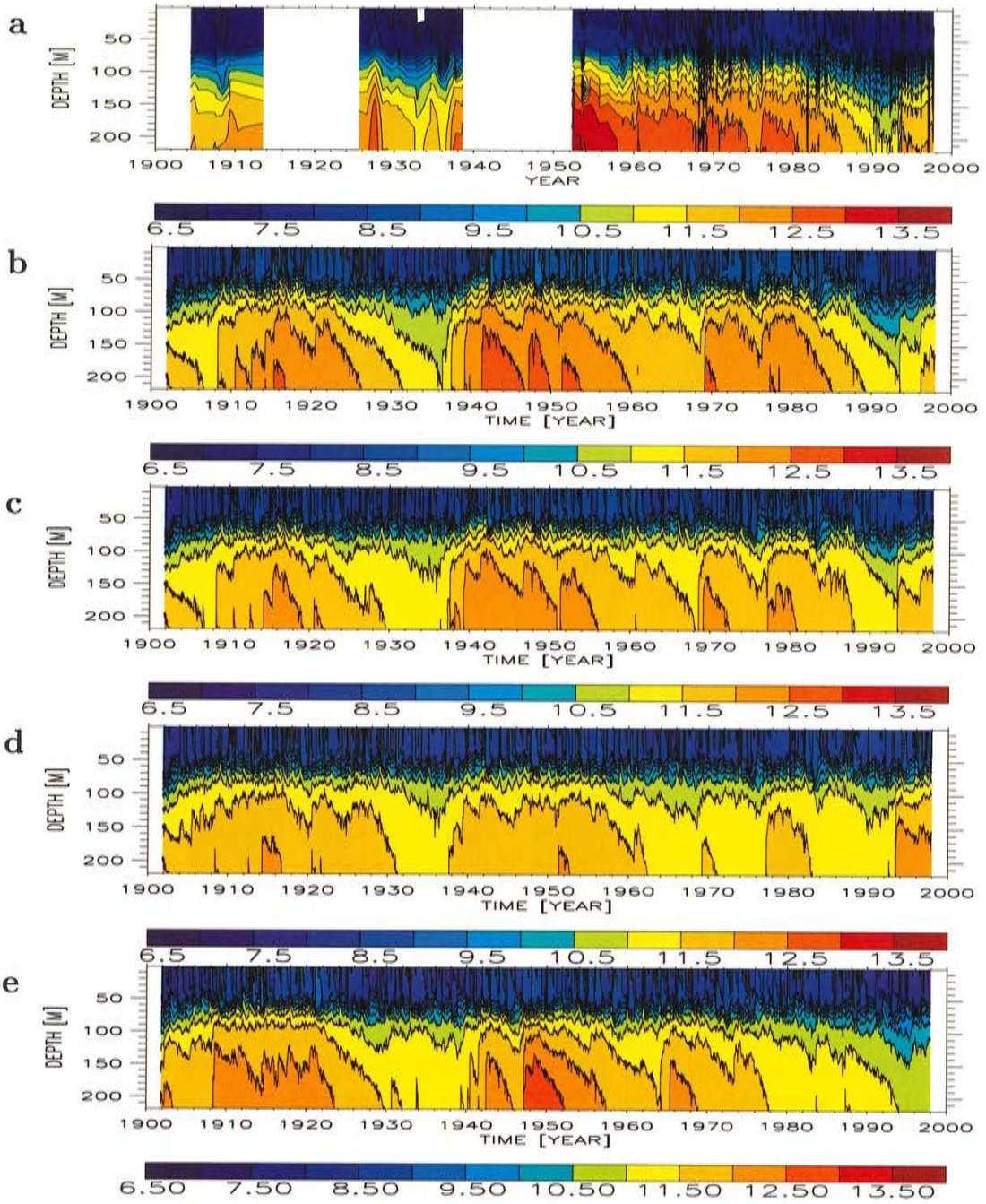

Figure 46: *Isohaline depths (in psu) in the eastern Gotland Basin (BY15): (a) observations, (b) reference experiment (run 403, cf. Fig.17d), (c) as (b) but with climatological monthly mean river runoff and precipitation of the period 1902-1970 (run 409), (d) as (c) but with 4-year high-pass filtered SLP and correspondingly surface wind (run 418), (e) as (b) but forced with a series of random years for SLP, surface wind and sea level in Kattegat (run 410).*

changing the annual mean runoff. The comparison with the reference experiment (run 403) shows that river regulation has almost no impact on salinity at Gotland Deep (Fig.47).

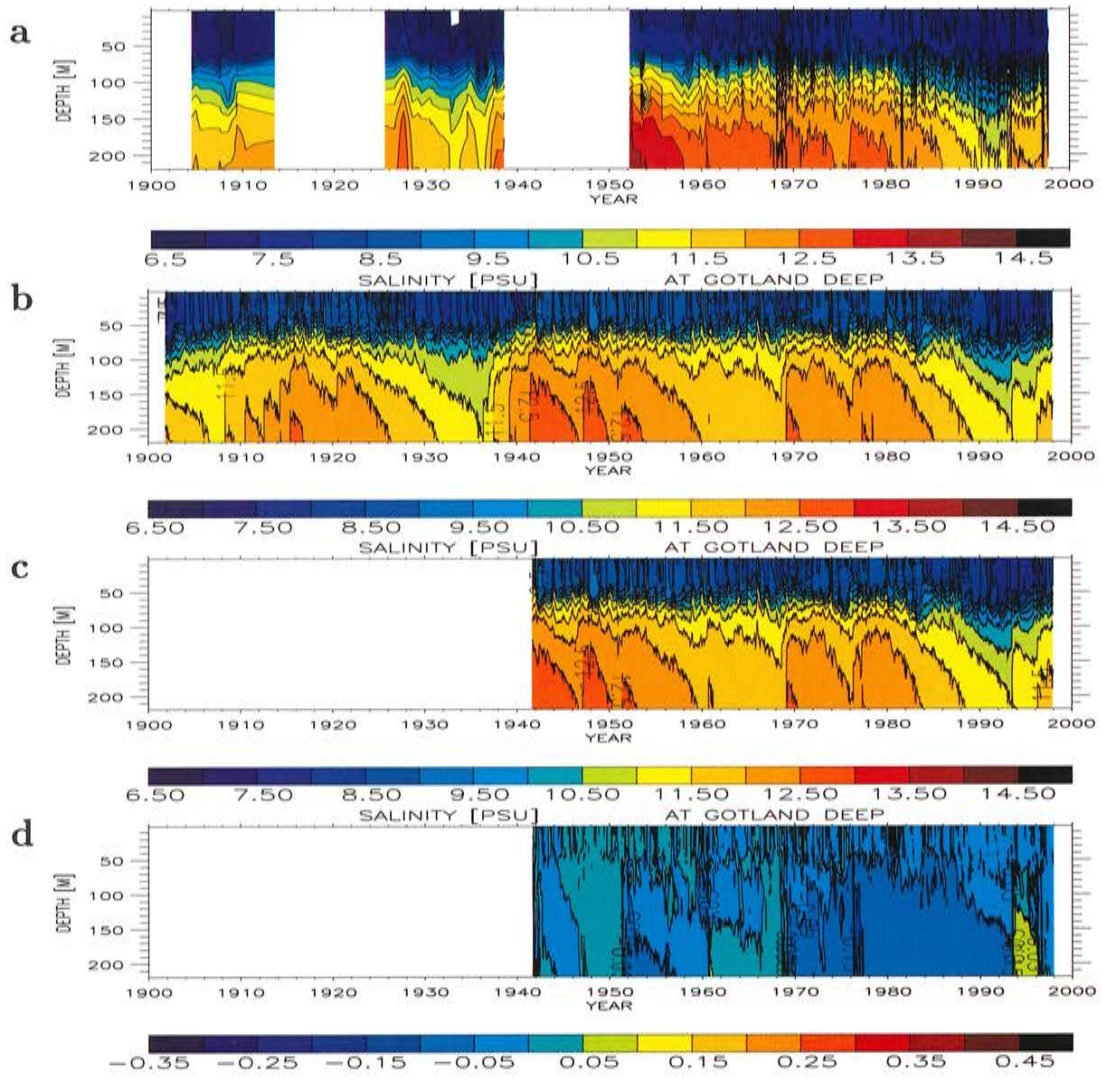

Figure 47: *Isohaline depths (in psu) in the eastern Gotland Basin (BY15): (a) observations, (b) reference experiment (run 403, cf. Fig.17d), (c) as (b) but with climatological monthly mean river runoff and precipitation of the period 1902-1970 and inter-annual variability for the period 1942-1998 (run 408), (d) difference between (c) and (b) (run 408 minus run 403).*

9.2.2 Saltwater inflows during 1902-1998

Volumes of high saline water (indicating saltwater inflows) of the previous mentioned sensitivity experiments (run 383, run 404, and run 393) in Arkona Basin, Bornholm Basin, and Gotland Basin are depicted in Figures 48 and 49. Results of the standard experiment (run 373b) are shown in Figure 19. For a discussion of the definition of saltwater inflows the reader is referred to Section 8.3. The results indicate that the freshwater inflow can modify the intensity of saltwater transports through Bornholm and Stolpe Channel significantly whereas the transports through the Danish Straits are relatively less affected.

The function of saltwater inflows into the Arkona Basin is completely different if the model is forced by a series of random years for SLP, surface wind and sea level in Kattegat, i.e. in run 393 (Fig.49). However, the record of high saline water in the Gotland Basin is amazingly

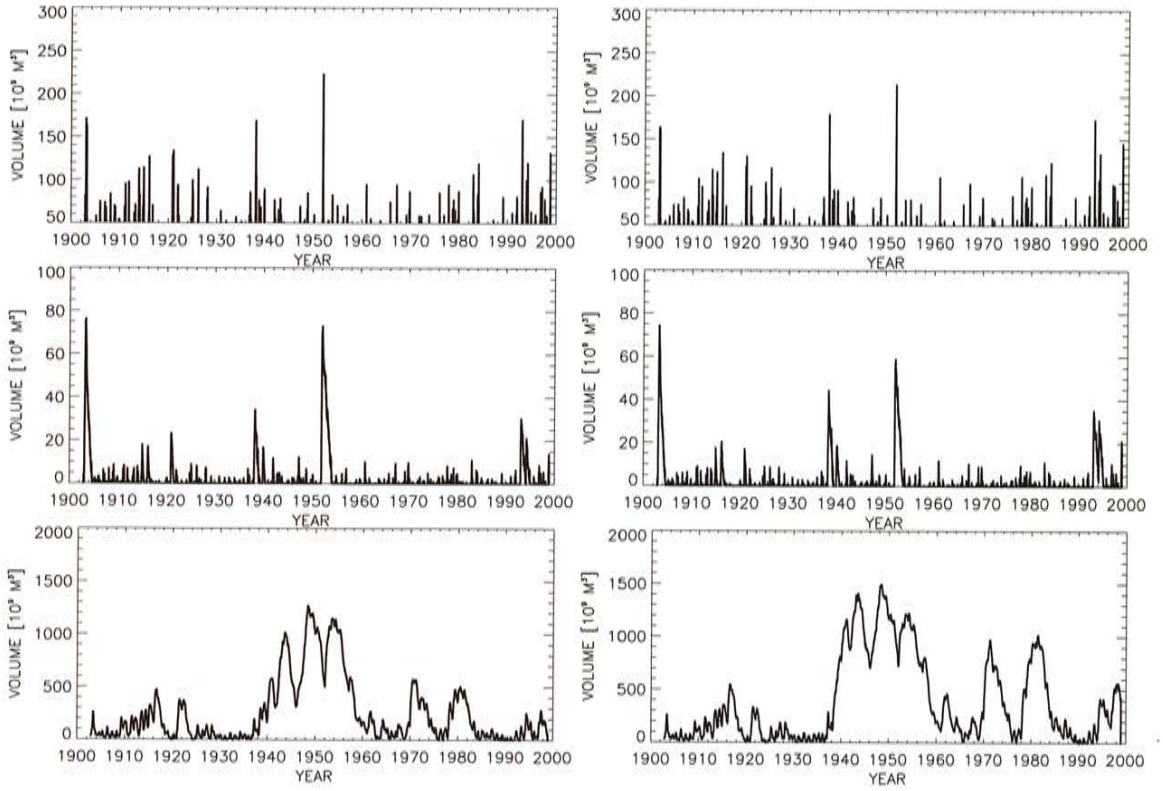

Figure 48: *Volume (in km^3) of high saline water in (upper panels) Arkona Basin ($S \geq 17\,psu$), (middle panels) Bornholm Basin ($S \geq 17\,psu$), and (lower panels) Gotland Basin ($S \geq 12\,psu$). The model results are from run 383 with climatological monthly mean river runoff of the period 1902-1998 (left) and from run 404 with climatological monthly mean river runoff and precipitation of the period 1902-1970 (right).*

similar compared to the reference experiment (Fig.19). For example, the largest during the last century observed (and simulated) saltwater inflow in November/December 1951 appears in 1987 but has only minor influence on salinity in the Baltic interior. Thereafter no strong major inflow occurs giving rise to the distinct salinity minimum in the Gotland Basin during the 1990s. Obviously the inflow of freshwater works as effective filter between the Bornholm Basin and the Gotland Basin hampering saltwater inflows during decades with increased runoff and precipitation. In Figure 50, the results of the reference experiment for the high saline water in the eastern Gotland Basin are rearranged in the same manner as the forcing for SLP, surface wind and sea level in Kattegat is calculated in run 393. The comparison with the lower panel in Figure 49 illustrates the non-linear filter function of the freshwater inflow.

The impact of the freshwater inflow and of the SLP decadal variability on the transports between sub-basins is visualized by calculating differences of volumes of high saline water in Arkona Basin, Bornholm Basin, and Gotland Basin (Figs.51 and 52). The standard run 403 is used here as a reference. Anomalously high river runoff hampers the inflow of high saline water ($S \geq 17\,psu$) into the Arkona Basin and Bornholm Basin. The change of the flow into the Bornholm Basin is a non-linear function of the discharge change indicating the complex impact of the Baltic Sea physics on the inflow. The volume of high saline water in Gotland Basin ($S \geq 12\,psu$) is significantly increased during periods with anomalously low

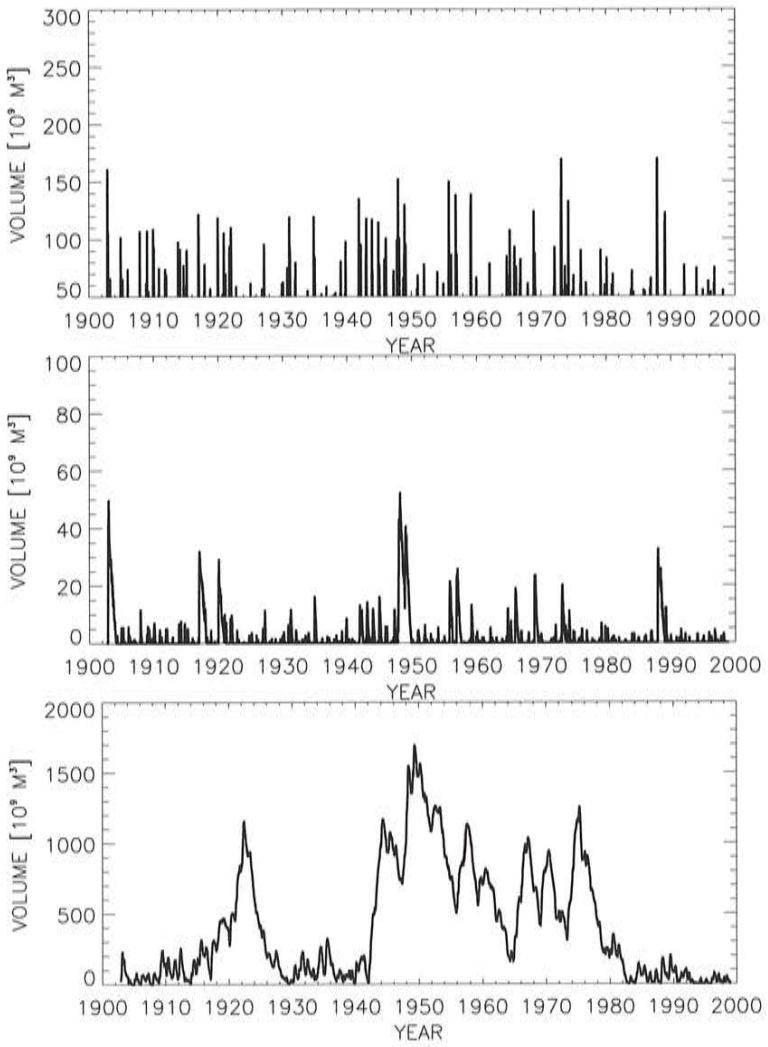

Figure 49: *Volume (in km^3) of high saline water in (upper panel) Arkona Basin ($S \geq 17\,psu$), (middle panel) Bornholm Basin ($S \geq 17\,psu$), and (lower panel) Gotland Basin ($S \geq 12\,psu$). The model results are from run 393 which is forced with a series of random years for SLP, surface wind and sea level in Kattegat.*

runoff. However, there is almost no change during periods with high runoff. This is caused by the definition of the salinity threshold of $S = 12\,psu$. In case of a threshold of $S = 9\,psu$, the difference is indeed negative (Fig.53). The volume changes of high saline water with $S \geq 9\,psu$ increase between Arkona Basin and Gotland Basin (Fig.53). This is explained by entrainment of water with $S < 9\,psu$ into the dense bottom currents.

The impact of the decadal SLP variability is similar. Increased westerlies during the 1920s and during the 1990s (see Section 9.2.5) reduce the volume of saline water with $S \geq 9\,psu$ in the Gotland Basin significantly. The stagnation periods caused by the freshwater inflow are shifted in time compared to the stagnation periods caused by the wind forcing. The first stagnation period caused by the wind forcing starts 1921 and ends 1934 whereas the first stagnation period caused by the freshwater inflow is lacking with 7 years. The latter starts 1928 and ends 1941. The second stagnation period starts 1989 (wind forcing) and 1985

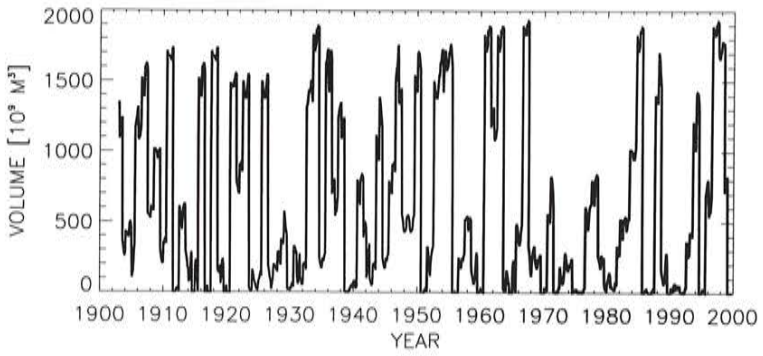

Figure 50: *Volume (in km^3) of high saline water in Gotland Basin ($S > 12\,psu$). The model results are from run 373b but monthly rearranged as in run 393.*

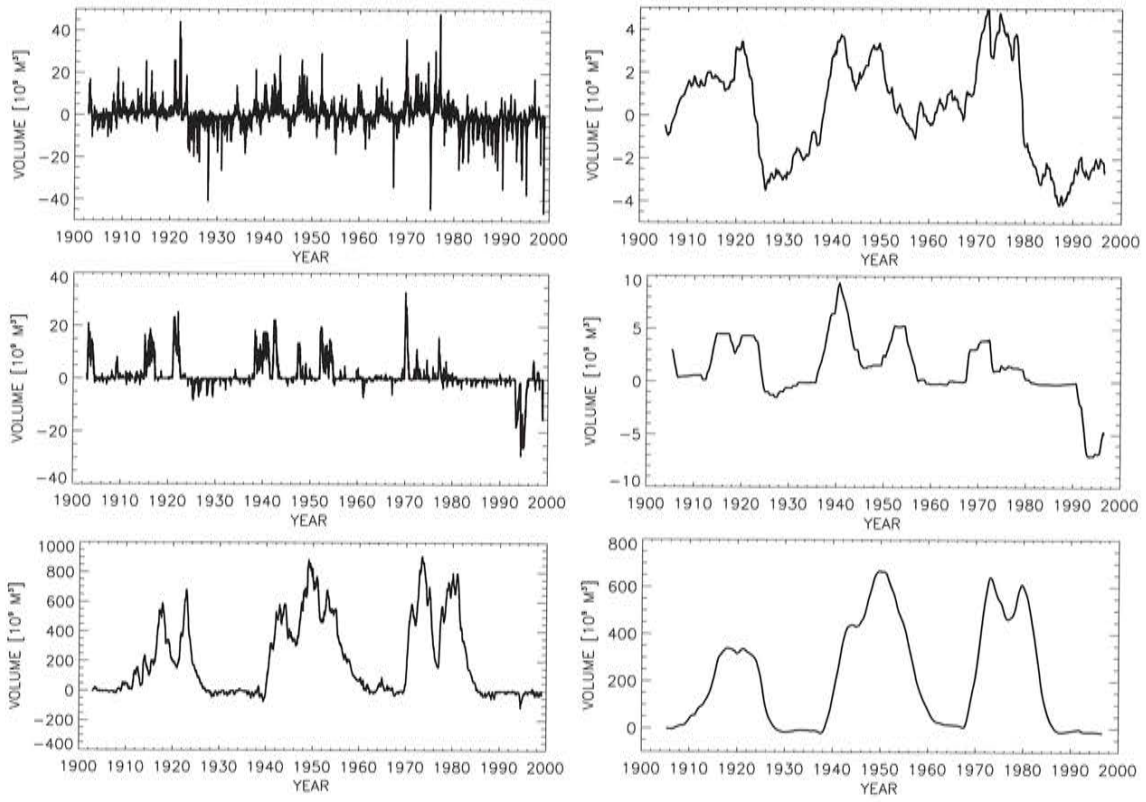

Figure 51: *Volume (in km^3) of high saline water in (upper panel) Arkona Basin ($S \geq 17\,psu$), (middle panel) Bornholm Basin ($S \geq 17\,psu$), and (lower panel) Gotland Basin ($S \geq 12\,psu$). Shown are unfiltered (left) and 4-year running mean (right) differences between model results from run 403 and run 409.*

(freshwater inflow).

The decadal variability of the forcing (runoff/precipitation and large-scale wind) has a relatively small impact on saltwater inflows across the Danish Straits into the Arkona Basin but a quite large impact on the entrainment rate of the salt transport between Bornholm Basin

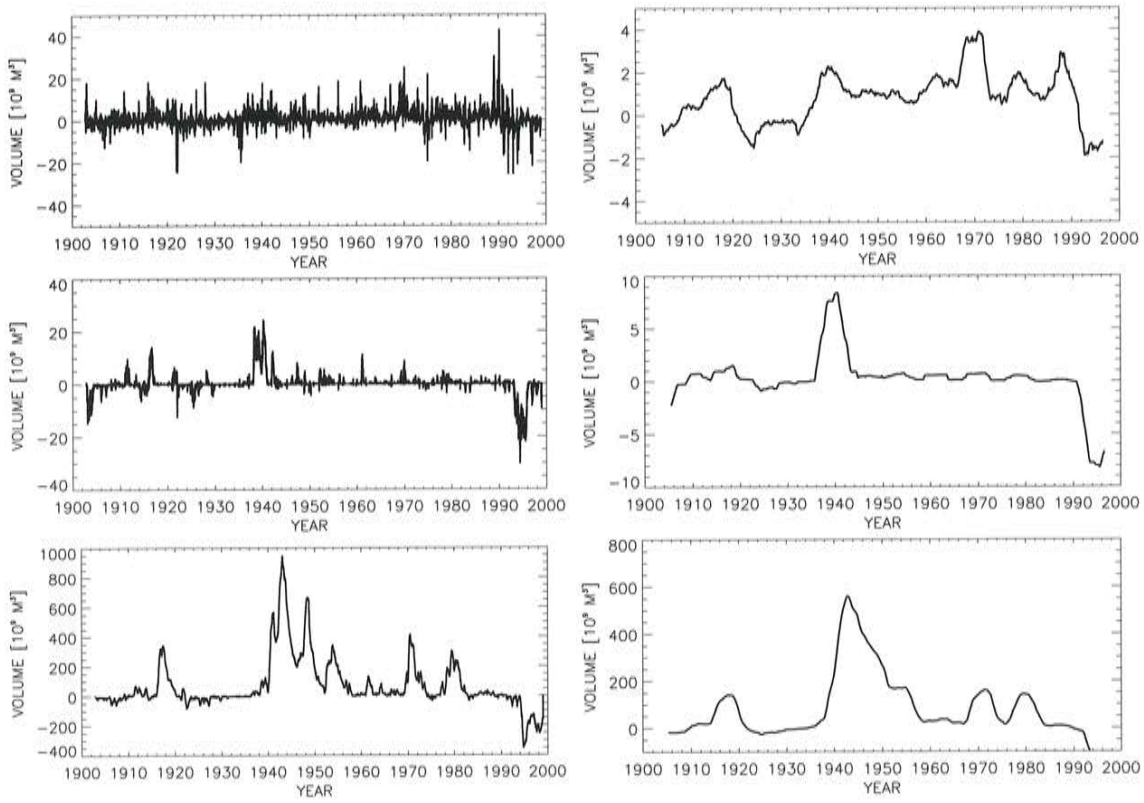

Figure 52: *Volume (in km^3) of high saline water in (upper panel) Arkona Basin ($S \geq 17\,psu$), (middle panel) Bornholm Basin ($S \geq 17\,psu$), and (lower panel) Gotland Basin ($S \geq 12\,psu$). Shown are unfiltered (left) and 4-year running mean (right) differences between model results from run 409 and run 418.*

and Gotland Basin.

9.2.3 Freshwater budget

As shown already in Section 8.7, the freshwater storage anomaly and the accumulated freshwater inflow are well correlated (Figs.54a and 55a). In this sub-section, the changes of the freshwater budget in the sensitivity experiments are discussed (Figs.54 and 55). When inter-annual variations of the freshwater forcing are omitted utilizing climatological monthly mean river runoff and precipitation (inter-annual variations of evaporation are very small), significant variability of the freshwater content is still found in the system (Figs.54c and 55b). The maxima of freshwater content during the 1920s and during the 1990s are quite pronounced.

A quite bad correlation is also found in the cases when the model is forced with a series of random years for SLP, surface wind and sea level in Kattegat (Figs.54d and 55d). The maximum of freshwater content during the 1930s and the minimum during the 1970s are smaller than in the reference experiments. Based on these results it is concluded that the observed variability of the freshwater content in the Baltic Sea can be explained only by the variations of both forcing functions, i.e. fresh- and saltwater inflows.

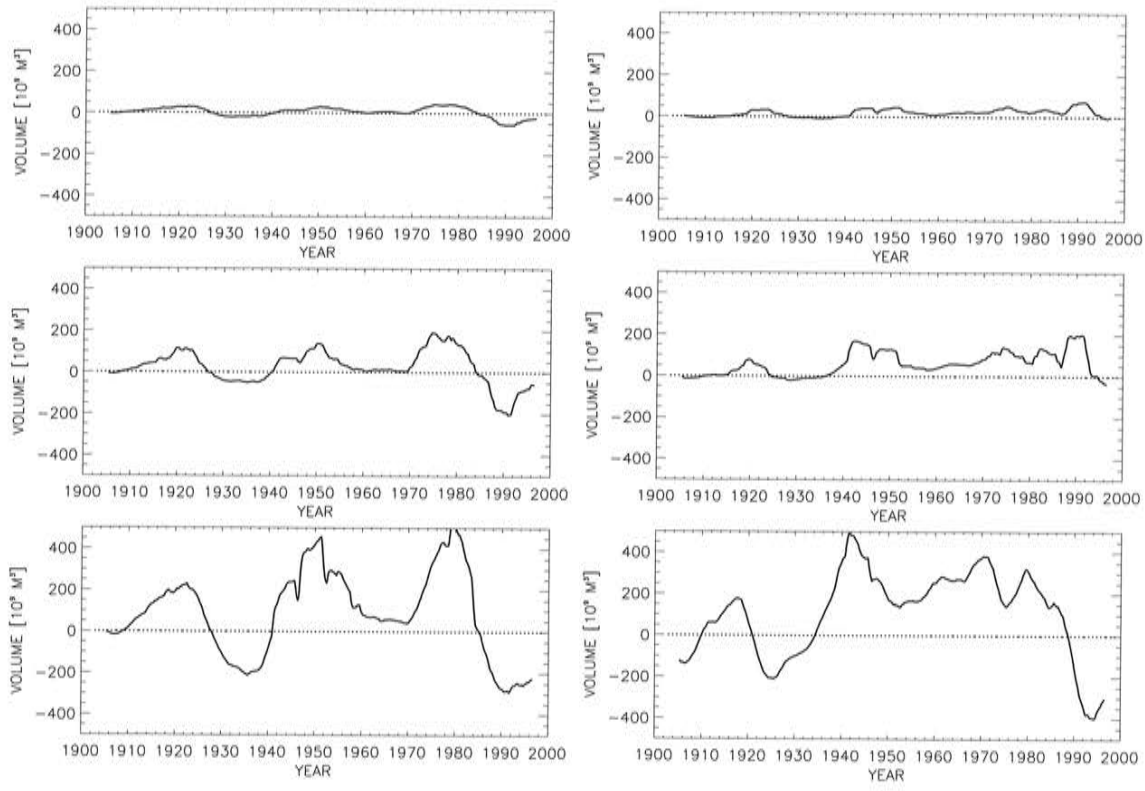

Figure 53: *Volume (in km^3) of high saline water ($S \geq 9\,psu$) in (upper panel) Arkona Basin, (middle panel) Bornholm Basin, and (lower panel) Gotland Basin. Shown are 4-year running mean differences between model results from run 403 and run 409 (left) and from run 409 and run 418 (right).*

The variability of the freshwater content in run 418 is further reduced when also the decadal variability of SLP is removed (Fig.55c). In addition to climatological mean freshwater inflow, in run 418 the daily SLP fields are high-pass filtered with a cut-off period of four years. Consequently, decadal variability of the surface wind fields is not considered. From the results of run 418 it is also evident that the model drifts towards higher salinities during the first two decades (Fig.55c). Similar conclusions can be drawn from the changes of mean salinity in the Baltic Sea (Fig.56).

9.2.4 The 1993 event

The question remains how the physical mechanisms works which control the strength of a saltwater inflow as a function of freshwater inflow. We have shown that an increase of winter runoff of 30 % (Tab.3) has almost no impact on the variability of salt in the Baltic proper if the annual discharge remains unchanged (Fig.47). However, as will be shown in Section 11 the overall increase of runoff by approximately the same amount (34 %) results in an extreme decrease of salinity on 100-year time scale. Thus, the important quantity is the accumulated freshwater inflow volume during decades instead of runoff on monthly to annual time scale. The high annual discharge variability (Fig.8) is just noise for the system because the Baltic Sea response time is about 36 years (Section 8.7).

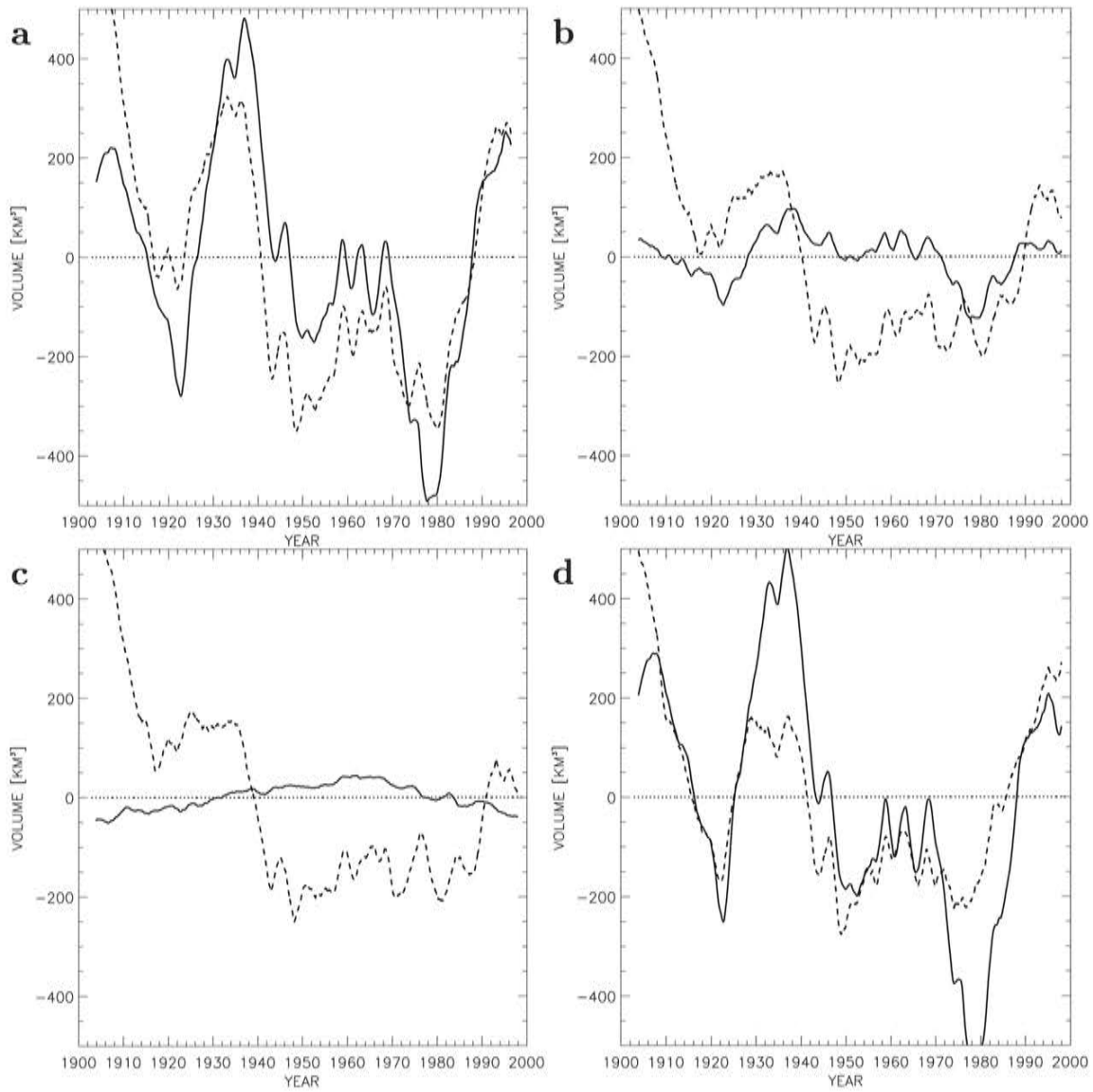

Figure 54: *2-year running mean of accumulated river runoff and net precipitation anomaly (solid) and 2-year running mean of freshwater storage anomaly (dashed), in km^3: (a) reference experiment (run 373b), (b) as (a) but with climatological monthly mean river runoff of the period 1902-1998 (run 383), (c) as (a) but with climatological monthly mean river runoff and precipitation of the period 1902-1970 (run 404), (d) as (a) but forced with a series of random years for SLP, surface wind and sea level in Kattegat (run 393).*

To address the Baltic response to runoff variations on a shorter time scale of up to one year, a series of sensitivity experiments have been performed using RCO with a horizontal resolution of 2 *nautical miles* which is considered as eddy permitting. The higher horizontal resolution has been chosen because there is evidence that the spreading of juvenile freshwater during spring and summer is connected to baroclinic eddies (Tapani Stipa FIMR, 2001, pers. comm.). The simulation period, May 1992 to June 1993, covers the major inflow event in January 1993. The model is started from observed temperature and salinity profiles and forced with atmospheric surface data of the SMHI database and with observed river runoff [9]. For further information concerning model setup and validation, the reader is referred to

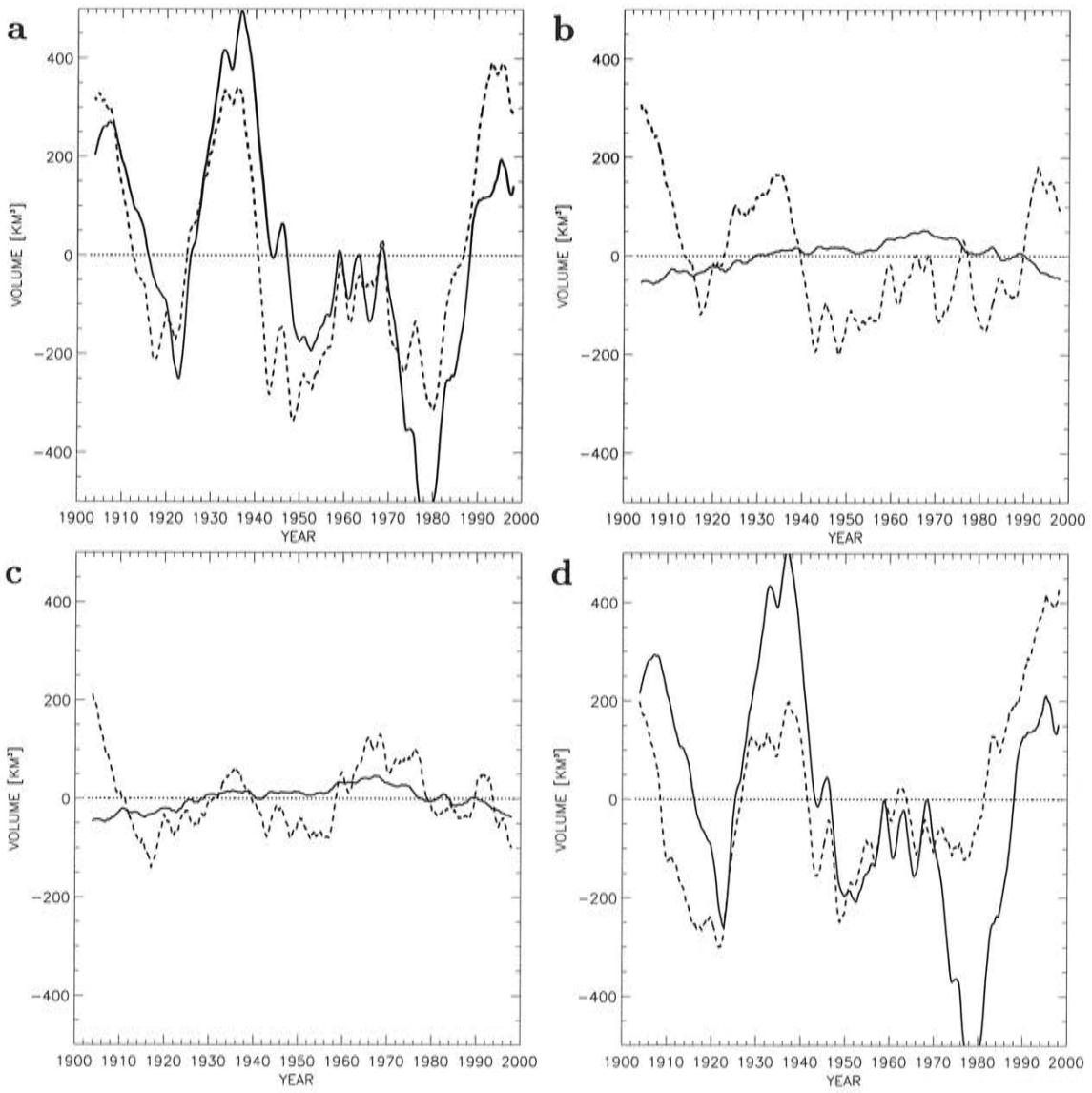

Figure 55: *2-year running mean of accumulated river runoff and net precipitation anomaly (solid) and 2-year running mean of freshwater storage anomaly (dashed), in km^3: (a) reference experiment (run 403), (b) as (a) but with climatological monthly mean river runoff and precipitation of the period 1902-1970 (run 409), (c) as (b) but with 4-year high-pass filtered SLP and correspondingly surface wind (run 418), (d) as (a) but forced with a series of random years for SLP, surface wind and sea level in Kattegat (run 410).*

[77].

As an annual mean runoff range of $-27\,\%$ to $+22\,\%$ is observed, sensitivity experiments with increased (run 350) and reduced runoff (run 367) of $\pm 22\,\%$ are performed. In the Arkona Basin (Bornholm Basin), the volume of high saline water is reduced by $10\,\%$ ($47\,\%$) or increased by $8\,\%$ ($44\,\%$) at the maximum (Fig.57). Thus, the model response is slightly asymmetric. The relative impact of changing runoff is larger for the Bornholm Basin than for the Arkona Basin. This is in accordance with the results of Section 9.2.2 (see Fig.53).

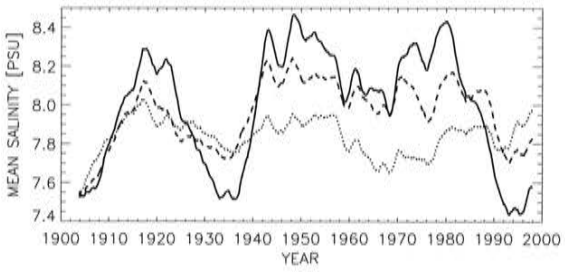

Figure 56: *2-year running mean salinity in the Baltic Sea without Kattegat (in psu): run 403 (solid), run 409 (dashed), and run 418 (dotted). The model results are uncorrected.*

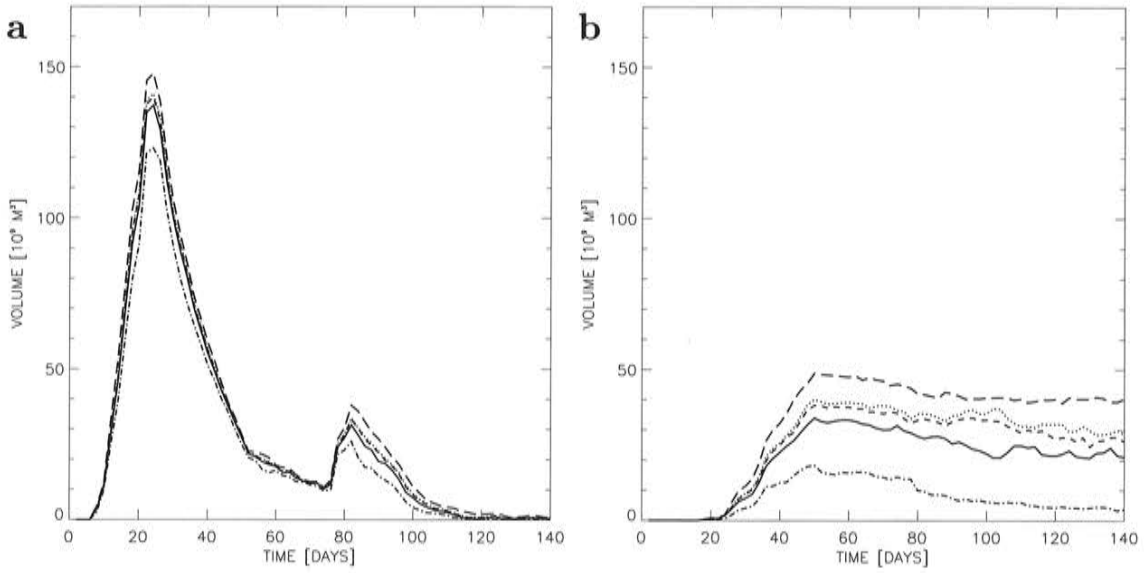

Figure 57: *Volume (in km^3) of high saline water (> 17 psu) in (a) Arkona Basin and (b) Bornholm Basin: reference run with observed runoff (run 349, solid line), 22 % increased runoff (run 350, dash-dotted line), 22 % reduced runoff (run 367, long-dashed line), unregulated runoff (run 354, short-dashed line), 9 % reduced runoff (run 399, dotted line). The time axis starts January 2, 1993.*

The effect of river regulation has been estimated by [91]. He found an increase of 9 % of the total discharge during winter (January to March) compared to the unregulated case. Using his estimates (run 354), we found that the impact on the major inflow in January 1993 is relatively small. The volume of high saline water in the Arkona Basin (Bornholm Basin) increased by only 2 % (12 %) without river regulation. In an additional experiment (run 399), the observed runoff has been decreased by 9 % over the whole period 1992/93. Whereas the annual mean runoff in run 354 is unchanged, spring and summer discharge is now also lower compared to the reference experiment (run 349). The results are almost the same than in run 354 (Fig.57). This indicates that the accumulated freshwater inflow volume during spring and summer has no significant impact on the saltwater inflow event in January because the time scale is too short for the system to respond.

9.2.5 Stolpe Channel and Gotland Deep transports

An important key region for the ventilation of the Baltic proper is the Stolpe Channel. A sill with a depth of about 60 m separates Bornholm Basin and the southern Gotland Basin at the western entrance of Stolpe Channel (see introduction). The high saline water has to pass the channel on its path into the Gotland Deep. As the mean wind blows from south-westerly direction, an Ekman transport in the surface layer has an eastward component (Fig.58a). In

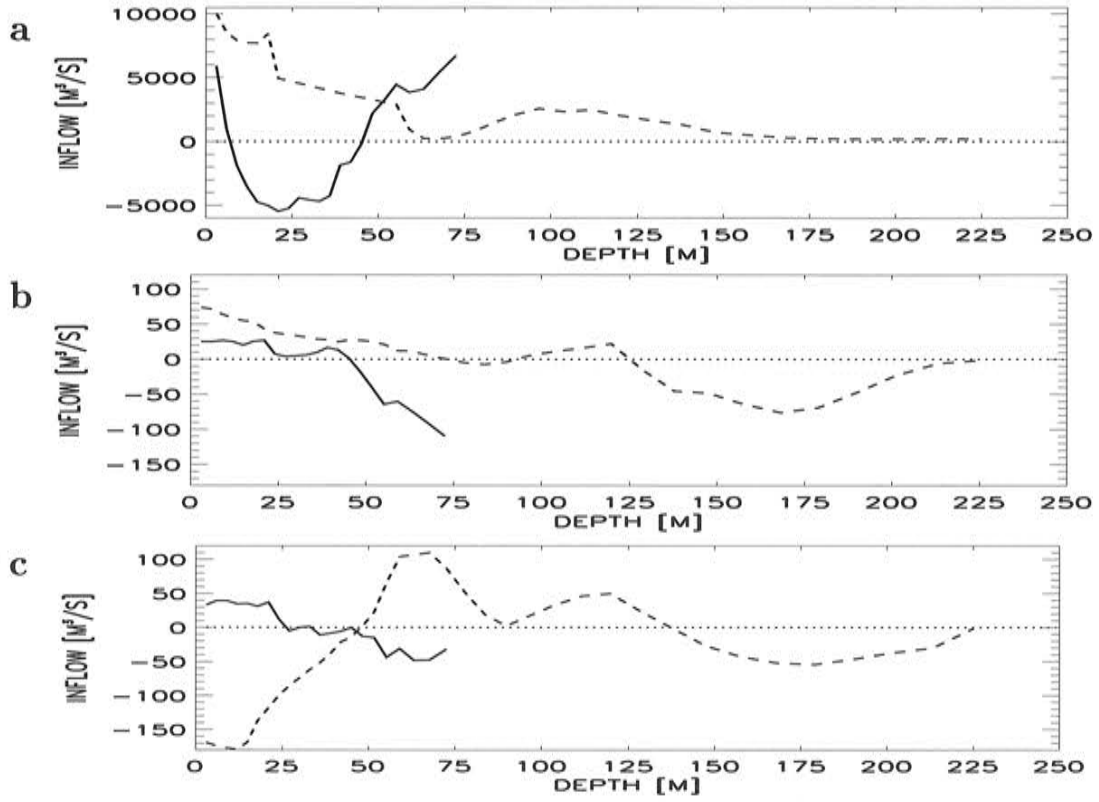

Figure 58: *Mean horizontally integrated transports across a basin-wide section at Stolpe Channel (solid) and in the eastern Gotland Basin between Gotland and Estonia (dashed) for the period 1902-1998: (a) standard experiment (run 403), (b) difference between run 403 and run 409, and (c) difference between run 409 and run 418. At Stolpe Channel (Gotland Deep) eastward (northward) transports are counted positive.*

depths below 48 m, the deepwater flow is also directed into the Gotland Basin. Between 9 and 45 m of depth the mean compensating flow of the vertical circulation is directed towards west. The transports at Stolpe Channel depicted in Figure 58 are horizontally integrated from coast to coast to subtract the horizontal cyclonic circulation. The qualitative results do not change if only the transports through the Stolpe channel are considered (not shown). The vertical integral of the profile yields the freshwater input from river discharge and net precipitation east of the chosen section.

In addition, the transport through a cross section between Gotland and Estonia at Gotland Deep has been calculated (Fig.58a). In the whole surface layer the transport is directed northwards with strong gradients in the profile at depths of the seasonal thermocline and of the permanent halocline. Local minimum and maximum transports are found in 68 m and 97 m

of depth, respectively. The latter maximum within the halocline is caused by interleaving of saline water from Stolpe Channel which is not heavy enough to replace the bottom water at Gotland Deep. In contrast to the results for the period 1979-1994 (Fig.27), we found no transport maximum at the bottom for the long period 1902-1998.

The mean difference transports at the two sections (Stolpe Channel and Gotland Deep) between the standard experiment (run 403) and the sensitivity experiments (run 409 and run 418) are shown in Figure 58b and c. Caused by the runoff variability during the past century, the deepwater flows at Stolpe Channel below $45\,m$ and at Gotland Deep in $170\,m$ depth are slightly reduced (Fig.58b). We found the largest differences in the eastern Gotland Basin caused by the variability of the large-scale wind forcing in the surface layer and at the depth of the minimum transport in $68\,m$ (Fig.58c). Differences at Stolpe Channel are only small.

The total mean transport differences between the experiments are small compared to differences occurring on decadal time scale (Fig.59). The two stagnation periods are clearly visible. The deepwater flows at Stolpe Channel and into the Gotland Deep are reduced due to the freshwater inflow and surface (bottom) layer transports are increased (reduced) due to the wind forcing. At Stolpe Channel Ekman transports with an east component are compensated by deepwater transports in opposite direction. This effect, first described by [55], is also dominant in our results on decadal time scale.

The 4-year running mean wind speed differences between run 409 and run 418 at Stolpe Channel are shown in Figure 60. Anomalous strong west winds during the 1920s and during the 1990s cause anomalous surface layer transports towards east and compensating deepwater flows towards west, i.e. the entrainment is reduced and the volume of high saline water in the Baltic proper decreases (Fig.53).

In addition, we compared the total mean profiles for the period 1902-1998 with the mean profiles for 1928-1934 and for 1989-1998 (not shown). We found no indication for significant changes of the zero crossing depth of the transport profile at Stolpe Channel.

9.2.6 Sea level

A comparison of the 10-year running mean sea levels at Landsort between run 403 (standard experiment) and run 409 (no variability of the freshwater forcing) shows no significant differences (not shown). Thus, decadal variability of the sea levels in the Baltic Sea is determined mainly by wind variations.

9.3 The influence of sea ice

[73] investigated the impact of salinity in the Baltic Sea on the seasonal sea ice cover. He compared the ice climate of the brackish water body as observed today and the climate of a lake. His results indicated that the sea ice cover is quite insensitive to salinity changes of this order of magnitude because the sea surface salinity is very low anyhow in the Gulf of Finland and the Gulf of Bothnia. These sub-basins are ice covered during a mean ice winter. Larger differences were found during severe ice winters.

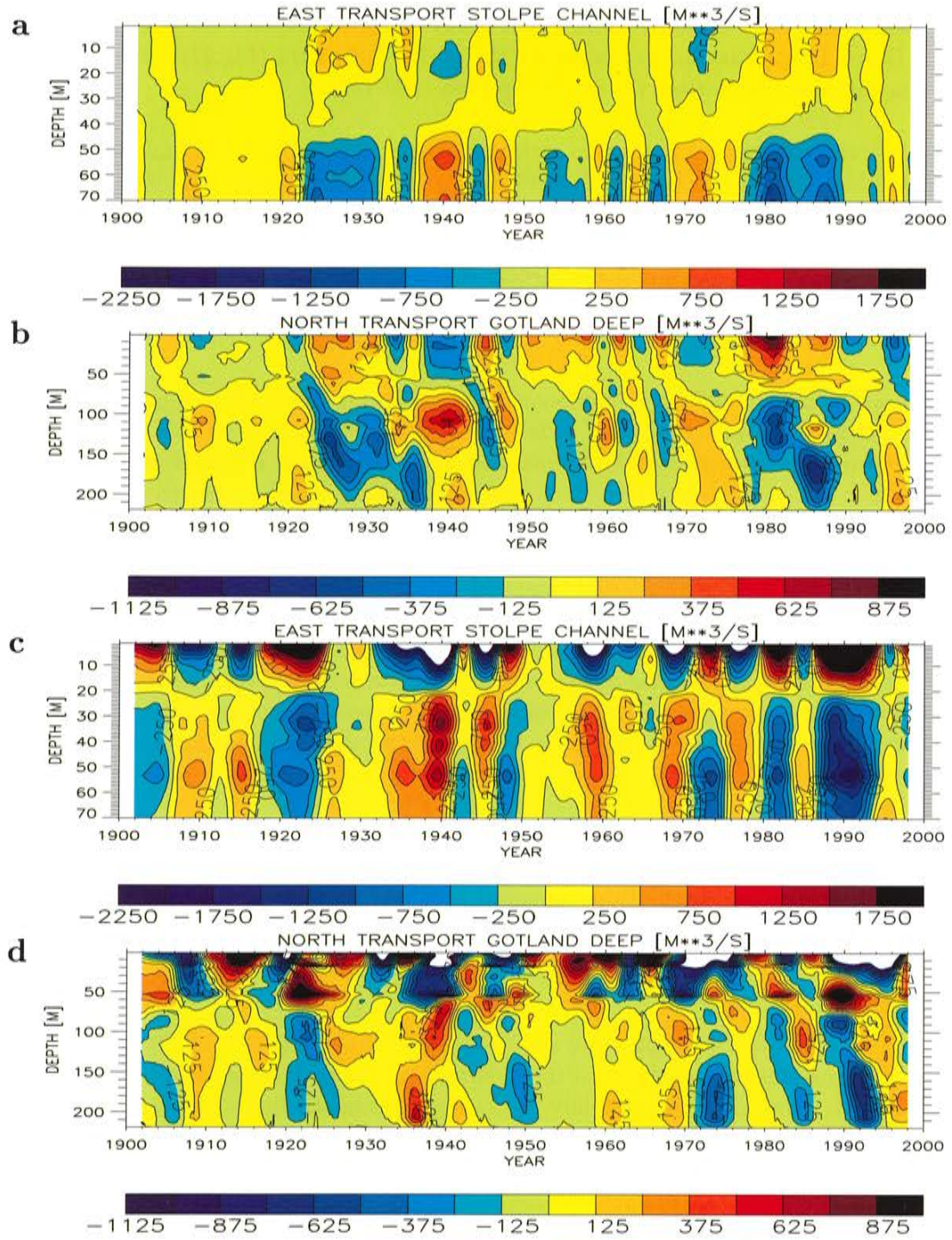

Figure 59: *4-year running mean horizontally integrated transport anomalies across a basin-wide section at Stolpe Channel (a, c) and in the eastern Gotland Basin between Gotland and Estonia (b, d) for the period 1902-1998: (a, b) difference between run 403 and run 409, (c, d) difference between run 409 and run 418. At Stolpe Channel (Gotland Deep) eastward (northward) transports are counted positive.*

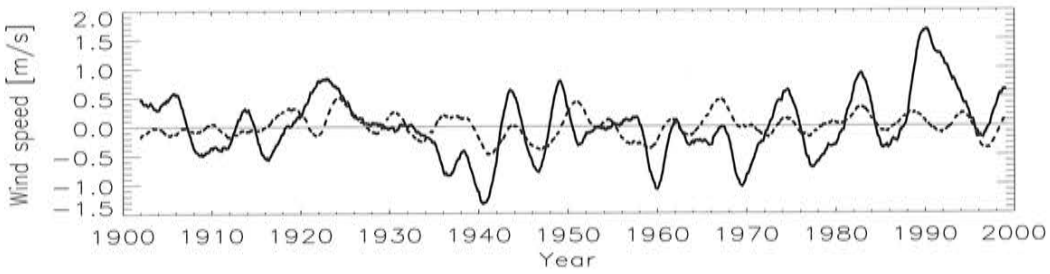

Figure 60: *4-year running mean wind speed difference between run 409 and run 418 at Stolpe Channel (55.5°N, 17.5°E): east component (solid), north component (dashed).*

In this sub-section the opposite case is studied, i.e. the impact of the sea ice cover on salinity in the Baltic proper. As explained in the introduction to Section 9, it might be possible that severe ice winters with ice coverage in the area of the Danish Straits prevent major Baltic inflows.

Therefore, an experiment with climatological monthly mean river runoff, precipitation, air temperature, specific humidity and cloudiness is performed (run 406). The climatological mean seasonal cycle is calculated for the period 1902-1970. Thus, in this sensitivity run only inter-annual variabilities of the input variables SLP, wind, and sea level in Kattegat are considered. Consequently, the ice season has no year-to-year variability. The salinity differences of the deepwater between this case and the corresponding reference experiment (run 404) are very small (Fig.45c). Thus, the inter-annual variability of sea ice during the past century has almost no impact on saltwater inflows.

A more extreme case is investigated when the air temperature of the calendar year 1941/42 is cyclic repeated (run 415), i.e. during every winter ice covers the entire surface area of the model domain. The climate of this 96-year run might be regarded as an extreme realization of the 'Little Ice Age'. Especially at the end of the 1930s, the increased inflow activity is hampered by the severe ice conditions (Fig.61). During the period 1938-1993 the salinity in the Baltic deepwater is lower due to the total ice cover compared to the standard experiment. However, the salinity changes are smaller than the changes due to the freshwater inflow variability (Fig.61c). We conclude that the impact of sea ice cover is only minor during todays climate and moderate during a 'Little Ice Age' climate with frequently occurring severe winters.

9.4 The influence of sea level in Kattegat

9.4.1 Salinity in the Gotland Basin

Two sensitivity experiments have been performed to illustrate the impact of the Kattegat sea level at the open boundary on the Baltic Sea stratification, one for the period 1980-1993 (run 315) and another one for the period 1902-1998 (run 411). In these experiments the sea level in Kattegat is calculated from the meridional SLP difference across the North Sea according to Equation (61) [36]. The results for salinity in Bornholm and Gotland Basin are shown in Figures 62, 63, and 64. With (61) more salt is transported into the deeper layer of the Bornholm Basin and into $100\,m$ of depth in the Gotland Basin during 1980-1993. As the

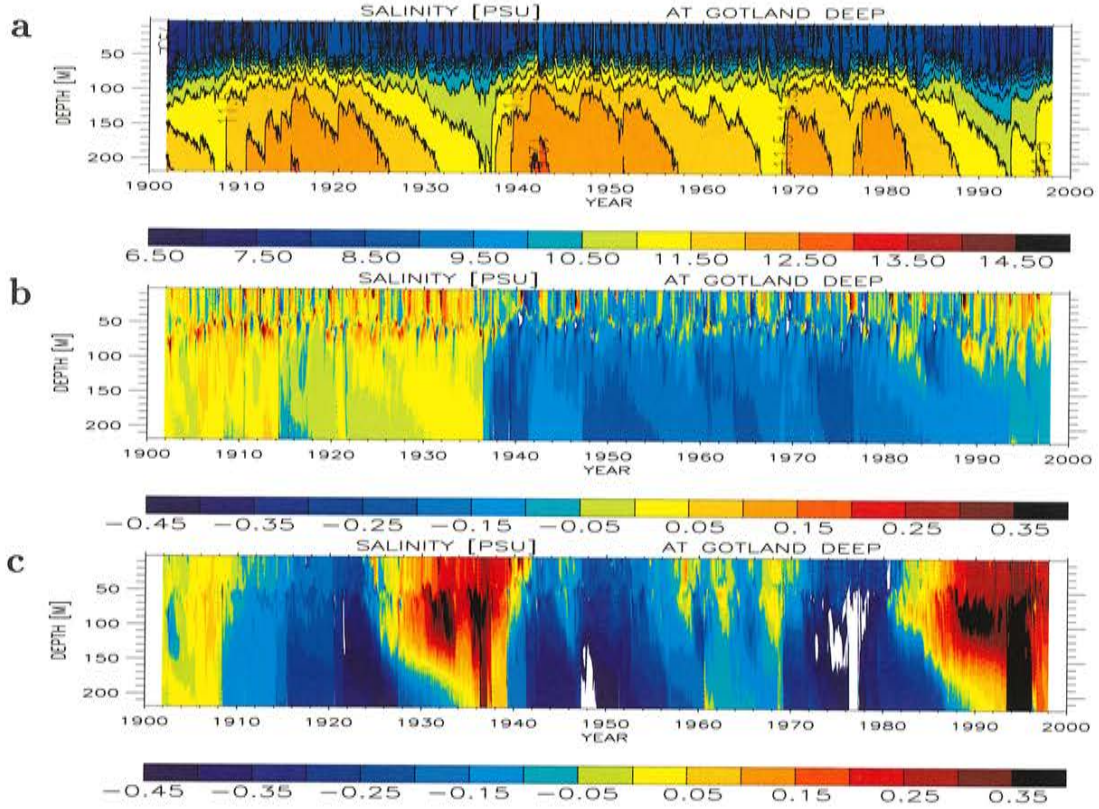

Figure 61: *Isohaline depths (in psu) in the eastern Gotland Basin (BY15): (a) sensitivity experiment with cyclic repeated air temperature from 1941/1942 (run 415), (b) difference between (a) and the standard experiment (run 403, Fig.17d), (c) difference between the experiment with climatological monthly mean river runoff and precipitation of the period 1902-1970 (run 409, Fig.46c) and the standard experiment (run 403, Fig.17d).*

bottom layer of the Gotland Basin is not ventilated during the stagnation period, the largest changes occur at the depth with the maximum inflow in about 100 m.

In the long simulation during 1902-1998 maximum salinity differences of more than 1 psu are found mainly at 50-100 m of depth (Fig.64). As the halocline is ventilated stronger using (61), this drift to higher salinities affects the bottom layer in the Gotland Basin after about three decades. We assume that the stronger salt transport into the Baltic Sea is caused by less mixing in the Danish Straits and in the western Baltic because the empirical relationship in (61) cannot explain the sea level variance for periods less than 15 days (see Fig.3 by [36]). The high daily variability of transports through the Danish Straits causes turbulence giving rise to mixing between the high saline inflows and the less saline outflows. The drift towards higher salinities is also illustrated in Figure 65 (mean salinity, cf. Fig.29b) and in Figure 66 (freshwater storage, cf. Figs.31b and 32b).

An additional experiment has been performed with high-pass filtered sea level data from Smögen and Strömstad prescribed at the open boundary (run 425). A cut-off period of four years was chosen. As expected we found no significant impact of the decadal variability of the sea level forcing on salinity in the Gotland Basin (not shown).

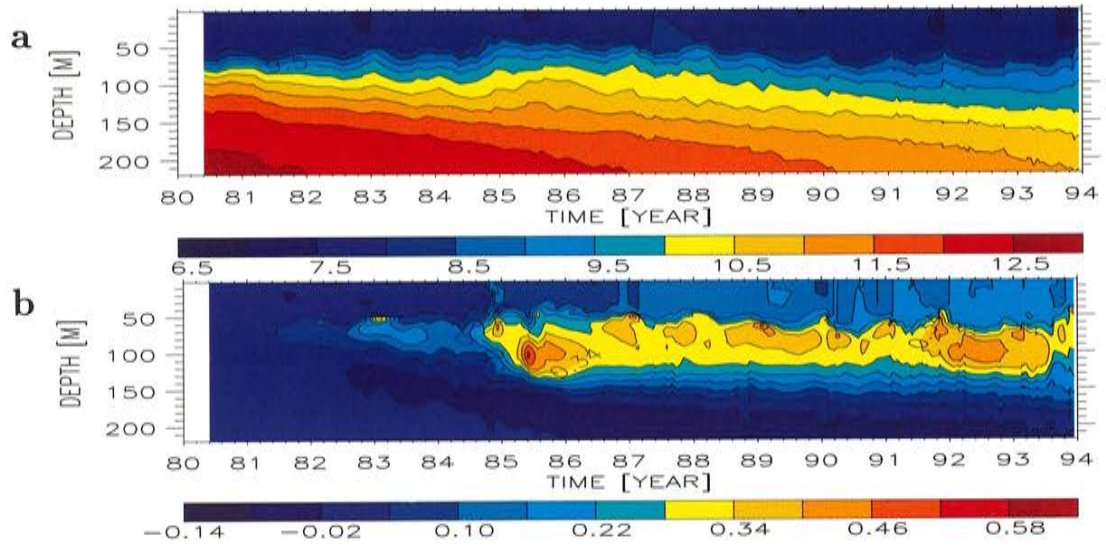

Figure 62: *Isohaline depths (in psu) in the eastern Gotland Basin (BY15): (a) experiment with sea level boundary condition in Kattegat according to [36] (run 315), (b) difference between (a) and the standard experiment (run 240, cf. Fig.40b).*

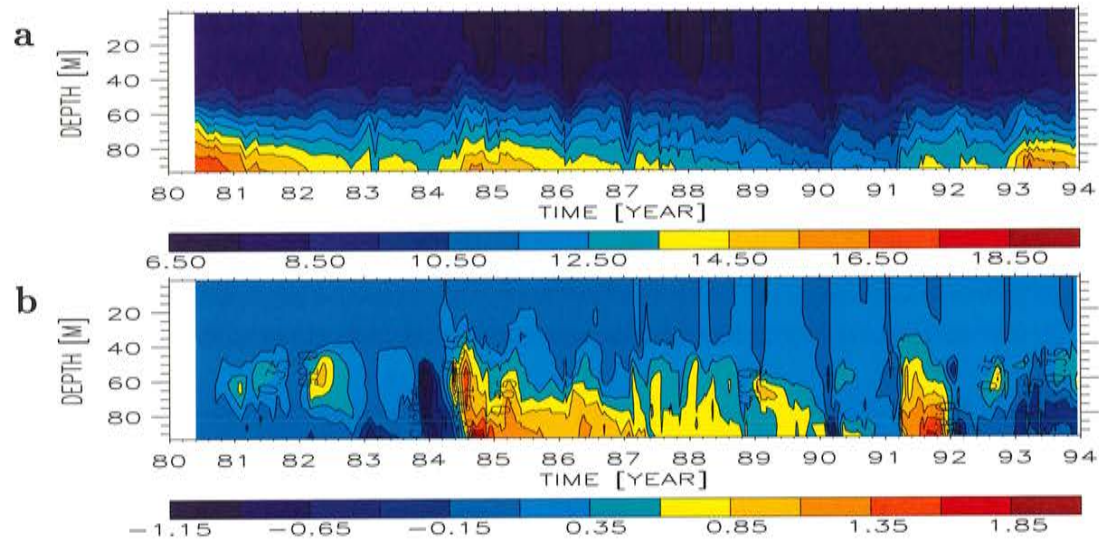

Figure 63: *As Fig.62, but isohaline depths (in psu) in Bornholm Basin (BY5): (a) experiment with sea level boundary condition in Kattegat according to [36] (run 315), (b) difference between (a) and the standard experiment (run 240, cf. Fig.39b).*

9.4.2 Sea levels at Landsort and Varberg

Utilizing (61) the sea level at Landsort in the Baltic proper is simulated with high quality compared to observations (Fig.67). The simulated 2-daily sea levels at Landsort (run 411) have a mean error of $ME = 3.2\,cm$ and a rms error of $RMSE = 12.0\,cm$ (Tab.4 in Section 8.1). These results are slightly worse compared to the results of the corresponding standard

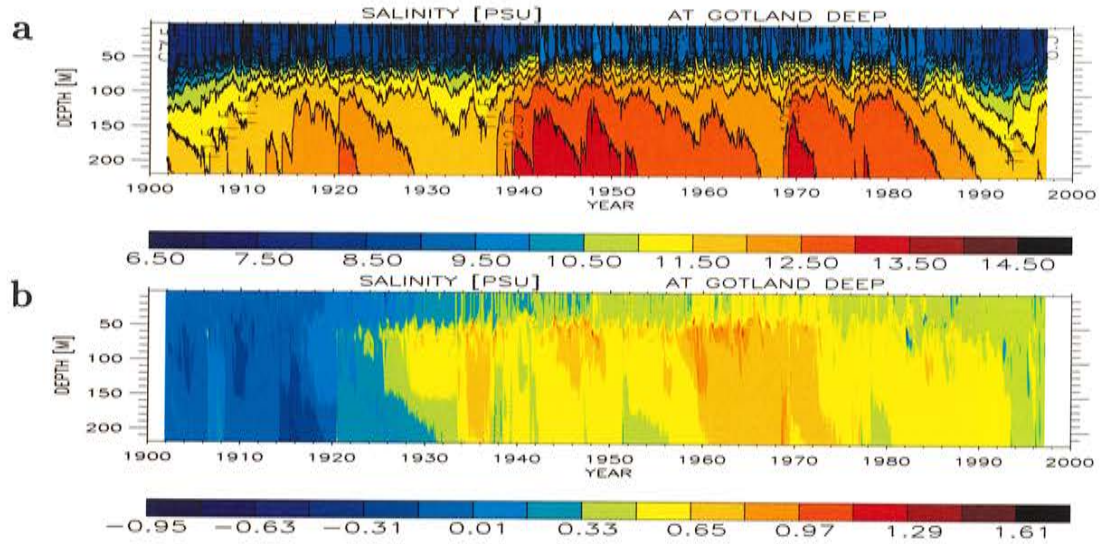

Figure 64: *Isohaline depths (in psu) in the eastern Gotland Basin (BY15): (a) experiment with sea level boundary condition in Kattegat according to [36] (run 411), (b) difference between (a) and the standard experiment (run 403, cf. Fig.17d).*

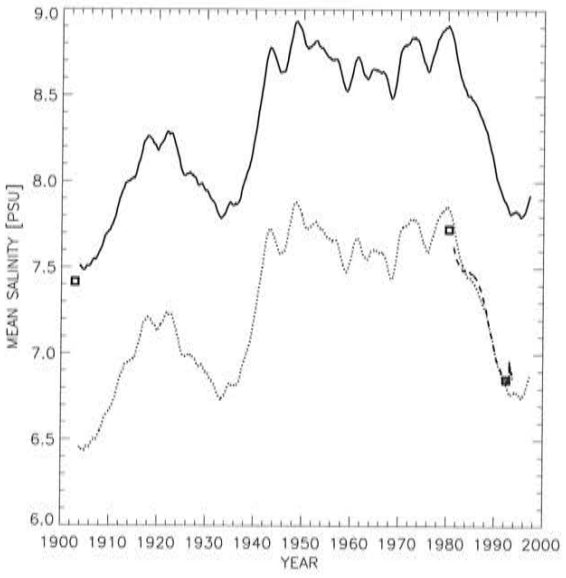

Figure 65: *2-year running mean salinity in the Baltic Sea without Kattegat (in psu): run 411 (solid), corrected run 411 (dashed), run 240 (dashed), run 349 (dashed-dotted).*

experiment (run 403, $ME = 3.0\,cm$, $RMSE = 11.3\,cm$) but much worse compared to the best standard experiment (run 373b, $ME = -0.4\,cm$, $RMSE = 9.3\,cm$). The simulated 10-year running mean sea levels at Landsort are well correlated with the observations (Fig.68). The differences between run 411 and run 403 are only small (cf. Fig.14b).

The low-frequency part of the sea level variability at Varberg calculated from (61) is compared to observations (Fig.69). We found small biases of the order of $1 - 2\,cm$ during the

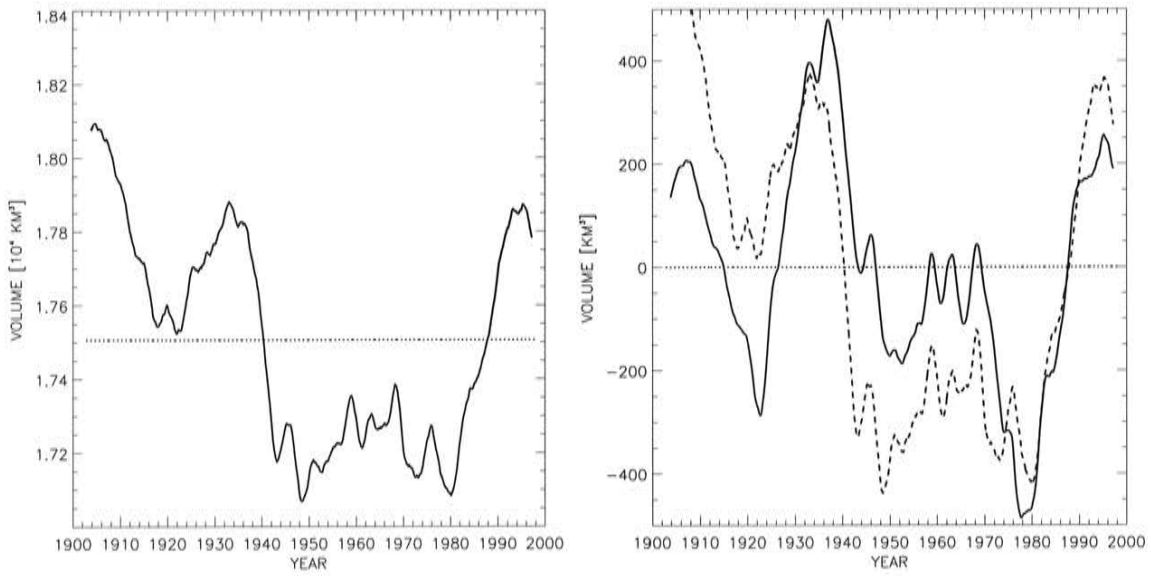

Figure 66: *Left: 2-year running mean of freshwater storage (in $10^4\,km^3$). Right: 2-year running mean of accumulated river runoff and net precipitation anomaly (solid) and 2-year running mean of freshwater storage anomaly (dashed), in km^3. Model results of run 411 are depicted.*

1910s, the 1920s, and the 1970s.

Based on 2-daily values the mean error of the sea level at Varberg/Ringhals in run 411 amounts to $ME = 2.3\,cm$ and the rms error amounts to $RMSE = 16.4\,cm$. As for the station Landsort, the results are much better in the best standard experiment (run 373b) with $ME = 1.8\,cm$ and $RMSE = 7.3\,cm$. Mean differences occur because the station Varberg/Ringhals is not exactly located at the open boundary. If the 2-daily sea levels calculated from (61), the input at the open boundary in run 411, were directly compared to the observations at Varberg/Ringhals, we found a mean error of $ME = 0.0\,cm$ (per definition) and a rms error of $RMSE = 16.8\,cm$.

10 The link to the large-scale atmospheric circulation

The most important forcing components of the system (salt- and freshwater inflows) are not independent functions (Section 9). Both are connected to each other via the large-scale atmospheric circulation as shown in this section.

10.1 Atmospheric teleconnection patterns

10.1.1 North Atlantic Oscillation (NAO)

The Baltic Sea is located in the transition zone between continental and maritime climate. Westerly winds associated to the pressure difference between the Azores High and the Icelandic Low transport warm and humid air into the region. These zonal wind fields and the

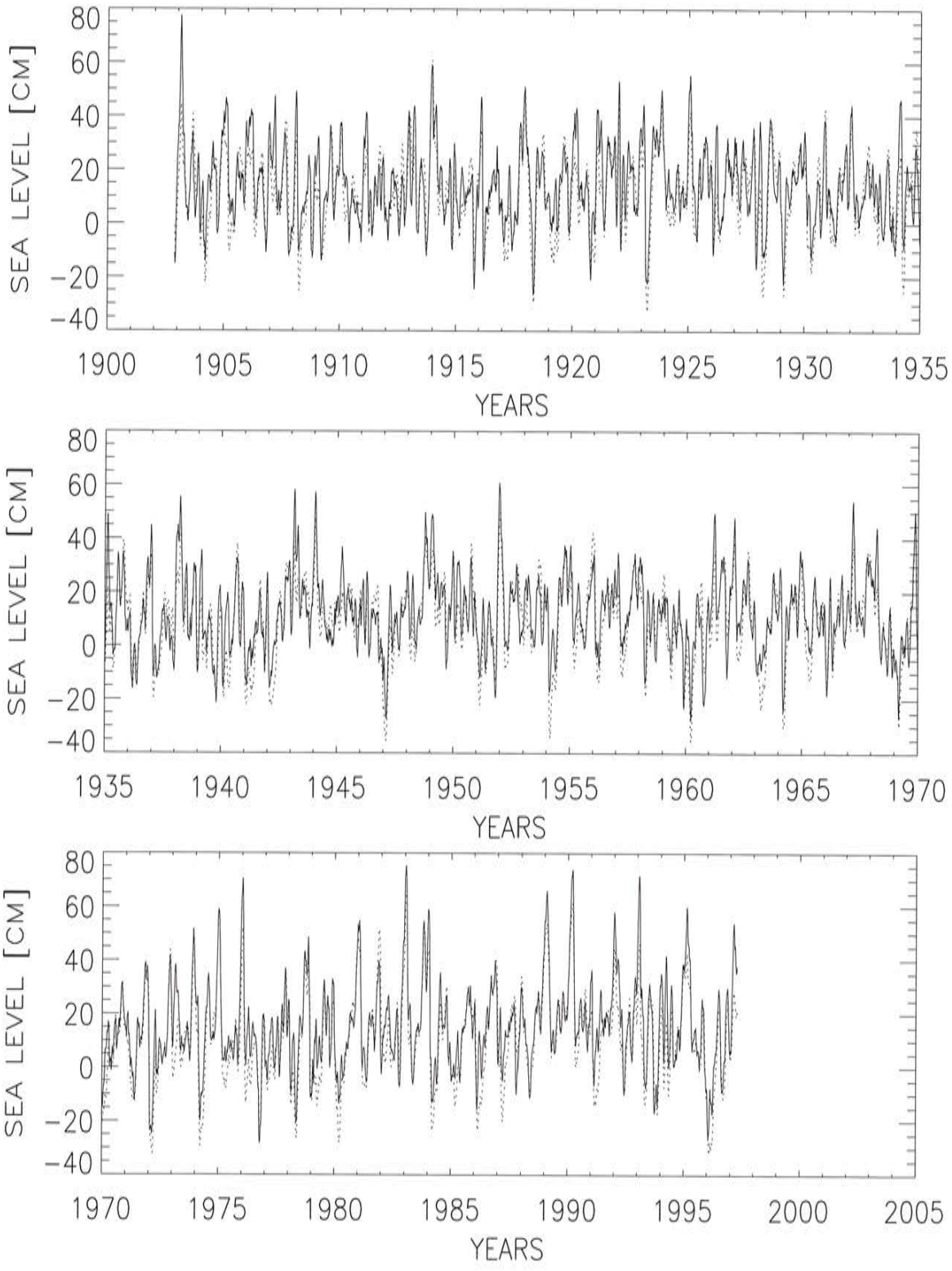

Figure 67: *Sea levels (in cm) at Landsort. Solid line: model results (run 411). Dotted line: observations. Both series are 20-day running means.*

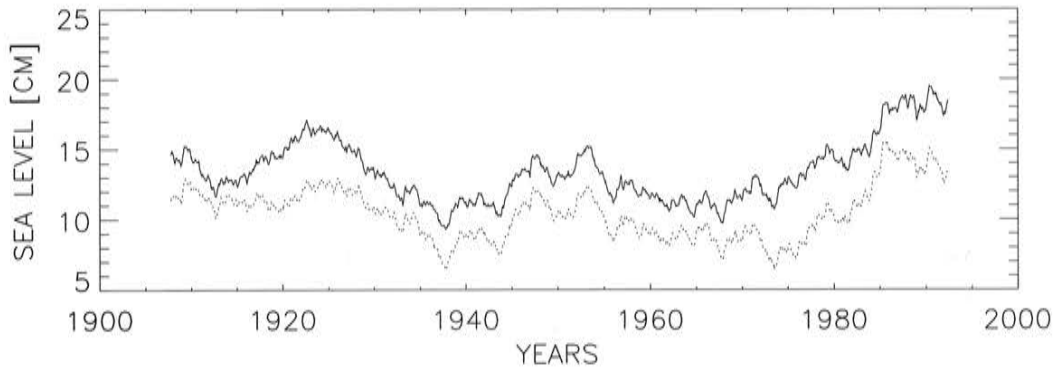

Figure 68: *10-year running mean sea levels (in cm) at Landsort. Solid line: model results (run 411). Dotted line: observations.*

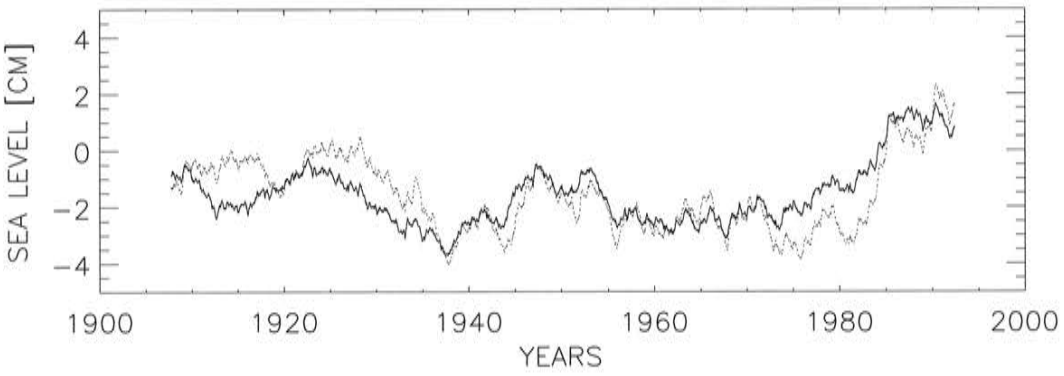

Figure 69: *10-year running mean sea levels (in cm) at Varberg/Ringhals. Solid line: input to model run 411. Dotted line: observations.*

corresponding pressure anomalies reveal a large variability known as North Atlantic Oscillation (NAO). The NAO is documented inter alia by [6]. The positive phase of the NAO reflects below-normal heights and pressure across the high latitudes of the North Atlantic and above-normal heights and pressure over the central North Atlantic, the eastern United States and western Europe (see http://www.cpc.ncep.noaa.gov/data/teledoc/telecontents.html). The negative phase reflects an opposite pattern of height and pressure anomalies over these regions. Both phases of the NAO are associated with basin-wide changes in the intensity and location of the North Atlantic jet stream and storm track. During the winter half of the year much of the variability of surface temperature and precipitation patterns over Europe are explained by the NAO [42]. Traditional definitions of the NAO index define it as the difference of normalized sea level pressure between a station in Iceland (Stykkisholmur/Reykjavik) and one in the Azores (Ponta Delgada). The record at Ponta Delgada can be extended back to 1865. A further extension of the NAO index back to 1823 using early instrumental pressure observations from Gibraltar and the Reykjavik area of south-west Iceland has been provided by [48] (http://www.cru.uea.ac.uk/~timo/projpages/nao_update.htm). In winter the two sites are located close to the centers of action that comprise the NAO. Positive values of the NAO index indicate stronger-than-average westerlies over the mid-latitudes whereas negative values indicate stronger impact of the continental climate over the Baltic Sea region. The NAO winter index has remained in a highly positive phase since 1980.

Although the NAO index is a useful presentation of the large-scale atmospheric circulation over Europe and the North Atlantic during the past decades, on even longer time scales a single time record cannot comprise decadal variability completely as the centers of action are changing location with time [41].

The monthly pressure variability in January over the Nordic countries is explained by less than 25 % by NAO. This is in agreement with results by [19]. They found that the monthly fluctuations of the NAO index can explain 21 % of the variance of the monthly air temperature in Sweden.

10.1.2 Scandinavia (SCAND)

For the Nordic countries, a larger part of the monthly SLP variability is explained by the Scandinavia (SCAND) pattern (http://www.cpc.ncep.noaa.gov/data/teledoc/telecontents.html). SCAND consists of a primary circulation center which spans Scandinavia and large portions of the Arctic Ocean north of Siberia. Two additional weaker centers with opposite sign to the Scandinavia center are located over western Europe and over the Mongolia/ western China sector. The Scandinavia pattern is a prominent mode of low frequency variability in all months except June and July, and has been previously referred to as the Eurasia-1 pattern by [6]. The positive phase of this pattern is associated with positive height anomalies, sometimes reflecting blocking anti-cyclones over Scandinavia and western Russia.

10.1.3 East Atlantic/ Western Russia (EATL/WRUS)

The East Atlantic/ West Russia (EATL/WRUS) pattern is one of two prominent modes that affects Eurasia during most of the year. This pattern is prominent in all months except June-August, and has been referred to as the Eurasia-2 pattern by [6]. In Winter, two main anomaly centers, located over the Caspian Sea and western Europe, comprise the East Atlantic/ West Russia pattern (http://www.cpc.ncep.noaa.gov/data/teledoc/telecontents.html). A three-celled pattern is then evident in the spring and fall seasons, with two main anomaly centers of opposite sign located over western/ north-western Russia and over northwestern Europe. The third center, having same sign as the Russia center, is located off the Portuguese coast in spring, but exhibits a pronounced retrogression toward Newfoundland in the fall.

The most pronounced and persistent negative phases of the East Atlantic/ West Russia pattern tend to occur in winter and early spring, with particularly large negative phases noted during the winters and early springs of 1969/70, 1976/77 and 1978/79. Pronounced positive phases of the pattern are less common, with the most prominent positive phase evident during late winter/ early spring of 1992/93. During this 1992/93 winter, negative height anomalies were observed throughout western and southwestern Russia, and positive height anomalies were observed throughout Europe and the eastern North Atlantic. These conditions were accompanied by warmer and wetter than normal conditions over large portions of Scandinavia and northwestern Russia, and by much colder and drier than normal conditions over the eastern Mediterranean Sea and the Middle East. During March through May 1993, the area of negative anomalies over western Russia persisted, the positive anomaly center over northwestern Europe became consolidated, and a negative anomaly center became established over the eastern North Atlantic. These conditions brought a continuation of warmer (colder) than

normal conditions to Scandinavia (eastern Mediterranean Sea sector), and drier than normal conditions to much of Europe.

For more information about teleconnection patterns the reader is referred to:
http://www.cpc.ncep.noaa.gov/data/teledoc/telecontents.html.

10.2 Correlations with the NAO index

In the following, we summarize briefly significant correlations between local variables in the Baltic Sea region and NAO.

10.2.1 Sea level

The linear correlation between winter (December through March) sea level at Smögen and winter NAO index amounts to $r = 0.76$ (Fig.70). For the 4-year running mean sea levels and

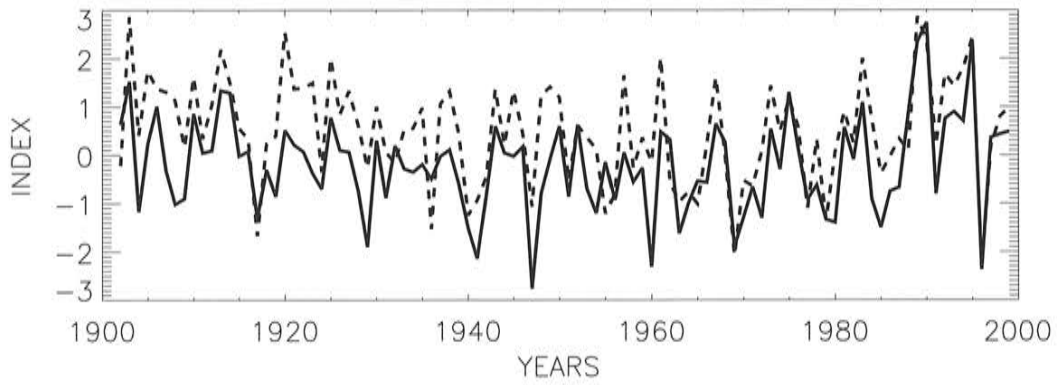

Figure 70: *Normalized (with one standard deviation) winter mean (December through March) sea level at Smögen (solid line) and winter NAO index (dashed line).*

NAO indices we found a correlation of even $r = 0.79$. High correlation is also found for the Landsort sea level which is a good measure of the Baltic Sea volume (e.g. [63]). The linear correlation between winter (January through March) sea level at Stockholm and winter NAO index amounts to $r = 0.74$ according to [3]. Thus, inter-annual variability of the Baltic Sea volume and transports through the Danish Straits are to a significant amount explained by the large-scale atmospheric circulation. The impact of decadal variability of runoff on the sea level variability is one order of magnitude smaller.

10.2.2 Sea ice

The high, temporal changing correlation between the annual maximum ice extent of the Baltic Sea (MIB) and the large-scale atmospheric circulation has been shown already by [109]. We have calculated the moving correlation between simulated MIB and winter NAO (Fig.71). The total correlation amounts to $r = -0.68$ in the model (run 403) and to $r = -0.57$ in the observations. The 31-year moving correlation is high during the 1940s and 1980s but quite low during the 1920s. The correlation between simulated MIB and NAO is higher than

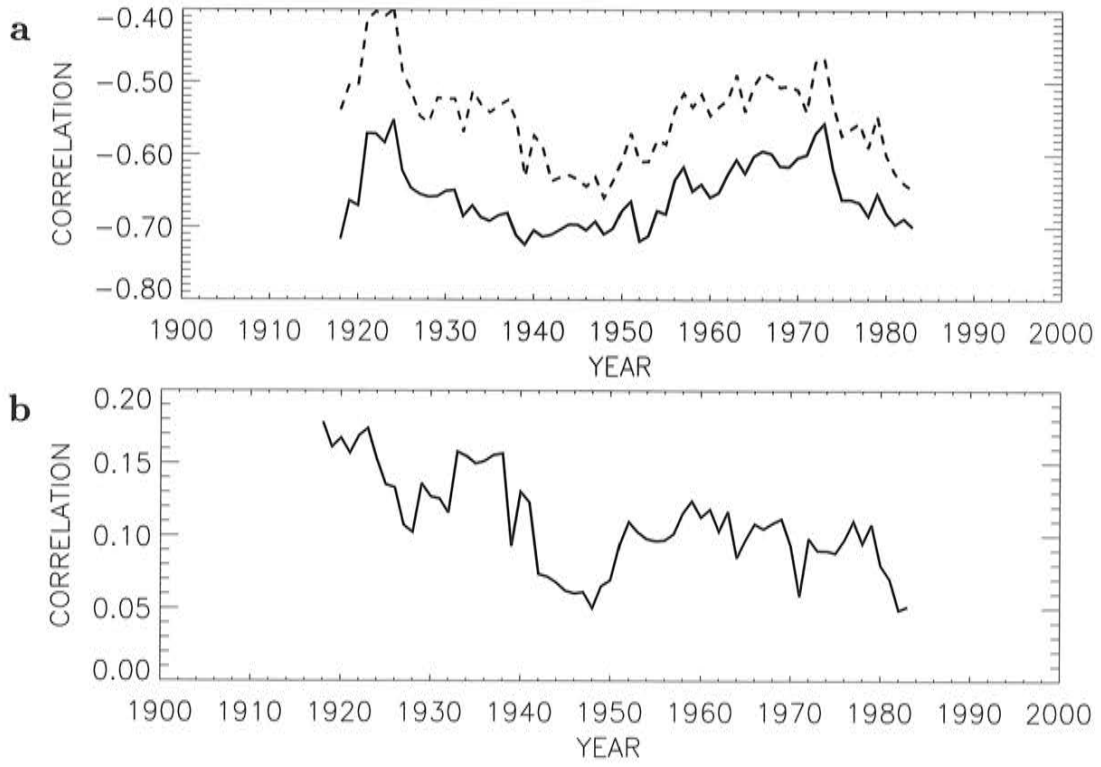

Figure 71: *(a) 31-year moving correlation between the annual maximum ice extent (MIB) and the winter mean NAO index. Solid line: simulated MIB (run 403). Dashed line: observed MIB. (b) Absolute difference of the simulated and observed correlations shown in (a).*

between observed MIB and NAO. Obviously, the statistical model used works well for the reconstruction of the large-scale variability but might have shortcomings for the reconstruction of the local-scale variability. The grid resolution of the predictand field is only $1° \times 1°$. As the MIB is a function of both, remote and local forcing, the correlation between simulated MIB and observed NAO is indeed expected to be higher than the correlation between observed MIB and observed NAO.

10.2.3 Runoff

The linear correlation between the winter (JFM) mean runoff and the winter (JFM) NAO index for the whole period 1902-1998 is only $r = 0.26$. A much higher correlation of $r = 0.72$ is found for the period 1960-1998. The 31-year moving correlation between the 4-year running mean winter (JFM) runoff and the 4-year running mean winter (DJFM) NAO index is shown in Figure 72. Based on the 4-year running mean records the total mean correlation for the period 1903-1996 amounts to $r = 0.18$ only. Again the correlation for the period 1960-1996 is much higher ($r = 0.85$). Thus, the winter variability of the whole freshwater inflow during the second stagnation period is linked fairly well to NAO because net precipitation and runoff are also strongly correlated (Section 6.2). However, the correlation between the annual mean runoff and NAO is quite low ($r = 0.26$ for the period 1903-1996 and $r = 0.43$ for the period 1960-1996).

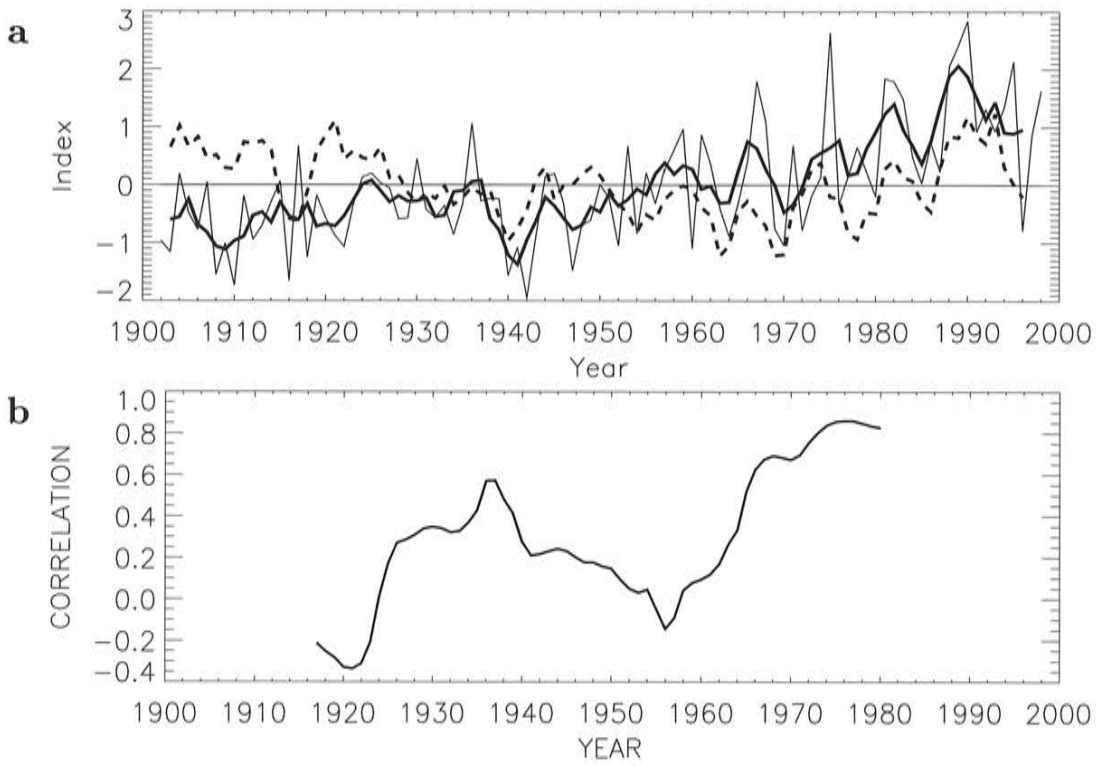

Figure 72: *(a) With one standard deviation normalized annual mean winter (January through March) river runoff (thin line) to the Baltic Sea without Kattegat, 4-year running mean winter river runoff (solid), and 4-year running mean winter (December through March) NAO index (dashed). (b) 31-year moving correlation between the 4-year running mean winter (January through March) river runoff to the Baltic Sea without Kattegat and the 4-year running mean winter (December through March) NAO index.*

10.2.4 Wind speed at Stolpe Channel

The correlation between the winter (DJFM) mean westerly wind anomaly at Stolpe Channel (i.e. the wind difference between run 409 and run 418) and the 4-year running mean winter NAO index is much higher than in case of winter runoff and amounts to $r = 0.67$ (Fig.73). As the filtered wind records do not contain the seasonal cycle anymore, the correlation between the annual mean wind speed anomaly and the 4-year running mean winter NAO index is almost the same ($r = 0.69$). Periods of exceptionally high correlation coincide with periods of exceptionally high correlation between winter runoff and NAO (Fig.72). We found low correlation between the local wind and NAO and between winter runoff and NAO at the beginning of the 1920s and during the 1950s.

10.2.5 Stolpe Channel transport

Increased westerly winds cause a decreased eastward transport through Stolpe Channel between 20 and $70\,m$ (Fig.59c). The correlation between the annual mean Stolpe Channel transport anomaly between 20 and $70\,m$ and the 4-year running mean winter NAO index amounts to $r = -0.67$.

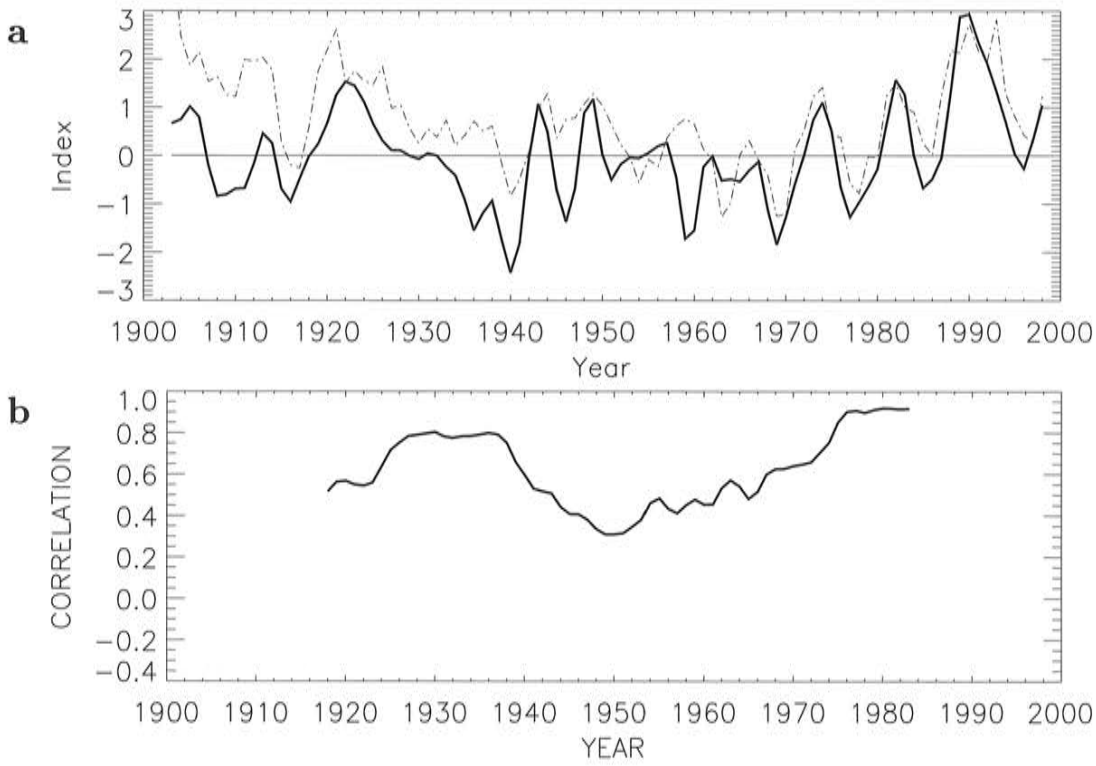

Figure 73: *(a) With one standard deviation normalized annual mean westerly wind anomaly at Stolpe Channel, i.e. the wind difference between run 409 and run 418 (solid), and the 4-year running mean winter (December through March) NAO index (dashed). (b) 31-year moving correlation between the annual mean westerly wind anomaly at Stolpe Channel (i.e. the wind difference between run 409 and run 418) and the 4-year running mean winter (December through March) NAO index.*

10.3 The winter SLP modes

The low-pass filtered records of the winter season SLP modes are shown in Figure 74. The first mode explains 72 % of the variance [51]. It has a relative maximum during the 1930s and a relative minimum at the end of the 1970s. These periods are close to the two stagnation periods defined earlier by the anomalous volume of high saline water in the eastern Gotland Basin in Section 9.2.1 (Fig.51), i.e. 1921-1934 and 1989-1998, but do not coincide completely. The time records of the winter season modes (especially of the first mode) are not related to the periods of intensified west winds over the Baltic proper which cause the stagnation periods (Fig.60). As shown below (Section 10.4), the inter-annual variability of SLP in winter over the Baltic Sea region is explained mainly by the variability of the NAO, SCAND and EATL/WRUS patterns. However, it is impossible to relate our local modes to large-scale modes of monthly variability because the whole range from daily to decadal time scales are included.

Although most of the daily variability is explained by the first mode, also the second and third mode have a significant impact on saltwater inflows (Fig.75).

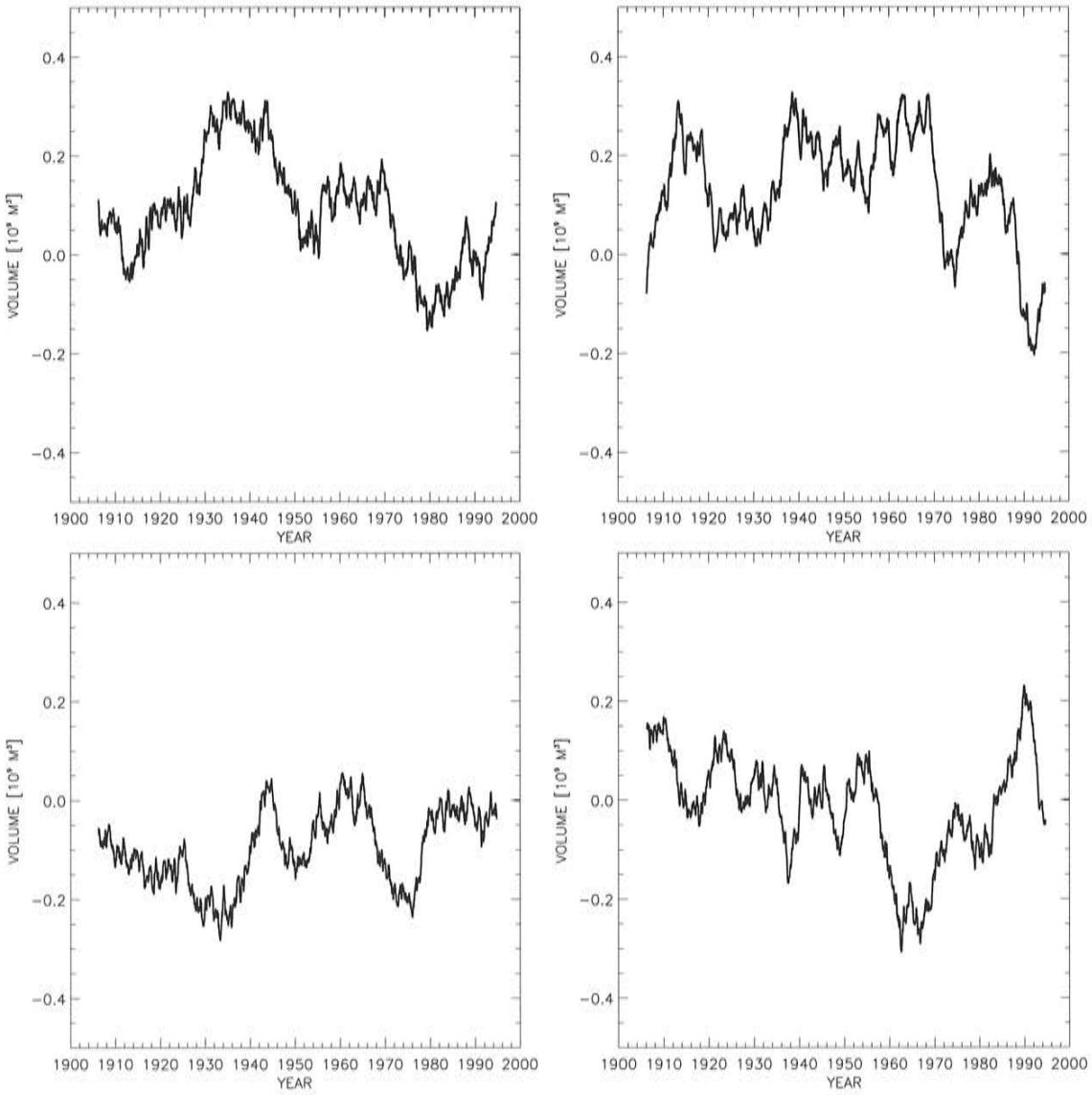

Figure 74: *4-year running mean winter SLP redundancy modes. The first four modes are shown (upper left: 1. mode, upper right: 2. mode, etc.).*

10.4 The role of the low-frequency SLP variability over Scandinavia

In run 418 the inter-annual variability of the freshwater inflow is removed and the daily SLP fields are high-pass filtered with a cut-off period of four years. The results have been discussed in Section 9.2 (see Figs.46d, 55c, and 56). We found that the SLP variability with periods larger than four years is connected to an anomalous west wind variability which causes increased or decreased deepwater flow into the Baltic proper. About half of the decadal variability of the mean salinity of the Baltic Sea is explained by the low-frequency variability of the SLP over Scandinavia. As shown in Section 10.2, in the Baltic Sea region the sea level, sea ice, air temperature, runoff and wind speed are correlated to the NAO. To analyze the modes of winter time (DJFM) variability of the reconstruction not connected to the NAO, we subtract the variability described by the NAO from the SLP anomalies. Then, an EOF-analysis of the residual field is performed. The first two EOFs describe 53 % and 13% of

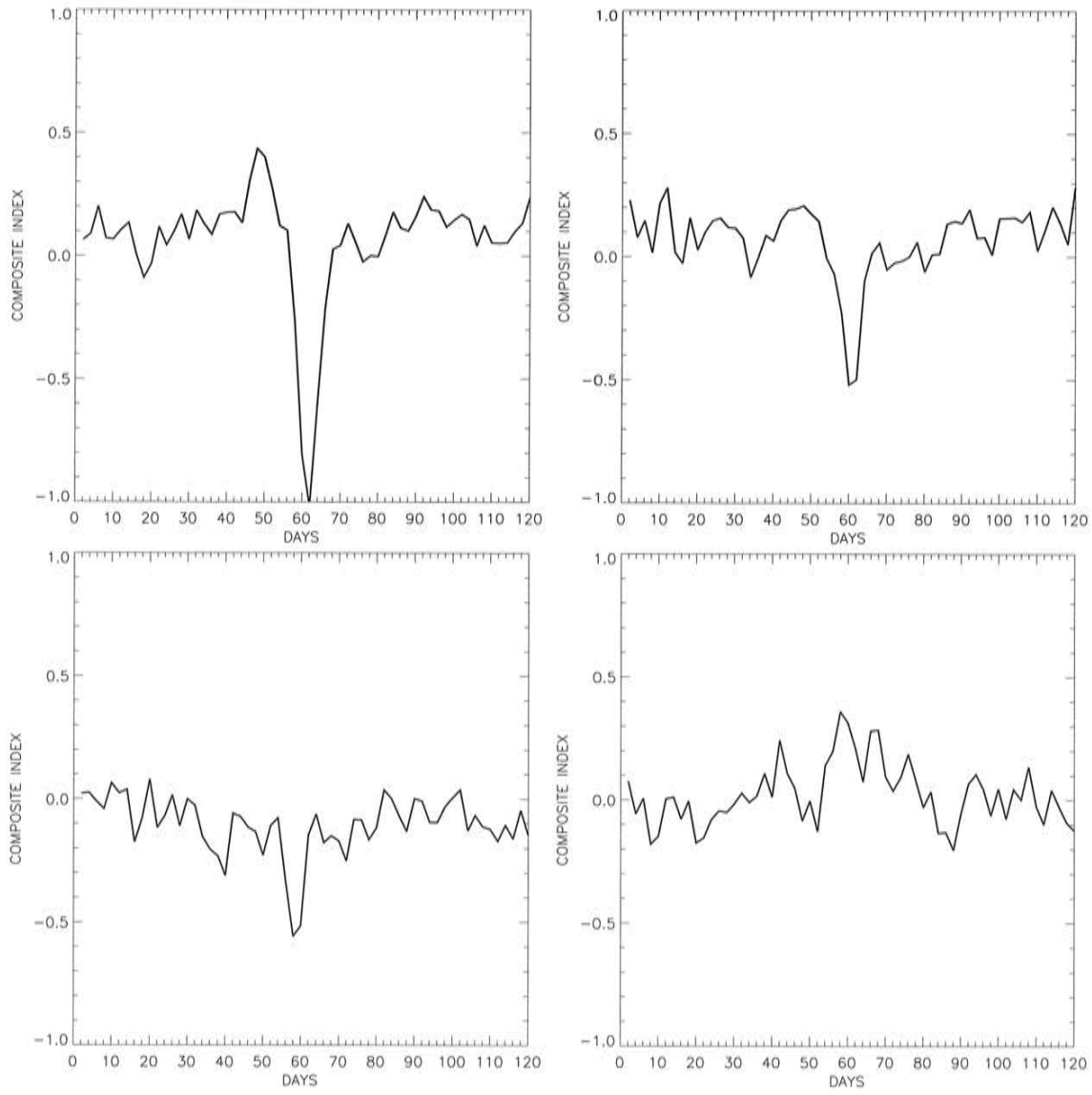

Figure 75: *Composites of time records of the winter SLP redundancy modes for saltwater inflows (in run 403). The first four modes are shown (upper left: 1. mode, upper right: 2. mode, etc.).*

the total variance. Further, the winter mean SLP field of the entire Northern Hemisphere is regressed upon the NAO index, and upon the first and second principal component of the residual field (Fig.76). The utilized data set of the Northern Hemisphere monthly SLP covers the period 1902 to 1998 [111], [112]. The regression pattern of the NAO displays the well-known dipole between Iceland and the Azores (Fig.76a). The SLP pattern associated with the first principal component shows a monopol over northeast Europe with high amplitudes (Fig.76b) and looks rather similar than SCAND. The SLP pattern associated with the second principal component displays a dipole with centers over Great Britain and West Russia (Fig.76c) and is interpreted as EATL/WRUS. Thus, the dominant SLP patterns over the Baltic Sea area can be traced back to well-known teleconnection patterns of the Northern Hemisphere. To illustrate the link to the large-scale atmospheric circulation we calculated

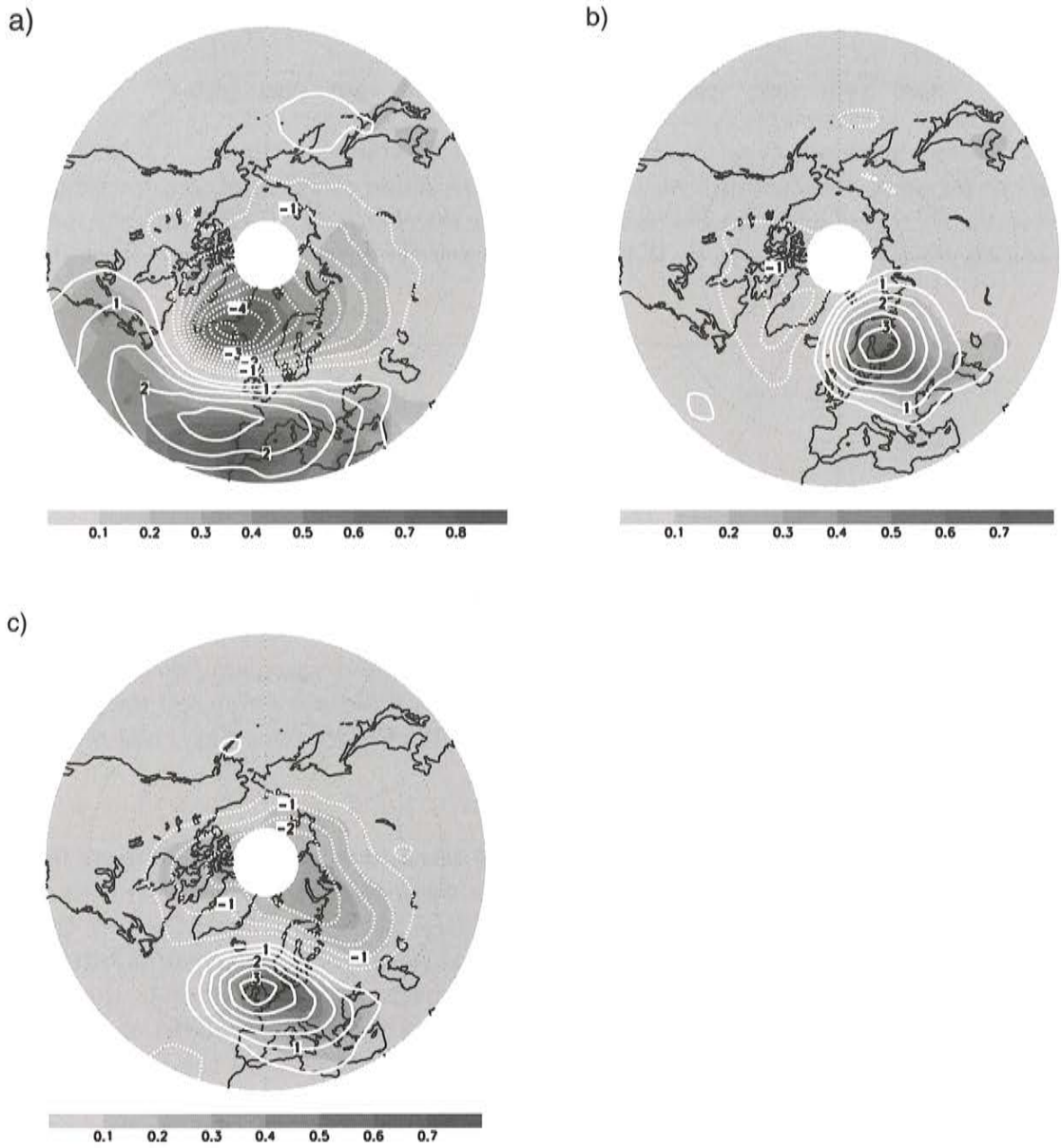

Figure 76: *The (a) winter SLP of [111] regressed upon the NAO, the (b) first, and (c) the second principal component. The contours give the regression coefficients [hPa]. The shading displays the local explained variances of the patterns.*

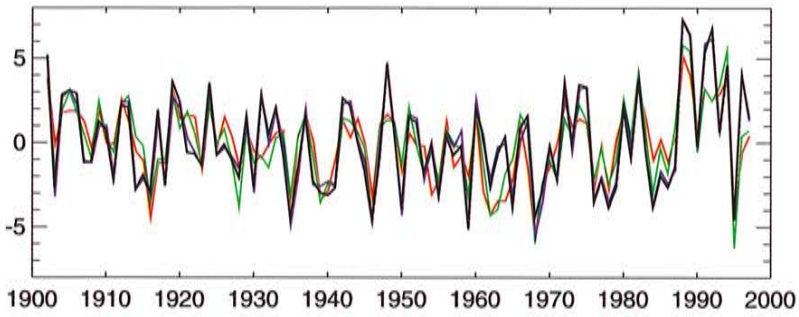

Figure 77: *The anomalous zonal component of the geostrophic wind (in $m\,s^{-1}$) for winter (DJFM) at Landsort: Calculated from the SLP reconstruction (black line), the fraction described by the NAO (red line), the fraction described by the NAO and SCAND patterns (green line), and the fraction described by the NAO, SCAND, and EATL/WRUS patterns (blue line).*

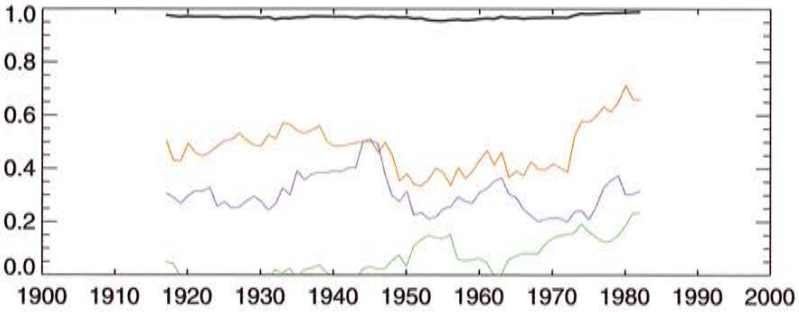

Figure 78: *31-year running explained variance between the zonal component of the geostrophic wind for winter (DJFM) at Landsort calculated from the SLP reconstruction and the fraction described by: NAO (red line), SCAND (green line), EATL/WRUS (blue line), and the sum of NAO, SCAND, and EATL/WRUS (black line).*

the zonal geostrophic wind at Landsort from the SLP reconstruction and alternatively from the dominant SLP modes. We found that 57 % of the variance of the reconstructed wind is explained by NAO, 12 % by SCAND, and 29 % by EATL/WRUS (Figs.77 and 78). All three modes together explain 98 % of the zonal wind variance at Landsort. In principal, the division into the dominant SLP modes works also for the total river runoff (not shown). However, the explained variance is much smaller. This is consistent with the calculated correlation between the annual mean winter runoff and NAO (Fig.72) and between the annual mean zonal wind anomaly at Stolpe Channel and NAO (Fig.73). The 31-year moving correlation with NAO is almost always higher in case of the zonal wind than in case of the winter runoff but the correlation shows similar minima and maxima in time. Further evidence (though indirect) for the linkage between the runoff and the large-scale circulation is given by [119]. They calculated the regression coefficients between the canonical time series associated with their North Atlantic zonal circulation pattern and the winter mean precipitation at stations around the Baltic Sea. At the stations located in the Baltic Sea catchment east of the Baltic, the regression coefficients are positive, indicating that seasons with stronger westerly winds are on average linked with higher than normal precipitation in the same season and probably with enhanced river runoff in the following spring due to snow accumulation. The same spatial distribution is found for the correlation between NAO and precipitation in Scandinavia

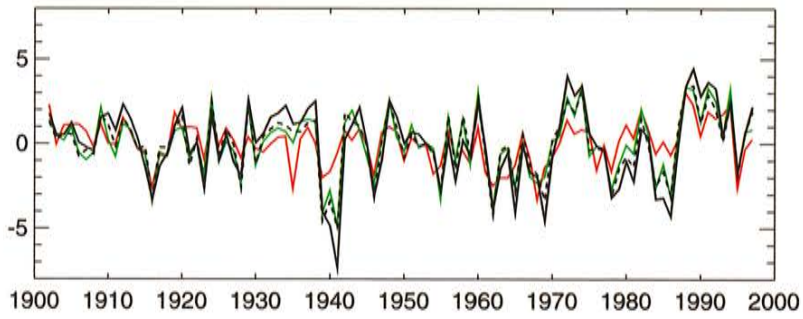

Figure 79: *The anomalous air temperature (in °C) in winter (DJFM) at Stockholm: Observed (black line), from the SAT reconstruction (black dashed line), the fraction described by the NAO (red line), and the fraction described by the NAO and the BO (green line).*

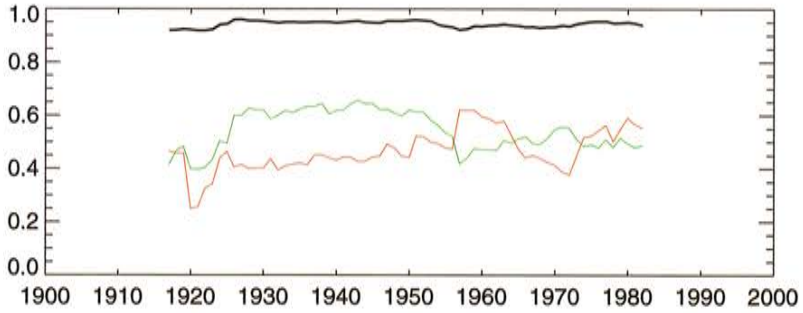

Figure 80: *31-year running explained variance between the reconstructed air temperature at Stockholm and the fraction described by the NAO (red line), the fraction described by the BO (green line), and by the sum (black line).*

[113].

The variability of the air temperature at Stockholm cannot be divided into the three dominant SLP modes, i.e. into NAO, SCAND, and EATL/WRUS. Therefore, we have repeated the procedure for the air temperature as sketched above for the SLP. We found that 50 % of the variance of the reconstructed air temperature at Stockholm is explained by NAO and 48 % by a SLP pattern similar to the *Barents Sea Oscillation (BO)* [104] (Figs.79 and 80). In an analysis presented by [110] the BO appears 'as a way to represent the non stationarity of the AO (NAO) spatial patterns', i.e. the BO describes shifts of the Icelandic low pressure center towards the Barents Sea. Both modes together explain 94 % (87 %) of the reconstructed (observed) air temperature variance at Stockholm. For further details the reader is referred to Kauker and Meier (Modeling decadal variability of the Baltic Sea. Part 1: Reconstructing atmospheric surface data for the period 1902-1998, submitted to Journal of Geophysical Research, 2002).

Summarizing, the two main forcing functions of the Baltic Sea salinity, the freshwater inflow and the local wind, are connected via the large-scale atmospheric circulation. Dominant patterns of inter-annual SLP variability in winter are NAO, SCAND, and EATL/WRUS. As the variability of precipitation depends on very local-scale processes, the link to the large-scale circulation is much weaker. The two exceptionally long stagnation periods, the 1920s to the

1930s and the 1980s to the mid 1990s, coincide with high positive values of the winter NAO index. However, we found only high correlations between local variables (runoff, precipitation, wind) and the NAO index during the second stagnation period (Figs.72 and 73). The lower correlation during the first stagnation period is caused by a strong variability of other modes.

11 Extreme states

In this section extreme states of the Baltic Sea stratification are studied. Simulations have been performed for the period 1902-1998 with increased and decreased saltwater inflow and with increased and decreased freshwater inflow. [72] has studied an extreme condition by integrating RCO for a period of 100 years while assuming that no major saltwater inflow occurs. River runoff was increased by 16% compared to the mean value of $14,085\,m^3\,s^{-1}$ for the period 1902-1998. In this sensitivity experiment (S2), salinity in the Gotland Basin decreases in the surface layer by about 3 to 4 psu and in the bottom layer by about 6 to 6.5 psu (Fig.81a). The final quasi-equilibrium is characterized by salinities of 2.8 psu (minimum at the surface) to 6.5 psu (maximum at the bottom). Upper and lower layer are still separated by a pronounced halocline which restricts the impact of wind mixing to the upper layer. Based on these results [72] concluded that it is very unlikely that the Baltic Sea will become a lake in future.

Results of additionally performed sensitivity experiments with extreme forcing are shown in Figures 81 and 82. Experiments with present-day saltwater inflow variability and with increased freshwater inflow of 34 % (run 407) and 100 % (run 416) have been performed. The salinity in the whole water column is reduced significantly (Figs.82a and b). However, even in the case of 100 % increased freshwater inflow we found still a halocline in about 60 to $100\,m$ of depth. Our 3D model results do not support the results of the semi-empirical model by [92]. [92] claimed that the Baltic Sea will become a lake when the freshwater inflow is larger than $21,500\,m^3\,s^{-1}$. Experiments with reduced freshwater inflow of 18 % (run 397), 21 % (run 417), and 69 % (run 431) underline the important role of the freshwater inflow for the system. We found significantly increased salinities (Figs.81c, 82c, and 82d).

Finally, an experiment with increased saltwater inflow and present-day freshwater inflow variability has been performed (run 395). SLP, wind forcing, and sea level in Kattegat of the calendar year 1951/52 have been used for the whole period 1902-1998. In November/December 1951 the largest during the last century observed (and simulated) saltwater inflow occurred. The large annually repeated saltwater inflow causes the Baltic Sea salinity to drift to significantly higher values (Fig.81d).

In Figure 83 the Baltic Sea mean salinity as a function of time is shown. Results of sensitivity experiments based on the standard run 403 are depicted. These are extreme cases with increased and decreased freshwater inflow as discussed above and experiments with omitted decadal variability of the freshwater inflow and of the SLP (see Section 9). The natural variability of the mean salinity is much smaller than the changes in the extreme cases. During the last 30 years (1969-1998) the mean salinity is almost constant in time (apart from natural fluctuations). The system is in a new steady-state. Freshwater inflows and steady-state salinities of the different experiments are summarized in Table 14. The phase diagram shows that the relationship between freshwater supply and mean salinity of the final steady-state is

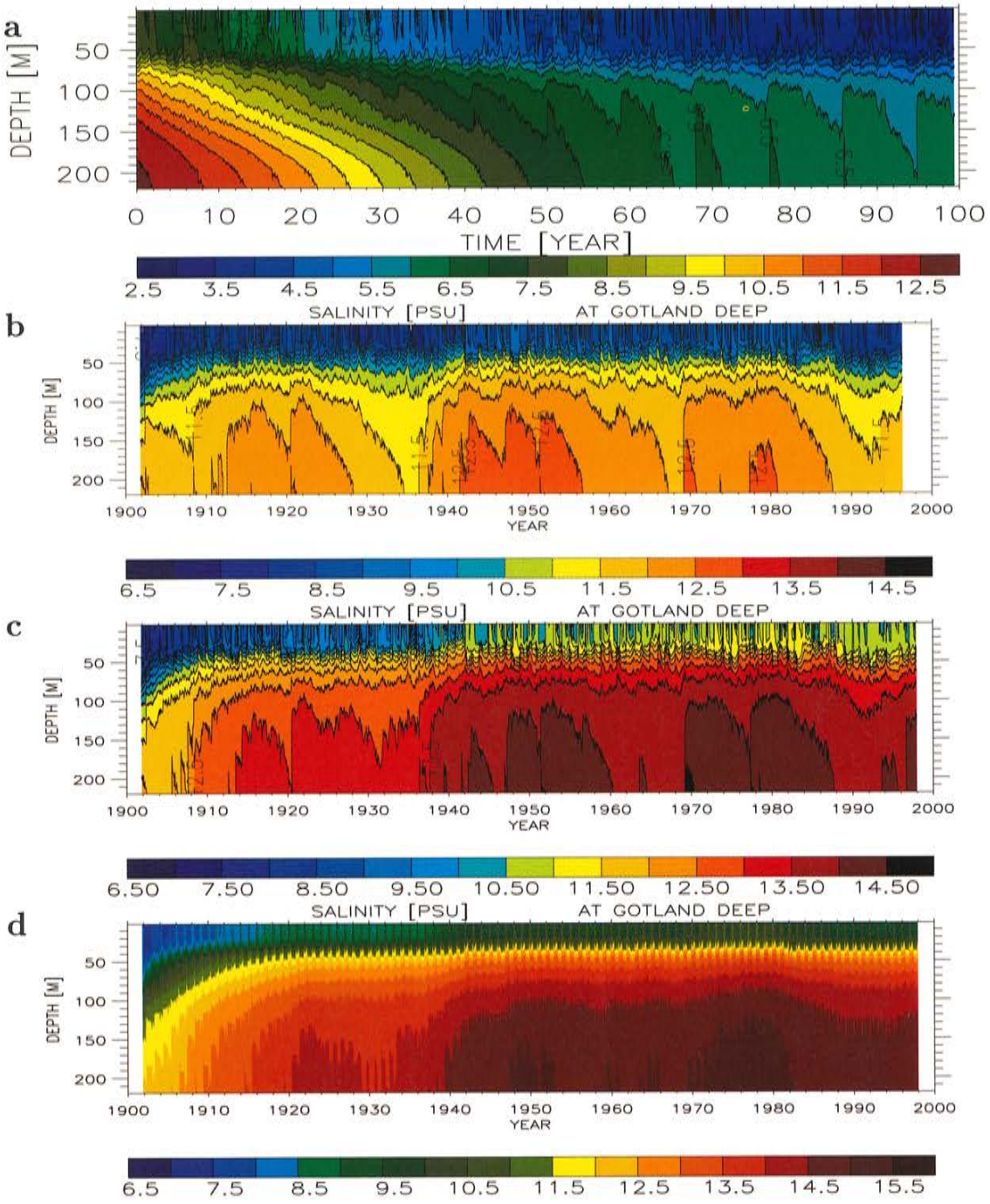

Figure 81: *Isohaline depths (in psu) in the eastern Gotland Basin (BY15): (a) with* 16 % *increased river runoff and no major saltwater inflows (S2), (b) standard experiment with present-day saltwater inflow variability (run 373b), (c) river runoff from 1976 for all years and present-day saltwater inflow variability (run 397), (d) sea level pressure and Kattegat sea level from 1951/52 for all years (run 395).*

non-linear (Fig.84).

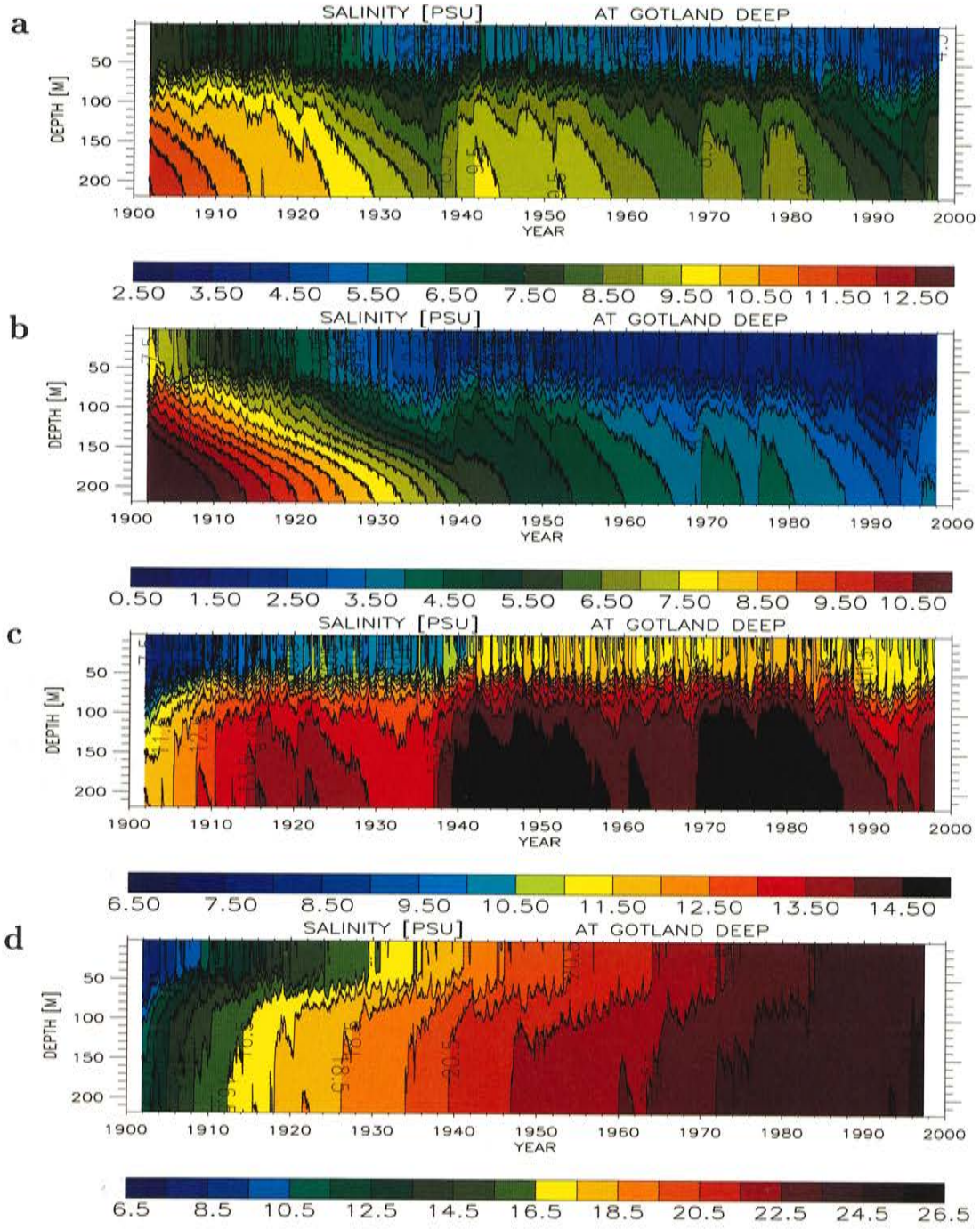

Figure 82: *Isohaline depths (in psu) in the eastern Gotland Basin (BY15): Experiments with present-day saltwater inflow variability and with (a)* 34 % *increased freshwater inflow (run 407), (b)* 100 % *increased freshwater inflow (run 416), (c)* 21 % *reduced freshwater inflow (corresponding to the mean runoff during 1976 of* $11,132\,m^3\,s^{-1}$*) (run 417), and (d)* 69 % *reduced freshwater inflow (run 431).*

12 Discussion

The RCO model has been validated earlier in hindcast simulations forced with observed atmospheric surface fields for the period 1980-1993 (e.g. [71], [72], [73], [77]). Therefore,

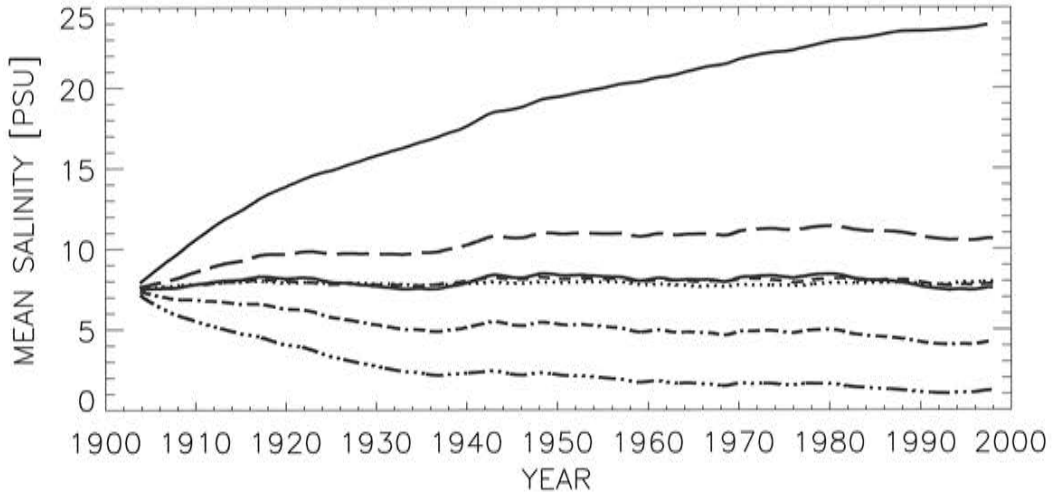

Figure 83: *2-year running mean salinity of the Baltic Sea without Kattegat (in psu): run 403 (solid), run 409 (dotted), run 418 (dashed), run 407 (dashed-dotted), run 416 (dashed-dotted with 3 dots), run 417 (long-dashed), run 431 (solid).*

	Runoff $(m^3\,s^{-1})$	Net precipitation $(m^3\,s^{-1})$	Sum $(m^3\,s^{-1})$	Change (%)	Mean Salinity (psu)
Observations	14,085				7.3
Run 403	14,085	2,030	16,115		7.98
Run 409	14,085	2,030	16,115		7.98
Run 418	14,085	2,030	16,115		7.83
Run 407	18,927	2,728	21,655	+ 34	4.56
Run 416	28,170	4,060	32,230	+ 100	1.36
Run 417	11,132	1,604	12,736	- 21	10.99
Run 431	4,370	630	5,000	- 69	22.99

Table 14: *Freshwater inflow and steady-state Baltic Sea mean salinity for the period 1969-1998. The relative change of the total freshwater inflow refers to the standard experiment run 403.*

we have focussed in our model validation on selected variables to detect artificial long-term trends caused by model biases or caused by shortcomings of the reconstruction procedure.

No trend of the simulated Landsort sea level is found. The errors (a mean error of 3.0 cm and a rms error of 11.3 cm) are of the same magnitude as found by [77] for the shorter period 1980-1993.

We found a systematic positive bias of the simulated ice cover even during the fitting period. Here, further work is still necessary. However, our results are not significantly worse than in previous studies using statistical models (e.g. [109], [83]).

As the halocline is too shallow in the simulation, the model drifts towards higher salinities during the first two decades of the century (Fig.56). The reason is unclear. Either mixing

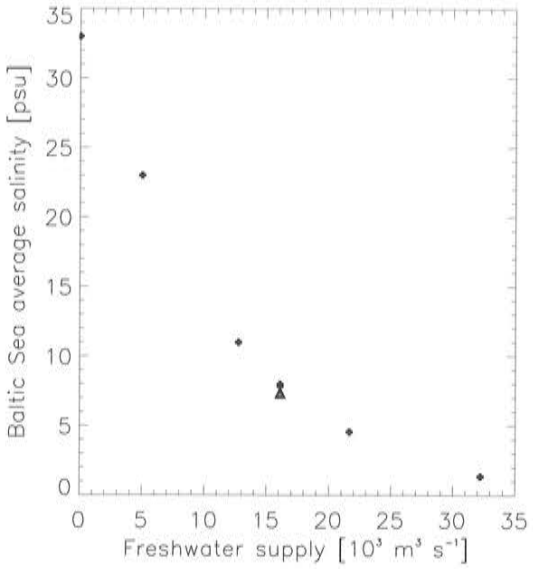

Figure 84: *Steady-state Baltic Sea mean salinity for the period 1969-1998 as a function of the freshwater supply calculated from observations (triangle) and from model results (plus signs: run 403, 409, 418, 407, 416, 417, 431; see Tab.14). For zero freshwater supply a mean salinity of* $33\,psu$ *is assumed.*

in the model is underestimated or re-stratification processes are overestimated. In the first case, underestimated extreme events of wind speed and unresolved processes generating turbulence, e.g. Langmuir circulation [5], are likely candidates.

Our results suggest that increased runoff and precipitation reduce the intensity of saltwater inflows but cannot explain the recent stagnation period (and the one during the 1930s) in the Baltic proper completely. Additional changes of the large-scale atmospheric circulation caused a reduced saltwater flow into the Baltic Sea during those periods. An anomalous positive westerly wind component on decadal time scale is found causing an anomalous high sea level in the Baltic. We believe that the deepwater flow is hampered due to the additional pressure gradient. Further investigations are still necessary to illuminate the mechanism. Our hypothesis differs from the conceptual model presented by [92]. They assumed that the mixing in the Danish Straits between the outflowing and the inflowing water is the most important factor determining the salinity of the Baltic Sea. Enhanced accumulated freshwater inflow increases the return flow of freshwater equivalents into the Baltic Sea at the Danish Straits. [117] claimed that this positive feedback mechanism explains the good correlation between the freshwater storage anomaly and the accumulated freshwater inflow.

Our model results agree well with the analysis results of long time series presented by [97]. [97] compared meteorological and oceanographic data during inflow seasons without and with major inflow events. Between November and April, [97] found significant differences only in river runoff and salinity at the Darss Sill. The significance of the wind speed differences is limited to isolated months.

[119] found that stronger than normal westerly winds are related to lower than normal salinities in the upper and lower layers in all areas of the Baltic Sea. Their analysis of this link

between the large-scale atmospheric circulation and annual salinity reveals that roughly one half of the salinity variability is correlated to the meridional atmospheric pressure gradient over the North Atlantic, and thus to the strength of the westerly zonal winds. These results are confirmed by our model study. We provided a dynamical explanation for the apparent inconsistency discussed by [119] that increased westerlies would cause more frequent and more intense major Baltic inflows.

13 Conclusions

The main conclusions are:

1. The first 100-year hindcast simulations of the Baltic Sea using a 3D coupled ice-ocean model have been presented. Due to technical limitations and due to lacking atmospheric surface data for the Baltic Sea region, 100-year simulations were not possible earlier. Baltic Sea climate of the period 1902-1998 is simulated realisticly with RCO. The reconstructed atmospheric forcing data have high quality.

2. The earlier problem of underestimated saltwater inflows is solved by the implementation of a new turbulence scheme in RCO. Our results suggest that the constant parameter $c_{\varepsilon 3}$ of the $k-\varepsilon$ model should be replaced by a turbulent Prandtl number dependent, negative function.

3. Net precipitation is found to be positive contributing to the total freshwater inflow with about 13 %. The decadal variabilities of runoff and precipitation are well correlated. On this time scale maximum variations of runoff and precipitation relative to the mean values are about 19 % and 10 %, respectively. The decadal variability of evaporation is relatively small.

4. The simulated freshwater storage anomaly agrees well with observations. Thus, our results confirm that the freshwater storage anomaly and the accumulated freshwater inflow are well correlated.

5. The total mean salinity of the Baltic Sea amounts to about $7\,psu$. Decadal variations are of the order of $1\,psu$. No long-term trend is found during the century in accordance with [117].

6. The vertical circulation of the Baltic Sea is very sensitive on internal mixing and on the surface wind fields. Both are important for saltwater inflows and for the energy flux to near-inertial motions generating turbulence. Stronger wind amplitudes cause increased mixing and consequently a deeper halocline. Good results for the halocline depth are obtained using an additional random component to the geostrophic wind derived from reconstructed SLP fields.

7. About half of the decadal variability of Baltic Sea salinity is related to the accumulated freshwater inflow.

8. If river regulation is assumed to change the discharge seasonality but not accumulated runoff on decadal time scale, the impact of river regulations on Baltic Sea variability is negligible.

9. The second half of the decadal variability of mean salinity is related to decadal variations of the large-scale SLP over Scandinavia. Stronger westerly winds during stagnation periods cause increased average Baltic sea levels and reduced saltwater transports into the Baltic Sea. In addition, eastward surface-layer transports are stronger than normal. Consequently, the mean eastward lower-layer transport through the Stolpe Channel is reduced. Thus, the entrainment of the deepwater flow between Bornholm Basin and the eastern Gotland Basin decreases.

10. During the last century two exceptionally long stagnation periods are found. Both periods are characterized by increased westerly winds and increased precipitation. The first stagnation period caused by the wind forcing starts 1921 and ends 1934 whereas the first stagnation period caused by the freshwater inflow is lacking with 7 years. The latter starts 1928 and ends 1941. The second stagnation period starts 1989 (wind forcing) and 1985 (freshwater inflow).

11. Although saltwater inflows have never been observed in the second part of the inflow season during severe winters, in general a rigid ice lid covering the entire Baltic surface area has only a small impact on saltwater inflows in present climate. For the period 1902-1998, we found only a few years when the impact is quite dramatic.

12. The high-frequency variability of the sea level in Kattegat at the open boundary of the Baltic Sea model is very important for the long-term behavior of mean salinity in the system. Variations with periods of about 10-20 days cause saltwater inflow events. Daily variability has an impact on mixing and consequently on the intensity of saltwater inflows. To the contrary, decadal variability of the Kattegat sea level is unimportant for salinity.

13. During both stagnation periods positive annual mean westerly wind anomalies at the Stolpe Channel and positive annual mean runoff anomalies coincide with exceptionally high NAO indices. We found fairly high correlations between the annual mean westerly wind anomaly and the winter NAO index and between the winter mean runoff and the winter NAO index during the second stagnation period. Dominant patterns of inter-annual SLP variability in winter are NAO, SCAND, and EATL/WRUS.

14. The sensitivity of the salinity is much smaller than in the semi-empirical model presented by [92]. We found that even with a 100 % increased freshwater supply compared to the period 1902-1998 the Baltic Sea cannot be classified as a lake. The relationship between freshwater supply and mean salinity of the final steady-state is non-linear.

14 Future outlook

It is planned to perform with RCO 100-year transient experiments for the Baltic Sea. Global coupled Atmosphere-Ocean General Circulation Models (AOGCMs) are typically too coarse to resolve regional scales of interest for climate change impact studies. One of the techniques being used to study climate change on the regional scale is dynamical downscaling. In this approach, a high-resolution limited-area atmosphere model is run with boundary data taken from a GCM simulation [94], [90]. So far, the results of the regional model has been used to calculate scenarios for the Baltic Sea during time slices [70], [37], [72], [73], [74], [25]. Also for the North Sea dynamical downscaling has been applied to regionalize climate change [52]. Assuming that the variability of the past 100 years will not change in future, it is now possible to simulate changing Baltic Sea climate gradually.

Acknowledgments

The SWECLIM program and the Rossby Centre are funded by the Foundation for Strategic Environmental Research (MISTRA) and by the Swedish Meteorological and Hydrological Institute (SMHI). The simulations have been performed on the Silicon Graphics Origin 3800 at the Swedish National Supercomputer Centre in Linköping, Sweden. Special thanks are given to Hans Alexandersson (SMHI) for providing sea level pressure station data and wind speed observations at Landsort, to Lars Axell (SMHI) for providing the optimized wind speed parameterization at Östergarnsholm, to Barry Broman (SMHI) for providing tide gauge data, to Bengt Carlsson (SMHI), Phil Graham (SMHI), and Jercy Cyberski (University of Gdansk, Institute of Oceanography, Gdynia, Poland) for providing river runoff data, to Frank Janssen (Baltic Sea Research Institute Warnemünde, Germany, IOW) for providing calibrated ice area data from the Global Digital Sea Ice Data Bank of the USA National Ice Center, to Jari Haapala (University of Helsinki, Finland) for providing maximum ice extent data, to Wolfgang Matthäus (IOW) for providing major Baltic inflow data, to Lars Meuller (SMHI) for providing gridded atmospheric surface data for the period 1970-2001, and to Ann-Sofi Smedman and hers group (Department of Earth Sciences, Meteorology, Uppsala University, Sweden) for providing wind speed observations at Östergarnsholm. Temperature and salinity profiles of the Marine Data Centre of the International Council for the Exploration of the Sea (ICES) are used. The North Atlantic Oscillation indices have been supplied by Phil Jones (Climatic Research Unit, University of East Anglia, Norwich, UK) via http://www.cru.uea.ac.uk/cru/data/nao.htm. Very helpful informations concerning the quality of Baltic Sea ice observations in general and the maximum ice extent data from the Finnish Institute of Marine Research (FIMR) in special are provided by Jouko Launiainen (FIMR). Torsten Seifert and Frank Janssen (IOW) contributed to the discussion about the long-term mean salinity of the Baltic Sea.

Appendix A: Overview of experiments performed

See Tables 15, 16 and 17.

Run	Period	Mixing	Atmos. forcing	River runoff	Sea level Kattegat	Comment	Ref.
Standard experiments 1980-93 (6 nm)							
240	1980-93	$k-\varepsilon$	SMHI (3h)	observed	observed (1h)		3.1, [71]
339	1980-93	$k-\varepsilon$	SMHI (3h)	observed	observed (1h)	without penetrating solar radiation	3.1
315	1980-93	$k-\varepsilon$	SMHI (3h)	observed	from daily SLP [36]	cf. run 240	9.4
Experiments 1992/93 and 1980-93 (2 nm)							
349	1992/93	$k-\varepsilon$	SMHI (3h)	observed	observed (1h)	2 nautical miles	9.2.4, [77]
350	1992/93	$k-\varepsilon$	SMHI (3h)	observed, +22%	observed (1h)	2 nautical miles, cf. run 349	9.2.4
367	1992/93	$k-\varepsilon$	SMHI (3h)	observed, −22%	observed (1h)	2 nautical miles, cf. run 349	9.2.4
399	1992/93	$k-\varepsilon$	SMHI (3h)	observed, −9%	observed (1h)	2 nautical miles, cf. run 349	9.2.4
354	1992/93	$k-\varepsilon$	SMHI (3h)	observed, unregulated [91]	observed (1h)	2 nautical miles, cf. run 349	9.2.4
353	1980-93	k	SMHI (3h)	observed	observed (1h)	2 nautical miles	8.8
Improved turbulence model 1980-93							
414	1980-93	improved k, $c_u = 1.1547$, $\alpha' = 1.5\,\alpha$	model (1d)	observed	observed (1h)	random wind component, cf. run 394	3.5
426b	1980-93	improved $k-\varepsilon$, $c_{\varepsilon 3} < 0$ (Eq.54), $\alpha' = 1.5\,\alpha$	model (1d)	observed	observed (1h)	random wind component, cf. run 394	3.5
413	1980-93	improved k, $c_u = 1.2$, $\alpha' = 1.5\,\alpha$	model (1d)	observed	observed (1h)	cf. run 373b	8.4.2
376	1980-93	improved k, $c_u = 1.1547$, $\alpha' = 1.5\,\alpha$	model (1d)	observed	observed (1h)	cf. run 375	8.4.2
402c	1980-93	improved k, $c_u = 1.1547$	model (1d)	observed	observed (1h)	$a_{red} = 0.78$, cf. run 403	8.4.2
Sensitivity mixing parameterization 1980-93							
264	1980-93	k	SMHI (3h)	observed	observed (1h)		9.1.1
361	1980-93	k, $m = 500$	model (1d)	observed	observed (1h)		9.1.1
362c	1980-93	k, $\alpha' = 1.5\,\alpha$	model (1d)	observed	observed (1h)		9.1.1
Standard experiments 1902-98							
373b	1902-98	improved k, $c_u = 1.2$, $\alpha' = 1.5\,\alpha$	model (1d)	observed basins	observed (1d)		8
403	1902-98	improved k, $c_u = 1.1547$	model (1d)	observed basins	observed (1d)	$a_{red} = 0.78$	8
394	1902-98	improved k, $c_u = 1.1547$, $\alpha' = 1.5\,\alpha$	model (1d)	observed basins	observed (1d)	random wind component	8

Table 15: *RCO experiments analyzed in this study. In the last column references to the corresponding sections of this study are listed. A statistical model is used to reconstruct daily sea level pressure and monthly surface air temperature, dew-point temperature, precipitation, and cloud cover fields [51]. Alternatively, atmospheric surface fields calculated from observations of the Swedish Meteorological and Hydrological Institute (SMHI) database are available since 1970 (see [51]). For further explanation see text.*

Run	Period	Mixing	Atmos. forcing	River runoff	Sea level Kattegat	Comment	Ref.
Sensitivity mixing parameterization 1902-98							
366	1902-98	k, $\alpha' = 1.5\,\alpha$	model (1d)	observed basins	observed (1d)	cf. run 373b	9.1.2
375	1902-98	improved k, $c_u = 1.1547$, $\alpha' = 1.5\,\alpha$	model (1d)	observed basins	observed (1d)	cf. run 373b	9.1.2
371	1902-98	improved k, $c_u = 1.5$, $\alpha' = 1.5\,\alpha$	model (1d)	observed basins	observed (1d)	cf. run 373b	9.1.2
368	1902-98	$k - \varepsilon$	model (1d)	observed basins	observed (1d)	cf. run 373b	9.1.2
396	1902-98	improved k, $c_u = 1.11$, $\alpha' = 1.5\,\alpha$	model (1d)	observed basins	observed (1d)	random wind component, cf. run 394	9.1.2
Sensitivity freshwater forcing 1902-98							
383	1902-98	improved k, $c_u = 1.2$, $\alpha' = 1.5\,\alpha$	model (1d)	monthly mean runoff 1902-98	observed (1d)	cf. run 373b	9.2
404	1902-98	improved k, $c_u = 1.2$, $\alpha' = 1.5\,\alpha$	model (1d), but monthly mean precip. 1902-70	monthly mean runoff 1902-70	observed (1d)	cf. run 373b	9.2
393	1902-98	improved k, $c_u = 1.2$, $\alpha' = 1.5\,\alpha$	model (1d), but random series of SLP and Kattegat sea level	observed basins	observed (1d)	cf. run 373b	9.2
408	1942-98	improved k, $c_u = 1.1547$	model (1d)	monthly mean runoff 1902-70 and inter-annual variability 1942-98	observed (1d)	$a_{red} = 0.78$, cf. run 403	9.2
409	1902-98	improved k, $c_u = 1.1547$	model (1d), but monthly mean precip. 1902-70	monthly mean runoff 1902-70	observed (1d)	$a_{red} = 0.78$, cf. run 403	9.2
410	1902-98	improved k, $c_u = 1.1547$	model (1d), but random series of SLP and Kattegat sea level	observed basins	observed (1d)	$a_{red} = 0.78$, cf. run 403	9.2
Sensitivity sea ice 1902-98							
406	1902-42	improved k, $c_u = 1.2$, $\alpha' = 1.5\,\alpha$	model (1d), but monthly mean t_{air}, t_{dew}, precip., cloud., 1902-70	monthly mean runoff 1902-70	observed (1d)	cf. run 373b	9.3
415	1902-98	improved k, $c_u = 1.1547$	model (1d), but t_{air} from 1941/42	observed basins	observed (1d)	$a_{red} = 0.78$, cf. run 403	9.3
Sensitivity Kattegat sea level 1902-98							
411	1902-98	improved k, $c_u = 1.1547$	model (1d)	observed basins	from daily SLP [36]	$a_{red} = 0.78$, cf. run 403	9.4
425	1902-42	improved k, $c_u = 1.1547$	model (1d)	observed basins	4-year high-pass filtered sea level	$a_{red} = 0.78$, cf. run 403	9.4
Sensitivity atmospheric forcing 1902-98							
420	1902-98	improved k, $c_u = 1.1547$	model (1d), but monthly mean cloudiness and humidity 1980-95	observed	observed (1d)	$a_{red} = 0.78$, cf. run 403	8.8
418	1902-98	improved k, $c_u = 1.1547$	model (1d), but monthly mean precip. 1902-70, 4-year high-pass filtered SLP	monthly mean runoff 1902-70	observed (1d)	$a_{red} = 0.78$, cf. run 403	9.2

Table 16: *As Table 15. Continuation of RCO experiments performed for this study.*

Run	Period	Mixing	Atmos. forcing	River runoff	Sea level Kattegat	Comment	Ref.
Extreme cases 1902-98							
395	1902-98	improved k, $c_u = 1.2$, $\alpha' = 1.5\,\alpha$	model (1d), but SLP and Kattegat sea level 1951/52	observed basins	observed (1d)	cf. run 373b	11
397	1902-98	improved k, $c_u = 1.2$, $\alpha' = 1.5\,\alpha$	model (1d)	runoff from 1976	observed (1d)	cf. run 373b	11
S2	2000-2100	$k - \varepsilon$	RCA1 scenario	HBV hindcast plus change	1980-89 subcycling		11, [72]
407	1902-98	improved k, $c_u = 1.1547$	model (1d), precip. plus 34%	observed basins plus 34%	observed (1d)	$a_{red} = 0.78$, cf. run 403	11
416	1902-98	improved k, $c_u = 1.1547$	model (1d), precip. plus 100%	observed basins plus 100%	observed (1d)	$a_{red} = 0.78$, cf. run 403	11
417	1902-98	improved k, $c_u = 1.1547$	model (1d), precip. minus 21%	observed basins minus 21%	observed (1d)	$a_{red} = 0.78$, cf. run 403	11
431	1902-98	improved k, $c_u = 1.1547$	model (1d), precip. minus 69%	observed basins minus 69%	observed (1d)	$a_{red} = 0.78$, cf. run 403	11

Table 17: *As Table 15. Continuation of RCO experiments performed for this study.*

Appendix B: Surface area and volume of the Baltic Sea

See Table 18.

	Area (km^2)		Volume (km^3)	
	Data	Model	Data	Model
Baltic only	377,400	391,481	21,200	23,107
Eastern Gotland Basin	-	95,531	-	7,297
Bornholm Basin	-	39,643	-	1,806
Arkona Basin	-	14,158	-	426
Belt Sea	18,740	27,754	270	424
The Sound	2,330	2,637	30	34
Kattegat	22,090	20,572	510	474
Total	420,560	442,446	22,010	24,039

Table 18: *Observed and modeled surface area and volume of the Baltic Sea. Independent data, so far available, are taken from [103]. The definition of the sub-basins in the model follows Fig.2 presented by [76] and might be quite different compared to [103].*

References

[1] H. Alexandersson, T. Schmith, K. Iden, and H. Tuomenvirta. Long-term variations of the storm climate over NW Europe. *The Global Atmosphere and Ocean System*, 6:97–120, 1998.

[2] H. Alexandersson, H. Tuomenvirta, T. Schmith, and K. Iden. Trends of storms in NW Europe derived from an updated pressure data set. *Clim. Res.*, 14:71–73, 2000.

[3] H. C. Andersson. Influence of long-term regional and large-scale atmospheric circulation on the Baltic sea level. *Tellus*, 54A:76–88, 2002.

[4] J.C. André and P. Lacarrère. Mean and turbulent structures of the oceanic surface layer as determined from one-dimensional, third-order simulations. *J. Phys. Oceanogr.*, 15(2):121–132, 1985.

[5] L. B. Axell. Wind-driven internal waves and Langmuir circulations in a numerical ocean model of the southern Baltic Sea. *J. Geophys. Res.*, 2002. In press.

[6] A. G. Barnston and R. E. Livezey. Classification, seasonality and persistence of low-frequency atmospheric circulation patterns. *Mon. Wea. Rev.*, 115:1083–1126, 1987.

[7] H. Baumert and H. Peters. Second-moment closures and length scales for weakly stratified turbulent shear flows. *J. Geophys. Res.*, 105:6,453–6,468, 2000.

[8] H. Baumert, J. Simpson, and J. Sündermann, editors. *Marine Turbulence*. Cambridge University Press, 2002. In press.

[9] S. Bergström and B. Carlsson. River runoff to the Baltic Sea: 1950-1990. *Ambio*, 23:280–287, 1994.

[10] B. Blanke and P.Delecluse. Variability of the tropical Atlantic Ocean simulated by a general circulation model with two different mixed layer physics. *J. Phys. Oceanogr.*, 23:1363–1388, 1993.

[11] K. Bumke and L. Hasse. An analysis scheme for the determination of true surface winds at sea from ship synoptic wind and pressure observations. *Boundary-Layer Meteorol.*, 47:295–308, 1989.

[12] K. Bumke, U. Karger, L. Hasse, and K. Niekamp. Evaporation over the Baltic Sea as an example of a semi-enclosed sea. *Contr. Atmos. Phys.*, 71:249–261, 1998.

[13] H. Burchard and H. Baumert. On the performance of a mixed-layer model based on the $k-\varepsilon$ turbulence closure. *J. Geophys. Res.*, 100:8,523–8,540, 1995.

[14] H. Burchard and K. Bolding. Comparative analysis of four second-moment turbulence closure models for the oceanic mixed layer. *J. Phys. Oceanogr.*, 31:1943–1968, 2001.

[15] H. Burchard and O. Petersen. Models of turbulence in the marine environment - A comparative study of two-equation turbulence models. *J. Mar. Sys.*, 21:29–53, 1999.

[16] H. Burchard, O. Petersen, and T.P. Rippeth. Comparing the performance of the Mellor-Yamada and the $k-\varepsilon$ two-equation turbulence models. *J. Geophys. Res.*, 103:10,543–10,554, 1998.

[17] V.M. Canuto, A. Howard, Y. Cheng, and M.S. Dubovikov. Ocean turbulence i: one-point closure model. Momentum and heat vertical diffusivities. *J. Phys. Oceanogr.*, 31:1413–1426, 2001.

[18] H. Charnok. Wind stress on a water surface. *Quart. J. Roy. Meteor. Soc.*, 81:639–640, 1955.

[19] D. Chen and C. Hellström. The influence of the North Atlantic Oscillation on the regional temperature variability in Sweden: spatial and temporal variations. *Tellus*, 51A:505–516, 1999.

[20] P.D. Craig. Velocity profiles and surface roughness under breaking waves. *J. Geophys. Res.*, 101:1265–1277, 1996.

[21] P.D. Craig and M.L. Banner. Modelling wave-enhanced turbulence in the ocean surface layer. *J. Phys. Oceanogr.*, 24:2546–2559, 1994.

[22] J. Cyberski and A. Wroblewski. Riverine water inflows and the Baltic Sea water volume 1901-1990. *Hydrology and Earth System Sciences*, 4:1–11, 2000.

[23] E. A. D'Asaro. The energy flux from the wind to near-inertial motions in the surface mixed layer. *J. Phys. Oceanogr.*, 15:1043–1059, 1985.

[24] J. Dera. *Marine Physics*. Oceanography Series Vol. 53. Elsevier, Warschau, 1992.

[25] R. Döscher and H. E. M. Meier. Baltic Sea ice in regional control and scenario runs based on Hadley Centre data. SWECLIM Newsletter No.12, 24-27, Swedish Meteorological and Hydrological Institute, SE-60176 Norrköping, Sweden, 2002.

[26] M. Ekman. A consistent map of the postglacial uplift of Fennoscandia. *Terra Nova*, 8:158–165, 1996.

[27] M. Ekman and J. Mäkinen. Mean sea surface topography in the Baltic Sea and its transition area to the North Sea: a geodetic solution and comparison with oceanographic models. *J. Geophys. Res.*, 101:11,993–11,999, 1996.

[28] J. Elken. Deep water overflow, circulation and vertical exchange in the Baltic Proper. Report Series No.6, Estonian Marine Institute, Tallinn, Estonia, 1996. 91 pp.

[29] H. Fischer and W. Matthäus. The importance of the Drogden Sill in the Sound for major Baltic inflows. *J. Mar. Sys.*, 9:137–157, 1996.

[30] H. Franck, W. Matthäus, and R. Sammler. Major inflows of saline water into the Baltic Sea during the present century. *Gerlands Beitr. Geophys.*, 96:517–531, 1987.

[31] B. Galperin, L.H. Kantha, S. Hassid, and A. Rosati. A quasi-equilibrium turbulent energy model for geophysical flows. *J. Atmos. Sci.*, 45:55–62, 1988.

[32] A.E. Gargett. Vertical eddy diffusivity in the ocean interior. *J. Mar. Res.*, 42:359–393, 1984.

[33] P. L. Graham. Modeling runoff to the Baltic Sea. *Ambio*, 27:328–334, 1999.

[34] G. Granqvist. Översikt av isarna vintern 1926-27. Havsforskningsinstitutets skrift No.55, p.1, Finnish Institute of Marine Research, Helsinki, Finland, 1928.

[35] B. G. Gustafsson. Time-dependent modeling of the Baltic entrance area. 2. Water and salt exchange of the Baltic Sea. *Estuaries*, 2:253–266, 2000.

[36] B. G. Gustafsson and H. C. Andersson. Modeling the exchange of the Baltic Sea from the meridional atmospheric pressure difference across the North Sea. *J. Geophys. Res.*, 106:19,731–19,744, 2001.

[37] J. Haapala, H. E. M. Meier, and J. Rinne. Numerical investigations of future ice conditions in the Baltic Sea. *Ambio*, 30:237–244, 2001.

[38] B. G. Håkansson, B. Broman, and H. Dahlin. The flow of water and salt in the Sound during the Baltic major inflow event in January 1993. In *ICES Statutory Meeting. Dublin, Ireland, ICES C.M. 1993/C:57*, 1993. 26 pp.

[39] J. Hänninen and I. Vuorinen. Climatic factors in the Atlantic control the oceanographic and ecological changes in the Baltic Sea. *Limnol. Oceanogr.*, 45:703–710, 2000.

[40] HELCOM. Fourth periodic assessment of the state of the environment of the Baltic marine area, 1994-1998. Baltic sea environment proceedings, Baltic Marine Environment Protection Commision, Helsinki, Finland, 2002. In press.

[41] M. Hilmer and T. Jung. Evidence for a recent change in the link between the North Atlantic Oscillation and Arctic sea ice export. *Geophys. Res. Lett.*, 27:989–992, 2000.

[42] J. W. Hurrell. Decadal trends in the North Atlantic Oscillation: Regional temperatures and precipitation. *Science*, 269:676–679, 1995.

[43] F. Jakobsen. The major inflow to the Baltic Sea during January 1993. *Contin. Shelf Res.*, 6:227–240, 1995.

[44] F. Jakobsen. Hydrographic investigation of the Northern Kattegat front. *Contin. Shelf Res.*, 17:533–554, 1997.

[45] F. Janssen, C. Schrum, and J. Backhaus. A climatological dataset of temperature and salinity for the North Sea and the Baltic Sea. *Deut. Hydrogr. Z., Supplement*, 9:245 pp, 1999.

[46] N.G. Jerlov. *Optical oceanography.* Elsevier, 194 pp, 1968.

[47] M. Johansson, H. Boman, K.K. Kahma, and J. Launiainen. Trends in sea level variability in the Baltic Sea. *Boreal Env. Res.*, 6:159–179, 2001.

[48] P. D. Jones, T. Jonsson, and D. Wheeler. Extension to the North Atlantic Oscillation using early instrumental pressure observations from Gibraltar and South-West Iceland. *Int. J. Climatol.*, 17:1433–1450, 1997.

[49] R. Jurva. Über den allgemeinen Verlauf des Eiswinters in den Meeren Finnlands und über die Schwankungen der grössten Vereisung. Sitzungsberichte 1941, Finnische Akademie der Wissenschaften, Helsinki, Finland, 1944.

[50] T. Kõuts and A. Omstedt. Deep water exchange in the Baltic Proper. *Tellus*, 45A:311–324, 1993.

[51] F. Kauker and H. E. M. Meier. Reconstructing atmospheric surface data for the period 1902-1998 to force a coupled ocean-sea ice model of the Baltic Sea. Reports Meteorology and Climatology No.99, Swedish Meteorological and Hydrological Institute, SE-60176 Norrköping, Sweden, 2002. 30 pp.

[52] F. Kauker and H. von Storch. Regionalization of climate model results for the North Sea. GKSS-Report 2000/28, GKSS, Geesthacht, Germany, 2000.

[53] A.N. Kolmogorov. The equation of turbulent motion in an incompressible fluid. *Izv. Akad. Nauk SSSR, Ser. Fiz.*, 6:56–58, 1942.

[54] G. Koslowski and P. Loewe. The western Baltic Sea ice season in terms of a mass-related severity index: 1879-1992. Part 1: Temporal variability and association with the North Atlantic Oscillation. *Tellus*, 46A:66–74, 1994.

[55] W. Krauss and B. Brügge. Wind-produced water exchange between the deep basins of the Baltic Sea. *J. Phys. Oceanogr.*, 21:373–384, 1991.

[56] H.-U. Lass and W. Matthäus. On temporal wind variations forcing salt water inflows into the Baltic Sea. *Tellus*, 48A:663–671, 1996.

[57] A. Lehmann. The major Baltic inflow in 1993 - a numerical model simulation. In *ICES Statutory Meeting. St. Johns, Canada, ICES C.M. 1994/Q:9*, 1994. 18 pp.

[58] A. Lehmann, W. Krauss, and H.-H. Hinrichsen. Effects of remote and local atmospheric forcing on circulation and upwelling in the Baltic Sea. *Tellus*, 54A:299–316, 2002.

[59] G. Lindström. Vattentillgång och höga flöden i Sverige under 1900-talet. Elforsk rapport, Elforsk, Stockholm, 2002. 39 pp.

[60] P. Loewe and G. Koslowski. The western Baltic Sea ice season in terms of a mass-related severity index: 1879-1992. Part 2: Spectral characteristics and association with the NAO, QBO, and solar cycle. *Tellus*, 50A:219–241, 1998.

[61] R. Lueck and R. Reid. On the production and dissipation of mechanical energy in the ocean. *J. Geophys. Res.*, 89:3,439–3,445, 1984.

[62] L.N. Ly. Numerical studies of the surface-wave effects on the upper turbulent layer in the ocean. *Tellus*, 42A:557–567, 1990.

[63] W. Matthäus and H. Franck. Characteristics of major Baltic inflows - a statistical analysis. *Cont. Shelf Res.*, 12:1375–1400, 1992.

[64] W. Matthäus and H.-U. Lass. The recent salt inflow into the Baltic Sea. *J. Phys. Oceanogr.*, 25:280–286, 1995.

[65] W. Matthäus, H.-U. Lass, and R. Tiesel. The major Baltic inflow in January 1993. In *ICES Statutory Meeting. Dublin, Ireland, ICES C.M. 1993/C:51*, 1993. 16 pp.

[66] W. Matthäus and H. Schinke. The influence of river runoff on deep water conditions of the Baltic Sea. *Hydrobiologia*, 393:1–10, 1999.

[67] H. E. M. Meier. *A regional model of the western Baltic Sea with open boundary conditions and data assimilation (in German).* PhD thesis, University of Kiel, Institute of Marine Research, D-24105 Kiel, Germany, 1996. In: Ber. Inst. f. Meereskunde No.284, 117 pp.

[68] H. E. M. Meier. First results of multi-year simulations using a 3D Baltic Sea model. Reports Oceanography No. 27, Swedish Meteorological and Hydrological Institute, SE-60176 Norrköping, Sweden, 1999. 48 pp.

[69] H. E. M. Meier. The use of the $k-\varepsilon$ turbulence model within the Rossby Centre regional ocean climate model: parameterization development and results. Reports Oceanography No.28, Swedish Meteorological and Hydrological Institute, SE-60176 Norrköping, Sweden, 2000. 81 pp.

[70] H. E. M. Meier. The first Rossby Centre regional climate scenario for the Baltic Sea using a 3D coupled ice-ocean model. Reports Meteorology and Climatology No.95, Swedish Meteorological and Hydrological Institute, SE-60176 Norrköping, Sweden, 2001. 63 pp.

[71] H. E. M. Meier. On the parameterization of mixing in 3D Baltic Sea models. *J. Geophys. Res.*, 106:30,997–31,016, 2001.

[72] H. E. M. Meier. Regional ocean climate simulations with a 3D ice-ocean model for the Baltic Sea. Part 1: Model experiments and results for temperature and salinity. *Clim. Dyn.*, 19:237–253, 2002.

[73] H. E. M. Meier. Regional ocean climate simulations with a 3D ice-ocean model for the Baltic Sea. Part 2: Results for sea ice. *Clim. Dyn.*, 19:255–266, 2002.

[74] H. E. M. Meier and R. Döscher. First regional downscaling results for Baltic Sea temperature and salinity based on Hadley Centre boundary data from HadAM3. SWECLIM Newsletter No.12, Swedish Meteorological and Hydrological Institute, SE-60176 Norrköping, Sweden, 2002. 21-24.

[75] H. E. M. Meier and R. Döscher. Simulated water and heat cycles of the Baltic Sea using a 3D coupled atmosphere-ice-ocean model. *Boreal Env. Res.*, 7, 2002. In press.

[76] H. E. M. Meier, R. Döscher, A. C. Coward, J. Nycander, and K. Döös. RCO - Rossby Centre regional Ocean climate model: model description (version 1.0) and first results from the hindcast period 1992/93. Reports Oceanography No.26, Swedish Meteorological and Hydrological Institute, SE-60176 Norrköping, Sweden, 1999. 102 pp.

[77] H. E. M. Meier, R. Döscher, and T. Faxén. A multiprocessor coupled ice-ocean model for the Baltic Sea: application to salt inflow. *J. Geophys. Res.*, 2002. Accepted.

[78] H. E. M. Meier and T. Faxén. Performance analysis of a multiprocessor coupled ice-ocean model for the Baltic Sea. *J. Atmos. Oceanic Technol.*, 19:114–124, 2002.

[79] G.L. Mellor and T. Yamada. A hierarchy of turbulence closure models for planetary boundary layers. *J. Atmos. Sci.*, 31:1791–1806, 1974.

[80] G.L. Mellor and T. Yamada. Development of a turbulence closure model for geophysical fluid problems. *Rev. Geophys. Space Phys.*, 20:851–875, 1982.

[81] Z. Mikulski. Inflow from drainage basin. In *Water balance of the Baltic Sea - Baltic Sea Environment Proceedings*, volume 16, pages 24–34, Baltic Marine Environment Protection Commision, Helsinki, Finland, 1986.

[82] A. Omstedt and L. Axell. Modeling the seasonal, interannual and long-term variations of salinity and temperature in the Baltic proper. *Tellus*, 50A:637–652, 1998.

[83] A. Omstedt and D. Chen. Influence of atmospheric circulation on the maximum ice extent in the Baltic Sea. *J. Geophys. Res.*, 106:4,493–4,500, 2001.

[84] A. Omstedt, L. Meuller, and L. Nyberg. Interannual, seasonal and regional variations of precipitation and evaporation over the Baltic Sea. *Ambio*, 26:484–492, 1997.

[85] A. Omstedt and L. Nyberg. Response of Baltic Sea ice to seasonal, interannual forcing and climate change. *Tellus*, 48 A:644–662, 1996.

[86] A. Omstedt, J. Sahlberg, and U. Svensson. Measured and numerically-simulated autumn cooling in the Bay of Bothnia. *Tellus*, 35A:231–240, 1983.

[87] T. J. Osborn, K. R. Briffa, S. F. B. Tett, and P. D. Jones. Evaluation of the North Atlantic Oscillation as simulated by a coupled climate model. *Clim. Dyn.*, 15:685–702, 1999.

[88] E. Palosuo. A treatise on severe ice conditions in the central Baltic. Havsforskningsinstitutets skrift No.156, Finnish Institute of Marine Research, Helsinki, Finland, 1953.

[89] C.A. Paulson and J.J. Simpson. Irradiance measurements in the upper ocean. *J. Phys. Oceanogr.*, 7:952–956, 1977.

[90] J. Räisänen, M. Rummukainen, and A. Ullerstig. Downscaling of greenhouse gas induced climate change in two GCM's with the Rossby Centre regional climate model for northern Europe. *Tellus*, 53A:168–191, 2001.

[91] R. Rödel. *The impact of historical river regulation on runoff to the Baltic Sea (in German).* PhD thesis, University of Greifswald, Greifswald, Germany, 2001.

[92] J. Rodhe and P. Winsor. On the influence of the freshwater supply on the Baltic Sea mean salinity. *Tellus*, 54A:175–186, 2002.

[93] W. Rodi. *Turbulence models and their application in hydraulics - a state-of-the-art review.* Int. Assoc. for Hydraul. Res., Delft, Netherlands, 1980. 104 pp.

[94] M. Rummukainen, J. Räisänen, B. Bringfelt, A. Ullerstig, A. Omstedt, U. Willén, U. Hansson, and C. Jones. A regional climate model for northern Europe - model description and results from the downscaling of two GCM control simulations. *Clim. Dyn.*, 17:339–359, 2001.

[95] M. Samuelsson. Interannual salinity variations in the Baltic Sea during the period 1954-1990. *Cont. Shelf Res.*, 16:1463–1477, 1996.

[96] M. Samuelsson and A. Stigebrandt. Main characteristics of the long-term sea level variability in the Baltic Sea. *Tellus*, 48A:672–683, 1996.

[97] H. Schinke and W. Matthäus. On the causes of major Baltic inflows - an analysis of long time series. *Cont. Shelf Res.*, 18:67–97, 1998.

[98] C. Schrum, F. Janssen, and U. Hübner. Recent climate modelling in North Sea and Baltic Sea. Part A: Model description and validation. Ber. Zentrum f. Meeres- u. Klimaforschung No.37, Zentrum f. Meeres- u. Klimaforschung, Hamburg, Germany, 2000. 60 pp.

[99] U. Schumann and T. Gerz. Turbulent mixing in stably stratified shear flows. *J. Appl. Meteorol.*, 34, 1995.

[100] T. Seifert and B. Kayser. A high resolution spherical grid topography of the Baltic Sea. *Meereswiss. Ber., Warnemünde*, 9:73–88, 1995.

[101] A. Seinä. Ice time series of the Baltic Sea. In M. Leppäranta and J. Haapala, editors, *Proceedings of the first workshop on the Baltic Sea ice climate*, number 27 in Report Series in Geophysics, pages 87–90, Department of Geophysics, University of Helsinki, Finland, 1993.

[102] A. Seinä and E. Palosuo. The classification of the maximum annual extent of ice cover in the Baltic Sea 1720-1992. Meri No.20, Finnish Institute of Marine Research, Helsinki, Finland, 1993.

[103] B. Sjöberg, editor. *Sea and Coast.* The National Atlas of Sweden. Almqvist and Wiksell International, Stockholm, Sweden, 1992. 128 pp.

[104] P. Skeie. Meridional flow variability over the Nordic seas in the Arctic Oscillation framework. *Geophys. Res. Lett.*, 27:2569–2572, 2000.

[105] A. Smedman, U. Högström, H. Bergström, A. Rutgersson, K. Kahma, and H. Pettersson. A case-study of air-sea interaction during swell conditions. *J. Geophys. Res.*, 104:25,833–25,851, 1999.

[106] A. Stigebrandt. A model for the exchange of water and salt between the Baltic and the Skagerrak. *J. Phys. Oceanogr.*, 13:411–427, 1983.

[107] A. Stigebrandt. A model of the vertical circulation of the Baltic deep water. *J. Phys. Oceanogr.*, 17:1772–1785, 1987.

[108] U. Svensson. A mathematical model of the seasonal thermocline. Report No.1002, Dep. of Water Resour. Eng., Univ. of Lund, Lund, Sweden, 1978. 187 pp.

[109] B. Tinz. On the relation between annual maximum extent of ice cover in the Baltic Sea level pressure as well as air temperature field. *Geophysica*, 32:319–341, 1996.

[110] L. B. Tremblay. Can we consider the Arctic Oscillation independently from the Barents Sea Oscillation? *Geophys. Res. Lett.*, 28:4227–4230, 2001.

[111] K.E. Trenberth and D.A. Paolino. The Northern Hemisphere sea level pressure data set: Trends, errors, and discontinuities. *Mon. Weather Rev.*, 108:855–872, 1980.

[112] K.E. Trenberth and D.A. Paolino. Characteristic patterns of variability of sea level pressure in the Northern hemisphere. *Mon. Weather Rev.*, 109:1169–1189, 1981.

[113] C.B. Uvo and R. Berndtsson. North Atlantic Oscillation - a climatic indicator to predict hydropower availablity in Scandinavia. *Nordic Hydrology*, 2002. In press.

[114] D. J. Webb, A. C. Coward, B. A. de Cuevas, and C. S. Gwilliam. A multiprocessor ocean circulation model using message passing. *J. Atmos. Oceanic Technol.*, 14:175–183, 1997.

[115] P. Welander. Two-layer exchange in an estuary basin, with special reference to the Baltic Sea. *J. Phys. Oceanogr.*, 4:542–556, 1974.

[116] J. Willebrand. Theorie der Turbulenz. Technical report, University of Kiel, Kiel, Germany, 1994. Unpublished manuscript of the turbulence lecture, summer term '94.

[117] P. Winsor, J. Rodhe, and A. Omstedt. Baltic Sea ocean climate: an analysis of 100 yr of hydrographic data with focus on the freshwater budget. *Clim. Res.*, 18:5–15, 2001.

[118] Z.-H. Zhang and M. Leppäranta. Modeling the influence of ice on sea level variations in the Baltic Sea. *Geophysica*, 31:31–45, 1995.

[119] E. Zorita and A. Laine. Dependence of salinity and oxygen concentrations in the Baltic Sea on large-scale atmospheric circulation. *Clim. Res.*, 14:25–41, 2000.

SMHIs publications

SMHI publishes six report series. Three of these, the R-series, are intended for international readers and are in most cases written in English. For the others the Swedish language is used.

Names of the Series	**Published since**
RMK (Report Meteorology och Climatology)	1974
RH (Report Hydrology)	1990
RO (Report Oceanography)	1986
METEOROLOGI	1985
HYDROLOGI	1985
OCEANOGRAFI	1985

Earlier issues published in RO

1 Lars Gidhagen, Lennart Funkquist and Ray Murthy (1986)
Calculations of horizontal exchange coefficients using Eulerian time series current meter data from the Baltic Sea.

2 Thomas Thompson (1986)
Ymer-80, satellites, arctic sea ice and weather.

3 Stig Carlberg et al (1986)
Program för miljökvalitetsövervakning - PMK.

4 Jan-Erik Lundqvist och Anders Omstedt (1987)
Isförhållandena i Sveriges södra och västra farvatten.

5 Stig Carlberg, Sven Engström, Stig Fonselius, Håkan Palmén, Eva-Gun Thelén, Lotta Fyrberg och Bengt Yhlen (1987)
Program för miljökvalitetsövervakning - PMK. Utsjöprogram under 1986.

6 Jorge C. Valderama (1987)
Results of a five year survey of the distribution of UREA in the Baltic sea.

7 Stig Carlberg, Sven Engström, Stig Fonselius, Håkan Palmén, Eva-Gun Thelén, Lotta Fyrberg, Bengt Yhlen och Danuta Zagradkin (1988).
Program för miljökvalitetsövervakning - PMK. Utsjöprogram under 1987

8 Bertil Håkansson (1988)
Ice reconnaissance and forecasts in Storfjorden, Svalbard.

9 Stig Carlberg, Sven Engström, Stig Fonselius, Håkan Palmén, Eva-Gun Thelén, Lotta Fyrberg, Bengt Yhlen, Danuta Zagradkin, Bo Juhlin och Jan Szaron (1989)
Program för miljökvalitetsövervakning - PMK. Utsjöprogram under 1988.

10 L. Fransson, B. Håkansson, A. Omstedt och L. Stehn (1989)
Sea ice properties studied from the icebreaker Tor during BEPERS-88.

11 Stig Carlberg, Sven Engström, Stig Fonselius, Håkan Palmén, Lotta Fyrberg, Bengt Yhlen, Bo Juhlin och Jan Szaron (1990)
Program för miljökvalitetsövervakning - PMK. Utsjöprogram under 1989.

12 Anders Omstedt (1990)
Real-time modelling and forecasting of temperatures in the Baltic Sea.

13 Lars Andersson, Stig Carlberg, Elisabet Fogelqvist, Stig Fonselius, Håkan Palmén, Eva-Gun Thelén, Lotta Fyrberg, Bengt Yhlen och Danuta Zagradkin (1991)

14 Lars Andersson, Stig Carlberg, Lars Edler, Elisabet Fogelqvist, Stig Fonselius, Lotta Fyrberg, Marie Larsson, Håkan Palmén, Björn Sjöberg, Danuta Zagradkin, och Bengt Yhlen (1992)
Haven runt Sverige 1991. Rapport från SMHI, Oceanografiska Laboratoriet, inklusive PMK - utsjöprogrammet. (The conditions of the seas around Sweden. Report from the activities in 1991, including PMK - The National Swedish Programme for Monitoring of Environmental Quality Open Sea Programme.)

15 Ray Murthy, Bertil Håkansson and Pekka Alenius (ed.) (1993)
The Gulf of Bothnia Year-1991 - Physical transport experiments.

16 Lars Andersson, Lars Edler and Björn Sjöberg (1993)
The conditions of the seas around Sweden. Report from activities in 1992.

17 Anders Omstedt, Leif Nyberg and Matti Leppäranta (1994)
A coupled ice-ocean model supporting winter navigation in the Baltic Sea.
Part 1. Ice dynamics and water levels.

18 Lennart Funkquist (1993)
An operational Baltic Sea circulation model. Part 1. Barotropic version.

19 Eleonor Marmefelt (1994)
Currents in the Gulf of Bothnia. During the Field Year of 1991.

20 Lars Andersson, Björn Sjöberg and Mikaell Krysell (1994)
The conditions of the seas around Sweden. Report from the activities in 1993.

21 Anders Omstedt and Leif Nyberg (1995)
A coupled ice-ocean model supporting winter navigation in the Baltic Sea.
Part 2. Thermodynamics and meteorological coupling.

22 Lennart Funkquist and Eckhard Kleine (1995)
Application of the BSH model to Kattegat and Skagerrak.

23 Tarmo Köuts and Bertil Håkansson (1995)
Observations of water exchange, currents, sea levels and nutrients in the Gulf of Riga.

24 Urban Svensson (1998)
PROBE An Instruction Manual.

25 Maria Lundin (1999)
Time Series Analysis of SAR Sea Ice Backscatter Variability and its Dependence on Weather Conditions.

26 Markus Meier[1], Ralf Döscher[1], Andrew, C. Coward[2], Jonas Nycander[3] and Kristofer Döös[3] (1999). RCO – Rossby Centre regional Ocean climate model: model description (version 1.0) and first results from the hindcast period 1992/93.
[1] Rossby Centre, SMHI [2] James Rennell Division, Southampton Oceanography Centre, [3] Department of Meteorology, Stockholm University

27 H. E. Markus Meier (1999)
First results of multi-year simulations using a 3D Baltic Sea model.

28 H. E. Markus Meier (2000)
The use of the $k-\varepsilon$ turbulence model within the Rossby Centre regional ocean climate model: parameterization development and results.

29 Eleonor Marmefelt, Bertil Håkansson, Anders Christian Erichsen and Ian Sehested Hansen (2000)
Development of an Ecological Model System for the Kattegat and the Southern Baltic. Final Report to the Nordic Councils of Ministers.

SMHI
Swedish Meteorological and Hydrological Institute
SE 601 76 Norrköping, Sweden.
Tel +46 11-495 80 00 · Fax +46 11-495 80 01

ISSN 0283-1112